December 2015

Part I. The Development of Non-secosteroidal Vitamin D Receptor Modulators Part II. The Development of a Universal GTP-ase Assay

Kelly Ann Teske
University of Wisconsin-Milwaukee

PART I. THE DEVELOPMENT OF NON-SECOSTEROIDAL VITAMIN D RECEPTOR MODULATORS

PART II. THE DEVELOPMENT OF A UNIVERSAL GTPase ASSAY

by

Kelly A. Teske

A Dissertation Submitted in

Partial Fulfillment of the

Requirements for the Degree of

Doctor of Philosophy

in Chemistry

at

The University of Wisconsin-Milwaukee

December 2015

ABSTRACT

PART I. THE DEVELOPMENT OF NON-SECOSTEROIDAL VITAMIN D RECEPTOR MODULATORS

by

Kelly A. Teske

The University of Wisconsin-Milwaukee, 2015
Under the Supervision of Professor Alexander (Leggy) Arnold

The vitamin D receptor is a nuclear hormone receptor that regulates cell proliferation, cell differentiation, calcium homeostasis and immunomodulation. The receptor is activated by the vitamin D metabolite, 1,25-dihydroxyvitamin D_3, which induces a cascade of events including the recruitment of coactivators that activate transcription of specific VDR target genes. Thousands of VDR agonists have been synthesized based on the secosteroid scaffold of 1,25-dihydroxyvitamin D_3. However, most of these ligands are metabolically unstable, have sub-optimal drug-like properties, and induce hypercalcemia *in vivo.* The limited numbers of VDR antagonists reported bear the same secosteroid scaffold and thus exhibit similar problems encountered by VDR agonists. VDR has been implicated with many diseases including cancer, allergies, sarcoidosis and autoimmune diseases like Crohn's disease. Therefore, the synthesis and biochemical evaluation of novel, non-secosteroidal modulators for VDR were developed and reported herein.

First, VDR inhibitors were rationally designed to directly target the interactions between VDR and coactivator SRC2. A fluorescence polarization-based assay evaluated the binding of these molecules. Next, a high throughput screening campaign with the NIH chemical and genomics center (NCGC) identified GW0742 as a novel VDR anatagonist. Originally developed by

GlaxoSmithKline as a selective PPARδ agonist, GW0742 was used as a scaffold for the synthesis of VDR inhibitors with decoupled activity towards PPARδ. Biochemical, cell-based, solubility and permeability assays determined drug-like properties of over 100 GW0742 analogs. Finally, secondary bile acids, which are known to bind VDR and modulate transcription without inducing hypercalcemia, lead to a study of phase 1 and phase 2 metabolites of lithocholic acid. In addition to biochemical and cell-based assays, a semi-quantitative real time polymerase chain reaction was used to confirm the ability of lithocholic acid derivatives to induce the transcription of VDR target genes.

ABSTRACT

PART II. THE DEVELOPMENT OF A UNIVERSAL GTPase ASSAY

by

Kelly A. Teske

The University of Wisconsin-Milwaukee, 2015
Under the Supervision of Professor Alexander (Leggy) Arnold

GTPases act as a molecular switches in which their “on” and “off” functions are triggered by the binding and hydrolysis of GTP. Due to their relationship to many diseases, numerous GTPase targeting drugs have been developed. One third of all drugs targeting proteins are either interacting with kinases (22% of drugs) or GTPases (15% of drugs). The growing interest in GTPase targeting drugs has promoted the development of assays that can efficiently test these compounds in a high throughput and inexpensive way. AviMed Pharmaceuticals, LLC, a local company founded by Dr. Daniel Sem, pursued the development of a universal kinase/GTPase assay kit that would be affordable and commercially available for industry and research labs to test potential drug candidates. The assay designed was based on previous research conducted by the founder and relies on a beta thiol substituted ATP (GTP for GTPases) that would be enzymatically hydrolyzed to produce ADP (GDP). The exposure of the thiol makes it nucleophilic and reactive towards thiol-sensitive fluorescent or calorimetric reagents such as Thiofluor 623. Herein, we report the synthesis of the assay reagents and the preliminary development of a universal, inexpensive, sensitive GTPase assay kit that directly detects the GTPβ-S hydrolysis product, GDPβ-Se.

I would like to dedicate my dissertation to my Pops (Grandpa Teske) and Grandpa Pete.

TABLE OF CONTENTS

LIST OF FIGURES

LIST OF TABLES

LIST OF SCHEMES

LIST OF ABBREVIATIONS

UV- ultraviolet

25(OH)D_3- 25-hydroxyvitamin D_3

1,25$(OH)_2D_3$- 1,25-dihydroxyvitamin D_3

DBP- vitamin D binding protein

VDR- vitamin D receptor

NRs- nuclear receptors

DBD- DNA binding domain

LBD- ligand binding domain

CTE- C-terminal extension

RX- 9-*cis* retinoic acid receptor

VDREs- vitamin D-responsive elements

DR direct repeats

RNA Pol II- RNA polymerase II

AF-2- activation function

AD- activating domain

GTFs- general transcription factors

NCoR1- nuclear receptor corepressor

SMRT- silencing mediator for retinoic acid and thyroid hormone receptors

HDACs- histone deacetylases

TFIIB- transcription factor IIB

PIC- preinitiation complex

SRC- p160/steroid receptor coactivator

DRIP- vitamin D receptor interacting protein complex

HAT- histone acetyl transferase activity

CBP- CREB- binding protein

p/CAF- p300/CBP-associated factor

TAFs- TATA binding accessory factors

RANKL- receptor activator of NF-κB ligand

PTH- parathyroid hormone

OVX- ovariectomized

NMU- nitrosomethyl urea

ROS- reactive oxygen species

uPA- urokinase-type plasminogen activator

tPA- tissue type plasminogen activator

KRS-2- kinase suppressor of ras 2 gene

OC- osteocalcin

SAR- structure-activity relationship

fatty acid synthase (FASN)

MCRs- multi-component reactions

U-4CR- Ugi four component reaction

EDCI- 1-ethyl-3-(3-dimethylaminopropyl)carboiimide

HOBt- Hydroxybenzotriazole

DIPEA- N, N-Diisopropylethylamine

EtOAc- ethyl acetate

TLC- thin layer chromatography

MeOH- methanol

THF- tetrahydrofuran

AcOH- acetic acid

FP- fluorescence polarization

LBP- ligand binding pocket

ADME- absorption, distribution, metabolism, and excretion

HTS- High Throughput Screening

NCGC- NIH chemical and genomics center

ME- 2-mercaptoethanol

PPARδ- peroxisome proliferator activated receptor δ

TRβ- thyroid hormone receptor β

AR- androgen receptor

ERα and β- estrogen receptors α and β

CMV- cytomegalovirus promoter

DMSO- dimethylsulfoxide

DCM- dichloromethane

APCI- atmospheric-pressure chemical ionization

ESI- electrospray ionization

LC-MS- liquid chromatography mass spectrometry

NMR- nuclear magnetic resonance

HPLC- high performance liquid chromatography

DUIS- dual ion source

GI-tract- gastrointestinal tract

PAMPA- parallel artificial membrane permeability assay

PBS- phosphate buffered saline

TMS- trimethylsilyl

TBS- *t*-butyldimethylsilylether

dNTPs- deoxynucleoside triphosphates

dsDNA- double stranded

qRT-PCR- semi-quantitative real time polymerase chain reaction

MOE- Molecular Operating Environment

LXR- liver X receptor

ERR- estrogen related receptor

RAR- retinoic acid receptor

PXR- pregnane X receptor

TEAB- triethylammonium bicarbonate

TEA- Triethylamine

ACKNOWLEDGMENTS

These past years have been an incredible journey that would not have happened if it were not for the amazing people supporting me along the way. I would like to first and foremost thank my research advisor, Dr. Leggy Arnold, for pushing me to be a better chemist. Although I had days of frustration, you were always there to help me reach my goal.

Thank you to my amazing research group who are the best people I could have ever wished for to share this experience with. A huge thank you to the outrageously crazy "Ladies of Chemistry" who helped me keep my sanity in and out of school. You always knew how to cheer someone up after a long day in the lab.

Thank you to my family, in particular my Mom, Dad and two sisters, Kari and Meghan, who constantly supported me. Mom and Dad thank you for providing me with the opportunity to go to college and better educate myself. I would also like to thank my extended family including my Grandma Teske and Grandma Marge, my aunts and uncles and all my cousins for encouraging me during my studies.

Of course I would have never made it to graduate school if it weren't for the incredible education I received from Illinois State University. Dr. Frank Shaw, III, thank you for introducing me to chemical research. You opened my eyes to all the possibilities achievable through chemistry. To all my ISU friends, thank you. Your constant support through the good and bad times over these past five years have been astounding. I could not have asked for better friends.

Last but not least, I would like to thank my amazing and wonderful boyfriend, Mike Poe, who too endured long days in the lab but always found a way to be positive for the both of us,

especially when I felt frazzled from research. You always found the best way to calm my stress and think about the big picture. Thank you for that. You have been the perfect partner in crime.

PART I. THE DEVELOPMENT OF NON-SECOSTEROIDAL VITAMIN D RECEPTOR MODULATORS

CHAPTER 1: INTRODUCTION

1.1 The History of Vitamin D

Prior to the twentieth century, vitamins and pre-vitamins were largely unknown although evidence existed that certain foods can prevent diseases such as Scurvy and Beri-Beri.[12] In 1910, Drs. Hopkins and Funk separately demonstrated that diets of purified carbohydrates, proteins, fats and salts were unable to support growth in animals thus concluding that "vital amines" or vitamins were present in natural foods and therefore providing sustenance for life.[13, 14] In 1914, McCollum et al. isolated a fat-soluble, non-saponifiable factor from butter fat that was necessary for normal growth and prevention of the eye disease xerophthalmia in young rats. This substance became known as "fat soluble factor A" or vitamin A.[15] This quickly led to McCollum's discovery of the water soluble vitamin, vitamin B, that deemed necessary for the prevention of polyneuritis.[16] During this time, the skeletal disease rickets was becoming an epidemic in England. This was mainly brought on by the sudden urbanization of rural areas during the "Industrial Revolution" that caused a large production of pollutants in the atmosphere blocking the sun. Thinking the disease was caused by a deficiency in vitamin A, people were given cod liver oil, a substance known to contain vitamin A, for the treatment of rickets. Although this treatment worked, McCollum questioned whether vitamin A was responsible. In 1922, he conducted a pivotal experiment where he heated and bubbled oxygen through cod liver oil to destroy the vitamin A activity and found that this preparation was incapable of treating vitamin A deficiencies (i.e. xerophthalmia) but still retained its ability to cure rickets. This surprising result

prompted McCollum to conclude that the factor that cures rickets was a new vitamin which they named vitamin D.[17, 18]

Around the same time, the German scientist, Huldschinsky, made the important observation that the health of rachitic children as well as their calcium deposition improved by being exposed to sunlight or artificial ultraviolet (UV) light.[19] This was later confirmed by Harriette Chick in 1922 while working with severely malnourished children in Vienna. She found that therapeutic exposure to sunlight provided results that were indistinguishable from those patients receiving cod liver oil.[20] This treatment triggered investigations into the active form of vitamin D.

Many scientist contributed to the long history of the isolation and identification of vitamin D analogs in the 1920's and 1930's including early vitamin D pioneers H. Steenbock (Wisconsin), A. F. Hess (New York), O. Rosenheim (London) and A. Windaus (Germany).[21] Steenbock found that by irradiating food with UV light, specifically the non-saponifiable lipid fraction, the vitamin D content increased and promoted growth and bone-calcifying properties in rachitic rats.[22] He concluded that an inactive lipid in the diet and skin could be converted by UV light into an active antirachitic substance.[23] This led to tremendous advances in public health by adding vitamin D to milk and other foods to prevent disease. Hess et al. isolated sitosterol from cottonseed oil and found that upon irradiation this inactive non-saponifiable sterol was then active against rickets. He also observed this phenomenon with "pure" cholesterol isolated from rat brains thus allowing him to hypothesize that the cholesterol in skin can be converted by UV-irradiation and rendered an active form of vitamin D.[24] However, the sample of cholesterol used by Hess was found to be impure, which led him to collaborate with the chemists Windaus and Rosenheim to purify the

sample. Because physical methods such as recrystallization and saponification had proven incapable of purifying the cholesterol mixtures to begin with, they converted cholesterol into its dibromide form, recrystallized it and recovered cholesterol upon treatment with sodium amalgam. The purified cholesterol, after irradiation, no longer possessed antirachitic properties making it evident that the impurity was the pro-vitamin they were looking for.

Askew et al. were the first to successfully isolate and determine the structure of vitamin D or ergocalciferol, better known as Vitamin D_2, from ergosterol (a fungal steroid from ergot).[25] Windaus and Hess also found that the most highly active antirachitic compound upon irradiation was ergosterol.[26] Furthermore it was determined that ergosterol (Figure 1, A) was a provitamin

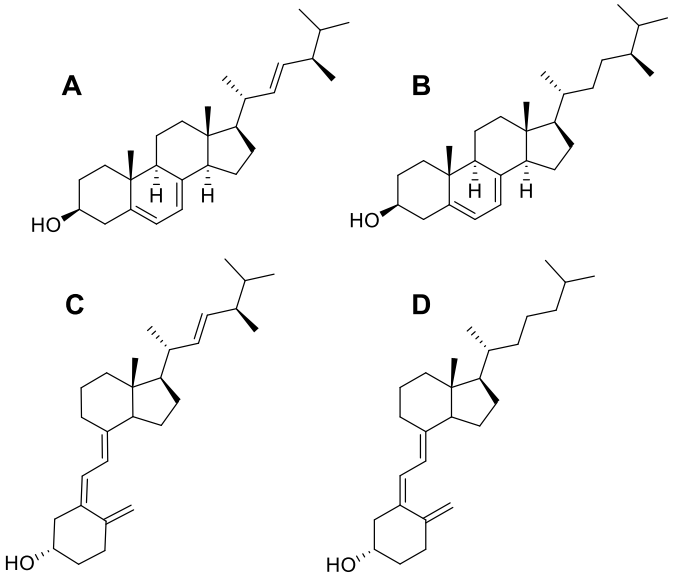

Figure 1. Structure of A) ergosterol, B) 7-dehydrocholesterol, C) ergocalciferol or Vitamin D_2, and D) cholecalciferol or Vitamin D_3.

with its irradiation product being ergocalciferol or vitamin D_2 (Figure 1, C) in plants.[27] In 1936, Windaus et al. isolated 7-dehydrocholesterol (Figure 1, B) from hog skin that provided evidence

that it was the provitamin found in humans for the production of vitamin D_3 cholecalciferol (Figure 1, D).[28, 29]

In the 1950's, Egan Kodicek investigated the metabolism of vitamin D_2. He used ^{14}C-labeled vitamin D_2 to monitor its activity and metabolism in the body. However, the degree of labeling was not sufficient to allow the administration of physiological doses of vitamin D_2, which

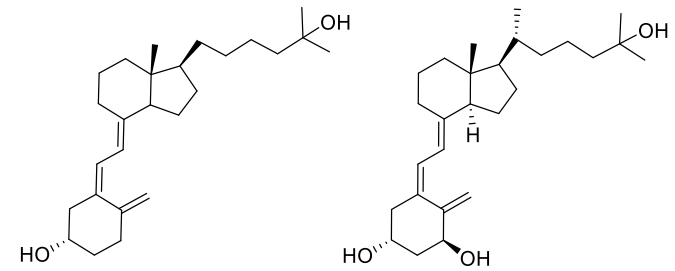

Figure 2. The active Vitamin D metabolites, 25(OH)D_3 and 1,25$(OH)_2D_3$, determine by Deluca *et al.* at the University of Wisconsin.

increased the storage of the vitamin D rather than its metabolism. After a decade he concluded that vitamin D_2 was the active biological compound and that no metabolic change was required.[30, 31] However, we know today that hydroxylation is essential to activate vitamin D, which was discovered in Wisconsin led by DeLuca *et al.* in 1967 using radiolabeled Vitamin D_3. Upon administration, detection of metabolites were seen within 1-2 hours and when isolated and given to vitamin D-deficient animals proved to be more potent and faster acting than vitamin D_3 in supporting calcium transport. This led to the isolation and identification of the active metabolite, 25-hydroxyvitamin D_3 (25(OH)D_3), in 1968 (Figure 2).[32, 33] However, when radiolabeled 25(OH)D_3 was administered further metabolism occurred. Holick and DeLuca identified these metabolites by feeding 1,600 Vitamin D-deficient chickens radiolabeled Vitamin

D_3 and isolating Vitamin D metabolites from the intestines. Analysis conducted by mass spectrometry and derivatization lead finally to the identification of the most active hormonal form of vitamin D, 1,25-dihydroxyvitamin D_3 ($1,25(OH)_2D_3$) (Figure 2).[34, 35]

1.2 A Brief Overview of the Activating Enzymes of Vitamin D_3

Vitamin D_3 can either be absorbed from various food sources in the intestine or synthesized in the skin by a two-step reaction starting with 7-dehydrocholesterol undergoing a UV-induced, electrocyclic ring opening reaction to make pre-vitamin D_3 followed by an antarafacial sigmatropic [1,7] hydride shift induced by thermal isomerization to make vitamin D_3 (Figure 3). Once formed, vitamin D_3 and its analogs bind specifically to the vitamin D binding protein (DBP), which transports these molecules in the blood to cells and organs such as the liver and kidney.[36, 37] DeLuca found that the liver is the primary site of the first enzymatic activation of vitamin D_3 where hydroxylation of the C-25 position to $25(OH)D_3$ occurs.[38] The mitochondrial enzyme responsible for this process is 25-hydroxylase, a cytochrome P450 mixed-function oxidase that in humans is encoded by the CYP2R1 gene.[39] $25(OH)D_3$ binds tightly to DBP and enables it transport to the kidneys. Within the kidneys, specifically the renal tubules, $25(OH)D_3$ is hydroxylated at C-1 by 1α-hydroxylase, a different cytochrome P450 enzyme encoded by the CYP27B1 gene.[40] This enzymatic reaction forms the final hormonal form of vitamin D_3,

$1,25(OH)_2D_3$, which is the most potent ligand of the vitamin D receptor (VDR) and is responsible for the physiological actions of vitamin D throughout the body.

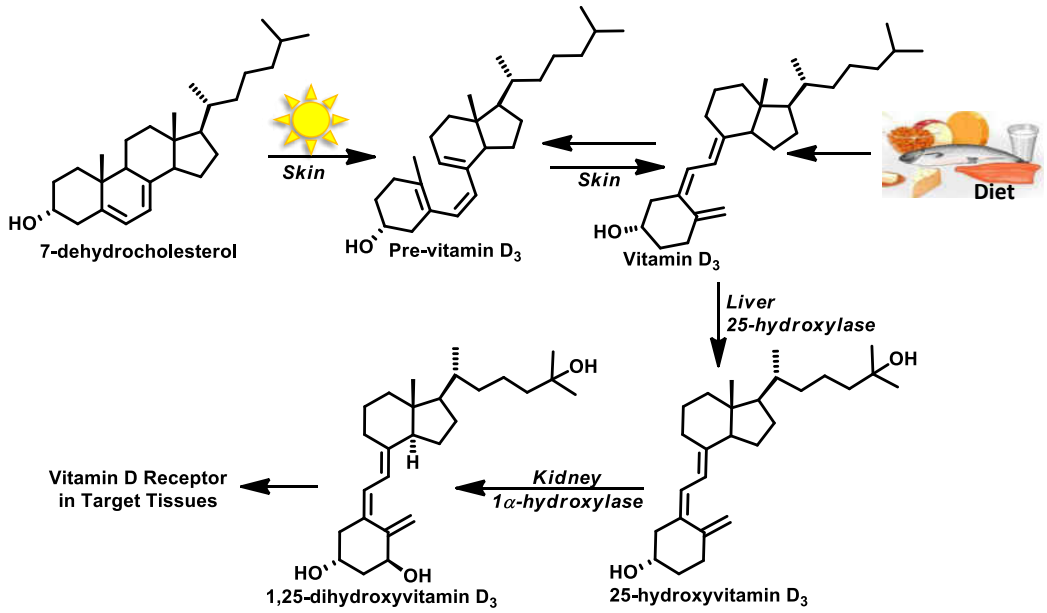

Figure 3. The activation of vitamin D_3 obtained either from the diet or the photo-catalyzed reaction of 7-dehydrocholesterol. CYP enzymes catalyze reactions in the liver and kidneys make the potent VDR hormone, $1,25(OH)_2D_3$, which get distributed to different target tissues in the body.

1.3 The Vitamin D Receptor: Structure and Function

In 1969, Haussler and Norman first identified VDR in chicken intestinal chromatin extracts that demonstrated a preferential uptake of $1,25(OH)_2D_3$ through a protein mediated process. They also showed that this process was saturable at low concentrations.[41] Work done by Brumbaugh and Haussler in 1975 provided substantial evidence that the protein must function as a nuclear receptor when observing that cytosol-derived VDR could bind to chromatin fractions in a hormone-sensitive manner.[42, 43] VDR was cloned in the late 1980's and eventually crystallized at the turn of the century, which gave much insight into the structure and function of this hormone activated protein.[8, 44]

Today we know that VDR is a transcription factor that belongs to a superfamily of nuclear receptors (NRs). As a transcription factor, VDR functions within the nucleus where it regulates gene expression through hormone-activation of the receptor. So far 48 identified proteins belong to this superfamily. They share similarities in structural and functional features in spite of the wide variation in their ligands.[45] All NRs are modular proteins that typically contain six domains (A-F) based on regions of similar sequence and function (Figure 4). The nonconserved N-terminal A/B domain that mediates activation by other molecules is followed by the DNA

Figure 4. The functional domains of typical NRs, which consist of a variable N-terminal region (A/B), a conserved DNA binding domain (C), a variable hinge region (D), a conserved LBD (E), and a variable C-terminal region (F). VDR does not contain an F domain.

binding domain (DBD, domain C). The D domain or hinge region is a highly flexible region that links the NR's DBD to its ligand binding domain (LBD, domain E) making receptor dimerization possible. The highly conserved LBD region mediates the interaction with ligands and other proteins, such as co-repressors and co-activators that are important to fine-tune the transcriptional activity of VDR. Finally, the F domain is extensively variable among NRs and absent in VDR.[46, 47]

The centrally located VDR DBD consists of a 66 residue core in humans and is made up of two modules each containing zinc-coordinated structures. The zinc atoms are individually coordinated in a tetrahedral fashion through four cysteine residues that serve to stabilize the zinc-finger structure (Figure 5).[48, 49] Although the two zinc modules appear structurally similar, they are not related topologically due to the difference in chirality of the residues that coordinate the zinc in each module. Thus, each module possesses their own unique function. The amino-terminal module directs specific DNA binding in the major grove of the DNA binding site, while

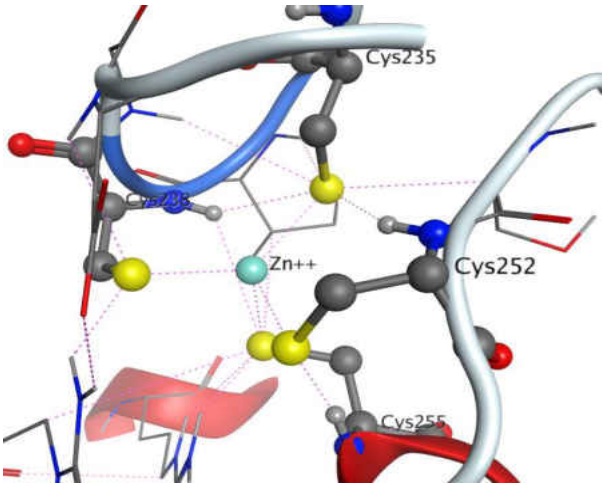

Figure 5. Crystal structure VDR DBD with Zn^{2+} coordinated with four cysteine residues. (PDB: 1YNW)[1-4]

the carboxy-terminal module serves as a dimerization interface for interaction with other proteins.[3, 50] An extra string of residues known as the adjacent C-terminal extension (CTE) of the DBD provides additional dimerization specificity for VDR (Figure 6, B). Although VDR can occasionally partner with itself, it commonly heterodimerizes with any of the three isoforms of the 9-*cis* retinoic acid receptor (RXR). The VDR-RXR complex binds DNA and activates transcription by recognizing vitamin D-responsive elements (VDREs) on specific VDR target genes.

Response elements typically consist of two hexameric half-sites with a spacer of neutral base pairs (Figure 6, A). Diversity and specificity of binding is dictated largely by variations of the half-

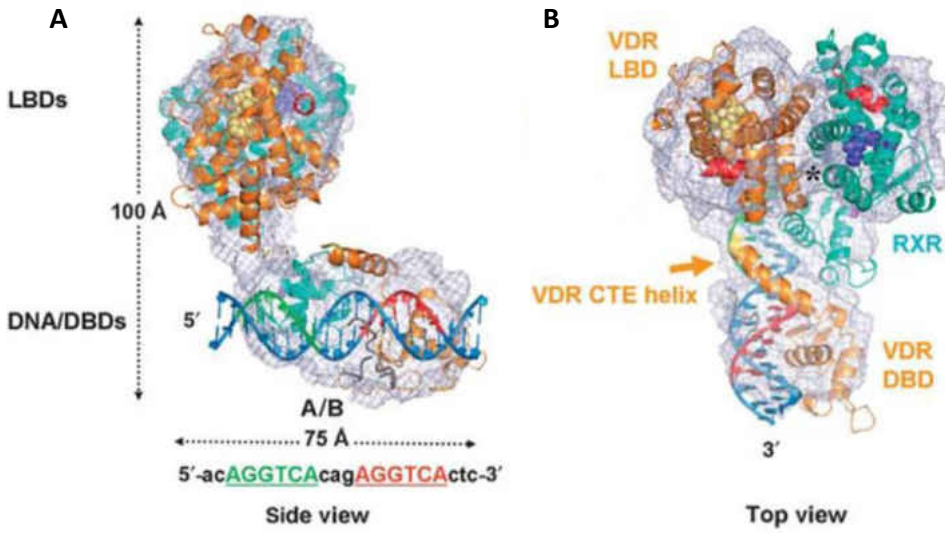

Figure 6. Cryo electron microscopy (cryo-EM) structure of the heterodimeric complex of the human RXR and VDR activated by 1,25(OH_2)D_3 and bound to a consensus DNA response element forming a direct repeat (DR3). This was done by fitting known crystal structures of LBDs and DNA bound DBDs with cryo EM maps of the nuclear receptor complex. No crystal structure of RXR-VDR-DR3 DNA has been reported yet. A) Side view with 5′ DNA end on the left. The fitted LBD and DBD/DNA heterodimer parts are shown in their backbone secondary structure. The DNA is shown in blue with the first half-site of the response element green and the second half-site in red. B) Top view of complex as seen along the pseudo two-fold axis through the interface of the RXR and VDR LBDs (indicated by black star). The CTE helix of VDR is protruding from the DBD and cross the DNA minor groove indicated by the arrow.

sites relative to one another and the number of neutral base pairs separating the half-element repeats.[51, 52] For example, half-sites can be arranged as inverted, everted or direct repeats (DR), where VDR-RXR requires a direct repeat of typically 5′-AGGTCA-3′ with a three base pair spacer (DR3) for DNA binding to occur. In addition, VDR occupies the downstream 3′ half-site and the RXR occupies the upstream 5′ half-site, which influences the target gene selectivity and ultimately the rate of RNA polymerase II (RNA Pol II) directed transcription.[53]

The E domain or LBD, is a multifunctional region that has complete regulatory control over DNA-binding and transcription-modifying properties of VDR.[54] Within the LBD is a highly structured region known as the ligand-dependent activation function or AF-2 that acts as the major interface for dimerization with RXR (Figure 6, B), as well as, the interface for co-activators and co-repressors. AF-2 is only functional through the binding of VDR ligands (Figure 7). The general fold of NR's LBD involve a three-layered α-helical sandwich containing twelve α-helices designated as H1–H12 and three β-sheets. Upon binding of $1,25(OH)_2D_3$, helix H11 is repositioned in line with H10 to allow helix H12 to clamp down and seal the binding pocket. Helix H12, also referred to as the activating domain (AD) of the AF-2 function, stabilizes ligand binding by contributing to the hydrophobic environment and making, in some cases, additional contacts with the ligand. When folded back onto the LBD, Helix H12 forms a hydrophobic cleft with charged surface-exposed residues on each end. The positively charged K246 (H3) and negatively charged E420 (H12) form the "charged clamp" that accommodate the recruitment of coregulators (Figure 7, A).[55]

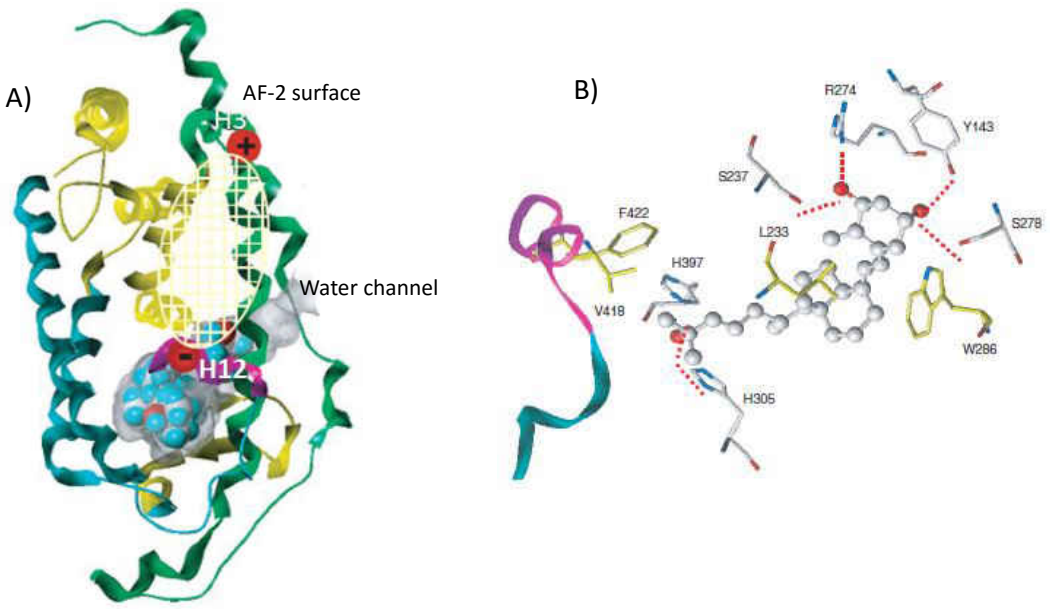

Figure 7. A) Side view of three layered sandwich fold of hVDR LBD in complex with $1,25(OH)_2D_3$ (ribbon model with colors indicating position: front is blue green, middle as yellow and rear as green). The AF-2 surface, where coactivators bind, is shown in transparent yellow oval with charge residues, K246 and E420, as red balls. B) Major interactions of ligand, $1,25(OH_2)D_3$ with the LBD pocket residues. Yellow residues indicate hydrophobic interactions while the red dotted lines indicate hydrogen bonds.

The crystal structure of $1,25(OH)_2D_3$ with hVDR reveals a ligand-binding pocket that is wider at H11 site than many other NRs with $1,25(OH)_2D_3$ occupying 56% of the pocket volume.[8] Upon binding, the ligand obtains an extended configuration with the A ring in the β chair conformation with the 1α-OH in the equatorial position. The side chain is in proximity of H11, while the A ring extends into the β-turn region. $1,25(OH)_2D_3$ is anchored in the pocket by six hydrogen bond interactions: the 1α-OH bonds with Ser237 (H3) and Arg274 (H5), the 3β-OH hydrogen bonds with Tyr143 (loopH1-H2) and Ser278 (H5) and the 25-OH group forms two hydrogen bonds with His305 (loop H6-H7) and His 397 (H11) when using the hVDR numbering (Figure 7, B).[55, 56]

1.4 General Transcription Factors and Coregulators of VDR-mediated Gene Expression

VDR-mediated transcription is regulated by a series of temporary macromolecular interactions, which includes both general transcription factors (GTFs) and coregulatory proteins.[57] Coregulators interact directly with the VDR-RXR heterodimer LBDs and can affect transcription in either a positive or negative fashion. These positive and negative modulators are known as coactivators and corepressors, respectively. VDR-coactivator interactions are mediated by $1,25(OH)_2D_3$ binding to VDR-LBD and corepessor binding occurs typically in the absence of ligand.

The classic and most simplified model of the ligand induced switch between transcription "off" and transcription "on" using coregulators begins with unliganded VDR loosely associated with RXR and nonspecifically bound to DNA. At this point, VDR and RXR are in a favorable conformation for binding corepessors because helix 12 of the AF2 domain is left in an "open", inactive position.[58] The best characterized corepressors for VDR are the nuclear receptor corepressor (NCoR1) and the universally expressed silencing mediator for retinoic acid and thyroid hormone receptors (SMRT or NCoR2). Both possess a LXXH/IIXXXI/L motif (where x is any amino acid, L is leucine and I is isoleucine) that interacts with the hydrophobic groove of the heterodimer (Figure 8).[59] NCoR and SMRT both associate with enzymes known as histone deacetylases or HDACs.[60] HDACs interfere with gene transcription by removing acetyl groups from chromatin and allowing for tight compaction of negatively charge DNA with positively

Peptide	-7	-6	-5	-4	-3	-2	-1	1	2	3	4	5	6	7	8	9	10	11	12
SRC1-1	Y	S	Q	T	S	H	K	L	V	Q	L	L	T	T	T	A	E	Q	Q
SRC1-2	L	T	A	R	H	K	I	L	H	R	L	L	Q	E	G	S	P	S	D
SRC1-3	E	S	K	D	H	Q	L	L	R	Y	L	L	D	K	D	E	K	D	L
SRC2-1	D	S	K	G	Q	T	K	L	L	Q	L	L	T	T	K	S	D	Q	M
SRC2-2	L	K	E	K	H	K	I	L	H	R	L	L	Q	D	S	S	S	P	V
SRC2-3	K	K	K	E	N	A	L	L	R	Y	L	L	D	K	D	D	T	K	D
SRC3-1	E	S	K	G	H	K	K	L	L	Q	L	L	T	S	S	S	D	D	R
SRC3-2	L	Q	E	K	H	R	I	L	H	K	L	L	Q	N	G	N	S	P	A
SRC3-3	K	K	E	N	N	A	L	L	R	Y	L	L	D	R	D	D	P	S	D
DRIP-1	K	V	S	Q	N	P	I	L	T	S	L	L	Q	I	T	G	N	G	G
DRIP-2	N	T	K	N	H	P	M	L	M	N	L	L	K	D	N	P	A	Q	D
NCoR-2	D	P	A	S	N	L	G	L	E	D	I	I	R	K	A	L	M	G	S
SMRT-2	H	A	S	T	N	M	G	L	E	A	I	I	R	K	A	L	M	G	K

Figure 8. Amino acid sequence of corepressors NCoR-2 and SMRT-2 and SRC family of coactivators and DRIP coactivators with each specific NR box motif indicated. The LXXLL NR box motif is labeled red and the LXXH/IIXXXI/L is labeled green for coactivators and corepressors, respectively.[9]

charged histones. In addition to HDACs and corepressors, the inactive VDR complex may also associate with an activating GTF known as transcription factor IIB (TFIIB) (Figure 9).[61] The true mechanism of TFIIB is not well understood but it might associate with unliganded DNA-bound VDR and help sequester TFIIB into the vicinity of specific vitamin D-responsive promoter areas. Once $1,25(OH)_2D_3$ binds to VDR, TFIIB might assemble with preinitiation complex (PIC) to help facilitate VDR-mediated transcription.[62]

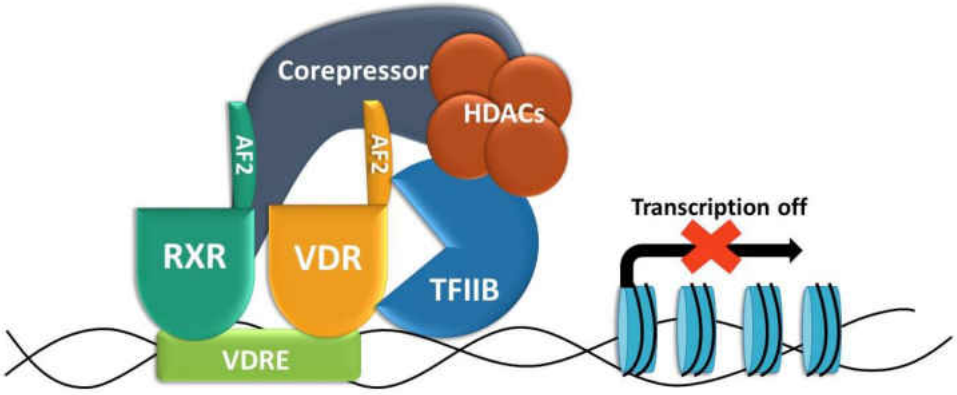

Figure 9. A generalized cartoon of unliganded VDR-RXR loosely associated heterodimer including its proposed interactions with corepressor (NCoR or SMRT), TFIIB and HDACs. The corepressor is bound to VDR when the AF2 domain is in the open configuration and attracts HDACs to repress chromatin.[3, 5]

The transcriptional machinery required for the VDR-mediated transcription is a very complex and includes sequential recruitment of many different VDR interacting proteins. This process is summarized in Figure 10. In the first step, transcription is switched "on" with the binding of 1,25(OH_2)D_3 to VDR. During these first activation steps RXR and VDR associate with a higher affinity, specific VDREs are recognized and the AF2 domains in both VDR-LBD and RXR-LBD are repositioned (Figure 10, A).[3] This conformational change promotes favorable coactivator binding and the dissociation of corepressor/HDAC complex. Several different coactivators can be recruited including the p160/steroid receptor coactivator (SRC) family, which consist of SRC-1 (also known as NCoA1), SRC-2 (also known as NCoA2, GRIP-1, and TIF2) and SRC-3 (also known as NCoA3, p/CIP, RAC3, ACTR, AIB-1, and TRAM-1), and the large vitamin D receptor interacting protein complex (DRIP or Mediator D complex).[63] Important for VDR binding are multiple highly conserved LXXLL-containing NR boxes where L is leucine and X is any amino acid (Figure 10).[64] The coactivator NR box forms an amphipathic α-helix that interacts with VDR's AF2 domain. The preference of certain NR boxes for particular NRs have been reported. For example in the case of SRC-3, VDR has preferential interaction with NR box III.[9, 65] SRC coactivators also possess histone acetyl transferase activity (HAT), that may include the secondary recruitment of CREB-binding protein (CBP)/p300 cointegrator and p300/CBP-associated factor (p/CAF) (Figure 10, A).[66] HAT activity remodels the chromatin by covalently adding acetyl groups onto the carboxyl-terminal lysine residues of histones. This weakens the electrostatic interaction between the DNA and histone tail thus priming it for the binding and assembly of PIC, which includes TATA binding

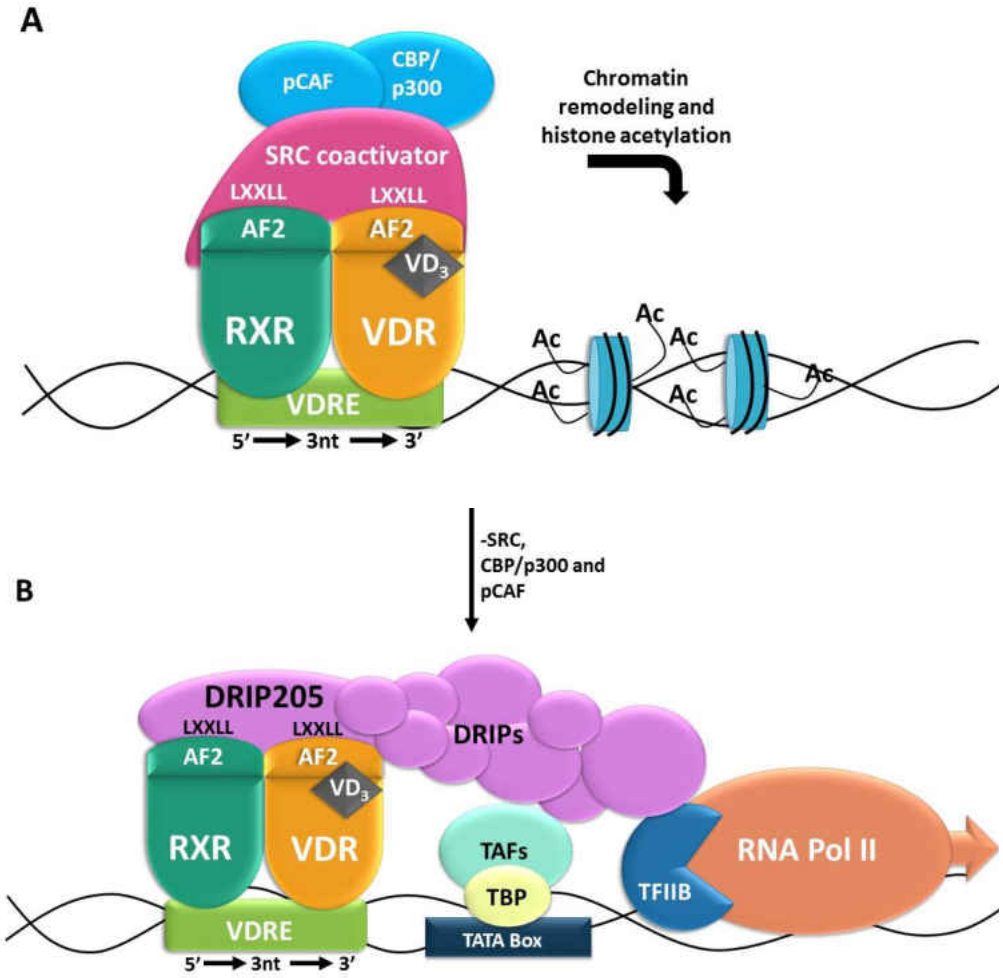

Figure 10. A generalized cartoon for the VDR-RXR-coactivator complex in VDR-activated transcription. A) $1,25(OH)_2D_3$ binds to VDR and the AF2 domains of the RXR-VDR heterodimer seals the LBD pocket. Primary (SRC) and secondary coactivators (pCAF and CBP/p300) provide HAT activity and prime DNA for transcription. B) SRC and secondary coactivators dissociate and mediator D-complex DRIP205 binds and stimulates assembly of PIC components such as TAFs and TFIIB and the recruitment of RNA Pol II to the repressed chromatin.[3-5]

accessory factors (TAFs) that target TATA box protein and TFIIB (Figure 10, B).[67] Furthermore, the mediator D complex (DRIP) acts as a bridge between VDR and GTFs that promote the formation and function of PIC with RNA Pol II.[57] It is composed of at least ten different proteins anchored by DRIP205 that interacts directly with the VDR-RXR heterodimer through their second of two LXXLL motifs.[68] Although DRIP may recruit RNA Pol II to the promotor, the polymerase is

not tightly bound thus allowing for its release and efficient initiation of transcription (Figure 10, B).[69]

1.5 Vitamin D analogs and Their Pharmacological Effects

VDR is expressed in many different cells and has been affiliated with calcium and phosphate homeostasis as well as differentiation and proliferation of cells. Novel therapies based on vitamin D receptor ligands are currently developed to treat skin and metabolic disorders, gastrointestinal diseases, cardiovascular problems, inflammatory diseases, and notably cancer.[70] The major hurdle for VDR ligand-based treatments is tissue selectivity in order to exert pharmacological activity in a particular tissue. For instance inducing anti-proliferation in cancer tissue without increasing the calcium concentration in blood or to increase the bone mineral density without inducing hypercalciuria. More than 2,000 VDR ligands have been synthesized and characterized during the last decades but only a very limited number of compounds have been approved for the treatment of human diseases. This section will describe the pharmacological effects of two drugs eldecalcitrol (osteoporosis) and EB1089 (cancer) and their modulation of vitamin D receptor function.

1.5.1 Vitamin D and Osteoporosis (Calcium Homeostasis)

Osteoporosis is the dysfunction of bone resorption and bone formation due to aging. Bone is the primary location for the resorption of Ca^{2+} and PO_4^{3-}; a process that is regulated by osteoblasts and osteoclasts. Osteoblasts control both the formation and breakdown of bone necessary for bone remodeling. Osteoblasts also activate osteoclast differentiation and formation, which is responsible for the resorption of bone.[71] Osteoblasts respond to $1,25(OH)_2D_3$

via the regulation of the receptor activator of NF-κB ligand (RANKL) mediated by VDR and independently to the parathyroid hormone (PTH) (Figure 11).[72, 73]

The RANKL gene is regulated by VDR thus eldecalcitrol (aka ED-71) and other vitamin D

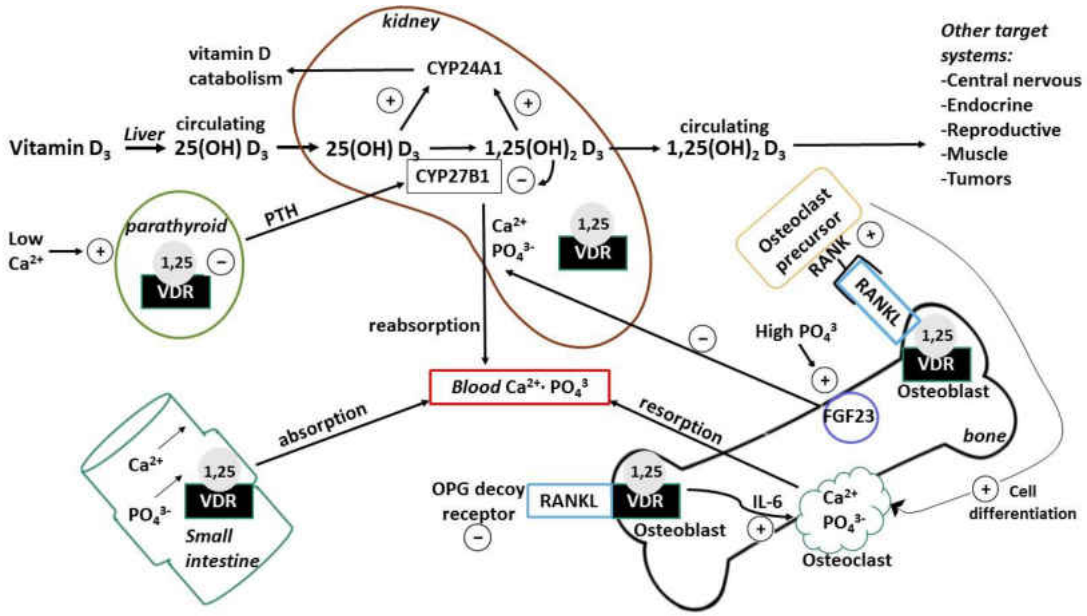

Figure 11. Summarized cartoon of the metabolism and biological action of vitamin D via VDR with particular emphasis to calcium and phosphate balance and bone mineralization.[3]

ligands regulate osteoclastgenesis by inhibiting the maturation of osteoclast progenitor cells or reducing the activation of osteoclasts via IL-6.[71] However, decelerated osteoclastgenensis can reduce Ca^{2+} levels, which in turn is sensed by the parathyroid glands, which to restore Ca^{2+} balance, rapidly enhances the secretion of PTH. Elevated PTH levels induce Ca^{2+} resorption from the bone independent from VDR and stimulates the expression and activity of renal CYP27B1 that produces $1,25(OH)_2D_3$. This classic negative feedback loop ends by $1,25(OH)_2D_3$ suppressing PTH synthesis and renal CYP27B1 activity.[74] Therefore, vitamin D ligands developed for osteoporosis should selectively regulate the VDR target genes RANKL and PTH. Furthermore, VDR ligands can

activate the transcription of genes encoding osteocalcin and osteopontin, two proteins involved in bone remodeling by osteoblasts.

Osteoblast differentiation is important for bone mineralization and is mediated by $1,25(OH)_2D_3$, which initiated the synthesis of Vitamin D_3 analogs by organic chemist and pharmaceutical companies with aim to separate the calcemic action of $1,25(OH)_2D_3$ from its ability to regulate cells growth and differentiation.[75] ED-71 was among those analogs introduced by Chugai Pharmaceuticals for the treatment of osteoporosis (Figure 12). Patients with osteoporosis experience low serum levels of $25(OH)D_3$, which is common in older or postmenopausal patients partially due to their low intake of vitamin D, decreased sun exposure, and impaired renal function. In turn this dysfunction decreases intestinal calcium absorption and reduces VDR activation. Therefore, a successful osteoporosis drug would need to be given within a small therapeutic window where calcium levels would increase to maintain bone homeostasis without causing adverse sides effects such as hypercalciuria, urinary tract stones, and hypercalcemia. Compared to $1,25(OH)_2D_3$, ED-71 has a higher affinity for serum DBP, binds more weakly to VDR and shows lower potency in suppression of serum PTH. The plasma half-life of eldecalcitol is also longer than that of $1,25(OH)_2D_3$ probably due to its higher affinity for DBP.[76] Preclinical *in vivo* studies using ovariectomized rat (ovx-rat) models for osteoporosis showed that ED-71 suppresses osteoclastic bone resorption and increases bone mass density to a greater extent than alfacalcidiol, a frequently prescribed anti-osteoporosis drug in many countries

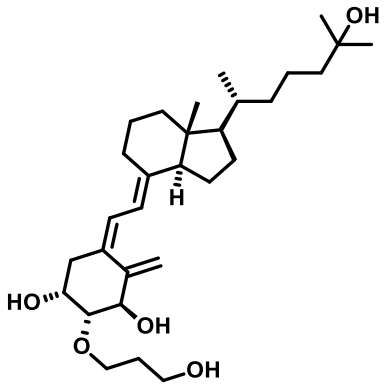

Figure 12. Eldecalcitol, also known as ED-71, is approved osteoporosis drug.

including Japan.[77] Furthermore, there is no significant difference in calcium absorption and serum PTH suppression between ED-71 and alfacalcidol thus suggesting the effect of increasing bone mass density by ED-71 to be independent of calcium metabolism. Phase III clinical trials revealed that patients had a lower incidence of vertebral and wrist fractures while taking ED-71 compared to alfacalcidol. Very few adverse effects were observed at this stage which included an increase of calcium levels found in serum and urine and a small number of patients (0.4%) developing hypercalcemia when given ED-71.[78, 79] As of 2013, this drug is prescribed in Japan and is awaiting approval in other countries.

1.5.2 Vitamin D and Cancer (Cell Proliferation)

The inhibition of cancer cell growth in the presence of 1,25-$(OH)_2D_3$ was first shown in 1979.[80, 81] During the last decades many groups have reported similar antiproliferative effects of VDR ligands *in vitro* and *in vivo*. Human clinical studies with 1,25$(OH)_2D_3$ and analogs are dose-limited because of hypercalcemia and hypercalciurea, which can cause psychosis, bone pain, calcification of soft tissue, coronary artery disease, and, in severe cases, coma and cardiac arrest.[82, 83] These side effects prompted the synthesis of thousands of 1,25$(OH)_2D_3$ analogs to develop VDR ligands with lower calcemic activity. Two synthetic VDR ligands EB1089 and ILX23-7553 were tested in clinical trials.[84, 85] Seocalcitol (EB1089, Figure 13) has shown to be 50 times more potent than 1,25$(OH)_2D_3$ *in vitro* and when given orally it dose dependently inhibits growth of nitrosomethyl

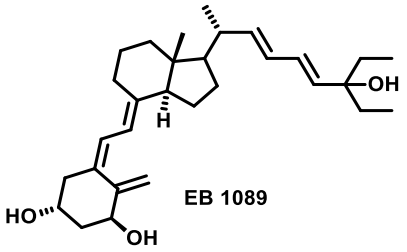

Figure 13. EB 1089, a VDR agonist that exhibits anti-tumor and anti-proliferative activity with reduced hypercalcemic effects.

urea (NMU) induced rat mammary tumors and MCF-7 xenografts without increasing serum calcium.[86] In addition, anti-proliferation, apoptosis, and anti-metastases effects of EB1089 have shown to be enhanced with co-administration with paclitaxel[87], retinoic acid[88] or radiation[89]. VDR-mediated anti-proliferation is facilitated by its' ability to modulate the cell cycle (Figure 14). Proliferating cells progress through the cell cycle, which comprises of the G_0/G_1 phase (differentiation and protein synthesis), the S phase in which new DNA is synthesized, and the G2 phase that is followed by mitosis or M phase upon which cells can reenter G_0/G_1 phase. Breast cancer cells treated with VDR ligands have been observed to undergo cell cycle arrest in the G_0/G_1 phase within 48 hours.[90] This arrest is associated with upregulation of genes that code for the cyclin-dependent kinase inhibitors CDKN1A (p21) and CDKN1B (p27) and act as control switches for the cell cycle. Depending on the cell type, G_1 arrest is due to inhibition of cyclic-dependent kinase (CDK) activity including CDK2-associated histone H1 kinase, cyclin D1/CDK4, and cyclin A/CDK2.[91, 92] In other situations, VDR interacts with protein phosphatases PP1c and PP1Ac to inactivate the p70 S6 kinase which is essential for G_1/S phase transition.[93] Thus, vitamin D

analogs have the potential to inhibit breast cancer cell growth by preventing their entry into the S phase thus leading to accumulation of these cells in the G_1 phase.

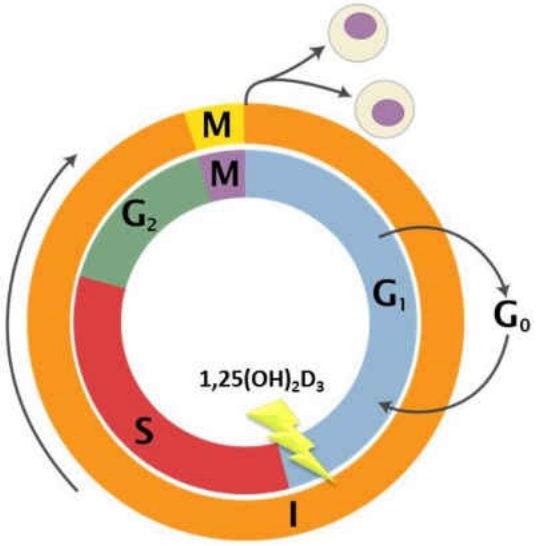

Figure 14. The cell cycle: Gap 0 (G_0) where cells can leave the cycle and quit dividing, Gap1 (G_1) is where the cell increases in size and produce RNA, synthesis (S) phase is where DNA replication occurs, in Gap 2 (G_2) the cell continues to grow and produce protein. The cell growth and production stops at the mitosis (M) phase where the cell divides into two similar daughter cells.

In addition to anti-proliferative effects, $1,25(OH)_2D_3$ and other vitamin D analogs induce cell shrinkage, chromatin condensation, and DNA fragmentation characteristic for apoptosis. Studies have shown that $1,25(OH)_2D_3$ mediated apoptosis affects the relative expression and/or subcellular localization of the Bcl-2 family and other pro-apoptotic proteins. When MCF-7 cells are treated with $1,25(OH)_2D_3$ or VDR agonist, EB1089, a redistribution of Bax, a member of the pro-apoptotic Bcl-2 family, from the cytosol to the mitochondria occurred and induced down-regulation of Bcl-2.[94, 95] Bax translocation triggers reactive oxygen species (ROS) generation, dissipation of the mitochondrial membrane potential, and release of cytochrome C into the cytosol, which are features of mitochondrial apoptosis.[96]

Metastasis is the process by which tumor cells invade secondary sites which requires degradation of the extracellular matrix and is facilitated by angiogenesis or the growth of new blood vessels connecting the developing tumor. When ER-negative breast cancer cells (i.e. SUM159PT), which are invasive *in vitro* and metastatic *in vivo*, are treated with $1,25(OH)_2D_3$ or vitamin D analogs invasion of cancer cells is inhibited.[97] This effect may be linked to regulation of extracellular protease such as MMP-9, urokinase-type plasminogen activator (uPA), and tissue type plasminogen activator (tPA).[98] Furthermore, $1,25(OH)_2D_3$-mediated inhibition of angiogenesis has been observed in the chick embryo chorioallantoic membrane assay and in tumor-cell induced angiogenesis assays in mice.[99]

1.6 Inhibition of the VDR-Coactivator Interactions

Many VDR ligands, commonly VDR agonists, have been developed to treat vitamin D related diseases. Only a limited number of VDR antagonists have been described with the ability to either directly or allosterically inhibit the interaction between VDR and its coactivators.[100-102] The following VDR ligands will be discussed in this section: direct VDR antagonists (allosteric VDR-coactivator inhibitors) and direct VDR-coactivator inhibitors.

1.6.2 Direct VDR Antagonists or Allosteric VDR-Coactivator Inhibitors

The synthesis of new synthetic analogs of $1,25(OH)_2D_3$ resulted in the identification of new VDR ligands that bind VDR but only weakly promote VDR–coactivator interactions. Usually, the biological effects of these antagonists have been determined in the presence of agonists like $1,25(OH)_2D_3$ giving results similar to the vehicle control. Interestingly, the degree of coactivator recruitment by VDR depends on the chemical structure of the VDR antagonist. Thus, the quality of a VDR antagonist can be defined by its residual agonistic activity. On the molecular level, this behavior is believed to be caused by the orientation of helix 12 (Figure 15). Depending on the structure, VDR antagonists may influence the equilibrium of VDR bound to coactivators, corepressors, or neither. Crystal structures of all three possible complexes have been reported for nuclear receptors. However, VDR prefers to crystallize solely with an agonistic arrangement.

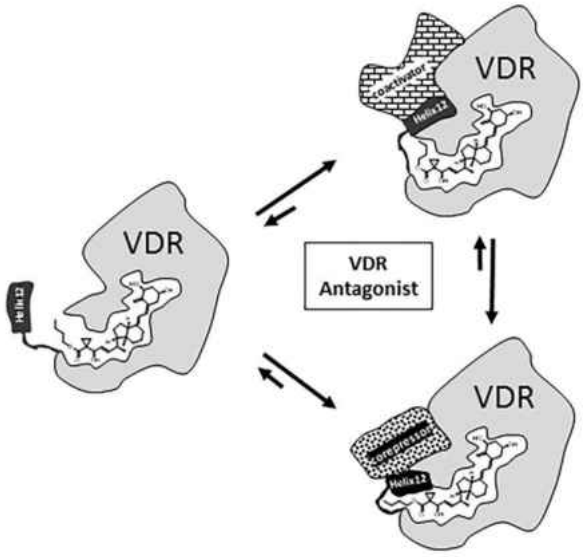

Figure 15. Possible equilibrium structure of VDR in the presence of antagonist.

One example is ZK159222 that exhibited a sub-nanomolar affinity for the VDR in the presence of $1,25(OH)_2D_3$ and inhibited VDR-mediated transcription with an IC_{50} value of 300 nM (Figure 16).[103, 104] SDS-page demonstrated three different conformations of ZK159222 liganded VDR.[105] These conformations may be responsible for the dissociation between liganded VDR and coactivators SRC1, SRC2, SRC3, and DRIP205.[106, 107] The interaction between corepressor NCoR and VDR was inhibited as well.[103] ZK159222 also inhibited the interaction between VDR and corepressor SMRT as demonstrated with a pull-down assay.[108] In human fetal osteoblastic cells, ZK159222 inhibited the expression of osteocalcin, alkaline phosphatase activity, and calcium contents, in the presence of $1,25(OH)_2D_3$.[109] In osteoblastic ST2 cells, ZK159222 blocked the activation of mRLD5 region of mRANKL in the presence of $1,25(OH)_2D_3$.[110] The calcemic activity of ZK159222 was 0.02% of that of $1,25(OH)_2D_3$ in mice after 5 days of 10 μg/kg/d.[111]

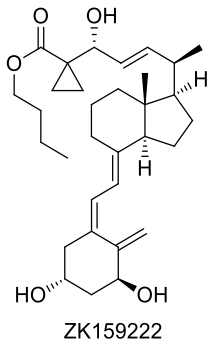

ZK159222

Figure 16. Structure of ZK159222.

In respect to anti-proliferation, ZK159222 also inhibited the differentiation of HL60 cells in the presence of $1,25(OH)_2D_3$ at a concentration of 6 nM.[112] The process involves the up-regulation of kinase suppressor of ras 2 gene (KRS-2), which was demonstrated to be inhibited by ZK159222.[113] In addition, ZK159222 inhibited the phosphorylation of Raf-1[114, 115] and the expression of pRb and c/EBPβ, two very important cancer genes, in the presence of $1,25(OH)_2D_3$.[116] ZK159222 inhibited the phosphorylation of phosphoinositide and Akt mediated by phosphatidylinositol 3-kinase in the presence of $1,25(OH)_2D_3$.[117] Weak induction of calbindin-D28K, a cytosolic calcium binding protein, and VDR itself was observed in the presence of

ZK159222 in choriocarcinom- derived cells (JEG-3). In the presence of $1,25(OH)_2D_3$, ZK159222 exhibited strong antagonist effects in these cells.[118]

1.6.3 Direct VDR-Coactivator Inhibitors

The identification of the central coactivator LXXLL motif as being essential to mediate nuclear receptor binding prompted investigations into peptide-based VDR–coactivator inhibitors that would evaluate the function of this protein-protein interaction. Pioneered by McDonnell *et al* for the estrogen receptor, a phage display library of synthetic LXXLL peptides was generated and screened with two hybrid assays against a panel of nuclear receptors including VDR.[119-121] Peptides, C33, D47, EBIP41 and EBIP44, were identified to bind VDR (Figure 17). Importantly when C33, D47, EBIP41 and EBIP44 peptides were expressed as Gal4 DBD fusions in cells, they

																				Target
C33	H	V	E	M	H	P	L	L	M	G	L	L	M	E	S	Q	W	G	A	**VDR**
D47	H	V	Y	Q	H	P	L	L	L	S	L	L	S	S	E	H	E	S	G	**VDR**
EBIP41	R	R	D	D	F	P	L	L	I	S	L	L	K	D	G	A	L	S	Q	**VDR**
EBIP44	Y	G	L	K	M	S	L	L	E	S	L	L	R	E	D	I	S	T	V	**VDR**
F6	G	H	E	P	L	T	L	L	E	R	L	L	S	G	T	S	V	A	E	**RxR**
3	L	S	E	T	H	P	L	L	W	T	L	L	S	S	E	G	D	S	M	**VDR**
4	M	Q	E	R	F	P	M	L	W	D	L	L	D	L	P	S	P	T	S	**VDR**
5	L	G	E	S	H	P	L	L	M	Q	L	L	T	E	N	V	G	T	H	**VDR**

Figure 17. Sequences of coactivator peptides that inhibit the interaction between VDR and coactivators.

inhibited the VDR-mediated transcription in a reporter assay under control of an osteocalcin (OC) promoter.[122] In addition, RXR-selective peptide F6 was able to inhibit VDR-mediated transcription demonstrating transactivation between RXR and VDR. A more exhaustive phage display library identified three more LXXLL peptides (Figure 17, compounds 3,4, and 5) that not only bind VDR in a two hybrid assay but also inhibit VDR-mediated transcription when expressed in cells.[106] These peptides exhibited a consensus sequence of (H/F)P(L/M)LXXLL. Importantly, the binding of these peptides to VDR was more pronounced in the presence of VDR agonists than

VDR antagonists. However, these peptides possess limitations in their inability to regulate endogenous VDR target genes.

To overcome limitations in cell-based assays such as inactivity when transfected as a fusion peptide or limited cell permeability and stability, new peptide-based inhibitors were generated.[123] Misawa *et al.* introduced stabilized cyclic heptapeptides that were composed of L-leucine residues and a stapled side chain as VDR inhibitors (Figure 18).[124, 125] These stapled linkers consisting of a long hydrocarbon chain have been reported to increase stability and oral bioavailability. A dramatic IC_{50} value change from 220 µM to 3.2 µM was observed by changing the nonfunctional linker (Figure 18, DPI-06) to a functionalized linker (Figure 18, DPI-07).

Rational drug design resulted in the first small molecules that inhibit the VDR–coactivator interaction in 2010.[126] Using a rational design approach, a benzodiazepine scaffold was substituted with branched hydrophobic groups to mimic the *i*, *i*+3, and *i*+4 position of leucine of coactivator DRIP205 (Figure 19).[127] Docking studies revealed that compound 2 might form

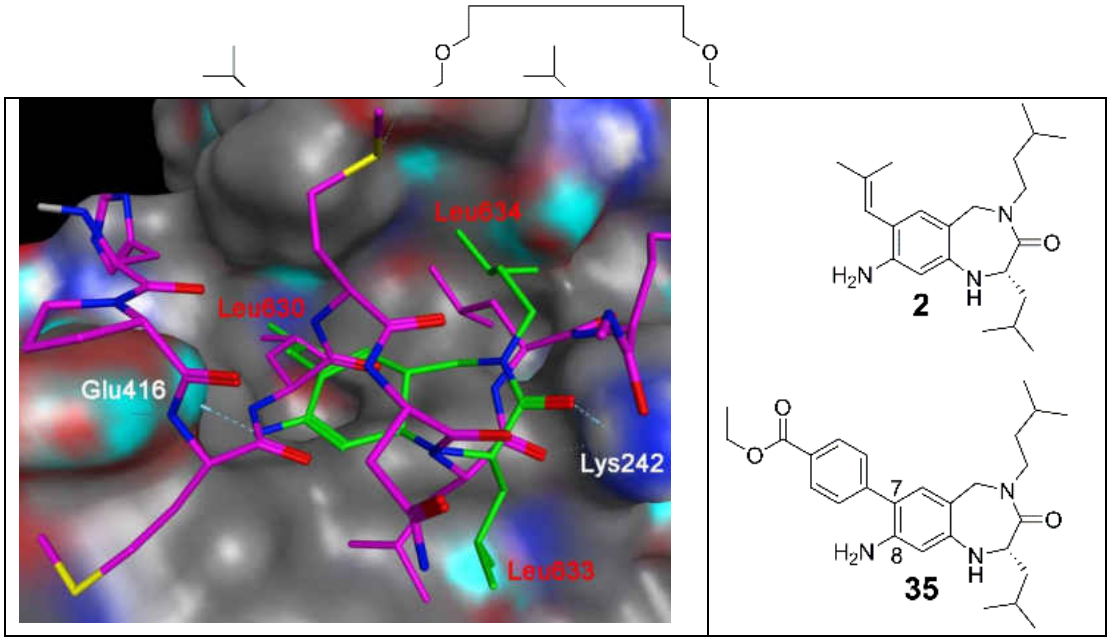

Figure 19. Overlay between a crystal structure of VDR and coactivator peptide DRIP205 and docked conformation of compound 2 and structures of compound 2 and 35.

hydrogen bonds with rat VDR clamp residues Glu416 and Lys242. The inhibition activity of compound 2 (IC_{50}= 17 μM) was confirmed in cells with a reporter gene assay. The results prompted a more exhaustive structure-activity relationship (SAR) study reported in 2013 by the same group.[128] Despite the large number of analogs with various substituents in the 7- and 8-position, only marginal improvement (IC_{50}= 14 μM) was observed for compound 35 (Figure 19). However, the aniline function in the 8-position was confirmed to be important for binding, probably interacting with Glu417 of VDR.

In 2012, Arnold *et al.*, identified the first irreversible VDR–coactivator inhibitors using high throughput screening.[129] Among 275,000 compounds, 140 inhibitors with cellular activity were identified, including a group of 3-indolylmethanamines. A comprehensive SAR study around the 3-indolylmethanamine scaffold identified compound 31B as the most active VDR–coactivator inhibitor in cells (IC_{50} = 4.2 μM, Figure 20, A). In addition, a linear free energy relationship between inhibition rates of 3-indolylmethanamines bearing different electronic substituents

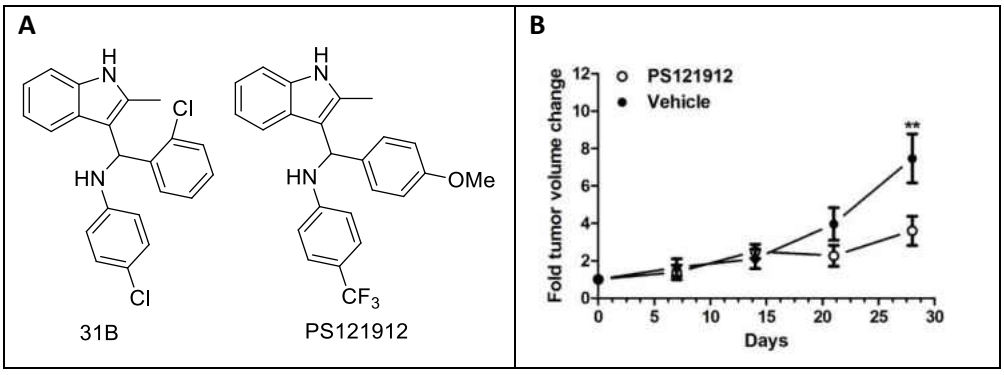

Figure 20. A) Structure of 31B and PS121912; B) Anti-proliferative effects of PS121912 in a HL-60 xenograft model.

confirmed irreversibility. Due to the unique mode of binding, a high selectivity of 31B toward VDR in respect to other nuclear receptors was observed. In addition, 31B is selective towards the interaction between VDR and coregulator peptide SRC2-3 among other LXXLL coregulator peptides. Importantly, down-regulation of VDR target gene *TRPV6* by 31B was observed in the

presence of 1,25$(OH)_2D_3$ for DU145 cancer cells leading to anti-proliferation at higher concentration. Inhibition of VDR-mediated transcription and anti-proliferation in the presence of 31B was also observed for ovarian cancer cells OVCAR8 and SKOV3 and endometrial cancer cells ECC-1.[130] In cis-platinum resistant SKOV3 cells, other markers of anti-proliferation and apoptosis were upregulated in the presence of 31B such as activation of caspase 3, phosphorylation of MAP kinases p38 and SAPN/JNK, upregulation of P21, and cell-cycle arrest. In a cisplatin-resistant SKOV3 xenograft tumor model, 31B treatment, delivered 5 times a week at a dose of 5 mg/kg, led to suppressed tumor growth after two weeks. In addition, reduced tumor formation was partially caused by a compromised *de novo* production of fatty acids due to lower expression of fatty acid synthase (FASN) in the tumor. Further SAR studies resulted in a discovery of 3-indolylmethanamine PS121912, a VDR–coactivator inhibitor that inhibited VDR-mediated transcription with an IC_{50} of 590 nM (Figure 20).[131] Similar to 31B, PS121912 is selective towards VDR and has a preference for the interaction between VDR and coregulator peptide SRC2-3. Importantly, ChIP studies revealed that in HL60 leukemia cells PS121912 was able to reduce the DNA occupancy of VDR and binding of SRC2. However, PS121912 promoted the recruitment of NCoR to the VDR–DNA complex.[132] PS121912 reversed the regulation of VDR target genes in the presence of 1,25$(OH)_2D_3$ at a concentration of 500 nM and modulated the transcription of many genes affiliated with cell cycle control. Elevated levels of P21 protein levels were observed for the PS121912 in the presence and absence of 1,25$(OH)_2D_3$ in HL60 cells as well as increased levels of pro-apoptotic serine protease HTRA. In a mouse HL60 xenograft model at 3 mg/kg five times a week, a significant change in tumor volume was observed after three weeks of treatment (Figure 20, B). The blood calcium levels and animal weight did not differ from the control group.

CHAPTER 2: THE RATIONAL DESIGN AND SYNTHESIS OF THIAZOLE-BASED VDR-COACTIVATOR MODULATORS

2.1 Introduction

The rational design of drugs can be defined as the discovery of a lead molecule with desirable properties determined prior to its actual identification based upon the information known about a specific target.[133] With advancing computer technology and growing combinatorial libraries, this form of lead identification has become more and more streamlined. The rational design of a drug is unique from that of other drug discovery processes such a high throughput screening. High throughput screening can easily become a game of luck depending on the size and diversity of compound libraries screened and the quality of assay being used. However, rational drug discovery isn't without its own drawbacks. To be truly a *de novo* rational design, structural and chemical knowledge must be known about the targeted receptor and compounds that bind to it. From this, a pharmacophore model can be developed in which set parameters must be met by the compound in order to bind the active site. Without this, the method must employ empirical information to base its claims thus becoming more of a "semi-rational" approach. As established in chapter 1, VDR is a well-studied receptor whose crystal structure with ligands has been solved. Furthermore, the interaction between VDR and many of its coactivators have been greatly investigated. Therefore, we were able to use a rational approach to design a novel inhibitor of the interactions between VDR and its coactivator, SRC2.

In Figure 21, coactivator peptide (stick model), SRC2, makes specific interaction with VDR (grey/red) through an LXXLL motif. We hypothesized that by replacing the peptide backbone

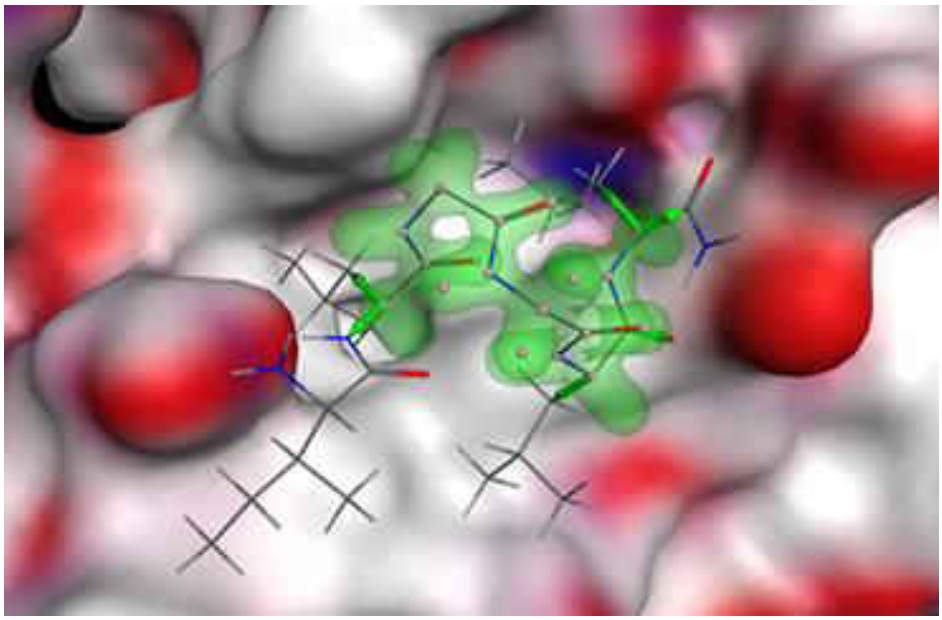

Figure 21. Molecular Operating Environment (MOE) was used for fragment-based design to replace the peptide backbone with a small molecule scaffold.[6]

(shown in green) with a small molecule scaffold while keeping the leucine residues within the same space orientation as in SRC2, we could mimic this interaction and successfully inhibit a coactivator from binding. In addition to the leucine residues, the pharmacophore model required that the small molecule contained an electron donating group, as well as, the ability to H-bond with glutamic acid while possessing drug-like properties. A linker database containing approximately 3,000 different scaffolds was virtually screened against this pharmacophore developed in the program Molecular Operating Environment (MOE) and yielded a thiazole

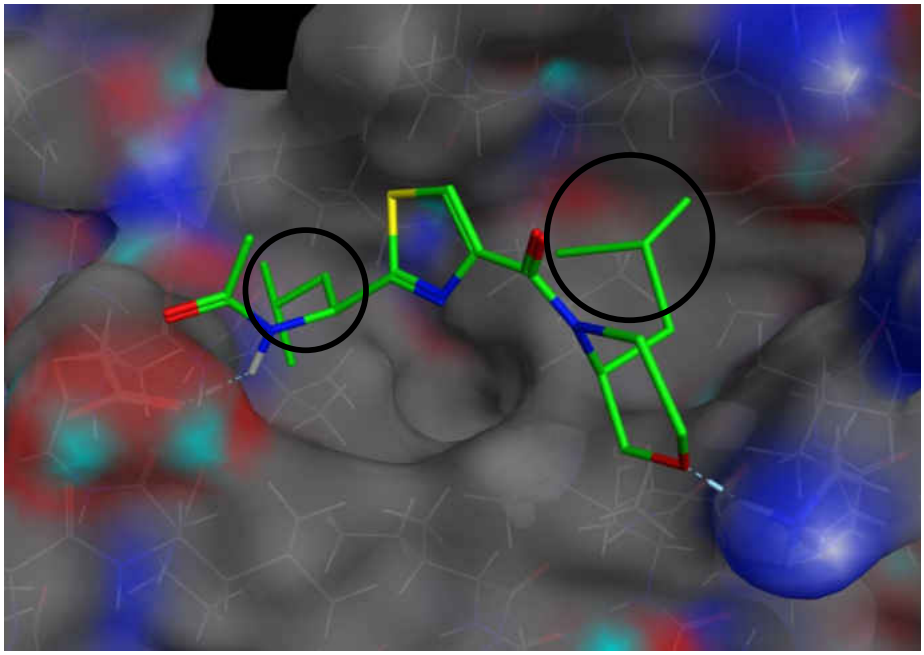

Figure 22. The thiazole molecule found as a suitable scaffold for peptide replacement.[6]

scaffold containing two leucine like residues (Figure 22). Research into the synthesis of this molecule revealed a quick three step route utilizing an efficient multi-component.[134]

In general, multi-component reactions (MCRs) are defined as any process in which three or more reactants combine in one pot to form a product that incorporates structural features of each reagent (Figure 23).[135] There are many advantages to using MCRs including simplicity, greater efficiency, higher yields, and higher atom economy over conventional chemical reactions. These convergent reactions involve all atoms within the chemical process therefore producing little chemical waste. This makes them a green synthetic method for pharmaceutical and drug discovery research. In 1850, the Strecker 3-component reaction (S-3CR) was the first official

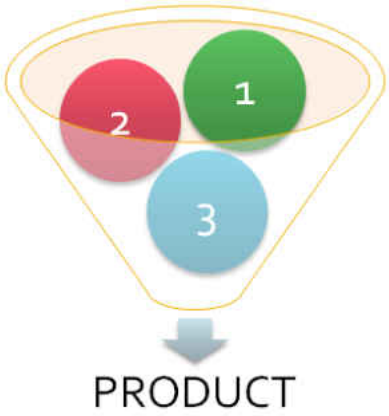

Figure 23. Simplistic model of how multi-component work.

MCR discovered for the synthesis of α-aminonitriles by the reaction of ammonia, hydrocyanic acid, and carbonyl compounds.[136] Since then, organic chemist have invented numerous MCR reactions that are now key players in combinatorial chemistry with their ability to quickly produce large and diverse compound libraries. The reactions have especially grown in popularity in part due to the arrival and growth of high throughput screening techniques that enable rapid screening of these compounds.

Reactions involving isocyanides provide additional benefits to the rapidly developing field of MCRs. As a very reactive functional group, isocyanides are unique in their ability to react with nucleophiles and electrophiles at the same carbon atom resulting in a stable C-C bond.[137] In many cases, reactions with isocyanides are chemo-, regio- and stereoselective as well as highly effective and versatile.[138] The most important and vastly studied isocyanide-based MCR is the Ugi four component reaction (U-4CR) developed in 1959 by Ivar Ugi (Figure 24). Advantages of this reaction includes variable products by changing the amine (ammonia, primary and secondary),

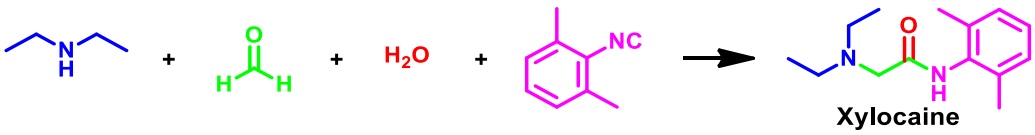

Figure 24. The original U-4CR was used to produce Xylocaine with dimethylamine, carbonyl compounds (ketone or aldehyde), and isocyanides without sensitivity to steric bulk.[139]

Herein, we report the use of a U-4CR to synthesize novel, non-secosteroidal inhibitors of VDR. These molecules were rationally designed to directly inhibit the interactions between VDR and its coactivator SRC2. Biochemical evaluation was conducted using a fluorescence polarization binding assay.

2.2 Chemistry

2.2.1 Synthetic Strategy

A U-4CR was used to synthesize the thiazole ring (Scheme 1).[139] In one pot, (2,4-dimethoxyphenyl)methanamine (2.1) and isovaleraldehyde (2.2) were initially added together to undergo a condensation reaction to form the corresponding imine as seen in the reaction mechanism (Figure 25). With the addition of thioacetic acid (2.3) and isocyanoacrylate (2.4), a

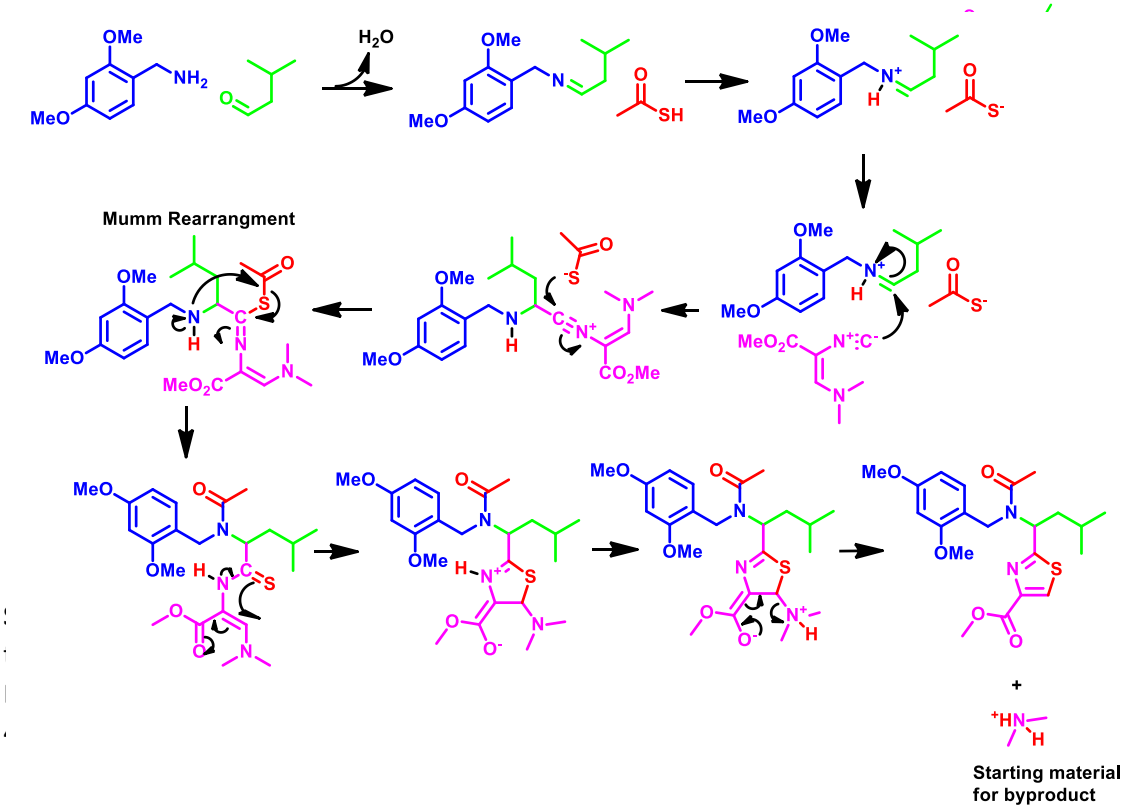

Figure 25. Mechanism for U-4CR reaction. This reaction produces the final thiazole product in addition to one equivalent of dimethylammonium ion that can go back into the reaction as an amine source.

proton exchange occurred with thioacetic acid thus activating the imine for nucleophilic addition of the isocyanoacrylate and formation of a nitrilium ion. Next, a second nucleophilic addition took place with the thioacetate anion. This was followed by a unique rearrangement termed a

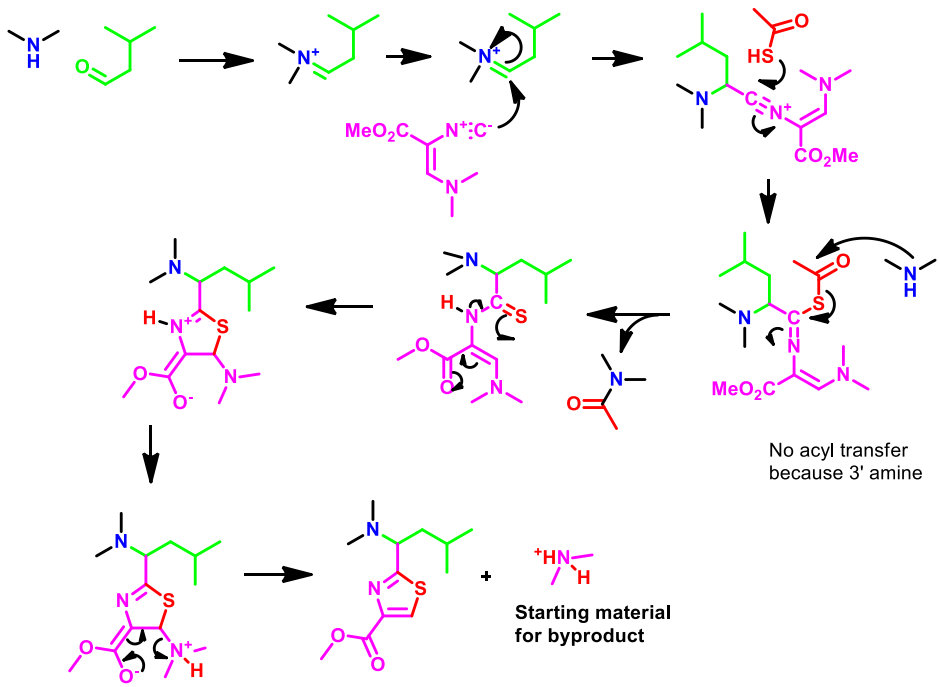

Figure 26. The dimethylammonium byproduct reaction mechanism.

Mumm rearrangement where the acyl group transfers from the sulfur to the nitrogen followed by ring closure and production of an amide thiazole ring product (KAT011311) and a dimethylammonium byproduct. This byproduct was able to participate in the synthesis as a starting material and produced the dimethylamine thiazole ring product (KAT052711) as seen in Figure 26. This was not initially evident due to their overlapping spots on the TLC but with the addition of 1% acetic acid the two compounds could be easily separated. The acetic acid protonated the dimethylamine and transformed it into a salt that retained longer on the column than the desired amide product. Because they were easily purified, KAT052711 was used in the subsequent coupling reactions in addition to the KAT011311. Deprotection of KAT011311 was carried out using TFA at elevated temperatures to produce compound KAT030711 (Scheme 1). Wang *et al.* previously published the successful amidation to the methyl ester position using morpholine with 30% triazabicyclodecene (TBD), a bicyclic guanidine base, at 80°C for several

hours.[134] This method was successful for the coupling of a morpholine to KAT030711 and KAT052711 to produce KAT080411 and KAT031312. Unfortunately these conditions were not suitable when 3-isobutylmorpholine was used. Alternatively, the hydrolysis of the ester to a carboxylic acid followed by peptide coupling using EDCI, HOBt, and DIPEA yielded the two desired 3-isobutylmorpholine amides, KAT021712 and KAT021112.

2.2.2 Characterization

Commercially available staring materials were used as received. Dry solvents were bought in sure-seal bottles and handled under dry conditions using syringe technique. All glassware was dried overnight at 100^{o}C before use. Thin layer chromatography was performed on pre-coated silicia gel 60 F254 plates (Fisher Scientific). Synthesized compounds were purified by normal phase flash chromatography (SPI Biotage, silica gel 230-400 mesh) and concentrated under vacuum. All pure compounds were stored as solids at -20°C. Compound characterization was performed using a Shimadzu 2020 LC-MS (single quadrupole) instrument or Surveyor & MSQ LC-MS (APCI or ESI) with compounds directly injected. NMR spectra were recorded on a Bruker 300MHz instrument with samples diluted in either $CDCl_3$ or DMSO- D_6.

General Procedure for 4-CR Ugi Reaction: Isovaleraldhyde (107.3 µL, 1 mmol), (2,4-dimethoxyphenyl)methanamine (167 mg, 1 mmol) and dry methanol (2 mL) with 4 Å molecular sieves were added together at room temperature and stirred for 1 hour. Then (z)-methyl-3-(dimethylamino)-2-isocyanoacrylate (154 mg, 1 mmol) and thioacetic acid (71.4 µL, 1 mmol) were added to the reaction mixture and stirred at room temperature for 24 hours. The mixture was concentrated by rotary evaporation. To the crude 1 mL of acetic acid was added and mixed thoroughly before being purified by column chromatography using EtOAc-Hexanes (2-80%

strong). Two products were obtained, KAT011311 as a yellow oil and KAT052711 as a cream colored solid.

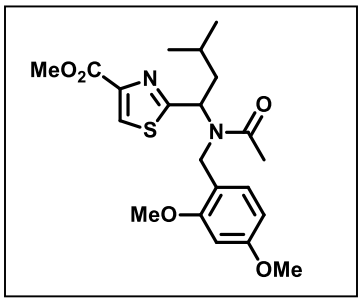

KAT011311 64 % yield; ^{1}H-NMR (300 MHz) ($CDCl_3$) δ 8.06 (s, 1H), 6.39-6.90 (d, 1H, J=9 Hz), 6.37-6.35 (m, 2H), 5.71-5.67 (t, 1H, J= 6Hz)), 4.49 (s, 2H), 3.91 (s, 3H), 3.77 (s, 3H), 3.78 (s, 3H), 2.16 (s, 3H), 2.06-1.96 (m, 2H), 1.59-1.50 (m, 1H), 0.90-0.86 (m, 6H, J= 13.5Hz, 7.5Hz); ^{13}C-NMR δ 171.90, 170.96, 161.83, 159.27, 157.58, 145.90, 128.60, 127.50, 117.20, 103.93, 98.48, 64.78, 55.33, 55.05, 41.59, 25.22, 22.68, 22.46. MS APCI ($^{+}$ve) calcd. *m/z* for $C_{21}H_{28}N_2O_5S$[(M)] 420, found [$(M+H)^{+}$] 421.2.

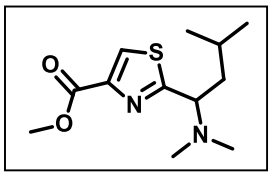

KAT052711 16% yield; ^{1}H-NMR (300 MHz) ($CDCl_3$) δ 8.32 (s, 1H), 4.89-4.85 (dd, 1H, J=9Hz, 3Hz), 3.98 (s, 3H), 2.85 (s, 6H), 1.43-1.26 (m, 3H), 0.97-0.90 (dd, J=15Hz, 6Hz); ^{13}C-NMR δ. 172.78, 162.05, 146.11, 127.89, 64.72, 52.36, 42.26, 41.60, 25.06, 22.85 (isobutyl CH_3), 22.38 (isobutyl CH_3). MS APCI ($^{+}$ve) calcd. *m/z* for $C_{12}H_{20}N_2O_2S$[(M)] 256.1, found [$(M+H)^{+}$] 257.1.

General Procedure for Deprotection Reaction: 1 mL of TFA was added to KAT011311 (85 mg, 0.2 mmol) and the mixture was heated to 60^{o}C for 1 hour. Reaction was monitored by TLC (4:1 EtOAc- Hexanes) by taking an aliquot of reaction and working up a fraction with ammonium chloride to remove acid. Upon complete conversion, the solution was concentrated and purified by column chromatography using EtOAc and Hexanes with 1% AcOH (2-80% strong). A yellow solid was obtained.

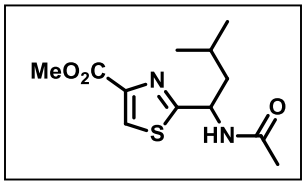

KAT030711 66% yield; ^{1}H-NMR (300 MHz) ($CDCl_3$) δ 8.11 (s, 1H), 6.23-6.22 (d, 1H, J=6Hz), 5.46-5.40 (m, 1H), 3.96 (s, 3H), 2.04 (s, 3H), 1.97-1.81 (m, 2H), 1.68-1.59 (m, 1H), 1.00-0.96 (dd, 6H, J= 6Hz, 3Hz) ; ^{13}C-NMR δ 172.72, 169.72, 161.75, 146.70, 127.36, 52.50, 49.34, 44.40, 24.97, 23.16, 22.75, 22.01. MS APCI ($^{+}$ve) calcd. *m/z* for $C_{12}H_{18}N_2O_3S$ [(M)] 270.1, found [$(M+H)^{+}$] 271.1.

General Procedure for 3-isobutylmorpholine Coupling: 40 mg, 0.148 mmol of either KAT030711 (amide) or KAT052711 (dimethyl amine) were dissolved in 1 mL of THF, 400 µL of a 0.5M LiOH solution (1:1 THF: H_2O). The solution was stirred overnight under 0°C. Product conversion was determined by TLC (4:1 EtOAc-Hexanes, R_f= baseline). To the solution, 100 µL 4M HCl Dioxane was added to neutralize the base and stirred for 20 minutes. The mixture was concentrated by rotary evaporation to yield an oil of the acid. The prepared acid was diluted with 2 mL of dichloromethane and to it of EDCI (28.4 mg, 0.148 mmol), HOBt (20.0 mg, 0.148 mmol), DIPEA (95.5 mg, 0.74 mmol, 128.8 µL) and 3-isobutylmorpholine (26.6 mg, 0.148 mmol) were added at 0°C and warmed to room temperature and stirred overnight. The reaction was monitored by TLC (3:2 MeOH-EtOAc, 1% acetic acid, R_f= 0.75). Upon conversion, the crude was diluted with dichloromethane and washed with water, dried over Na_2SO_4 and evaporated. The crude sample was purified on silica gel with EtOAc-MeOH (2%-60% strong, with 1% Ac) using normal phase flash chromatography system.

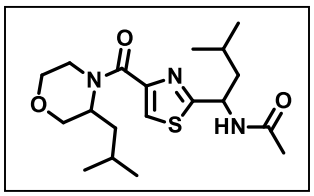

KAT021712 3% yield; ^{1}H-NMR (300 MHz) ($CDCl_3$) δ 7.91 (s, 1H), 5.33-5.28 (m, 1H), 4.01-3.56 (m, 7H, morpholine ring), 2.02(s, 3H), 1.98-1.69 (m, 6H), 1.02-0.97 (dd, 12H, J= 9Hz, 6Hz); MS APCI ($^{+}$ve) calcd. *m/z* for $C_{19}H_{31}N_3O_3S$ [(M)] 381.5, found [$(M+H)^{+}$] 382.3.

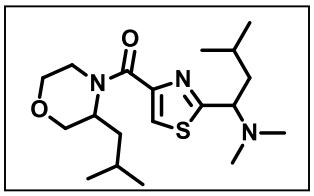

KAT021112 5% yield; ^{1}H-NMR (300 MHz) ($CDCl_3$) δ 8.00 (s, 1H), 4.56 (m, 1H), 3.99-3.55 (m, 7H, moropholine ring), 2.30 (s, 6H), 1.95-1.50 (m, 6H, isobutyl CH_2 and CH), 0.98-0.92 (dd, 12H, J= 10.5Hz, 7.5Hz); MS APCI ($^{+}$ve) calcd. *m/z* for $C_{19}H_{33}N_3O_2S$ [(M)] 367.3, found [$(M+H)^{+}$] 368.2.

General Procedure for Morpholine Coupling: 48 mg (0.177 mmol) of either KAT030711 (amide) or KAT052711 (dimethyl amine) were diluted with 1 ml of dried THF. To the solution 30% TBD and 0.355 mmol of morpholine were added and stirred at 40°C overnight. Reaction was monitored by TLC (4:1 EtOAc- Hexanes, R_f= 0.75). After full conversion, the mixture was concentrated to dryness and purified on silica gel with EtOAc-MeOH (2%-60% strong, with 1% acetic acid) using normal phase flash chromatography system.

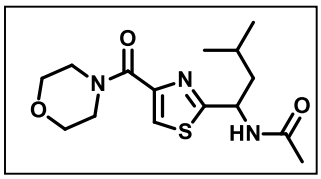

KAT080411 35% yield; ^{1}H-NMR (300 MHz) ($CDCl_3$) δ 7.83 (s, 1H), 6.02-6.00 (d, 1H, J= 6Hz), 5.44-5.36 (m, 1H), 3.77 (m, 8H, morpholine CH_2), 2.06 (s, 3H), 1.94-1.84 (m, 2H), 1.79-1.71 (m, 1H), 1.00-0.97 (dd, 6H, J= 3Hz, 6Hz); ^{13}C-NMR δ 171.57, 169.55, 162.62, 149.76, 124.32, 67.00, 49.51, 44.61, 24.99, 23.23, 22.73, 22.10. MS APCI ($^{+}$ve) calcd. *m/z* for $C_{15}H_{23}N_3O_3S$ [(M)] 325.3, found [$(M+ H)^{+}$] 326.

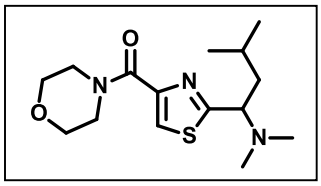

KAT031312 30% yield; ^{1}H-NMR (300 MHz) ($CDCl_3$) δ 7.96 (s, 1H), 4.39-4.37 (d, 1H, J= 6Hz), 3.99-3.76 (m, 8H, morpholine CH_2), 2.30 (s, 1H), 1.79-1.73 (m, 2H), 1.64-1.53 (m, 1H, J= 9Hz, 6Hz); ^{13}C-NMR δ 171.09, 162.78, 149.48, 125.40, 66.98, 64.53, 41.51, 41.13, 29.66, 25.24, 23.10, 22.04. MS APCI ($^{+}$ve) calcd. *m/z* for $C_{15}H_{25}N_3O_2S$ [(M)] 311.4, found [$(M+H)^{+}$] 312.2.

2.3 Modulation of VDR-Coactivator Binding with Rationally Designed Thiazole Derivatives

A fluorescence polarization-based (FP) assay was used to quantify the binding between VDR and coactivator in the presence of small molecules. Synthesized compounds displaying

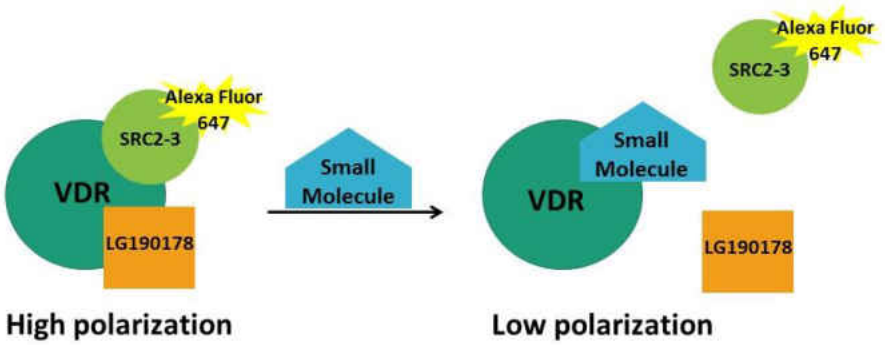

Figure 27. Cartoon of the FP-assay used to determine if newly synthesized molecules are competitive inhibitors of the VDR-coactivator interaction.

agonistic binding induce the interactions between VDR and Alexa Fluor 647-labeled coactivator peptide through favorable conformational changes of the VDR protein. Therefore, high fluorescence polarization is observed upon its binding to VDR-LBD. In contrast, low polarization is observed when the LXXLL mimic molecule competes with the coactivator for binding in the presence of $1,25(OH)_2D_3$ (Figure 27).

Potency and efficacy are determined directly from the dose-response curve produced for each compound. Potency is recorded as a median effective concentration (EC_{50}) or a median inhibition concentration (IC_{50}) value for agonist and antagonist binding, respectively. The maximal efficacy reflects the limit of the dose-response relation on the response axis. For example, a full agonist occupies the ligand binding pocket (LBP) of VDR more efficiently than partial agonists. This is seen by the lower response produced by the partial agonists compared to a full agonists (Figure 28). It is important to note that the failure of partial agonists to produce a maximal response is not due to decrease affinity for VDR. [140] Although partial agonist do not elicit a maximal therapeutic response it may be beneficial in limiting the drug's propensity to cause a toxic effect.

2.3.1 Experimental Procedure

Reagents and Instrumentation: The assay buffer was prepared with 18MΩ water, 25mM PIPES

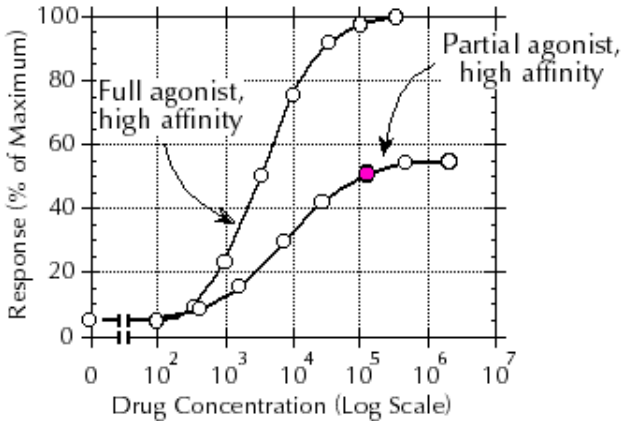

Figure 28. General dose-response showing example curves of a partial and full agonist.

(piperazine-N,N'-bis(2-ethanesulfonic acid)) (Sigma), 50mM NaCl (Fisher), and 0.01% NP-40 (Thermo Scientific) a detergent used to reduce any non-specific binding. The pH was adjusted to

6.75 and filtered to remove any particulates. LG190178 (a VDR agonist) was synthesized following a published procedure and used as a positive control (Figure 29).[141, 142] CBT1 (a VDR-coactivator inhibitor) was used as second positive control and was synthesized using a previously published method (Figure 30).[143] The expression and purification of VDR-LBD was performed as described by previous literature.[9] SRC2-3 (CKKKENALLRYLLDKDDTKD) was purchased and labeled with cysteine-reactive Alexa Fluor 647 or Texas Red maleimide. Labeled peptides were purified by reverse phase quantitative HPLC using a C18 column and stored at -20°C. All fluorescence readings were performed on a Tecan Infinite M1000 plate reader. Small volume transfers were performed on the Tecan Freedom EVO liquid handling system with a 100 nL pin tool transfer (V&P Scientific). Serial dilutions were done in 96-well polypropylene plates (Corning, #3365) and assays were conducted in 384- well black polystyrene microplates (Nunc, #262260).

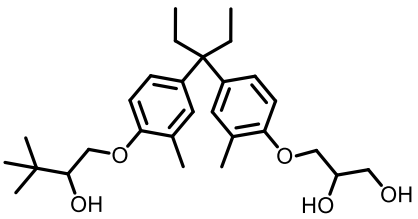

Figure 29. LG190178, a synthetic agonist for VDR that binds with an K_i= 150 nM

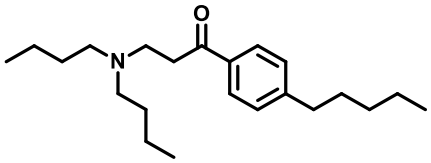

Figure 30. CBT is known to inhibit the interactions between VDR and its coactivator.

Fluorescence Polarization-based Binding Assay Protocol: To 30 mL of buffer, 1 µL of the Alexa Fluor 647-labeled SRC2-3 (7.5 nM final concentration) was added. The optimal concentration of VDR-LBD (EC_{90}) was determined by serially diluting VDR protein ranging from 35 to 0.017 µM and combined it with the coactivator containing solution in a 384-black well black plate. To the plate a solution of LG190178 was transferred using the pin tool at a final concentration of 2 µM. The calculated EC_{90} obtained determined was 0.1 µM VDR-LBD. The optimal LG190178 concentration

was determined by combining a serial diluted LG190178 solution ranging from 20µM-0.1nM to a solution containing VDR-LBD (0.1µM) and Alexa Fluor 647-labeled SRC2-3 (7.5 nM). The calculated EC_{90} determined was 0.75 µM. 10 mM stock solutions of synthesized compounds made in DMSO were serially diluted (1:3) in 96-well plates. Four 14 µL aliquots of each compound concentration was transferred to opaque 384-well plates for storage. 600 nl of each compound concentration was transferred into 20 µl assay solution resulting in a final maximum concentration of 300 µM. Agonistic binding was determined in the absence of LG190178 while antagonistic binding was determine in the presence of LG190187. Fluorescence polarization was detected after 30 minutes at an emission/excitation wavelength of 635/685 nm (Alexa Fluor 647). LG190178 and DMSO were used as positive and negative controls in the agonistic binding assay, respectively. In the antagonist binding assay CBT1 was the positive control while DMSO was used as a negative control. Controls were measured within each plate to determine the z' factor (Equation 1), which assed the quality of the assay and enabled data normalization. Three independent experiments were carried out in quadruplicate, and data was analyzed using nonlinear regression with a variable slope (GraphPrism, Equation 2).

Equation 1: $$Z' = 1 - \left(\frac{3 \times (Standard\ Deviation\ Positive + Standard\ Deviation\ Negative)}{|Average\ Positive - Average\ Negative|}\right)$$

Equation 2: $$\frac{Bottom+(top-bottom)}{(1+10^{(logIC50-X)(HillSlope)})}$$

2.3.2 Results and Discussion

Table 1 summarizes the binding results for the rationally designed thiazole molecules. Although these compounds showed great promise as VDR-coactivator inhibitors in the initial molecular modeling they did not exhibit any agonistic or antagonistic effects in the binding assay.

Table 1. Modulation of VDR-Coactivator binding in the presence of rationally designed thiazole ligands.

Compound	Recruitment of SRC-2-3 to VDR EC_{50} (μM)	Inhibition of SRC2-3 VDR Interaction IC_{50} (μM)
KAT011311	Inactive	Inactive
KAT052711	Inactive	Inactive
KAT030711	Inactive	Inactive
KAT021712	Inactive	Inactive
KAT021112	Inactive	Inactive
KAT080411	Inactive	Inactive
KAT031312	Inactive	Inactive

The maximum concentration used for this assay was 300 μM of each compound.

2.3.3 Conclusion

Although these initial rationally designed molecules did not bind to VDR and inhibit coactivator interactions, further computer modeling could aid in the development of active molecules. Also, these molecules may behave differently within cells and potentially exhibit transcriptional modifying properties. Further evaluation would be needed to determine this.

CHAPTER 3: GW0742

Introduction

High throughput screening (HTS) has quickly evolved over the last decades to become one of the main methods for the identification of lead compounds in drug discovery. As seen in Figure 31, it includes many different stages of the drug discovery process such as assay development, screening, hit compound selection, and the measurement of absorption, distribution, metabolism, and excretion (ADME) as well as toxicity.[7] Early drug discovery was simpler and focused more on the disease than on specific targets. Studies were carried out *in vivo* and required large amounts of each compound. Due to the identification of many new biological targets that mediate various diseases, more economic processes have been developed that include HTS using miniaturization and automation. The HTS revolution all began in 1951 with the invention of the microwell plate by Dr. Gyula Takatsky that was quickly commercialized as a plastic microplate later that decade.[144] With the development of microplate readers by Biotek that accepted different microwell plates, the concept really started to increase in popularity. By the 1990s, many companies were producing microplates and readers with many different features. In addition, automation was adopted which led to automated instruments,

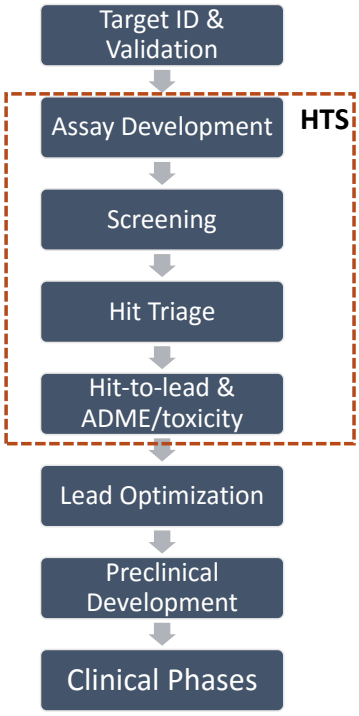

Figure 31. Stages of drug discovery and development and the involvement of HTS activities.[7]

automated liquid-handling systems, and automated screening systems that integrated more than 20 different instruments. Furthermore, the increase of publications containing detailed HTS assay adaptations helped mature HTS automation and detection systems. It was not long before standardization of microplates was necessary. The Society for Biomolecular Screening (SBS) was founded in 2002, which established a Microplate Standards Working group with the goal of introducing HTS standards and distributing knowledge among researchers in this field.

Today, HTS is more than assay development, validation and screening. It is a collective term that encompasses a range of multidisciplinary activities, ranging from the creation of specialized cell lines and purified enzymes for screening to compound design using computational chemistry and novel parallel chemistry approaches and even engineers creating suitable robots and instrumentation. HTS is constantly advancing with the development of new technology that increase throughput (i.e. ultraHTS) and decreases costs and waste.[144]

Drug target selection is an important starting point for drug discovery. Understanding the biology and pharmacological aspects of a biological target is essential before beginning a HTS campaign. There are many things to consider including the "drug-ability" of a target. For example, is there any evidence to support that a target is amendable to modulation by small molecules? In our case, nuclear receptors are known to be modulated by small molecules called hormones. Between 2001-2004, GlaxoSmithKline (GSK) had a 72% success rate of identifying new lead compounds for nuclear receptors among diverse libraries of small molecules.[145, 146] In addition, these compounds had ideal, drug-like chemical structures and exhibited a SAR. It is essential to note that the success of finding a hit compound is dependent upon the diversity of a compound library. The "chemical space" is quite large with an estimated 10^{40}-10^{100} compounds.

When considering that HTS is currently carried out with 0.5-1 million compounds, a selection process has to occur in order to make this approach successful.[147] By taking the structure of current drugs into account, Lipinski introduced the rule of five for drug-like molecules: 1. No more than five hydrogen-bond donors; 2. no more than ten hydrogen-bond acceptors; 3. a molecular mass less than 500 Daltons; 4. an octanol-water partition coefficient logP ≤ 5.[148]

In a general sense, HTS assays used for the identification of lead compounds are either biochemical or cell-based assays. The detection of activity can include fluorescence, luminescence, radioactive elements, heat of binding, and mass spectrometry.[149] Biochemical assays can include purified proteins such as receptors, enzymes, transporters and many more.[7] They offer the advantage of clear drug-target interactions leading to SAR during hit-to-lead optimization without being convoluted by other processes that can occur in cell-based assays. However, by assessing a compound within the environment of a cell, we are able to determine the quality and biological relevance of a hit compound in addition to any off-target effects it may have.[144]

In 2011, we conducted a screening campaign in collaboration with the NIH chemical and genomics center (NCGC) to identify a potential VDR inhibitor (AID: 504847, pubchem).[150] Approximately 390,000 compounds were screened using a FP assay where an inhibiting compound would disrupt the interaction between VDR and a fluorescently labeled peptide, SRC2-3. This primary screen found that 1,938 compounds exhibited IC_{50} values ≤ 40 μM. Two alternative FP assays, one with a Texas Red-labeled SRC2-3 and the other with a fluorescein-labeled SRC2-3, were employed to further validate the primary results. The Texas Red-labeled SRC2-3 revealed that out of the 1,938 initial hit compounds 69% of the compounds exhibited an

IC_{50} value of ≤ 40 μM. 83% of the compounds with the fluorescein-labeled SRC2-3 possessed an IC_{50} value of ≤ 40 μM. A good correlation was observed when Texas Red-labeled SRC2-3 and fluorescein-labeled SRC2-3 assay results were combined with those of the Alexa Fluor 647 assay. Accordingly, 747 compounds were selected based on diverse scaffold structures and functionality. To discriminate those compounds that might inhibit coactivator binding by irreversibly reacting with cysteine residues of the VDR-LBD protein, the VDR-SRC2-3 FP assay was conducted in the presence of 2-mercaptoethanol (ME). The idea was that the electrophilic compounds would react with the excess nucleophilic ME rather than the nucleophilic VDR protein residues such as cysteine. A significant decrease in the inhibition of VDR-SRC2-3 interaction was observed in the presence of 100 mM ME in comparison to 1 mM ME (Figure 34) thus suggesting

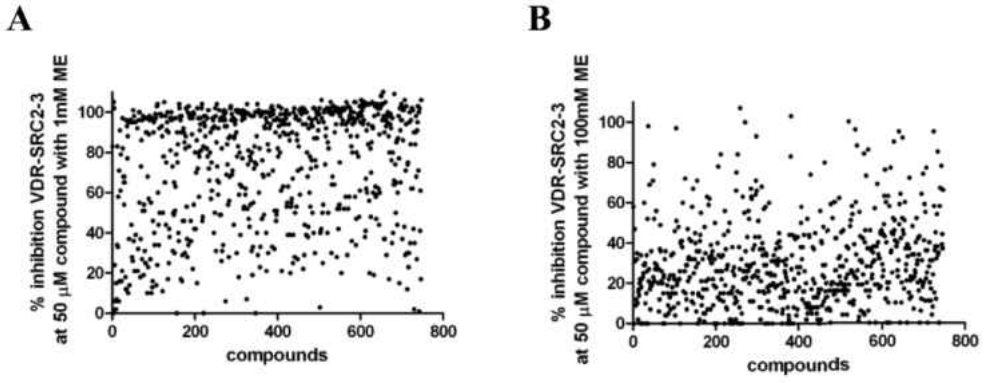

Figure 32. Inhibition of VDR-SRC2-3 Alexa Fluor 647 interaction by small molecules (50μM) in the presence of A) 1mM ME and B) 100mM ME.

that a large number of the primary hits may inhibit VDR-coactivator interactions through modifications of surface cysteine residues. However, a small number of compounds were not influenced by ME at high concentrations. Among these was GW0742 shown in Figure 33, A.

GW0742 was originally developed by GlaxoSmithKline in 2003 as a selective agonist for the peroxisome proliferator activated receptor δ (PPARδ) (EC_{50} = 0.001 μM).[151] The biological

role of PPARδ had remained elusive, in part, due to its broad tissue expression and the lack of good chemical tools to distinguish the pharmacology between the PPAR isoforms (α, γ, and δ). Thus, with the development of the selective GW0742 agonist, the function of PPARδ was investigated in cell-based assays and *in vivo* to reveal its role in hypertension, diabetes, inflammation, obesity, and cancer.

In our lab, GW0742 was evaluated in a dose responsive manner with a number of different assays. FP assays were used to determine the inhibition of VDR-SRC2-3 interaction with three different probes and IC_{50} values of 14 µM (Alexa Fluor 647), 25.1 µM (Fluorescein), and inconclusive (Texas Red) were determined. A cell-based transcription assay showed GW0742 inhibited VDR-mediated transcription with an IC_{50}= 26 µM as well as maximal response of 30% in the absence of $1,25(OH)_2D_3$. A cytotoxicity assay using HEK293T cells found that GW0742 encouraged 18% cell death at a concentration of 45.8 µM. In addition, a FP-assay using VDR and a rhodamine-labeled VDR ligand determined that GW0742 was binding the VDR ligand binding pocket and not the coactivator binding site with an IC_{50}= 8.7 ± 1.7 µM (Figure 33, B).

The selectivity of GW0742 with respect to its ability to inhibit the interaction between

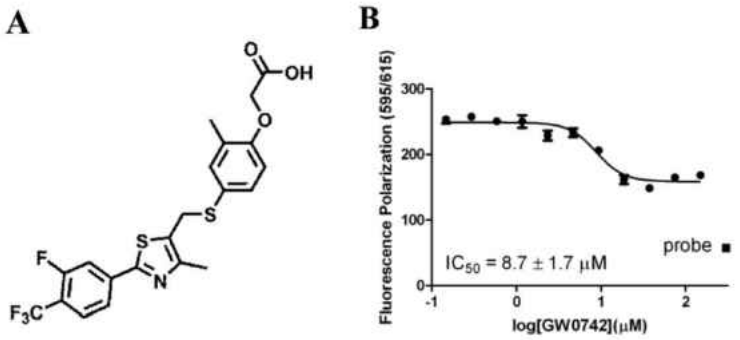

Figure 33. A) Structure of GW0742; B) FP-assay competing GW0742 against rhodamine-labeled VDR ligand.

other NRs and their coactivators was evaluated by using a FP assay with different Alexa Fluor 647

labeled coactivator peptides. The NR-coactivator pairs investigated included VDR and SRC2-3, the thyroid hormone receptor β (TRβ) and SRC2-2, PPARγ and DRIP2 (derived from coactivator DRIP205), and the androgen receptor (AR) and SRC2-3. GW0742 was able to disrupt NR-coactivator interactions from strongest to weakest potency as follows: AR-SRC2-3 (6.6 ± 1.5 μM), VDR-SRC2-3 (27.2 ± 2.7 μM), TRβ-SRC2-2 (59.9 ± 9.5 μM) and PPARγ-DRIP2 (>86 μM). Other groups have investigated GW0742 with respect to other nuclear receptors in a variety of assay.[151] GlaxoSmithKline used PPARα, PPARγ, and PPARδ cell-based transactivation assays (alkaline phosphatase as the reporter enzyme) to determine GW0742 agonistic activity EC_{50}= 2.0 ± 1.3 μM (PPARγ), 1.1 ± 0.109 μM (PPARα) and 0.001 ± 0.002 μM (PPARδ).[151]

GW0742 was evaluated in an array of nuclear receptor-mediated transcription assays using HEK293-T cells to confirm the pan nuclear receptor-coactivator inhibition caused by high concentrations of GW0742 in the FP assay. The nuclear receptors investigated were VDR, PPARα, PPARγ, PPARδ, AR, RXRα, TRα, TRβ, and ERα in the presence or absence of their endogenous ligands or synthetic agonists with different concentrations of GW0742. The EC_{50} and IC_{50} values are summarized in Table 2. As expected GW0742 was able to activate transcription mediate by PPARα, PPARγ, and PPARδ among the nuclear receptors tested with EC_{50} values in agreement with previously reported results. In contrast, inhibition of transcription was found for all NRs with GW0742 showing significantly lower IC_{50} values for VDR and AR with 12.1 μM and 14.7 μM, respectively. In addition, a cytotoxicity assay found that GW0742 at 37.5 μM was nontoxic (93%

of cells were alive). Interestingly, GW0742 exhibited an agonistic effect at lower concentrations and an antagonistic effect at higher concentrations. For PPARγ GW0742 exhibited EC_{50} values

Table 2. Evaluation of GW0742 in different nuclear receptor reporter assays.

NUCLEAR RECEPTOR	AGONIST EC_{50} (μM)	ANTAGONIST IC_{50} (μM)
VDR	Inactive	14.7 ± 1.5[a]
PPARα	1.3 ± 0.3	37.4 ± 8.2[b]
PPARγ	2.8 ± 0.7	20.2 ± 5.4[c]
PPARδ	0.0037 ± 0.0014	21.6 ± 4.9[d]
AR	Inactive	12.1 ± 5.3[e]
RXRα	Inactive	22.9 ± 3.8[f]
TRα	Inactive	31.4 ± 4.0[g]
TRβ	Inactive	25.8 ± 5.2[h]
ERα	Inactive	21.3 ± 7.2[i]

[a]1,25$(OH)_2D_3$ (10nM), [b]GW7647 (30nM), [c]Rogsiglitazone (300nM), [d]GW0742 (50nM), [e]DHT (10nM), [f]Bexarotene (200nM), [g]T3 (10nM), [h]T3 (10nM), [i]Estradiol (10nM). Three independent experiments were conducted in quadruplicate and data were analyzed using nonlinear regression with a variable slope (Graphpad Prism).

between 2.6 μM to 2.8 μM, whereas at concentrations higher than 20 μM GW0742 inhibited PPARγ-mediated transcriptional. The interaction between PPARγ-LBD and DRIP2 was inhibited at concentrations higher than 86 μM.

Together with the NIH NCGC, our goal was to develop novel, non-secosteroidal VDR modulators based on the GW0742 scaffold that 1) did not influence PPARδ signaling and 2) inhibited VDR-coactivator interactions. Reducing GW0742's ability to bind PPARδ might be accomplished by modulating the interaction with key LBP amino acid residues. Compared to VDR, PPARδ has a larger LBP that contains three different regions that can make contact with the ligand. GW0742 occupies this Y-shaped space by making a total of 29 ligand interaction with the pocket.[10] Region I (Figure 34, yellow residues) is mostly polar with residues that line the C-

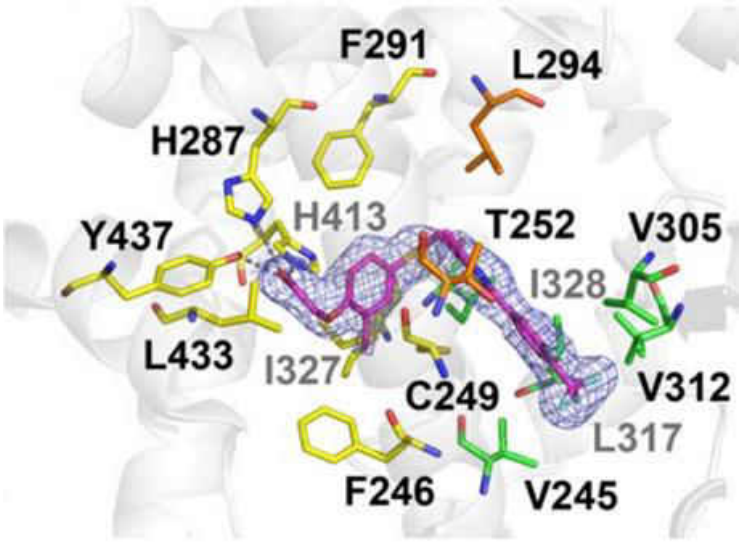

Figure 34. Stereo view of the binding site of PPARδ-LBD (grey cartoon) interacting with GW0742 (pink). The ligand makies interactions with residues belonging to region I (yellow), region II (green) and region III (orange).[10]

terminal activation of helix 12. Region II (Figure 34, green residues) and region III (Figure 34, orange residues) are predominately hydrophobic. GW0742 hydrophilic carboxylate group interacts with region I and its hydrophobic tail group containing the thiazole and the fluorine substituted phenyl ring is positioned mostly in region II. Therefore, it can be assumed that molecules lacking the ability to bind in this orientation would make poor PPARδ agonists.

Figure 35 depicts the SAR scheme followed to develop such GW0742 analogs reported within this chapter. Part 1 discusses changes made in the carboxylate region (blue) of GW0472. Part 2 includes over 100 analogs that have changes in the phenyl (pink), linker (green), methyl (light blue), and carboxylate (blue) regions. Finally, part 3 describes the synthesis and biochemical effects associated with a thiazole-oxazole switch. All compounds were investigated using nuclear receptor binding assays, transcription and toxicity assays to evaluate the selectivity and potency of GW0742 analogs to interact with VDR and PPARδ.

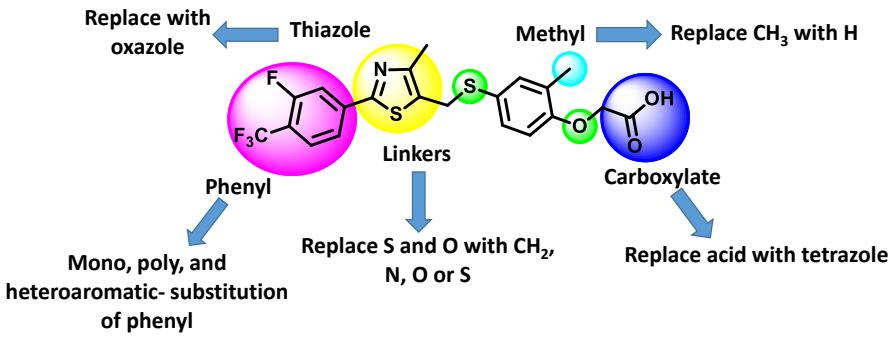

Figure 35. SAR scheme for the synthesis of GW0742 analogs.

Part 1: Evaluation of Coactivator Recruitment by the Vitamin D Receptor or the Peroxisome Proliferator-Activated Receptor δ in the Presence of GW0742 Analogs

3.1 Purpose

As previously discussed, our lab introduced GlaxoSmithKline's compound, GW0742,[151] as a novel antagonist for VDR.[152] In addition, GW501516, another GSK molecule that possesses a

1000-fold selectivity for PPARδ over other PPAR subtypes was found to inhibit VDR mediated transcription (IC_{50}= 16.0 ± 3.6 μM).[151] The compounds differ in structure by a *m*-fluorine substituent. Within this chapter, GW0742 and GW501516 analogs containing an ester (compound 2) or alcohol moiety (compound 3) in the carboxylate region were investigated for agonistic and antagonistic effects towards VDR and PPARδ. We hypothesized that analogs with appropriate substitution in the carboxylate region could diminish PPARδ binding. Therefore, we focused on the decrease of hydrogen bond interactions with important residues His413 and Tyr437 in region I. Virtual docking of compound 3 overlaid with GW0742 in the PPARδ LBP in Figure 36 visualizes the decrease in hydrogen bonding due to alcohol functionality.

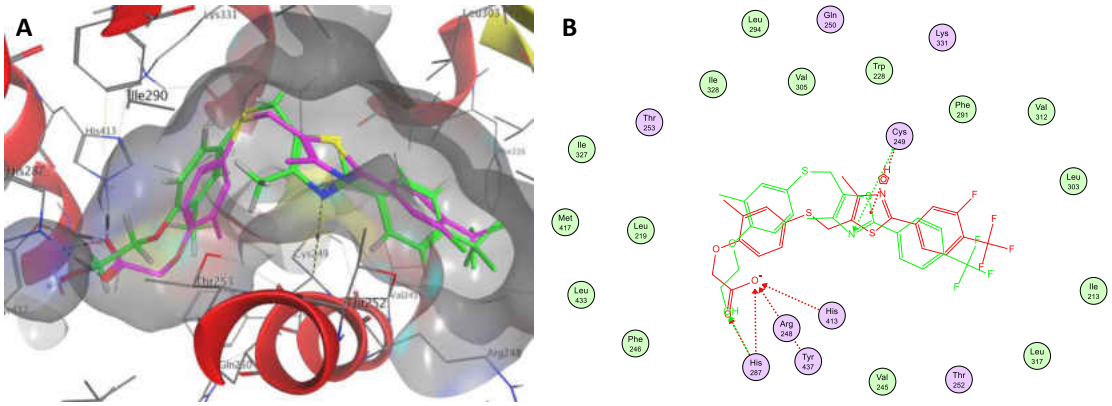

Figure 36. Virtual docking with PPARδ co-crystallized with GW0742 (PBD: 3TKM) were used to visualize the affects carboxylate substitution had on binding. A) GW501516 alcohol analog (lime green) overlaid GW0742 (pink). Hydrogen bonding is shown in black dashes and hydrogen pi bonds are shown in yellow. B) A 2D depiction of the interactions GW0742 (red) and GW501516 alcohol analog (lime green) have with PPARδ LBD.

3.2 Modulation of VDR-Coactivator Binding by GW0742 Analogs

The activities of compounds 1-3 with respect to VDR were determined using a FP assay employing recombinant VDR-LBD, Alexa Fluor 647 labeled SRC 2-3 peptide, and the synthetic VDR ligand LG190178.[129] The results are presented in Table 3. Compounds 1-3 possess no agonistic

Table 3. Summary of EC_{50} and IC_{50} values of compounds 1-3 for VDR determined by fluorescence polarization.

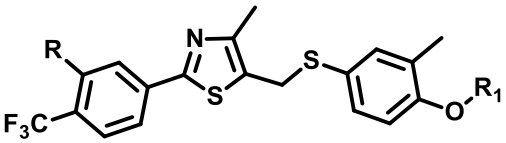

Compound	R	R_1	Agonist EC50 (μM)	Antagonist[a] IC50 (μM)
1 GW0742	F	CH_2COOH	Inactive	7.73 ± 1.68
2	H	CH_2COOCH_3	Inactive	>30
3	H	CH_2CH_2OH	Inactive	9.03 ± 5.5

A VDR-LBD concentration used was 0.1μM. [a] Inhibition of VDR-SRC2-3 interaction in the presence of LG190178 (0.75 μM). Three independent experiments were conducted in quadruplicate and data were analyzed using a nonlinear regression with a variable slope (GraphPad Prism).

activity thus the inability to initiate the interaction between VDR-LBD and coactivator peptide SRC2-3. The antagonistic behavior of all compounds was determined in the presence of VDR agonist LG190178.[153] Compound 1, GW0742, was the most active inhibitor with an IC_{50} of 7.73 ± 1.68 μM in the presence of 100 nM VDR-LBD. We observed that higher concentrations of VDR-LBD resulted in ligand depletion and therefore higher IC_{50} values for instance the recently reported IC_{50} of 27.2 ± 2.7 μM for GW0742 in the presence of 600 nM VDR-LBD.[152] Interestingly, compound 2 bearing a carboxylic ester functionality instead of the carboxylic acid is significantly less active. The corresponding alcohol 3 however has a similar inhibitory activity as GW0742 with an IC_{50} of 9.03 ± 5.5 μM.

3.3 Modulation of VDR and PPARδ-Mediated Transcription by GW0742 Analogs

Unlike fluorescence polarization-based binding assays, which provide information on favorable compound binding or inhibition, cell-based assays provide information about compound cell permeability, biological relevance and overall toxicity of novel compounds. Three specific assays were conducted using highly transfectable HEK-293T kidney cells: 1) VDR transcription assay; 2) A PPARδ transcription assay; and 3) a cell viability assay. The VDR transcription assay applies two plasmids. VDR is overexpressed under control of a cytomegalovirus promoter (CMV) and the reporter plasmid possesses a luciferase reporter gene under control of a CYP24A1 promoter (Figure 37). In the presence of an agonist like $1,25(OH)_2D_3$,

VDR is activated and recognizes the VDRE found on the CYP24A1 promoter region and induces the transcription of the luciferase reporter gene. A bioluminescent reaction in the presence of

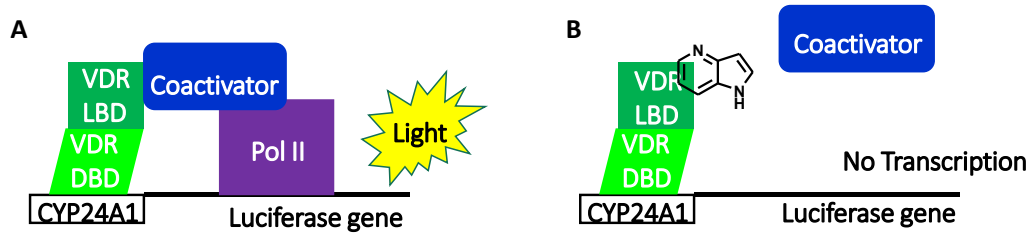

Figure 37. Cartoon describing luminescence-based transcription assay. A) Activated VDR transcribes the luciferase gene and produces light. B) In the presence of an inhibitor, VDR is unable to transcribe the luciferase gene and produce light.

its substrates (i.e. luciferin, ATP, Mg^{2+} and O_2) creates light that is directly proportional to the amount of expressed enzyme, and thus, the transcriptional activity of VDR (Figure 37, A). An inhibitor induces a conformational change to VDR that is unfavorable for coactivator binding and thus transcription of the luciferase gene does not occur (Figure 37, B).

The PPARδ transcription assay is a 2-hybid assay that includes a vector of PPARδ's ligand binding domain fused to a GAL4 DNA domain. The reporter plasmid includes a luciferase genes under control of a UAS. In the presence of an agonist like GW0742, PPARδ is activated and binding of GAL4 to the UAS induces transcription of the luciferase gene, thus the ability to produce light. Because we are trying to diminish PPARδ-activated transcription with the GW0742 analogs, a decrease in light production would indicate poor agonistic effects and the desired discrimination against PPARδ.

The cytotoxicity assay allows for the direct quantification of the ATP present in viable cells, which is an indicator of metabolically active cells. Because ATP is a necessary substrate for

luciferase enzyme, living cells producing it will promote a bioluminescent reaction through this enzyme.

3.3.1 Experimental Procedure

Reagents and Instrumentation: Human embryonic kidney (HEK) 293T cells were purchased (ATCC) and cultured in 75 cm^2 flasks (CellStar) coated in matrigel (BD Bioscience, #354234), a gelatinous protein secreted by mouse sarcoma that helps cells adhere to the flask. Cells are grown in DMEM/High Glucose (Hyclone, #SH3024301) media to which non-essential amino acids (Hyclone, #SH30238.01), 10 mM HEPES (Hyclone, #SH302237.01), 5 x 10^6 units of penicillin and streptomycin (Hyclone, #SV30010), and 10% of heat inactivated fetal bovine serum (Gibco, #10082147) were added. Cells are harvested using 0.05% Trypsin (Hyclone, #SH3023601), which disrupts the cell monolayer and proteolytically cleaves the bonds between the cells and flask. The assay is conducted in DMEM/High Modified buffer without phenol red (Hyclone, #SH30284.01) that contains all the above mentioned additives plus 10 mM sodium pyruvate and 2% percent charcoal treated FBS (Invitrogen, #12676-011) instead of HI FBS. Cell transfection was conducted by lipid-based methods using Lipofectamine™ reagent with PLUS™ reagent (Life Technologies, #15338020). VDR and PPARδ-mediated transcription was determined using Bright-Glo™ Luciferase Assay Kit (Promega, Madison, WI). Controls used with VDR were $1,25(OH)_2D_3$ (10 nM in DMSO, purchased form Endotherm) and DMSO while PPARδ controls were GW0742 (30 nM in DMSO, purchased from Tocris). Bright-Glo™ contains all substrates (luciferin, ATP, and Mg^{2+}) necessary for expressed luciferase to produce a light. The cell viability assay was evaluated using Cell Titer-Glo™ Luminescent Cell Viability Assay Kit (Promega, Madison, WI)

which contains luciferase and all its substrate but ATP. The controls for the cytotoxicity assay used were 3-dibutylamino-1-(4-hexyl-phenyl)-propan-1-one (100 µM in DMSO, positive, Figure 38) and DMSO (negative). Cell culture was performed in a Baker Company Class II Biological Safety Cabinet. All luminescence readings were performed on a Tecan Infinite M1000 plate reader. Small volume transfers were performed on the Tecan Freedom EVO liquid handling system with a 100 nL pin tool transfer (V&P Scientific). Serial dilutions were done in 96-well polypropylene plates (Corning, #3365) and assays were conducted in 384- well white optical bottom plates (Nunc, #142762).

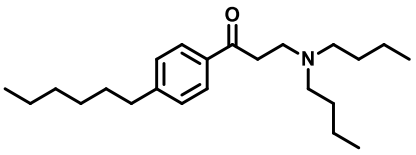

Figure 38. 3-dibutylamino-1-(4-hexyl-phenyl)-propan-1-one

Luminescence-Based VDR-Mediated Transcription Assay Protocol: Cell transfection was carried out with 70-80% confluent HEK 293T cells that had been cultured in 75 cm^2 flasks. For VDR transfection, 2 mL of untreated DMEM/High Glucose media (without additives) containing 0.7 µg of VDR-CMV plasmid, 16 µg of a CYP24A1-luciferase reporter gene, Lipofectamine™ LTX (75 µl), and PLUS™ reagent (25 µl) was added to the flask. For PPARδ transfection, 2 mL of untreated DMEM/High Glucose media (without additives) containing 1.5 µg of PPARδ GALx4 plasmid, 16 µg of a GALx4RE luciferase reporter gene, Lipofectamine™ LTX (75 µl), and PLUS™ reagent (25 µl) was added to the flask . After 16 hours of incubation at 37°C with 5% CO_2, the cells were harvested with 3mL of 0.05% Trypsin, added to 10mL of the assay buffer, DMEM/High Modified buffer without phenol red, and spun down for 2 minutes at 1000 rpm. The media was removed and cells were resuspended in the DMEM assay media. Prior to adding cells to sterile white, optical bottom 384-well plates, plates were treated with 20 µL per well of a 0.25% matrigel

solution. To each well, 20 µL of cells were added to yield a final concentration of 15,000 cells per well. The plates were then spun down for 2 minutes at 1000 rpm. After 4 hours, plated cells were treated with 100 nL of small molecules and controls which were added using the pin tool. In the competitive inhibition assay, $1,25(OH)_2D_3$ (10 nM) was also added to the small molecule wells. After 16 hours of incubation at 37°C with 5% CO_2, 20µL of Bright-Glo™ Luciferase Assay Kit (transcription assay) or Cell Titer-Glo™ Luminescence Assay Kit (cytotoxicity assay) were added and luminescence was read. Controls were measured within each plate to determine the z' factor (Equation 1) and to enable data normalization. Three independent experiments were performed in quadruplicate and data was analyzed using nonlinear regression with variable slope (GraphPrism, Equation 2).

3.3.2 Results and Discussion

To further explore the biological role of compounds 1-3, transcription assays mediated by VDR and PPARδ were employed using transiently transfected HEK293-T cells.[129] The results are summarized in Table 4.

Table 4. Summary of transcriptional activation and deactivation mediated by VDR and PPARδ in the presence of GW0742 analogs.

Cmpd	R[a]	R_1[a]	VDR EC_{50} (µM)	VDR IC_{50} (µM)	PPARδ EC_{50} (**nM**)	PPARδ IC_{50} (µM)	Toxicity LD_{50} (µM)
1 GW0742	F	CH_2COOH	Inactive	12.7 ± 8.0	3.5 ± 0.31	3.9 ± 2.4	>50
2	H	CH_2COOCH_3	0.15 ± 0.08 (11%)[b]	0.95 ± 0.30	3.9 ± 0.38 (35%)[c]	0.26 ± 0.12	5.47 ± 3.3 (70%)[d]
3	H	CH_2CH_2OH	0.12 ± 0.03 (38%)[b]	0.36 ± 0.055	40 ± 19 (13%)[c]	0.63 ± 0.22	1.73 ± 0.14

[a]For structure see Table 1; [b] percent partial VDR activation in reference to calcitriol; [c] Percent partial PPARδ activation in reference to compound GW0742; [d] Percent partial toxicity

As expected, GW0742 was inactive as a VDR agonist but could inhibit VDR-mediated transcription with an IC_{50} value of 12.7 ± 8.0 µM (Table 4). Furthermore, we confirmed the activation of PPARδ

at nanomolar concentrations of GW0742 (EC_{50} 3.5 ± 0.31 nM) and inhibition of PPARδ-mediated transcription at higher concentration (IC_{50} 3.9 ± 2.41 μM).[152] Interestingly, compounds 2 and 3, which were not able to initiate the interaction between VDR-LBD and SRC2-3 peptide (Table 3) exhibited partial VDR agonistic effects at concentrations between 110-150 nM (Table 4, entries 2 and 3). Compound 3 activated the VDR-mediated transcription with a 38% efficacy in respect to VDR agonist calcitriol and an affinity of 0.12 ± 0.03 μM (EC_{50}). For the activation of PPARδ-mediated transcription compound 2 was superior to compound 3 with an EC_{50} of 3.9 ± 0.38 nM and an efficacy of 35% in comparison to GW0742. Importantly, compound 2 and 3 inhibited PPARδ- and VDR-mediated transcription at sub-micromolar concentrations. In addition, the toxicity of analogs 2 and 3 is more pronounced than that of GW0742. Compound 2 has three-fold selectivity towards the inhibition of PPARδ-mediated transcription with an IC_{50} of 0.26 ± 0.12 μM and compound 3 is two-fold more active to inhibit VDR-mediated transcription with an IC_{50} of 0.36 ± 0.055 μM.

3.4 Conclusion

Overall, we demonstrated agonistic behaviors of GW0742 and its analogs at lower concentrations for PPARδ and inhibition of PPARδ-mediated transcription at higher concentrations. In addition, GW0742 analogs 2 and 3 exhibited a similar behavior for VDR but at significantly higher concentrations for the partial agonist effect. The toxicity of both compounds is significant and may play a role in the relatively low inhibition of transcription for the both receptors.

Part 2: A High Throughput Approach to Identify Novel Nuclear Receptor Ligands Based on the GW0742 Scaffold

3.1 Purpose

In this part, molecules with substitutions made in the phenyl, linker, methyl and carboxylate regions of GW0742 were synthesized to investigate their effects on PPARδ and VDR

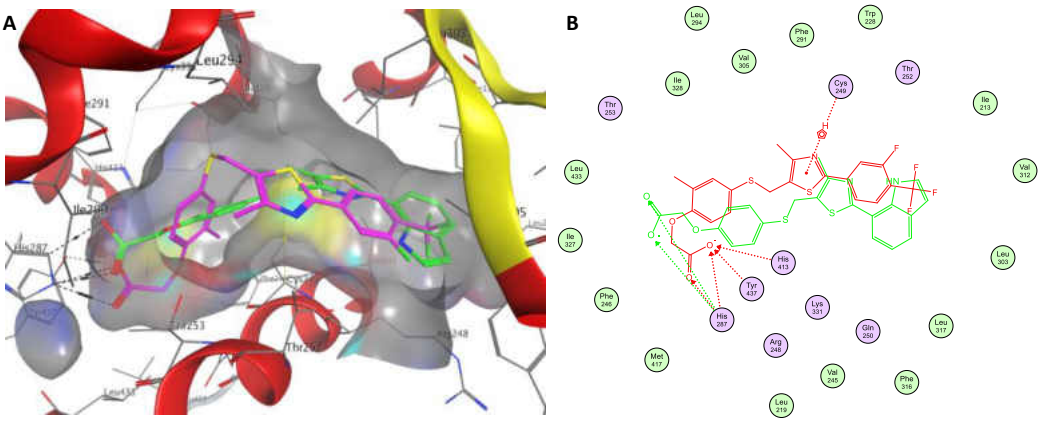

Figure 39. Virtual screening docking with PPARδ co-crystallized with GW0742 (PBD: 3TKM) were used to visualize the affects phenyl substitution had on binding. A) GW0742 analog, NCGC00344919-01, possessing a 1*H*-indol-4-yl substituent in the phenyl position (lime green) overlaid GW0742 (pink). Hydrogen bonding is shown in black dashes and hydrogen pi bonds are shown in yellow. B) A 2D depiction of the interactions GW0742 (red) and NCGC00344919-01 (lime green) have with PPARδ LBP.

transcription. As before, we wanted to deactivate PPARδ-mediated transcription by creating unfavorable interactions with its LBD while creating a potent VDR inhibitor. As seen in figure 39, the addition of a heteroaromatic ring system such as an indole in the phenyl position would create steric bulk and diminish favorable hydrogen bonding interactions with Tyr437, His413, and His287.

Furthermore, by adding different electron donating and accepting groups on the phenyl substituent, itself, may also create the necessary interactions needed for a potent VDR inhibitor.

The addition of bioisosteric linkers such as nitrogen, oxygen and carbon provided diversity in bond angles and molecule length that might decrease PPARδ activation. Figure 40 depicts how a sulfur/oxygen switch changes the orientation of a GW0742 analog caused by increased polar surface and reduced molecule length.

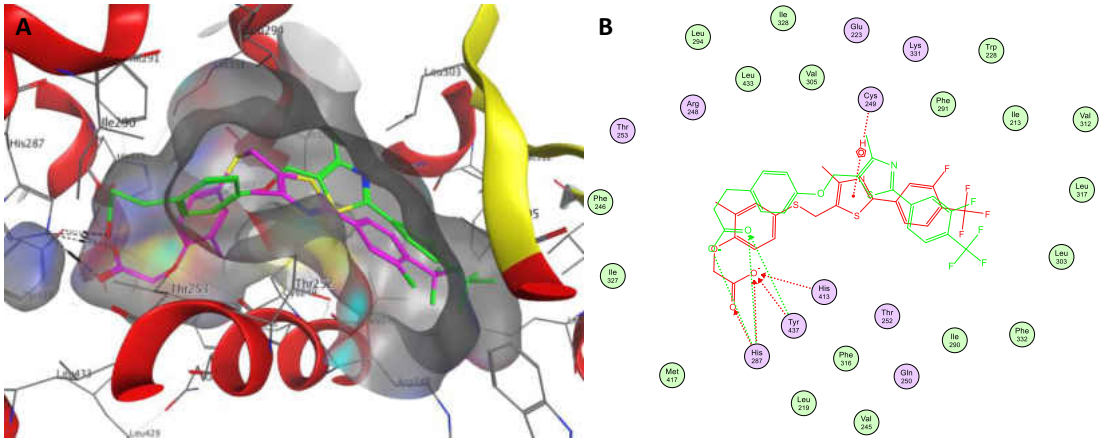

Figure 40. Virtual screening docking with PPARδ co-crystallized with GW0742 (PBD: 3TKM) were used to visualize the affects linker substitution had on binding. A) GW0742 analog containing an oxygen and carbon linkers (lime green) overlaid GW0742 (pink). Hydrogen bonding is shown in black dashes and hydrogen pi bonds are shown in yellow. B) A 2D depiction of the interactions GW0742 (red) and GW0742 with oxygen and carbon linkers (lime green) have with PPARδ LBP.

3.2 Chemistry

3.2.1 Synthetic Strategy

Synthetic route developed by UWM (Scheme 1): The synthesis of mono-substituted GW0742 analogs included the reduction of ethyl 2-bromo-5-methylthiazole-4-carboxylate to obtain primary alcohol (KAT051412).[154] This compound was coupled with methyl 3-(4-hydroxyphenyl)propionate under Mitsunobu reaction conditions yielding thiazole ester KAT091212.[155] Originally a two-step reaction was applied transforming KAT051412 into the corresponding chloride in the presence of methanesulfonyl chloride followed by the subsequent

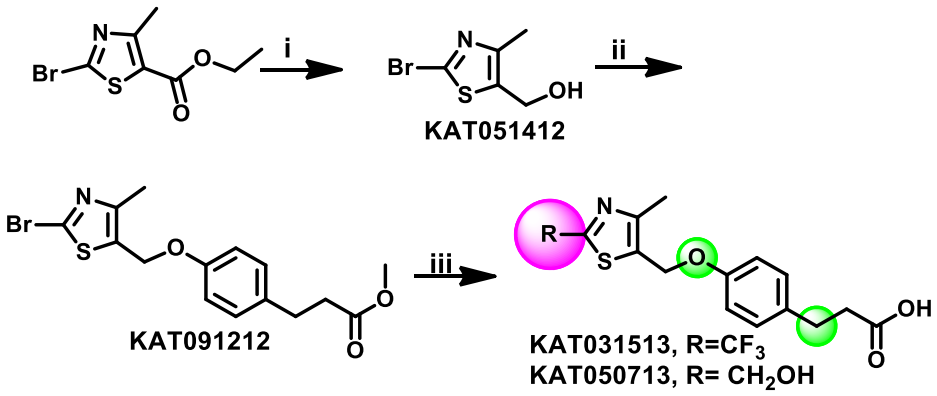

Scheme 2. Synthesis of phenyl ring-subsituted ligands containing oxygen and carbon linkers: i) $NaBH_4$, EtOH, room temperature, 4 hrs; ii) PPh_3, DIAD, DCM, methyl 3-(4-hydroxyphenyl) propionate, room temperature, 2hrs; iii) a) 4-(trifluoromethyl)boronic acid (KAT031513) or 3-(hydroxymethyl)phenyl) boronic acid (KAT050713), $PdCl_2(PPh_3)_2$, $Na_2CO_3 \cdot H_2O$, DME/H_2O/EtOH, 160°C, 10minutes, MW, b) (3-(hydroxymethyl)phenyl)boronic acid, $PdCl_2(PPh_3)_2$, $Na_2CO_3 \cdot H_2O$, DME/H_2O/EtOH, 160°C, 10 min, MW.

reaction with methyl 3-(4-hydroxyphenyl)propionate. However, the overall yield was still lower than the one step Mitsunobu reaction at 25%. A microwave assisted Suzuki reaction allowed for the introduction of the third aromatic ring.[156] Conveniently, carbon-carbon bond formation and hydrolysis occurred under microwave conditions to form final carboxylic acids KAT031513 and KAT050713 with a para-trifluoromethyl or meta-methylene hydroxy substituent, respectively.

Synthetic route developed by NIH: Mono, poly, and heteroaromatic-substituted GW0742 analogs were synthesized according to reaction scheme 3. Similar to our reaction, methyl 2-bromo-5-methylthiazole-4-carboxylate was reduced to a primary alcohol. A substitution to produce a corresponding chloride (compound 3.1) was accomplished with thionyl chloride followed by the coupling with 4-hydroxy-3methylthiophenol in the presence of cesium carbonate. Alkylation of the phenol with *tert*. butyl bromoacetate afforded compound 3.2. A Suzuki coupling was applied to enable diversity in this position with different boronic acids utilizing a unique solid supported diphenylphosphine palladium (II) heterogeneous catalyst that

could be recycled and used again. The resulting esters were hydrolyzed with trifluoroacetic acid in DCM to afford the final carboxylic acid products.

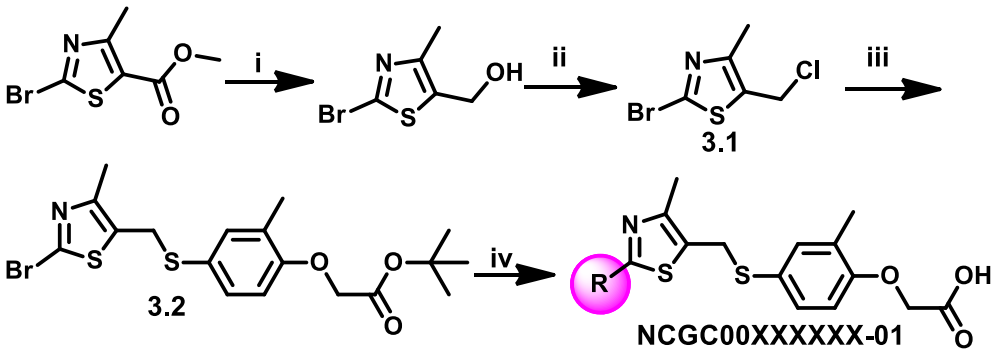

Scheme 3. Synthesis of mono, poly, and heteroaromatic-substituted ligands: i) $NaBH_4$, EtOH, room temperature, ii) $SOCl_2$, DCM, rt; iii) a) 4-hydroxy-3methylthiophenol, Cs_2CO_3, acetonitrile, room temperature; b) *tert*. butyl bromoacetate, Cs_2CO_3, acetonitrile, room temperature; iv) a) boronic acid Na_2CO_3, SiliaCat® DPP-Pd, DME, 150°C, MW, 0.5 h; b) TFA, DCM, room temperature, 1h.

Bioisosteric substitution is a common approach in medicinal chemistry to improve potency, selectivity or toxicity in a drug while maintaining similar physical (i.e. size, shape, polarity) and chemical properties (i.e. pKa). In our case a tetrazole ring was introduced in place of the carboxylate as depicted in scheme 4. Therefore, cyano-substituted analogs were treated with sodium azide to form tetrazoles by a traditional [2+3] cycloaddition.

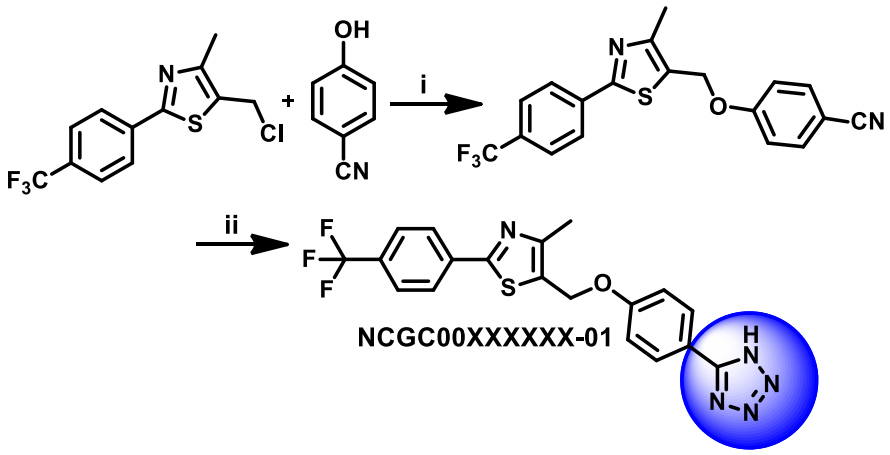

Scheme 4. Synthesis of bioisostere-substituted ligands. i) Cs_2CO_3, CAN, room temperature, 2 hours; ii) NaN_3, NH_4Cl, DMF, 100°C, overnight.

3.2.2 Characterization

General Chemistry: Starting reagents such as ethyl 2-bromo-4-methylthiazole-5-carboxylate, methyl 3-(4-hydroxyphenyl)propionate, 4-(trifluoromethyl)boronic acid, and 3-(hydroxymethyl)phenyl)boronic acid were purchased from Sigma-Aldrich. Anhydrous solvents were purchased in sure-seal bottles and handled under dry conditions using syringe technique. All glassware was dried overnight at 100°C before use. Thin layer chromatography was performed on pre-coated silica gel 60 F254 plates (Fisher Scientific). Microwave reactions were performed using a CEM Discover SP instrument. Synthesized compounds were purified by normal phase flash chromatography (SPI Biotage, silica gel 230-400 mesh) and concentrated under vacuum. All pure compounds were stored as solids at -20°C. Compound characterization was performed using a Shimadzu 2020 LC-MS (single quadrupole) instrument or Surveyor & MSQ LC-MS (APCI or ESI) with compounds directly injected. NMR spectra were recorded on a Bruker 300MHz instrument with samples diluted in either $CDCl_3$ or DMSO- D_6.

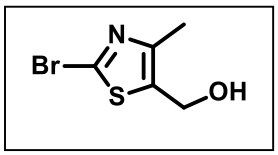

KAT051412: 60% yield; To an ice cold solution of ethyl 2-bromo-5-methylthiazole-4-carboxylate (2.6g, 15.6 mmol) in ethanol (60mL) and water (1 mL) a solution of $NaBH_4$ (2.36g, 62.4mmol) and ethanol (50mL) was added slowly over 40 minutes. Once added, the reaction was warmed to room temperature and stirred overnight. The reaction was monitored by TLC using EtOAc-hexanes (4:1, v/v). Next, ethanol was removed using rotary evaporation. The oily residue was resuspended in EtOAc and carefully washed with saturated NH_4Cl. The aqueous layer was then washed with EtOAc three times, combined, dried over Na_2SO_4 and concentrated to dryness. The crude product was purified on silica gel with EtOAc-hexanes (2%-60% strong) using normal phase flash chromatography system. The pure product was a cream colored solid. ^{1}H-NMR (300 MHz) ($CDCl_3$) δ 4.78 (s, 2H), 2.39 (s, 3H); ^{13}C-NMR δ 149.05, 135.73, 134.18, 56.43, 50.47, 14.96. MS APCI ($^+$ve) calcd. *m/z* for C_5H_6BrNOS [(M)] 207.0, found [$(M+H)^+$] 208 and [$(M+H+2)^+$] 211.1.

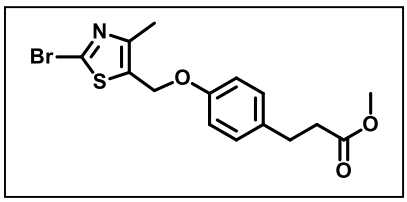

KAT091212: 25% yield; Methyl 3-(4-hydroxyphenyl)propionate (87 mg, 0.48 mmol) and triphenylphosphine (164 mg, 0.63 mmol) were added to a solution of (2-bromo-4-methylthiazol-5-yl)methanol (100 mg, 0.48 mmol, compound KAT051412) and DCM (5mL) and cooled to 0ºC. Diisopropyl azodicarboxylate (123.1 µL, 0.63mmol) was added dropwise and allowed to stir for 15 minutes before being warmed to room temperature. The reaction was monitored by TLC using EtOAc-hexanes (4:1, v/v). Upon completion, the solvent was removed and purification was conducted with EtOAc-Hexanes (2%-60% strong). Pure fractions were isolated and dried under high vacuum to obtain a cream colored solid. ^{1}H-NMR (300 MHz) ($CDCl_3$) δ 7.17-7.14 (d, 2H, J= 9Hz), 6.90-6.87 (d, 2H, J= 9Hz), 5.07 (s, 2H), 3.69 (s, 3H), 2.95-2.90 (t, 2H, J= 7.5 Hz), 2.65-2.60 (t,

2H, J= 7.5Hz), 2.40 (s, 3H); ^{13}C-NMR δ 173.30, 156.32, 150.40, 149.18, 133.89, 129.44, 129.18, 115.04, 61.95, 51.62, 35.87, 30.08, 15.28. MS DUIS calcd. *m/z* for $C_{15}H_{16}BrNO_3S$ [(M)] 369.2, found [$(M+H)^+$] 370.0 and [$(M+H+2)^+$] 372.0.

General Procedure for Suzuki Coupling Reaction: In a 10 mL microwave reaction vessel methyl 3-(4-((2-bromo-4-methylthiazol-5-yl)methoxy)phenyl)propionate (50 mg, 0.14 mmol, compound KAT091212), 4-(trifluoromethyl)boronic acid or 3-(hydroxymethyl)phenylboronic acid (0.20 mmol, 1.5 equiv.), $Na_2CO_3 \cdot H_2O$ (25 mg, 1.5 equiv.), bis(triphenylphosphine)palladium(II) dichloride (1 mg, 0.0014 mmol, 0.01 equiv.) were dissolved in a mixture of DME-H_2O-EtOH (7:3:2, v/v/v). The reaction mixture was treated with nitrogen to remove traces of oxygen and capped. The reaction was heated in a microwave reactor to 160^{o}C for 10 minutes. TLC using EtOAc-Hexanes with 1% AcOH (4:1, v/v) was used to confirmed conversion of the starting material (KAT091212) and appearance of a new product. The crude reaction was dried, resuspended in saturated NH_4Cl and extracted with EtOAc (2x) and DCM (2x). The organic layers were combined, dried over Na_2SO_4 and concentrated to dryness. The crude mixture was purified with silica gel using EtOAc-Hexanes with 1% AcOH (2-80% strong).

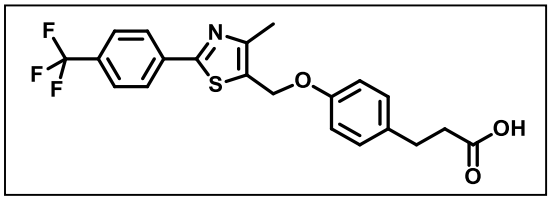

KAT031513: 36% yield; ^{1}H-NMR (300 MHz) (DMSO-D_6) δ 8.14-8.11 (d, 2H, J= 9Hz), 7.86-7.83 (d, 2H, J= 9Hz), 7.19-7.16 (d, 2H, J= 9Hz), 6.98-6.95 (d, 2H, J= 9Hz), 5.31 (s, 2H), 2.79-2.74 (t, 2H, J= 7.5Hz), 2.51-2.50 (t, 2H), 2.47 (s, 3H); ^{13}C-NMR δ 174.21, 163.73, 156.36, 152.01, 144.83, 137.00, 134.27, 129.76, 129.63, 127.06, 126.64, 122.78, 115.36, 62.06, 35.99, 29.92, 15.56; ^{13}CDEPT-135 NMR δ Negative (-), CH_2: 62.07, 36.08, 30.02, Positive

(+): 129.76, 127.05, 126.64, 115.36, 15.55; ESI-MS (+ve and –ve) calcd. *m/z* for $C_{21}H_{18}F_3NO_3S$ [(M)] 421, found [$(M+H)^+$] 422.2 and [$(M-H)^-$] 420.

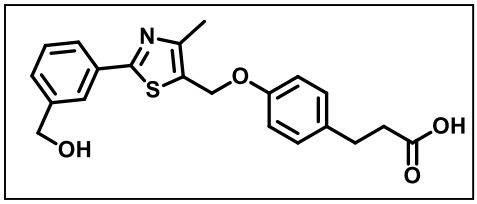

KAT050713: 33% yield; ^{1}H-NMR (300 MHz) (DMSO-D_6) δ 7.88 (s, 1H), 7.77-7.75(1H, d, J= 6Hz), 7.46-7.38 (m, 2H), 7.18-7.15 (d, 2H, J=9Hz), 6.97-6.94 (d, 2H, J= 9Hz), 5.28 (s, 2H), 4.57 (s, 2H), 2.79-2.74 (t, 2H, J= 7.5Hz), 2.51 (m, 2H), 2.44 (s, 3H); ^{13}C-NMR δ 174.29, 165.87, 156.55, 151.71, 144.19, 134.09, 133.25, 129.74, 127.76, 124.73, 124.13, 115.37, 62.91, 62.07, 36.02, 30.00, 15.56; ^{13}CDEPT-135 NMR δ Negative (-), CH_2: 62.91, 62.07, 36.02, 30.00, Positive (+): 129.74, 129.43, 128.62, 124.73, 124.13, 115.38, 15.56; ESI-MS (+ve) calcd. *m/z* for $C_{21}H_{21}NO_4S$ [(M)] 383, found [(M+H)] 384.

NIH General Chemistry: Preparative purification was run on a Waters semi-preparative HPLC system using a Phenomenex Luna C18 (5 micron, 30 x 75 mm) at a flow rate of 45 mL/min. A gradient of 10% to 50% acetonitrile in water over 8 minutes (each containing 0.1% trifluoroacetic acid) was used as a mobile phase during the purification. Fraction collection was triggered by UV detection (220 nm). Analytical analysis was performed on an Agilent LC/MS (Agilent Technologies, Santa Clara, CA). Method t1: A 7 minute gradient of 4% to 100% Acetonitrile (containing 0.025% trifluoroacetic acid) in water (containing 0.05% trifluoroacetic acid) was used with an 8 minute run time at a flow rate of 1 mL/min. A Phenomenex Luna C18 column (3 micron, 3 x 75 mm) was used at a temperature of 50° C. Method t2: A 3 minute gradient of 4% to 100% Acetonitrile (containing 0.025% trifluoroacetic acid) in water (containing 0.05% trifluoroacetic acid) was used with a 4.5 minute run time at a flow rate of 1 mL/min. A Phenomenex Gemini

Phenyl column (3 micron, 3 x 100 mm) was used at a temperature of 50° C. Method t3: Analysis was performed on an Agilent 1290 Infinity Series HPLC. UHPLC Long Gradient Equivalent 4% to 100% acetonitrile (0.05% trifluoroacetic acid) in water over 3.5 minutes run time of 4 minutes with a flow rate of 0.8 mL/min. Purity was determined using an Agilent Diode Array Detector for both Method t1, Method t2 and Method t3. Mass determination was performed using an Agilent 6130 mass spectrometer with electrospray ionization in the positive mode. ^{1}H NMR spectra were recorded on Varian 400 MHz spectrometer. Chemical shifts are reported in ppm with DMSO at 2.49 ppm as internal standard. High resolution mass spectrometry was recorded on Agilent 6210 Time-of-Flight LC/MS system. Confirmation of molecular formula was accomplished using electrospray ionization in the positive mode with the Agilent Masshunter software (version B.02).

3.3 Evaluation of GW0742-Based Analogs using Biochemical and Cell-based Assays

GW0742 analogs were characterized using a PPARδ-mediated transcription assay and toxicity assay.[157] The results are summarized in the following tables: mono-substituted analogs (Table 5), poly-substituted analogs (Table 6), heteroaromatic-substituted analogs (Table 7), tetrazole-substituted analogs (Table 8), and linker-substituted analogs (Table 9). PPARδ agonists with EC_{50} values greater than 1 μM were summarized into Table 10.

GW0742 analogs with non-substituted phenyl rings like compound NCGC00319174-01 exhibited low PPARδ activation (Table 5). This suggests that the substituents such as *p*-CF_3 and *m*-F of the parent compounds encourage favorable interactions with PPARδ LBP. Only three mono-substituted compounds modulated transcription with high potency. They were

NCGC00241455-04 (*p*-CF_3), NCGC00319058-01 (*p*-OCF_3), and NCGC00319066-01 (*p*-CO_2Et) with EC_{50} values lower than 15 nM. It was no surprise that compound NCGC00241455-04, also known as GW501516, was confirmed as a potent PPARδ agonist.[158] The other two compounds have not been reported but exhibit similar electron donating properties and significant hydrophobicity. Notably, the positioning of substituents around the phenyl ring affected the ligands ability to activate transcription. A para positioned substituent, in most cases, is a more potent PPARδ agonist than compounds that bear the same group in the ortho or meta position. This is observed with a methyl, trifluoromethyl, trifluoromethoxy and cyano substituents.

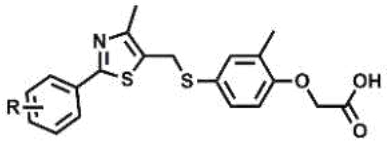

Table 5. Evaluation of mono-substituted GW0742 analogs

Entry	R	PPARδ EC_{50} (μM) [a,(b)]	Toxicity LD_{50} (μM)[c]
NCGC00319174-01	H	0.26 ± 0.35 (90)	>100
NCGC00319046-01	*o*-CH_3	0.60 ± 0.17 (66)	>100
NCGC00319053-01	*m*-CH_3	1.62 ± 0.41 (74)	>80
NCGC00319065-01	*p*-CH_3	0.05 ± 0.02 (100)	>80
NCGC00319061-01	*o*-Cl	0.58 ± 0.20 (71)	>80
NCGC00319050-01	*m*-Cl	0.50 ± 0.16 (74)	28.8 ± 5.0
NCGC00319056-01	*p*-Cl	0.13 ± 0.04 (66)	>100
NCGC00319063-01	*o*-F	0.26 ± 0.08 (94)	>80
NCGC00319048-01	*m*-F	0.43 ± 0.23 (96)	>100
NCGC00319055-01	*p*- F	0.16 ± 0.04 (93)	Non-toxic
NCGC00319064-01	*o*-CF_3	2.4 ± 0.95 (39)	>100
NCGC00319049-01	*m*-CF_3	1.1 ± 0.6 (79)	>50
NCGC00241455-04 (GW501516)	*p*-CF_3	0.013 ± 0.004 (100)	>33
NCGC00319047-01	*o*-OCH_3	2.3± 0.70 (27)	>100
NCGC00319052-01	*m*-OCH_3	2.36 ± 0.67 (96)	>80
NCGC00319051-01	*m*-OCF_3	0.45 ± 0.15 (100)	>50
NCGC00319058-01	*p*-OCF_3	0.014 ± 0.007 (49)	>50
NCGC00319036-01	*m*- CN	3.2 ± 1.0 (74)	>80
NCGC00319057-01	*p*-CN	0.12 ± 0.42 (100)	>80
NCGC00319069-01	*p*- $N(CH_3)_2$	0.16 ± 0.02 (100)	>50
NCGC00319067-01	*p*-$NHCH_3$	0.57 ± 0.24 (100)	Non-toxic
NCGC00319066-01	*p*- $COOCH_2CH_3$	0.009 ± 0.002 (100)	>80
NCGC00319054-01	*m*-methylsulfinyl	6.7 ± 3.2 (59)	Non-toxic
NCGC00319070-01	*p*-methanesulfonamide	>100	Non-toxic
NCGC00319071-01	*p*-$NHCOCH_3$	3.9 ± 2.3 (100)	>100
NCGC00319151-01	*m*-$CONH(CH_2)_3N(CH_3)_2$	2.4 ± 1.3 (70)	Non-toxic
NCGC00319150-01	*p*-$CONH(CH_2)_2N(CH_3)_2$	2.1 ± 1.4 (65)	Non-toxic
NCGC00319169-01	*p*-(4-methylpiperazinyl) methanone	6.9 ± 5.53 (70)	Non-toxic
NCGC00319072-01	*p*-piperazinyl	16.8 ± 5.7 (37)	>80
NCGC00319068-01	Morpholino-methanone	3.8± 1.5 (37)	Non-toxic

[a] Two-hybrid assay using a CMV-PPARδ-LBD-GAL4-DBD plasmid and a 6xGal4-luc reporter vector. The maximum concentration used for this assay was 100 μM of each compound; [b]Efficacy in PPARδ assay in respect to full activation with GW0742; [c]Cell-TiterGlo (Promega).

However, halide substituents (F and Cl) showed no significant difference between ortho, meta, or para positioning around the ring possibly due to their smaller atomic size or change in ligand orientation. Para positioned fluorine and chlorine substituents had similar but relative high EC_{50} values of around 0.14 µM (compounds NCGC00319055-01 and NCGC00319056-01). The least active PPARδ agonist was compound NCGC00319070-01 (SO_2NH_2) introducing high polarity with the ability to be both a hydrogen-bond donor and acceptor. Depending on its position within the LBP, the extra hydrogen bonding capability may not be favorable. Compound NCGC00319072-01 (piperazine) was another example where hydrogen bonding as a donor and acceptor may deactivate PPARδ with an EC_{50}= 16.8 ± 5.7.

Interestingly, many compounds possess partial agonistic activity against PPARδ although no evident trend was observed. Finally, most compounds exhibited LD_{50} values of higher then 80 µM. An exception was compound NCGC00319050-01 (*m*-Cl) with an LD_{50} of 28.8 µM. Poly-substituted phenyl rings found in Table 6 were also capable of activating PPARδ mediated transcription.

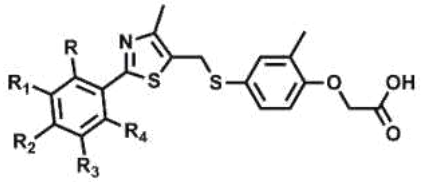

Table 6. Evaluation of poly-substituted GW0742 analogs.

Entry	R	R_1	R_2	R_3	R_4	PPARδ EC_{50} (μM)[a, (b)]	Toxicity LD_{50} (μM)[d]
NCGC00092344-05 (GW0742)	H	F	CF_3	H	H	0.0035 ± 0.00031 (100)	>50
NCGC00319082-01	H	CF_3	CF_3	H	H	0.99± 0.42 (46)	>50
NCGC00319145-01	CF_3	H	CF_3	H	H	0.20± 0.09 (50)	>50
NCGC00319172-01	Cl	H	CF_3	H	H	0.028 ± 0.013 (88)	>50
NCGC00344925-01	H	Cl	CF_3	H	H	0.007 ± 0.003 (75)	>33
NCGC00344922-01	H	Cl	OCF_3	H	H	0.009 ± 0.004 (69)	>50
NCGC00344921-01	H	F	OCF_3	H	H	0.020 ± 0.010 (100)	>50
NCGC00319077-01	H	OCH_3	OCH_3	H	H	1.06± 0.47 (44)	>100
NCGC00319159-01	H	F	OCH_3	H	H	0.074 ± 0.031 (100)	>100
NCGC00319154-01	H	CH_3	OCH_2CF_3	H	H	0.050± 0.028 (100)	>50
NCGC00319171-01	H	CF_3	F	H	H	0.49± 0.31 (100)	>50
NCGC00319147-01	F	F	F	H	H	0.042 ± 0.009 (100)	>80
NCGC00319168-01	H	F	F	F	H	0.046± 0.019 (100)	>100
NCGC00344924-01	H	Cl	F	H	H	0.18 ± 0.08 (43)	>50
NCGC00319153-01	H	CN	F	H	H	1.07± 0.59 (100)	>100
NCGC00319148-01	CF_3	H	Cl	H	H	0.18± 0.12 (63)	>50
NCGC00319143-01	H	CF_3	Cl	H	H	0.22± 0.09 (100)	>50
NCGC00344923-01	H	F	Cl	H	H	0.035 ± 0.011 (92)	>50
NCGC00319075-01	H	Cl	Cl	H	H	0.692 ± 0.137 (79)	>50
NCGC00319142-01	Cl	H	CN	H	H	0.066 ± 0.04 (100)	>100
NCGC00344926-01	H	Cl	H	F	H	0.17 ± 0.05 (62)	>50
NCGC00344927-01	H	CF_3	H	Cl	H	0.60 ± 0.28 (23)	>33
NCGC00319146-01	H	Cl	H	Cl	H	0.71± 0.27 (78)	>50
NCGC00344928-01	Cl	H	H	H	Cl	6.6 ± 4.8 (84)	>100
NCGC00344929-01	Cl	Cl	H	H	H	0.028 ± 0.017 (78)	>100
NCGC00344930-01	Cl	H	H	Cl	H	1.40 ± 0.74 (75)	>80
NCGC00319170-01	H	F	Benzyl-morpholine	H	H	4.3± 1.9 (50)	>100

[a] Two-hybrid assay using a CMV-PPARδ-LBD-GAL4-DBD plasmid and a 6xGal4-luc reporter vector. The maximum concentration used for this assay was 100 μM of each compound; [b]Efficacy in PPARδ assay in respect to full activation with GW0742; [c]Cell-TiterGlo (Promega).

The least active compound in our series was compound NCGC00344928-01 (*o,o*'Cl_2) with an EC_{50} of greater than 5 μM, indicating that two groups occupying both ortho positions of the phenyl ring is not favorable for PPARδ activation. Interestingly, by moving just one chloride to the R-3 position, like in compound NCGC00344929-01, greatly increased activity by 230-folds. The positioning of groups like CF_3, Cl, F and OCF_3 on phenyl ring positions gave some insight into PPARδ affinity. For example, by switching the *p*-CF_3 and *m*-F substituents on GW0742 to make compound NCGC00319171-01 (*m*-CF_3, *p*-F) a 500 fold decrease in potency was observed. When both those positions were occupied by CF_3 groups like in compound NCGC00319082-01, agonistic activity decreased 1000 fold compared to GW0742. If the CF_3 substituent was moved to the ortho position (compound NCGC00319145-01 (*o*-CF_3, *p*-CF_3)), an increase in potency was observed. An even more significant increase in activation was observed when the CF_3 group was changed to a chlorine (NCGC00319172-01 (*o*-Cl, *p*-CF_3) and even more when the chlorine was moved to the meta position (NCGC00344925-01 (*m*-Cl, *p*-CF_3) with a 7 nM affinity. With respect to all fluorine substituents, it appeared that two fluorine substituents were better than one regardless of their positioning, which was observed for all chlorine substituents as well. The toxicity of poly-substituted GW0742 analogs was, in general, higher than their mono-substituted counterparts, however none of them showed pronounced toxicity below 50 μM.

Heteroaromatic substituents were also coupled to the C-2 position of the thiazole ring and summarized in Table 7. Six compounds were able to activate PPARδ with an EC_{50} less than

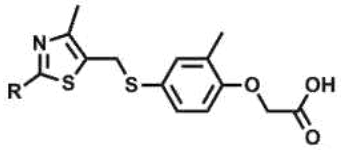

Table 7. Evaluation of heteroaromatic-substituted GW0742 analogs

Entry	R	PPARδ EC_{50} (μM) [a,(b)]	Toxicity LD_{50} (μM) [c]
NCGC00319037-01	3,5-dimethylisoxazol-4-yl	0.29± 0.12 (100)	>100
NCGC00319078-01	1*H*-indazol-4-yl	0.052± 0.035 (100)	>100
NCGC00319073-01	4-pyridine	9.1± 3.6 (81)	>80
NCGC00319074-01	2-(benzofuran-2-yl)	0.061± 0.028 (97)	>80
NCGC00319040-01	2,3-dihydrobenz[1,4]dioxin-6-yl	0.72± 0.23 (100)	>80
NCGC00319076-01	Naphthalene-1-yl	1.69± 0.34 (36)	>50
NCGC00319038-01	Benzo[1,3]dioxol-5-yl	0.26± 0.12 (52)	>50
NCGC00319039-01	Benzo[1,2,5]oxadiazol-5-yl	0.16± 0.04 (35)	>100
NCGC00319155-01	Furan-2-yl	6.0± 2.7 (96)	>100
NCGC00319173-01	Pyridin-3-yl	8.1± 5.6 (87)	>100
NCGC00319059-01	Benzothiophen-2-yl	0.026± 0.014 (100)	>100
NCGC00319162-01	Piperazin-1-yl	0.57± 0.39 (46)	>100
NCGC00319164-01	Pyrimidin-yl	1.57± 0.62 (51)	Non-toxic
NCGC00319149-01	1*H*-indazol-6-yl	3.18± 1.80 (100)	>100
NCGC00319160-01	Benzothiazol-6-yl	0.0738± 0.053 (100)	100
NCGC00319166-01	Isoquinolin-4-yl	0.35± 0.18 (51)	Non-toxic
NCGC00319163-01	6-fluoropyridin-3-yl	0.192± 0.082 (100)	Non-toxic
NCGC00319167-01	1-methyl-1*H*-indazol-6-yl	0.58± 0.34 (100)	>100
NCGC00319165-01	6-(trifluoromethyl)pyridin-3-yl	0.013 ± 0.006 (91)	>100
NCGC00319144-01	1-methyl-1*H*-indol-6-yl	0.52± 0.29 (100)	>100
NCGC00319157-01	1*H*-indol-5-yl	1.31± 0.42 (98)	>100
NCGC00319156-01	1*H*-pyrazol-4-yl	3.9 ± 1.7 (74)	Non-toxic
NCGC00319152-01	2-fluoropyridin-4-yl	3.3± 1.9 (100)	Non-toxic
NCGC00319158-01	1*H*-indazol-5-yl	1.44 ± 0.66 (64)	Non-toxic
NCGC00344920-01	Benzothiophen-5-yl	0.14 ± 0.08 (95)	>50
NCGC00344919-01	1*H*-indol-4-yl	>100	Non-toxic
NCGC00344918-01	1*H*-indol-2-yl	0.035 ± 0.015 (100)	>50

[a]Two-hybrid assay using a CMV-PPARδ-LBD-GAL4-DBD plasmid and a 6xGal4-luc reporter vector. The maximum concentration used for this assay was 100 μM of each compound; [b]Efficacy in PPARδ assay in respect to full activation with GW0742; [c]Cell-TiterGlo (Promega)

75 nM. Of these six, all but one had a bicyclic aromatic ring structure. This result was unexpected because of the rigidity and sheer bulkiness of the introduced substituents. However, it suggests that the LBD of PPARδ is spacious enough to accommodate such ligands, possibly through a

unique orientation unlike GW0742. From Table 5 we concluded that non-substituted phenyl ring structures such as compound NCGC00319174-01 made a poor PPARδ agonist. Similarly, substitution of the phenyl ring with a pyridine, as in compound NCGC319173-01, resulted in a poor PPARδ ligand. However, when the pyridine ring bears a trifluoromethyl group like compound NCGC319165-01, a 1600-fold increase in transcriptional activation was observed. This suggests the importance of the hydrophobic interactions between the trifluoromethyl of GW0742 with region II of PPARδ's LBP. The positioning of heterocyclic rings seemed to matter when comparing compounds NCGC00344918-01 and NCGC00344919-01. Both have an indole ring attached to C-2 of the thiazole but the 1*H*-indol-4-yl group (NCGC00344919-01) was nearly 3,000 times less potent than the 1*H*-indol-2-yl substituent (NCGC00344918-01). It could be speculated that the 1*H*-indol-4-yl ring unfavorably reaches into region III unlike GW0742, which interacts with region II of the Y-shaped PPARδ LBP. Interestingly, when docked in PPARδ LBP with respect to GW0742, the carboxylic acid region of NCGC00344919 reached out to region III residues (orange) and interacted with solvent molecules. This allowed for favorable hydrophobic interactions between region II residues (green) and 1*H*-indol-4-yl ring but an unfavorable conformation for a potent PPARδ agonist (Figure 41).

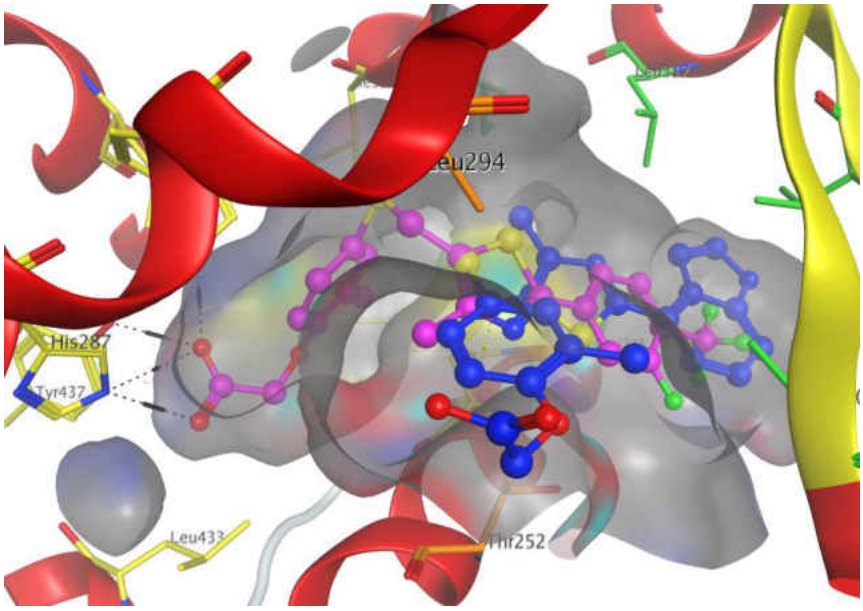

Figure 41. Overlay of GW0742 (pink) with compound NCGC00344919 (blue) in PPARδ LBP (PBD: 3TKM). Hydrogen bonding is shown in black dashes and hydrogen pi bonds are shown in yellow. Region I, II, and III are shown in yellow, green and orange, respectively.

Bioisoteric substitution of the carboxylate group with a tetrazole ring was used for several analogs to determine its effect on PPARδ-mediated transcription (Table 8). In general, increased toxicity and decreased potency was observed when compared to their carboxylate counterparts. Compound NCGC00264097-01 is most like GW0742 and had a 40 fold decrease in potency and a

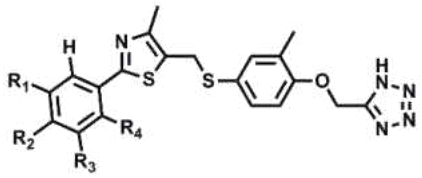

Table 8. Evaluation of tetrazole-substituted GW0742 analogs

Entry	R_1	R_2	R_3	R_4	PPARδ EC_{50} (μM) [a, (b)]	Toxicity LD_{50} (μM)[c]
NCGC00264097-01	H	CF_3	F	H	0.04± 0.018 (29)	>33
NCGC00344870-01	Cl	H	Cl	H	0.594 ± 0.435 (29)	>50
NCGC00344869-01	H	Cl	H	CF_3	0.51 ± 0.18 (51)	>33
NCGC00344871-01	H	Cl	Cl	H	0.24 ± 0.11 (26)	>33

[a]Two-hybrid assay using a CMV-PPARδ-LBD-GAL4-DBD plasmid and a 6xGal4-luc reporter vector. The maximum concentration used for this assay was 100 μM of each compound; [b]Efficacy in PPARδ assay in respect to full activation with GW0742; [c]Cell-TiterGlo (Promega).

two fold increase in toxicity. Although similar in acidity, the rigidity of the ring may decrease its ability to be a good hydrogen bond donor/acceptor with PPARδ. The two oxygens on the carboxylate group make hydrogen bonds with key residues like His413 (helix 10/11), Try437 (helix 12), His287 (helix 7) of PPARδ LBP and are implicated with maintaining the locked conformation of helix 12.[10] Overall, these compounds had the lowest efficacy ranging from 26-51% compared to any other series of thiazole compounds making them excellent partial agonist.

The replacement of the sulfur and oxygen linkers of GW0742 allowed investigations into geometry of successful PPARδ agonists (Table 9). In addition, the role of the methyl group on the

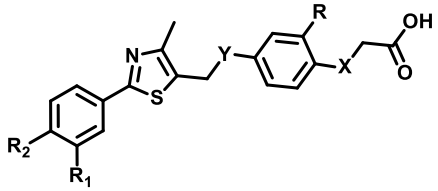

Table 9. Evaluation of linker-substituted GW0742 analogs.

Entry	R_1	R_2	Y	R	X	PPARδ EC_{50} (μM) [a,(b)]	Toxicity LD_{50} (μM)[c]
NCGC00264098-01	H	CF_3	S	CH_3	CH_2	0.039 ± 0.022 (87)	>100
NCGC00264099-01	F	CF_3	S	H	--	0.018 ± 0.010 (70)	>100
NCGC00263796-01	F	CF_3	S	H	O	0.026 ± 0.008 (84)	>100
NCGC00264094-01	F	CF_3	O	CH_3	O	0.02 ± 0.02 (73)	>100
NCGC00264104-01	F	CF_3	O	H	CH_2	0.032 ± 0.021 (77)	>100
NCGC00264093-01	F	CF_3	O	H	S	0.27 ± 0.023 (75)	>100
KAT-031513	H	CF_3	O	H	CH_2	0.703 ± 0.108 (100)	>100
NCGC00264101-01	F	CF_3	N	CH_3	O	0.18 ± 0.12 (61)	>100
NCGC00264103-01	F	CF_3	N	H	O	0.16 ± 0.045 (78)	>80
NCGC00264102-01	F	CF_3	N	H	CH_2	0.0576± 0.021 (95)	>80
KAT050713	CH_2OH	H	O	H	CH_2	18.2 ± 2.8 (47)	Non-toxic

[a]Two-hybrid assay using a CMV-PPARδ-LBD-GAL4-DBD plasmid and a 6xGal4-luc reporter vector. The maximum concentration used for this assay was 100 μM of each compound; [b]Efficacy in PPARδ assay in respect to full activation with GW0742; [c]Cell-TiterGlo (Promega).

linker was investigated in respect to its role in favorable PPARδ binding. Compound NCGC00263796-01 was structurally similar to GW0742 except for the removal of the methyl in the R position. Without the methyl group, this compound had an EC_{50} that was 10 times less

potent than GW0742 and surprisingly behaved as a partial agonist (84% in comparison with GW0742). A large decrease in potency was observed for compound KAT-031513 when Y was replaced with a smaller oxygen atom and X with a CH_2 in the absence of a fluoride and methyl group in positions R_1 and R, respectively. KAT-031513 was ~700 times less potent than GW0742. When compared to compound NCGC00264104-01 with a fluorine in the R_1 position this difference was only 22 fold less suggesting the necessity of the hydrophobic interactions between PPARδ LBP and the fluoride. However, if the Y linker was exchanged with a nitrogen, the presence of a fluoride on position R_1 did not benefit the activity of these compounds. Overall, the nitrogen linker produced compounds that were about 125 times less able to activate PPARδ transcription compared to GW0742. Only when the X linker is exchanged with a CH_2 group does the potency increase. When comparing NCGC00264101-01 and NCGC00264103-01, the presence or absence of an R positioned methyl had little effect on activation of transcription thus producing agonists that were 200 times less potent than GW0742. The least potent compound was KAT-050713 with the addition of a meta-CH_2OH substituent on the phenyl ring where the linkers were the same as that of KAT-031513. It was approximately 18,000 times less potent than GW0742 suggesting that hydrogen bond donor and acceptor moieties are not favorable for PPARδ binding.

The SAR study of GW0742 analogs has given us some inside in the structural requirements for successful GW0742 ligands. In addition, structural elements have been identified that significantly reduced the ability of ligands to activate PPARδ-mediated transcription. These ligands are summarized in Table 10 with EC_{50} values higher than 1 μM.

Table 10. Compounds that showed an activation of PPARδ greater than 1μM.

Entry	VDR-SRC2-3 interaction (IC_{50}) μM[a]	VDR transcription IC_{50} (μM)[b]
NCGC00319071-05	40.11± 9.26	inactive
NCGC00319064-01	32.27± 5.28	31.5± 9.1
NCGC00319047-01	45.18± 5.65	31.4± 8.1
NCGC00319036-01	>100	25.1± 10.0
NCGC00319054-01	>100	>100
NCGC00319151-01	30.28± 4.5	inactive
NCGC00319150-01	52.03± 12.79	>100
NCGC00319082-01	9.088± 0.982	15.0± 4.7
NCGC00319077-01	>10	>50
NCGC00319153-01	53.53± 15.95	23.7± 4.7
NCGC00344928-01	40.28± 8.07	33.0 ± 7.2
NCGC00344930-01	14.47±2.21	>50
NCGC00319073-01	43.88± 8.54	inactive
NCGC00319076-01	20.19± 1.89	26.3±0 8.3
NCGC00319068-01	>100	>100
NCGC00319170-01	68.79± 13.04	>50
NCGC00319155-01	>100	>50
NCGC00319173-01	>100	>100
NCGC00319164-01	>100	inactive
NCGC00319149-01	57.78± 8.69	inactive
NCGC00319157-01	15.07± 11.79	>50
NCGC00319156-01	>100	inactive
NCGC00319152-01	>100	>100
NCGC00319158-01	51.14± 5.55	inactive
NCGC00344919-01	28.93± 4.69	inactive
NCGC00319053-01	47.45± 6.61	38.2± 8.6
NCGC00319049-01	24.5± 2.27	19.0± 6.01
NCGC00319052-01	48.82± 6.56	26.3± 6.9
NCGC00319169-01	>100	24.5 ± 6.1
NCGC00319072-01	>100	inactive
KAT050713	inactive	inactive

[a]VDR-LBD concentration used was 0.1μM. Inhibition of VDR-SRC2-3 interaction in the presence of LG190178 (0.75 μM). The maximum concentration used for this assay was 300 μM of each compound; [b]Transcription assay using a CMV-VDR plasmid and a luciferase reporter plasmid under control of a 24-hydroxylase promoter with GW0742 analogs. The maximum concentration used for this assay was 100 μM of each compound. Data were analyzed using a nonlinear regression with a variable slope (GraphPad Prism).

Subsequently, a fluorescence polarization assay employing VDR and an Alexa Fluor 647 labeled SRC2-3 peptide was used to determine the ability of these compound to inhibit the interaction between VDR and coregulators. Inhibition of VDR-mediated transcription was evaluated in HEK293T cells in the presence of VDR ligand $1,25(OH)_2D_3$. None of the GW0742 analogs exhibited nanomolar activity in the VDR FP assay or the transcription assay thus selectivity towards VDR was not achieved. In addition, we found large differences for some compounds in regards to their activity determined in the biochemical and cell-based assay indicating the involvement of other mechanism. GW0742 is able inhibit VDR-coregulators interactions in the FP-assay at 7.73 μM and in the cell-based assays at 12.7 μM. NCGC00319082-01 bearing two trifluormethyl groups at the meta and para position of the phenyl ring exhibited similar activity towards VDR although its ability to activate PPARδ is more than 300-fold less than GW0742. Thus is seems that region II of PPARδ consisting of V305, V312, and V245 is less accommodating to larger groups perpendicular to the molecule axis than VDR. Compounds NCGC00319049-01 and NCGC00319076-01 are similar in this respect bearing a meta positioned trifluormethyl group and naphthalene group, respectively. As depicted in Figure 42A, the naphthalene group of NCGC00319076-01 is accommodated in what would be region I of PPARδ. This conformation is stabilized further by pi bond interactions between His397 and His 305 and the naphthalene ring. In Figure 42B, the naphthalene ring is forced into region II of PPARδ pocket thus forcing it into a sterically unfavorable conformation with residues like Val305.

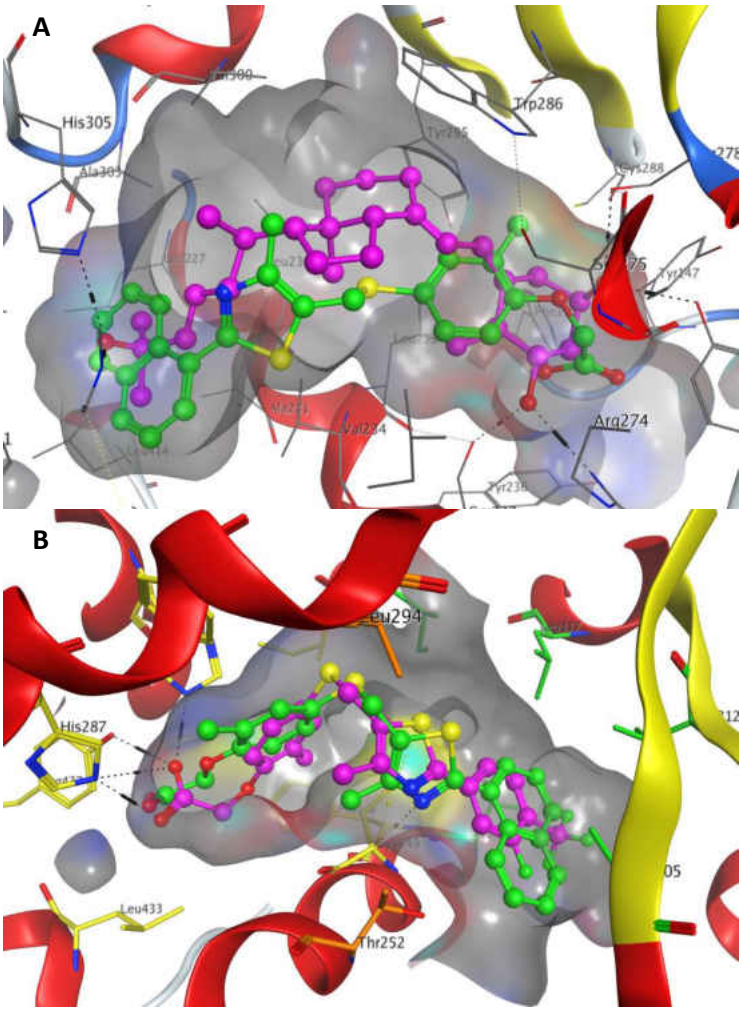

Figure 42. Docked in green is compound NCGC00319076. A) VDR LBP co-crystallized with 1,25$(OH)_2D_3$ (pink) (PDB: 1DBI)[8]. B) PPARδ LBP co-crystallized with GW0742 (pink) (PDB: 3TKM). Region I, II, and III are shown in yellow, green and orange, respectively.

3.3.3 Conclusion

The synthesis of analogs of GW0742 established a good SAR for the activation of PPARδ. Substituents such as CF_3, OCF_3 and $CO_2CH_2CH_3$ in the para-position of the GW scaffold were important for high activity suggesting a balance between hydrophobicity and electron density for successful interaction PPARδ. Additional aromatic substituents had a significant impact on the activity, with fluorine and chlorine substituents in the meta position being the most favorable. An attempt to substitute the phenyl ring with other heterocyclic groups did not yield in better ligands, however the results provided an insight of the size and tolerance of region III of PPARδ. The screen of the least active PPARδ ligands with VDR did not result in a clear SAR towards VDR binding. However a weak correlation between PPARδ and VDR binding was observed as depicted in Figure 43, when log of PPARδ EC_{50} (μM) was plotted against the log of VDR IC_{50} (μM). It was evident that when making a potent VDR inhibitor it often resulted in a potent PPARδ agonist.

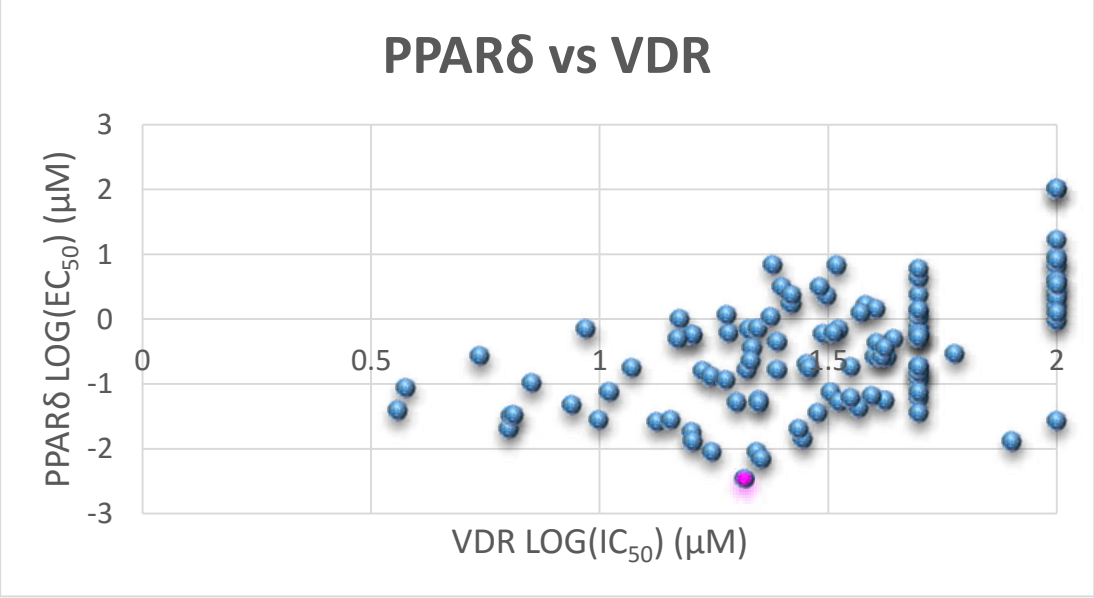

Figure 43. Log PPARδ EC_{50} (μM) was plotted against Log VDR IC_{50} (μM) to demonstrate the selectivity and potency of GW0742 analogs tested. GW0742 is highlighted in pink.

Unfortunately, most compounds exhibited poor inhibition of VDR, while still activating PPARδ in the sub-micromolar range or better as seen in the bottom right quadrant of the plot. Overall, we produced many potent PPARδ agonist that could be evaluated in PPARδ-related diseases such as obesity. Future experiments are ongoing in collaboration with Prof. Silvaggi here at UWM by attempting to co-crystallize any of the GW0742 analogs with VDR. With the crystal structure, computer based rational design could be used to develop a more potent and selective inhibitor of VDR based on the GW0742 scaffold.

Part 3: Development of Oxazole-Substituted GW0742 Analogs and Their Effect on Nuclear Receptor Mediated Transcription

3.1. Purpose

To improve the potency and selectivity of the GW0742-based VDR–coactivator inhibitors, we substituted the thiazole moiety with an oxazole, because GlaxoSmithKline reported that compound 7f had low activity towards all isoforms of PPAR (Table 11). In addition, our previous

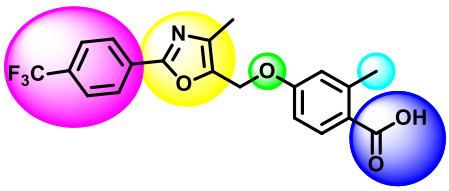

Table 11. Binding data reported by GlaxoSmithKline for compound 7f.

Cmpd	PPARα EC_{50} (μM)[a]	PPARγ EC_{50} (μM)[a]	PPARδ EC_{50} (μM)[a]	PPARδ IC_{50} (μM)[b]
7f	Inactive	Inactive	5.9 ± 5.5	5.5± 0.28

[a] Cell-based transactivation assay and [b]binding assay against human PPAR receptors.

study showed that GW0742 analogs with methoxy substitution such as *o*-OCH_3 (VDR IC_{50}= 31.4 ± 8.11 μM, PPARδ EC_{50}= 2.25± 0.69 μM) and *m*-OCH_3 (VDR IC_{50}= 26.3± 6.93 μM, PPARδ EC_{50}= 2.36±

0.67 µM) had relatively good VDR activity and poor PPARδ activity. Docking studies with an oxazole analog containing a *m*-OCH_3 substituted phenyl ring revealed that this shorter and more ridged molecule was unable to bind His413 and His287 but rather Tyr437 and His287 (Figure 44).

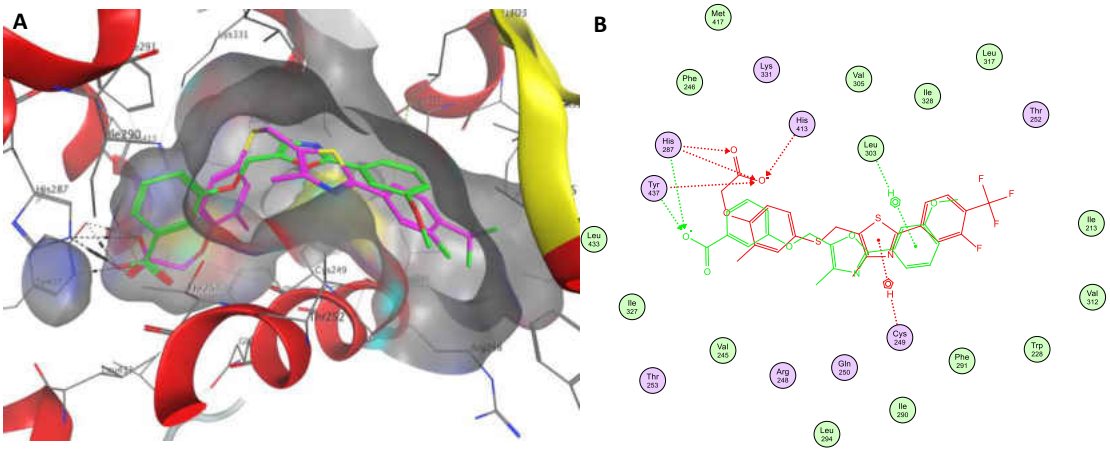

Figure 44. Virtual docking with PPARδ co-crystallized with GW0742 (PBD: 3TKM) were used to visualize the affects an oxazole substitution would have on binding. A) GW0742 analog containing an oxazole (lime green) overlaid GW0742 (pink). Hydrogen bonding is shown in black dashes and hydrogen pi bonds are shown in yellow. B) A 2D depiction of the interactions GW0742 (red) and GW0742 oxazole analog (lime green) have with PPARδ LBP.

Furthermore, the molecule did not reach as deeply into the pocket of region III, thus making less hydrophobic interactions. Within Part 3, we report the synthesis of the ortho and meta methoxy GW0742 oxazole analogs, which were evaluated using both biochemical and cell-based assays to determine their affinity and selectivity towards VDR and PPARδ. In addition to the acids, the corresponding methyl esters of the acids were studied. Furthermore, a solubility assay and a permeability assay were utilized to characterize both the ester and acid forms of the GW0742 derived oxazoles.

3.2 Chemistry

3.2.1. Synthetic Strategy

The formation of the oxazole ring was accomplished through a modified Hantzch reaction, where either 2- or 3-methoxybenzamide was reacted with ethyl 2-chloroacetoacetate (Scheme 5, i).[159, 160] The mechanism for the modified Hantzch reaction begins with a nucleophilic attack,

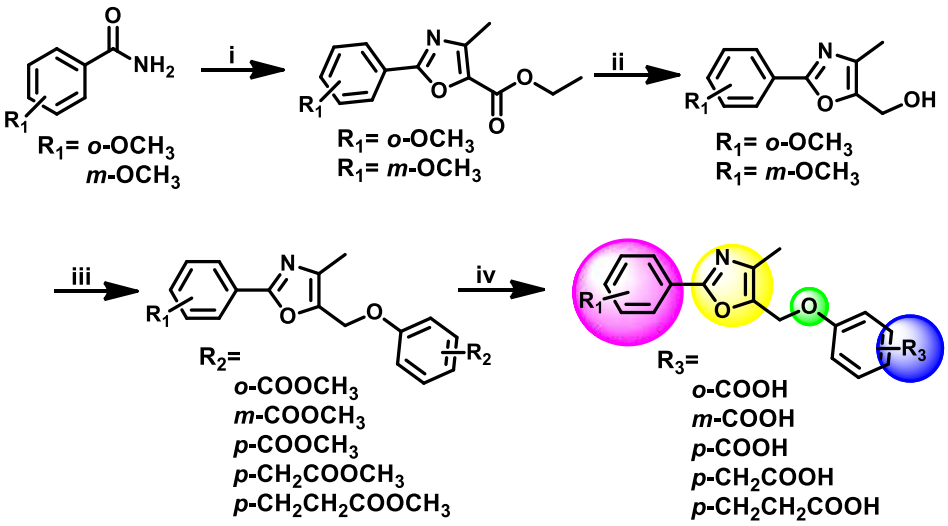

Scheme 5. Synthesis of GW0742-based analogs with an oxazole subsitituion. i) Ethyl-2-chloro acetoacetate, neat, 120-125°C, 3 days; i) $LiAlH_4$, THF, 0°C to room temperature, 3 hours; iii) a) $SOCl_2$, DCM, 1-2 hours, b) Cs_2CO_3, DMF, phenol; iv) a) THF, 2M NaOH aq., 40-70°C, overnight, b) HCl.

loss of HCl and the formation of an imine. Cyclization occurs with the nitrogen on the imine attacking the acetyl carbonyl (Figure 45). A loss of water affords the final oxazole product.

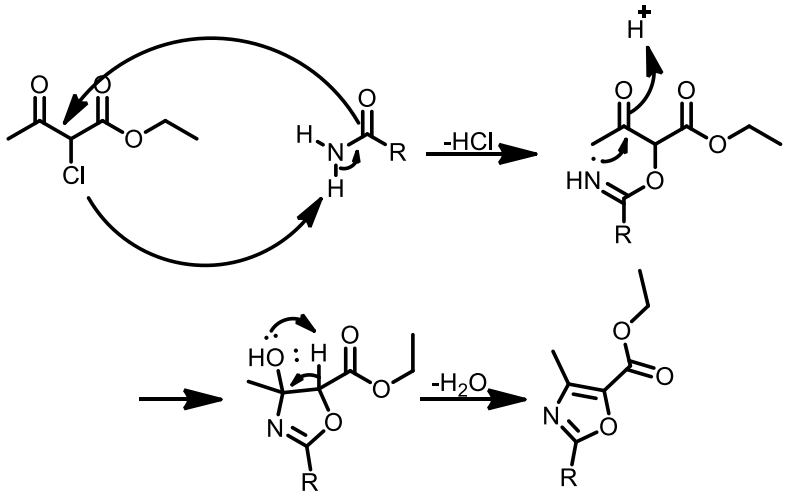

Figure 45. Mechanism for a modified Hantzch reaction.

$LiAlH_4$ was used to produce the corresponding primary alcohols, which were converted into chlorides using thionyl chloride. Subsequent coupling of different phenols afforded the corresponding esters, which were hydrolyzed in the presence of NaOH to yield the final carboxylic acids.

3.2.2 Characterization

All starting materials were purchased either from Sigma-Aldrich or Fisher Scientific without further purification. Anhydrous solvents were purchased in sure-seal bottles and handled under dry conditions using syringe technique. All glassware was dried overnight at 100^{o}C before use. Thin layer chromatography was performed on pre-coated silica gel 60 F254 plates (Fisher Scientific). Synthesized compounds were purified by normal phase flash chromatography (SPI Biotage, silica gel 230-400 mesh) and concentrated under vacuum. All pure compounds were stored at -20^{o}C. Compound characterization was performed using a Shimadzu 2020 LC-MS (single quadrupole) instrument with compounds directly injected. NMR spectra were recorded on a Bruker 300MHz instrument with samples diluted in either $CDCl_3$ or DMSO- D_6.

General Procedure for Hantzsch Reaction: To substituted benzamide (29.6 mmols), ethyl-2-chloro acetoacetate (148 mmols, 5 equiv.) was added. The solution was stirred neat at 120-125°C for 48-72hrs or until the disappearance of the benzamide on TLC using EtOAc-hexanes (4:1, v/v). To remove any unreacted ethyl-2-chloro acetoacetate, the resulting orange-yellow solution was subjected to vacuum distillation (60°C, 1.8 mbar) followed by purification on silica gel with EtOAc-hexanes (2-35% strong) using a normal phase flash chromatography system.

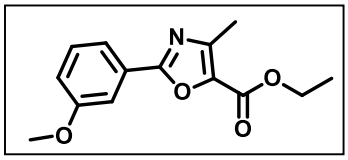

JWB071813 66 % yield; ^{1}H-NMR (300 MHz) ($CDCl_3$) δ 7.76-7.73 (d, 1H, J=9.0 Hz), 7.65 (s, 1H), 7.43-7.38 (t, 1H, J=8 Hz), 7.06 (d, 1H), 4.47-4.40 (q, 2H, J=7 Hz)), 3.91 (s, 3H), 2.57 (s, 3H), 1.46-1.42 (t, 3H, J=6 Hz); ^{13}C-NMR δ 162.1, 159.8, 158.8, 146.9, 137.4, 130.0, 127.6, 120.3, 118.2, 111.5, 61.1, 55.5, 14.4, 13.51. MS DUIS calcd. *m/z* for $C_{14}H_{15}NO_4$ [(M)] 261.3, found [$(M+H)^+$] 262.4 .

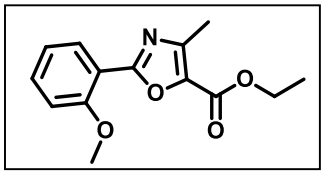

JWB080513-1 50% yield; ^{1}H-NMR (300 MHz) ($CDCl_3$) δ 8.04-8.01 (d, 1H, J= 9 Hz), 7.51-7.45 (t, 1H, J= 9 Hz), 7.09-7.03 (t, 2H, J= 9 Hz), 4.45-4.38 (q, 2H, J=8 Hz), 3.99 (s, 3H), 2.58 (s, 3H), 2.18 (s, 2H), 1.45-1.40 (t, 3H, J= 8 Hz); ^{13}C-NMR δ 161.0, 159.0, 158.2, 146.7, 137.0, 132.9, 130.9, 120.7, 115.4, 112.0, 61.0, 56.2, 14.4, 13.5. MS DUIS calcd. *m/z* for $C_{14}H_{15}NO_4$ [(M)] 261.3, found [$(M+H)^+$] 262.4.

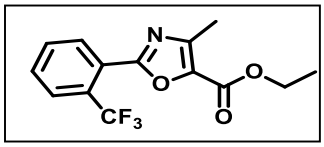

JWB080513-2 30% yield; ^{1}H-NMR (300 MHz) ($CDCl_3$) δ8.04-8.02 (d, 1H, J=), 7.87-7.84 (d, 1H, 7.71-7.62, ^{13}C-NMR δ160.0, 158.6, 146.6, 138.6, 131.8, 131.7, 131.0, 129.6-128.3 (m, fluorine coupling), 127.0-126.90 (m, fluorine coupling), 125.3, 121.5, 61.2, 14.2, 13.4.

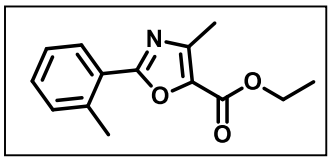

KAT090513 40% yield; ^{1}H-NMR (300 MHz) ($CDCl_3$) δ 8.10-8.08 (d, 1H, J= 6 Hz), 7.58-7.56 (d, 1H, J= 6 Hz), 7.42-7.32 (m, 2H), 4.46-4.39 (q, 2H, J= 7 Hz), 2.73 (s, 3H), 2.58 (s, 3H), 1.46-1.41 (t, 3H, J= 7.5 Hz) ; ^{13}C-NMR δ 162.8, 159.0, 146.68, 138.3, 131.7, 131.6, 129.6, 127.2, 126.1, 125.6, 61.0, 21.9, 14.4, 13.6; MS DUIS ($^{+}$ve) calcd. *m/z* for $C_{14}H_{15}NO_3$ [(M)] 245.3, found [$(M+H)^{+}$] 246.4.

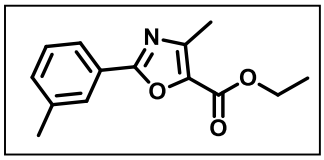

JWB072413 30% yield; ^{1}H-NMR (300 MHz) ($CDCl_3$) δ 7.96 (s, 1H), 7.95-7.92 (d, 1H, J=9 Hz), 7.40-7.31 (m, 2H), 4.46-4.39 (q, 2H, J=7 Hz), 2.55 (s, 3H), 2.43 (s, 3H), 1.43-1.41 (t, 3H, J= ; ^{13}C-NMR δ 162.9, 158.9, 147.0, 138.7, 137.3, 132.1, 128.8, 127.6, 126.2, 124.8, 61.1, 21.3, 14.7, 13.5. ^{13}C-NMR δ. MS DUIS ($^{+}$ve) calcd. *m/z* for $C_{14}H_{15}NO_3$ [(M)] 245.3, found [$(M+H)^{+}$] 246.4.

General Procedure for Reduction of Ester: $LiAlH_4$ (22.8 mmol, 2.5 eq) was slowly dissolved in dry THF (75mL) on ice. The appropriate oxazole ester, 1a or 2a, (9.12 mmol) was dissolved in dry THF (75mL) and added dropwise to the $LiAlH_4$. After addition was complete, the reaction was warmed to room temperature and stirred for 2.5 hours or until the disappearance of the starting material. The reaction was monitored by TLC using Hexanes-EtOAc (4:1, v/v). 3M HCl was added dropwise (pH= 1-2) to make a cloudy white solution. The solution was diluted in EtOAc and washed with brine and water, dried over anhydrous $MgSO_4$ and concentrated *in vacuo* to give a white solid. No further purification was needed.

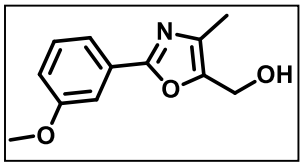

JWB072213 100% yield; ^{1}H-NMR (300 MHz) ($CDCl_3$) δ 7.61-7.59 (d, 1H, J= 6.0 Hz), 7.54 (s, 1H), 7.37-7.32 (t, 1H, J= 7.0 Hz), 7.01-6.89 (d, 1H, J= 6.0 Hz), 4.69 (s, 2H), 3.87 (s, 3H), 2.23 (s, 3H); ^{13}C-NMR δ 160.5, 159.9,

145.7, 134.8, 129.9, 128.2, 118.8, 117.2, 110.7, 55.4, 54.2, 11.4; MS DUIS ($^+$ve) calcd. *m/z* for $C_{12}H_{13}NO_3$ [(M)] 219.2, found [$(M+H)^+$] 220.4.

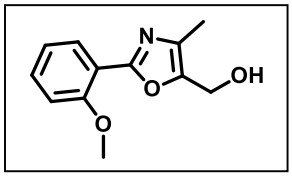

JWB082113-2 40% yield; ^{1}H-NMR (300 MHz) ($CDCl_3$) δ 7.84-7.82 (d, 1H, J= 6), 7.36-7.33 (t, 1H, J= 7.5), 6.99-6.94 (m, 2H), 4.60 (s, 2H), 3.88 (s, 3H), 2.13 (s, 3H); ^{13}C-NMR δ 158.8, 157.4, 145.4, 134.5, 131.6, 130.2, 120.6, 116.4, 111.8, 55.9, 53.9, 11.25; MS DUIS ($^+$ve) calcd. *m/z* for $C_{12}H_{13}NO_3$ [(M)] 219.2, found [$(M+H)^+$] 220.4

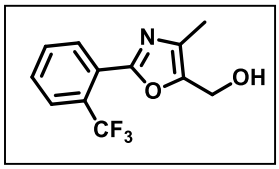

JWB080713 100% yield; ^{1}H-NMR (300 MHz) ($CDCl_3$) δ 8.01-7.98 (d, 1H, J=9 Hz), 7.83-7.80 (d, 1H, J= 9 Hz), 7.67-7.56 (m, 2H), 4.71 (s, 2H), 2.28 (s, 3H); ^{13}C-NMR δ 159.1, 147.6, 135.6, 132.6, 132.1, 131.0, 129.3, 128.7, 127.6, 127.5, 54.6, 11.7; MS DUIS ($^+$ve) calcd. *m/z* for $C_{12}H_8F_3NO_3$ [(M)] 257.2, found [$(M+H)^+$] 258.4

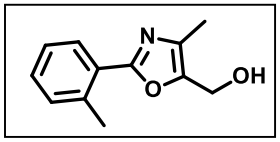

KAT092613 92% yield; ^{1}H-NMR (300 MHz) ($CDCl_3$) δ 7.98-7.95 (d, 1H, J= 9), 7.35-7.30 (m, 4H), 4.73 (s, 2H), 2.69 (s, 3H), 2.29 (s, 3H); ^{13}C-NMR δ 161.1, 145.1, 137.3, 134.6, 131.5, 129.9, 128.9, 126.5 125.9, 54.2, 21.8, 11.4; MS DUIS ($^+$ve) calcd. *m/z* for $C_{12}H_{11}NO_3$ [(M)] 203.2, found [$(M+H)^+$] 204.4

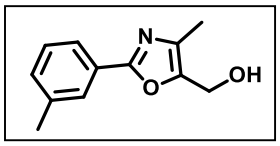

JWB082113-1 40% yield; ^{1}H-NMR (300 MHz) ($CDCl_3$) δ 7.84 (s, 1H), 7.81-7.79 (d, 1H, J=6 Hz), 7.35-7.24 (m, 2H), 4.68 (s, 2H), 2.40 (s, 3H), 2.22 (s, 3H); ^{13}C-NMR δ 160.7, 145.7, 138.5, 134.5, 131.2, 128.6, 127.0, 126.8, 123.4, 53.8, 21.3, 11.2; MS DUIS ($^+$ve) calcd. *m/z* for $C_{12}H_{11}NO_3$ [(M)] 203.2, found [$(M+H)^+$] 204.4

General Procedure for Chlorination and Coupling Reaction: The appropriate reduced oxazole (0.739 mmol) was mixed with thionyl chloride (3.69 mmol, 5 equiv.) in dry DCM (5mL). The

reaction was stirred at room temperature and monitored by TLC using EtOAc-Hexanes (3:2, v/v) for an hour or until completion. The reaction vessels were dried under vacuum to remove DCM. The crude product was used for the next reaction without purification. Phenol (0.738 mmol, 1 equiv.) and Cs_2CO_3 (1.48 mmol, 2 equiv.) were mixed in dry DMF (5mL) and stirred at room temperature for 30 minutes. A notable yellow color was observed after 30 minutes. The chloro oxazole in dry DMF (5mL) was added and the reaction was stirred at room temperature overnight. The reaction was monitored by TLC using EtOAc-hexanes (3:2, v/v). Once complete, the reaction was quenched by the slow addition of a saturated $NaHCO_3$ solution until carbon dioxide formation ceased followed by the extraction with EtOAc. The organic layer was dried over $MgSO_4$ and concentrated in vacuo to obtain a yellow oil. The oil was further purified on silica gel with hexanes- EtOAc (2-70%, strong) using a normal phase flash chromatography system.

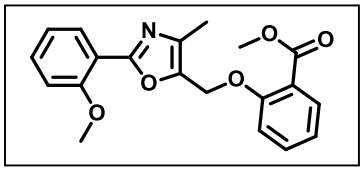

KAT092013-1 57% yield; ^{1}H-NMR (300 MHz) ($CDCl_3$) δ 7.91-7.89 (d, 1H, J= 6 Hz), 7.79-7.76 (d, 1H, J= 9Hz), 7.45-7.35 (m, 2H), 7.12-7.09 (d, 1H, J= 9), 7.04-6.97 (m, 3H), 5.15 (s, 2H), 3.91 (s, 3H), 3.82 (s, 3H), 2.25 (s, 3H); ^{13}C NMR δ 166.6, 159.4, 157.6, 157.5, 141.5, 137.0, 133.3, 131.9, 131.6, 130.3, 121.9, 121.6, 120.5, 116.3, 115.9, 111.81, 61.6, 56.0, 52.1, 11.6; MS DUIS ($^+$ve) calcd. *m/z* for $C_{20}H_{19}NO_4$ [(M)] 353.2, found [$(M+1)^+$] 354.4.

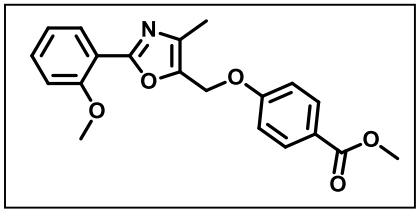

KAT092313-2 20% yield; ^{1}H-NMR (300 MHz) ($CDCl_3$) δ 8.04-8.01 (d, 2H, J= 9Hz), 7.93-7.91 (d, 1H, J=6 Hz), 7.45-7.39 (t, 1H, J= 7.5 Hz), 7.06-7.00 (t, 4H, J=9 Hz), 5.13 (s, 2H), 3.95 (s, 3H), 3.89 (s, 3H), 2.32 (s, 3H) ; ^{13}C NMR δ 170.1, 166.7, 162.0, 159.7, 157.6, 141.1, 137.2, 131.9, 131.6, 130.4,

123.2, 120.6, 116.6, 114.5, 111.9, 59.6, 56.0, 51.9, 11.7 ; MS DUIS ($^+$ve) calcd. *m/z* for $C_{20}H_{19}NO_4$ [(M)] 353.2, found [$(M+1)^+$] 354.4.

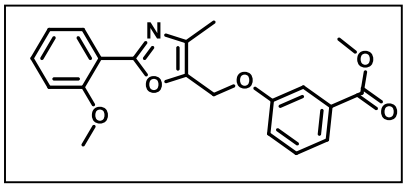

KAT092413-3 51% yield; ^{1}H-NMR (300 MHz) ($CDCl_3$) δ 7.93-7.90 (d, 1H, J=9Hz), 7.68 (s, 1H), 7.65 (s, 1H), 7.42-7.31 (m, 2H), 7.19-7.16 (d, 1H, J= 9Hz), 7.03-6.97 (t, 2H, J= 9Hz), 5.11 (s, 2H), 3.91 (s, 3H), 3.89 (s, 3H), 2.31 (s, 3H). ^{13}C NMR δ 166.75, 159.6, 158.2, 157.6, 141.31, 137.0, 131.8, 131.5, 130.3, 129.5, 122.7, 120.6, 120.5, 116.3, 115.1, 111.8, 60.4, 59.7, 56.0, 52.2, 11.65; MS DUIS ($^+$ve) calcd. *m/z* for $C_{20}H_{19}NO_4$ [(M)] 353.2, found [$(M+1)^+$] 354.4.

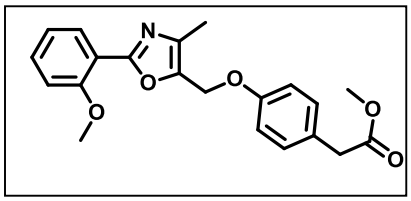

KAT092513-4 20% yield; ^{1}H-NMR (300 MHz) ($CDCl_3$) δ 7.94-7.92 (d, 1H, J= 6Hz), 7.46-7.40 (t, 1H, J= 9Hz), 7.25-7.22 (d, 2H, J= 9Hz), 7.07-6.97 (m, 4H), 5.08 (s, 2H), 3.95 (s, 3H), 3.70 (s, 3H), 3.59 (s, 2H), 2.31 (s, 3H); ^{13}C NMR δ 172.3, 159.5, 157.6, 157.5, 141.7, 126.8, 131.8, 131.8, 130.4, 126.9, 120.6, 116.4, 115.2, 111.9, 59.8, 56.1, 52.0, 40.3, 11.7 ; MS DUIS ($^+$ve) calcd. *m/z* for $C_{21}H_{21}NO_5$ [(M)] 367.4, found [$(M+H)^+$] 368.5.

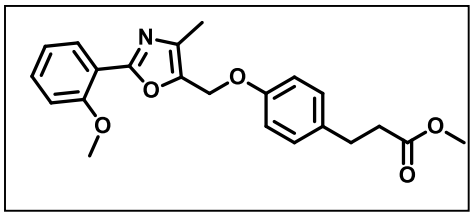

KAT092513-5 22% yield; ^{1}H-NMR (300 MHz) ($CDCl_3$) δ 8.14 (d, 1H), 7.46-7.40 (t, 1H, J= 9Hz), 7.17-7.14 (d, 2H, J= 9Hz), 7.07-7.02 (t, 2H, J= 7.5Hz), 6.97-6.94 (d, 2H, J= 9Hz), 5.06 (s, 2H), 3.96 (s, 3H), 3.68 (s, 3H), 2.95-2.90 (t, 2H, J= 7.5Hz), 2.65-2.60 (t, 2H, J= 7.5Hz), 2.31 (s, 3H); ^{13}C NMR δ 173.6, 159.5, 157.6, 156.8, 141.8, 136.7, 133.5, 131.8, 130.4, 129.3, 120.6, 116.4, 115.2, 111.9, 59.8, 56.1, 51.6, 35.9, 30.1, 11.6; MS DUIS ($^+$ve) calcd. *m/z* for $C_{22}H_{23}NO_5$ [(M)] 381.4, found [$(M+H)^+$] 382.4.

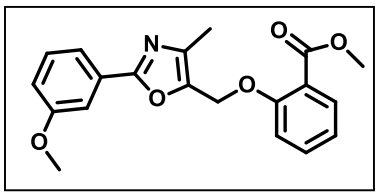

JWB091313-1 42% yield; ^{1}H-NMR (300 MHz) ($CDCl_3$) δ 7.83-7.81 (d, 1H, J= 6Hz), 7.65-7.63 (d, 1H, J= 6Hz), 7.57 (s, 1H), 7.52-7.47 (t, 1H, J= 7.5 Hz), 7.40-7.34 (t, 1H, J= 9Hz), 7.14-7.07 (m, 2H), 7.03-7.00 (d, 2H, J= 9Hz), 5.19 (s, 2H), 3.89 (s, 3H), 3.87 (s, 3H), 2.26 (s, 3H); ^{13}C NMR δ166.6, 160.9, 159.8, 157.5, 141.9, 137.3, 133.4, 131.7, 129.9, 128.4, 122.1, 121.8, 118.8, 117.1, 116.0, 110.8, 61.6, 55.4, 52.1, 36.4, 31.4, 11.5; MS DUIS ($^{+}$ve) calcd. *m/z* for $C_{20}H_{19}NO_5$ [(M)] 353.4, found [$(M+H)^{+}$] 354.4.

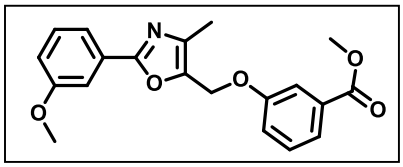

JWB091313-2 66% yield; ^{1}H-NMR (300 MHz) ($CDCl_3$) δ 7.72 (s, 1H), 7.70 (s, 1H), 7.66-7.63 (d, 1H, J= 9Hz), 7.57 (s, 1H), 7.42-7.34 (q, 2H, J= 8Hz), 7.22- 7.19 (d, 1H, J= 9Hz), 7.02-7.00 (d, 1H, J= 6Hz), 5.14 (s, 2H), 3.94 (s, 3H), 3.88 (s, 3H), 2.32 (s, 3H); ^{13}C NMR δ 166.7, 161.0, 159.8, 158.1, 144.8, 137.3, 131.5, 129.8, 129.6, 128.3, 122.8, 120.6, 119.7, 119.4, 117.1, 114.8, 110.8, 59.6, 52.2, 11.6. MS DUIS ($^{+}$ve) calcd. *m/z* for $C_{20}H_{19}NO_5$ [(M)] 353.4, found [$(M+H)^{+}$] 354.4.

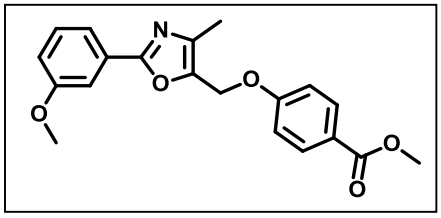

JWB091313-3 38% yield; ^{1}H-NMR (300 MHz) ($CDCl_3$) δ 8.07-8.04 (d, 2H, J= 9Hz), 7,67- 7.64 (d, 1H, J=9Hz), 7.60 (s, 1H), 7.41-7.35 (t, 1H, J= 9Hz), 7.07-7.04 (d, 1H, J= 9Hz), 7.01 (s, 1H), 5.14 (s, 2H), 3.92 (s, 3H), 3.90 (s, 3H), 2.33 (s, 3H); ^{13}C NMR δ 166.7, 161.9, 161.2, 159.9, 141.5, 137.5, 137.5, 131.7, 129.9, 128.3, 123.4, 118.9, 117.3, 114.4, 110.9, 59.5, 55.45, 51.9, 11.64; MS DUIS ($^{+}$ve) calcd. *m/z* for $C_{20}H_{19}NO_5$ [(M)] 353.4, found [$(M+H)^{+}$] 354.4.

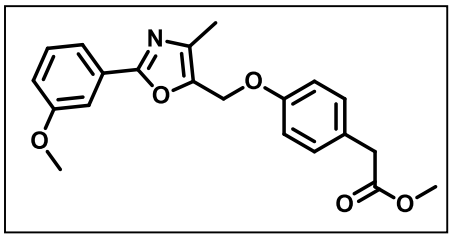

JWB091313-4 57% yield; ^{1}H-NMR (300 MHz) ($CDCl_3$) δ 7.63-7.61 (d, 1H, J= 6Hz), 7.56 (s, 1H), 7.35-7.30 (t, 1H, J= 7.5Hz), 7.23- 7.21 (d, 2H, 6Hz), 6.99 (s, 1H), 6.97-6.94 (d, 2H, J= 9Hz), 5.02 (s, 2H), 3.82 (s, 3H), 3.67 (s, 3H), 3.57 (s, 2H) 2.26 (s, 3H); ^{13}C NMR δ 172.3, 161.0, 159.9, 157.3, 142.2, 137.0, 130.4, 128.3, 127.1, 119.4, 118.9, 117.2, 110.8, 59.6, 55.4, 52.0, 40.3, 36.5, 11.5; MS DUIS ($^{+}$ve) calcd. *m/z* for $C_{21}H_{21}NO_5$ [(M)] 367.4, found [$(M+H)^{+}$] 468.5.

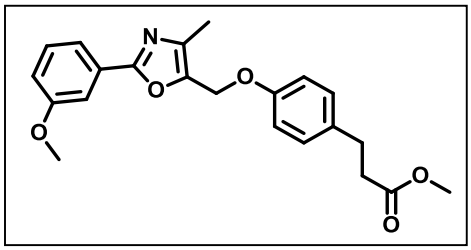

JWB091313-5 33% yield; ^{1}H-NMR (300 MHz) ($CDCl_3$) δ 7.65-7.63 (d, 1H, J= 6Hz), 7.58 (s, 1H), 7.39-7.34 (t, 1H, J= 7.5Hz), 7.18-7.15 (d, 2H, J= 9Hz), 7.02-7.00 (d, 1H, J= 6Hz), 6.96-6.93 (d, 2H, J= 9Hz), 5.05 (s, 2H), 3.88 (s, 3H), 3.68 (s, 3H), 2.95-2.90 (t, 2H, J= 7.5Hz), 2.65-2.60 (t, 2H, J= 7.5Hz), 2.29 (s, 3H); MS (ESI^{+}) calcd. *m/z* for $C_{22}H_{23}NO_5$ [(M)] 381.4, found [$(M+H)^{+}$] 382.5.

General Procedure for Saponifcation: The appropriate thiazole ester (0.06mmol) was dissolved in THF (3mL) and adjusted to pH= 9-10 with 2M NaOH. The reaction was stirred at room temperature overnight and monitored by TLC using EtOAc-Hexanes with 1% acetic acid (4:1, v/v). Acids that did not convert at room temperature were heated between 40^{o}C-70^{o}C and stirred for an additional 12 hours. Once the reaction was complete, THF was removed under reduced pressure and the left over residue was resuspended in water (5mL) and acidified with 2M HCl until pH=2. More water (5 mL) was added and the product was extracted with EtOAc (10 mL x 3). The organic layers were combined, dried over $MgSO_4$ and concentrated in *vacuo* to obtain white-cream colored solids. No further purification steps were taken.

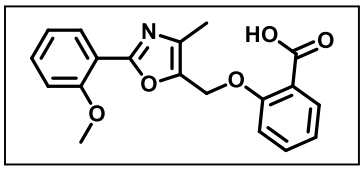

KAT120413-1 100% yield; ^{1}H-NMR (300 MHz) ($CDCl_3$) δ 7.81-7.79 (d, 1H, J= 6Hz), 7.65-7.62 (d, 1H, J= 9Hz), 7.56-7.48 (q, 2H, J= 8Hz), 7.32-7.30 (d, 1H, J= 6Hz), 7.21-7.18 (d, 1H, J=9 Hz), 7.09-7.04 (t, 2H, J= 7.5Hz), 5.25 (s, 2H), 3.85 (s, 3H), 2.2 (s, 3H^{13}CDEPT-135 NMR δ Negative (-): CH_2: 52.8 Positive (+): CH_3, CH: 136.2, 131.2, 130.7, 121.0, 119.7, 117.6, 56.3, 11.5 ; MS (ESI^+) calcd. m/z for $C_{19}H_{17}NO_5$ [(M)] 339.4, found [$(M+H)^+$] 340.0.

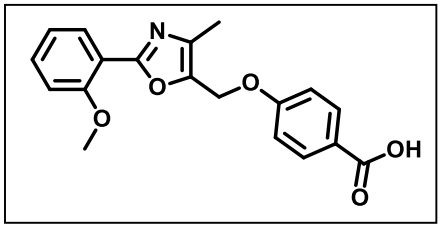

KAT101013-2 82% yield; ^{1}H-NMR (300 MHz) ($CDCl_3$) δ 7.94-7.91 (d, 2H, J= 9Hz), 7.82-7.80 (d, 1H, J= 6Hz), 7.53- 7.48 (t, 1H, J= 7.5Hz), 7.21-7.18 (d, 1H, J= 9Hz), 7.17 (s, 1H), 7.14 (s, 1H), 7.09-7.04 (t, 1H, J= 7.5Hz), 5.28 (s, 2H), 3.85 (s, 3H), 2.24 (s, 3H); ^{13}C NMR δ 167.4, 161.9, 159.5, 157.7, 143.2, 137.0, 132.7, 131.8, 130.5, 124.0, 121.0, 116.2, 115.2, 113.1, 59.6, 56.3, 11.6; ^{13}CDEPT-135 δ Negative (-): 132.7, 131.8, 130.5, 121.0, 115.2, 113.1, , 56.3, 11.6, Positive (+): 59.4; MS DUIS ($^+$ve) calcd. m/z for $C_{19}H_{17}NO_5$ [(M)] 339.4, found [$(M+H)^+$] 340.0.

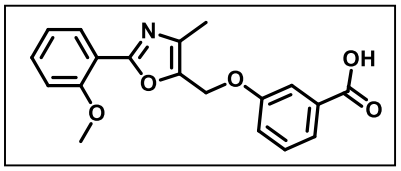

KAT101013-3 100% yield; ^{1}H-NMR (300 MHz) ($CDCl_3$) δ 7.82-7.79 (d, 1H, J= 9Hz), 7.60 (s, 2H), 7.53-7.42 (m, 2H), 7.32-7.29 (d, 1H, J= 9Hz), 7.21-7.18 (d, 1H, J= 9Hz), 7.08-7.03 (t, 1H, 7.5Hz), 5.26 (s, 2H), 3.84 (s, 3H), 2.24 (s, 3H). ^{13}C NMR δ 167.5, 159.5, 158.3, 157.7, 142.5, 136.8, 132.7, 132.7, 130.5, 130.2, 122.6, 121.0, 120.5, 116.3, 115.5, 113.1, 59.5, 56.3, 11.6; ^{13}CDEPT-135 NMR δ Negative (-): CH_2: 59.6, Positive (+): CH_3, CH: 132.7, 130.5, 130.1, 122.6, 121.0, 120.5, 115.5, 113, 56.3, 11.5; MS DUIS ($^+$ve) calcd. m/z for $C_{19}H_{17}NO_5$ [(M)] 339.4, found [$(M-H)^-$] 338.0.

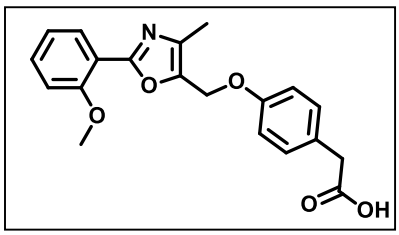

KAT101013-4 100% yield; ^{1}H-NMR (300 MHz) ($CDCl_3$) δ 12.24 (s, 1H), 7.83-7.79 (d, 1H, J= 9Hz), 7.53-7.48 (t, 1H, J= 7.5Hz), 7.09-6.99 (m, 3H), 5.15 (s, 2H), 3.85 (s, 3H), 3.51 (s, 2H), 2.51 (m, 2H, DMSO residual peak overlaps), 2.22 (s, 3H); ^{13}C NMR δ 173.29, 159.37, 157.64, 157.12, 142.76, 136.56, 132.60, 130.87, 130.46, 128.13, 120.99, 116.33, 115.23, 113.06, 59.37, 56.28, 11.58; ^{13}CDEPT-135 NMR δ Negative (-): CH_2: 59.25, 40.14, Positive (+): CH_3, CH: 132.60, 130.87, 130.15, 120.85, 115.12, 113.05, 56.11, 11.55; MS DUIS ($^{+}$ve) calcd. m/z for $C_{20}H_{19}NO_5$ [(M)] 353.4, found [$(M-H)^-$] 352.4.

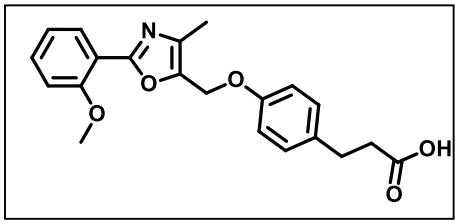

KAT100313-5 100% yield; ^{1}H-NMR (300 MHz) ($CDCl_3$) δ 12.09 (s, 1H), 7.82-7.79 (d, 1H, J= 9Hz), 7.53-7.47 (t, 1H, J= 9Hz), 7.21-7.16 (t, 3H, J= 7.5Hz), 7.09-7.04 (t, 1H, J= 7.5Hz), 6.98-6.95 (d, 2H, J= 9Hz), 5.13 (s, 2H), 3.85 (s, 3H), 2.79-2.74 (t, 2H, J= 7.5Hz), 2.51 (m, 2H, DMSO residual peak overlaps), 2.21 (s, 3H); ^{13}C NMR δ 174.2, 159.3, 157.6, 156.7, 142.8, 136.5, 133.9, 132.6, 130.5, 129.7, 121.0, 116.4, 115.3, 113.05, 59.3, 56.3, 36.0, 30.0, 11.6; ^{13}CDEPT-135 NMR δ Negative (-): CH_2: 59.4, 36.3, 30.1, Positive (+): 132.6, 130.5, 129.7, 121.0, 115.3, 113.1, 56.3, 11.6; MS DUIS ($^{+}$ve) calcd. m/z for $C_{21}H_{21}NO_5$ [(M)] 367.4, found [$(M-H)^-$ 366.4.

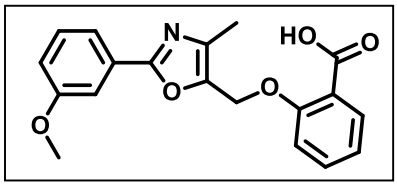

JWB111913-1 79% yield; ^{1}H-NMR (300 MHz) ($CDCl_3$) δ 7.65-7.63 (d, 1H, J= 6Hz), 7.56-7.42 (m, 4H), 7.33-7.30 (d, 1H, J= 9Hz), 7.12-7.07 (m, 2H), 5.28 (s, 2H), 3.83 (s, 3H), 2.21 (s, 3H) ; MS DUIS ($^{-}$ve) calcd. m/z for $C_{19}H_{17}NO_5$ [(M)] 339.1, found [$(M-H)^-$] 338.4.

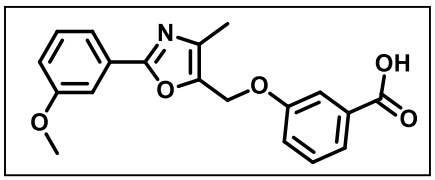

JWB111913-2 100% yield; ^{1}H-NMR (300 MHz) ($CDCl_3$) δ 7.63-7.54 (m, 3H), 7.47-7.41 (m, 3H), 7.29 (d, 1H, J= 6Hz), 7.10-7.01 (d, 1H, J= 6Hz), 5.29 (s, 2H), 3.83 (s, 3H), 2.25 (s, 3H); MS DUIS ($^{-}$ve) calcd. m/z for $C_{19}H_{17}NO_5$ [(M)] 339.1, found [$(M-H)^{-}$] 338.4.

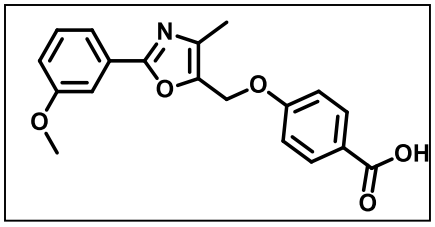

JWB111913-3 100% yield; ^{1}H-NMR (300 MHz) ($CDCl_3$) δ 7.94-7.91 (d, 2H, J= 9Hz), 7.56-7.54 (d, 1H, J= 6Hz), 7.48-7.42 (t, 2H, J= 9Hz), 7.17-7.14 (d, 2H, J= 9Hz), 7.12-7.10 (d, 1H, J= 6Hz), 5.31 (s, 2H), 3.83 (s, 3H), 2.26 (s, 3H); MS DUIS ($^{+}$ve) calcd. m/z for $C_{19}H_{17}NO_5$ [(M)] 339.1, found [$(M+H)^{+}$] 340.4.

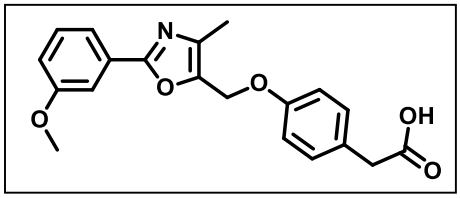

JWB111913-4 100% yield; ^{1}H-NMR (300 MHz) ($CDCl_3$) δ 7.56-7.53 (d, 1H, J= 9Hz), 7.47-7.42 (t, 2H, J= 7.5Hz), 7.22-7.19 (d, 2H, J= 9Hz), 7.12-7.09 (d, 1H, J= 9Hz), 7.02-6.99 (d, 2H, J= 9Hz), 5.18 (s, 2H), 3.83 (s, 3H), 2.51 (m, 2H, DMSO residual peak overlaps), 2.23 (s, 3H); δ MS DUIS ($^{+}$ve) calcd. m/z for $C_{20}H_{19}NO_5$ [(M)] 353.1, found [$(M+H)^{+}$] 354.4.

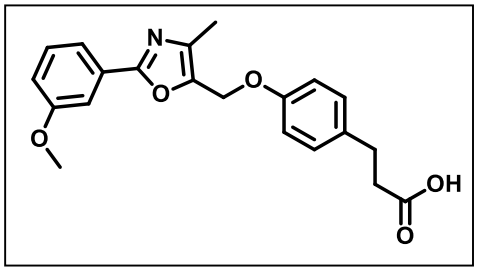

JWB111913-5 100**%** yield; ^{1}H-NMR (300 MHz) ($CDCl_3$) δ 7.66-7.63 (d, 2H, J= 9Hz), 7.58 (s, 1H) 7.40-7.34 (t, 1H, J= 9Hz), 7.20-7.17 (d, 1H, 9Hz), 7.03-7.00 (d, 2H, J= 9Hz), 6.97-6.94 (d, 2H, J= 9Hz), 5.06 (s, 2H), 3.89 (s, 3H), 2.97-2.86 (m, 2H), 2.70-2.65 (m, 2H), 2.29 (s, 3H); δ MS DUIS ($^{-}$ve) calcd. m/z for $C_{21}H_{21}NO_5$ [(M)] 367.4, found [$(M-H)^{-}$] 366.4.

3.3 Determining the Binding Between VDR and Coactivator in the Presence of Oxazole-Substituted GW0742 Analogs

The binding data obtained for both the ortho- and meta- methoxy GW0742 oxazole analogs (*o*-OCH_3 and *m*-OCH_3) are summarized in Table 12 and 13. This includes methyl esters as well as carboxylic acids. Surprisingly, all compounds did not bind to VDR and initiate or inhibit the interaction with coregulator peptide SRC2-3. Insufficient solubility was ruled out by the solubility

Table 12. Modulation of VDR-Coactivator binding in the presence of ortho-methoxy phenyl oxazole-based GW0742 analogs.

Compound	Recruitment of SRC2-3 VDR Interaction EC_{50} (μM)	Inhibition of SRC2-3 VDR Interaction IC_{50} (μM)
KAT092013-1	Inactive	Inactive
KAT092313-2	Inactive	Inactive
KAT092413-3	Inactive	Inactive
KAT092513-4	Inactive	Inactive
KAT092513-5	Inactive	Inactive
KAT120413-1	Inactive	Inactive
KAT101013-2	Inactive	Inactive
KAT101013-3	Inactive	Inactive
KAT100313-4	Inactive	Inactive
KAT101013-5	Inactive	Inactive

The maximum concentration used for this assay was 300 μM of each compound.

Table 13. Modulation of VDR-Coactivator binding in the presence of meta-methoxy phenyl oxazole-based GW0742 analogs.

Compound	Recruitment of SRC2-3 VDR Interaction EC_{50} (μM)	Inhibition of SRC2-3 VDR Interaction IC_{50} (μM)
JWB091313-1	Inactive	Inactive
JWB091313-2	Inactive	Inactive
JWB091313-3	Inactive	Inactive
JWB091313-4	Inactive	Inactive
JWB091313-5	Inactive	Inactive
JWB111913-1	Inactive	Inactive
JWB111913-2	Inactive	Inactive
JWB111913-3	Inactive	Inactive
JWB111913-4	Inactive	Inactive
JWB111913-5	Inactive	Inactive

The maximum concentration used for this assay was 300 μM of each compound.

assay reported later in this section. Changing the fluorophore attached to SRC2-3 to Texas Red did confirm the absence of activity. An alternative commercially available assay (Polarscreen™ VDR Competitor Assay) employing a fluorescent VDR ligand (Fluormone™ VDR Red) was purchased from Invitrogen but unfortunately we were unable to run this assay with our Tecan M1000 reader for unknown reasons. Currently, a coumarin-based probe is being developed in our laboratory to enable the identification of direct ligand inhibitors of VDR. Regardless of the FP results, the compounds were further tested for their ability to modulate transcription with respect to VDR and PPARδ in addition to cytotoxicity in cells.

3.4 Modulation of VDR and other NR-Mediated Transcription by Oxazole-Substituted GW0742 Analogs

Upon ligand binding, nuclear receptors undergo a conformational change that can induce recruitment of specific coactivators. In addition to the traditional two plasmid transcription assay, a two-hybrid assay was used to study the ligand-dependent interaction between VDR and coactivator SRC1 (Figure 46). The assay employs three plasmids. A fusion of SRC1 and a GAL4 DNA binding domain, a fusion between VDR LBD and VP16 plasmid and luciferase reporter

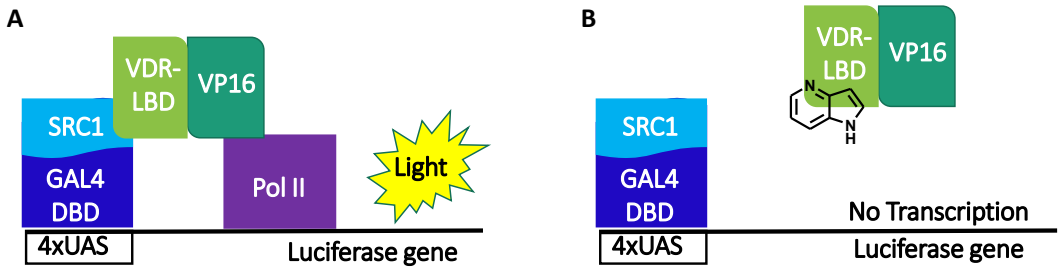

Figure 46. Cartoon describing luminescence-based 2-hybrid transcription assay. A) Activated VDR transcribes the luciferase gene and produces light. B) In the presence of an inhibitor, VDR is unable to transcribe the luciferase gene and produce light.

plasmid with a 4xUAS repeat. A VDR agonist would induce the binding between VDR LBD and SRC1 thus bringing the VP16 activation domain and GAL4 DNA domain together inducing the transcription of the luciferase gene.

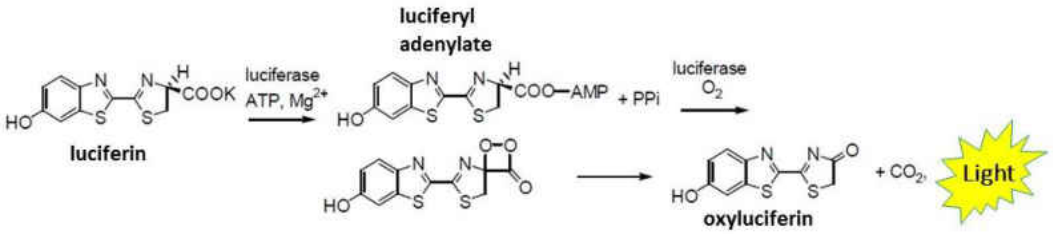

Scheme 6. Bioluminescent reaction that occurs when the luciferase enzyme is activated.

To determine if GW0742 oxazole analogs can inhibit the luciferase enzyme thus producing a false response in the transcription assay, a luciferase binding assay was conducted using Cell Titer-Glo™. This reagent, typically used for cell viability assays, contains already the luciferase enzyme that produces light through a series of reactions (Scheme 6). Important for the light reaction to occur are substrates luciferin, APT, and Mg^{2+}. Because Cell Titer-Glo is missing ATP, it must be added to the reaction in addition to the compounds.

3.4.1 Experimental Procedure

Luminescence-Based VDR-Mediated Transcription Assay Protocol: For complete details see Part 1 of this chapter. In addition to VDR and PPARδ transcription assays, PPARα, PPARγ, retinoid X receptor (RXRα), estrogen (ER, α and β isoforms) and thyroid (TR, α and β isoforms) receptor were evaluated for inhibitory activity with four different oxazole GW0742 analogs. For each competitive pan NR transcription assays, 2 mL of untreated DMEM containing 1.5 µg of NR plasmid, 16 µg luciferase reporter gene, Lipofectamine™ LTX (75 µl), and PLUS™ reagent (25 µl) was added to a flask of HEK293T cells. Inhibition was determined in the presence of the following

agonists: GW7647 (30 nM, PPARα), Rosiglitazone (300 nM, PPARγ), Bexarotene (200 nM, RXRα), estradiol (10 nM, ERα/β) and Triiodothyronine (100 nM, TRα/β). For the VDR two-hybrid assay, 2 mL of untreated DMEM containing 5.0 µg of VP16-VDR-LBD plasmid, 4.0 µg of SRC1-GAL4 plasmid, 16 µg of a luciferase reporter plasmid, Lipofectamine™ LTX (75 µl), and PLUS™ reagent (25 µl) were added. Due to cell sensitivity to DMSO concentrations greater than or equal to 1%, 30 mM rather than 10 mM stock solutions were made allowing for only a 100 nL transfer of compound into each well containing 20 µL of solution during the two hybrid assay.

Inhibition of Luciferase using Cell Titer Glo Assay Protocol: In a 384-well white optical bottom plates (Nunc, #142762), 20 µL of Cell Titer-Glo™ (Promega, Madison, WI) was added to each well. 30 mM stock solutions of synthesized compounds made in DMSO were serially diluted (1:3) in 96-well plates. Four 14 µL aliquots of each compound concentration was transferred to opaque 384-well plates for storage. 100 nl of each compound was transferred to the 384-well white optical bottom plate using the Tecan Freedom EVO liquid handling system (V&P Scientific). The plate was incubated for 45 minutes at 37°C. After incubation, 20 µL of a 1 µM ATP solution diluted in water was added to each well. Controls used were DMSO, DMSO and ATP, and ATP Cell Titer-Glo™. Luminescence readings were performed on a Tecan Infinite M1000 plate reader.

3.4.2 Results and Discussion

The transcriptional activity of oxazole analogs are summarized in Tables 14 and 15. None of the analogs activate VDR-mediated transcription up to a concentration of 150 µM.

Table 14. Modulation of VDR and PPARδ transcription in the presence of ortho-methoxy phenyl oxazole GW0742 analogs.

Compound	VDR Transcription EC_{50} (µM)[a]	VDR Transcription IC_{50} (µM)[a]	PPARδ Transcription EC_{50} (µM)[b]	Cytotoxicity LD_{50} (µM)[c]
KAT092013-1	Inactive	3.25 ± 1.4	Inactive	Non-toxic
KAT092313-2	Inactive	4.85 ± 2.2	Inactive	66.2 ± 5.4
KAT092413-3	Inactive	2.50 ± 1.2	Inactive	Non-toxic
KAT092513-4	Inactive	3.82 ± 1.3	Inactive	Non-toxic
KAT092513-5	Inactive	10.1 ± 1.7	Inactive	50.6 ± 5.9
KAT120413-1	>100	Inactive	Inactive	Non-toxic
KAT101013-2	Inactive	Inactive	8.7 ± 6.4 (16%)	Non-toxic
KAT101013-3	Inactive	Inactive	0.88 ± 0.47 (22%)	Non-toxic
KAT100313-4	Inactive	Inactive	11.0 ± 10.2 (48%)	Non-toxic
KAT101013-5	Inactive	>80	4.6 ± 3.1 (30%)	Non-toxic

[a]Transcription assay using a CMV-VDR plasmid and a luciferase reporter plasmid under control of a 24-hydroxylase promoter with GW0742-based oxazole analogs. [b]Transcription assay using a GALx4 PPARδ plasmid and a luciferase reporter plasmid under control of GALx4 promoter. Percent partial agonistic activity is shown in parenthesis. [b]Cell- TiterGlo (Promega). The maximum concentration used was 100µM.

Interestingly, the *o*-OCH_3 based esters were able to inhibit VDR-mediated transcription but not activate PPARδ-mediated transcription. On the contrary, PPARδ-mediated transcription was activated by most of the *o*-OCH_3 derived acids without inhibiting VDR-mediated transcription. The most potent VDR antagonist in this series was KAT092413-3 with an EC_{50} values of 2.5 µM that completely lacked the ability to activated PPARδ-mediated transcription like the parent compound GW0742.

Table 15. Modulation of VDR and PPARδ transcription in the presence of meta-methoxy phenyl oxazole GW0742 analogs.

Compound	VDR Transcription EC_{50} (μM)[a]	VDR Transcription IC_{50} (μM)[a]	PPARδ Transcription EC_{50} (μM)[b]	Cytotoxicity LD_{50} (μM)[c]
JWB091313-1	Inactive	6.75 ± 2.1	Inactive	48.0 ± 9.3
JWB091313-2	Inactive	5.56 ± 1.9	Inactive	95.8 ± 14.7
JWB091313-3	Inactive	5.67 ± 1.4	Inactive	>100
JWB091313-4	Inactive	0.66 ± 0.30	Inactive	90.8 ± 12.0
JWB091313-5	Inactive	2.88 ± 0.97	1.09 ± 0.58 (7.7%)	>33
JWB111913-1	Inactive	40.4 ± 13.4	Inactive	Non-toxic
JWB111913-2	Inactive	33.2 ± 15.2	Inactive	Non-toxic
JWB111913-3	Inactive	>100	2.62 ± 1.8 (2.1%)	Non-toxic
JWB111913-4	Inactive	3.60 ± 1.4	1.80 ± 0.79 (8.5%)	Non-toxic
JWB111913-5	Inactive	3.35 ± 1.5	1.39 ± 0.44 (13.7%)	Non-toxic

[a]Transcription assay using a CMV-VDR plasmid and a luciferase reporter plasmid under control of a 24-hydroxylase promoter with GW0742-based oxazole analogs. [b]Transcription assay using a GALx4 PPARδ plasmid and a luciferase reporter plasmid under control of GALx4 promoter. Percent partial agonistic activity is shown in parenthesis. [b]Cell- TiterGlo (Promega). The maximum concentration used was 100uM.

The series of *m*-OCH_3 analogs showed similar trends than the *o*-OCH_3 analogs, however the following differences were observed. Most of the *m*-OCH_3 esters showed a certain degrees of toxicity, whereas only two of the *o*-OCH_3 were slightly toxic. The *m*-OCH_3 esters and acids were able to inhibit VDR transcription, whereas one ester JWB091313-5 and some acids were able to activate PPARδ-mediated transcription. The most potent VDR antagonist was JWB091313-4 with an IC_{50} value of 660 nM. The compounds that activated PPARδ-mediated transcription exhibited partial agonism as low as 2.2% in respect to agonist GW0742. In general, this partial agonism was weaker for the *m*-OCH_3 and for the *o*-OCH_3 analogs.

Specificity towards a certain VDR-coactivator interaction was introduced with the two-hybrid assay. The results of the ester and acid analogs for this protein-protein inhibition assay are summarized (Table 16).

The results of the protein-protein interaction assays were similar to the VDR transcription assay confirming the interaction between VDR and coactivators as an essential interaction meditating VDR transcription. The average activities of both assays differed up to three-folds but higher standard deviations in the two hybrid assay resulted in non-significant differences between both IC_{50} values in most cases.

Table 16. Modulation of VDR transcription in the presence of ortho and metha-methoxy phenyl oxazole GW0742 analogs using a 2-hybrid cell assay.

Compound	2-Hybrid VDR Transcription IC_{50} (μM)	Compound	2-Hybrid VDR Transcription IC_{50} (μM)
KAT092013-1	20.2 ± 13.5	**JWB091313-1**	15.4 ± 11.6
KAT092313-2	17.9 ± 7.92	**JWB091313-2**	17.1 ± 5.2
KAT092413-3	7.33 ± 3.84	**JWB091313-3**	8.89 ± 2.5
KAT092513-4	11.13 ± 4.9	**JWB091313-4**	13.9 ± 11.5
KAT092513-5	13.6 ± 5.2	**JWB091313-5**	6.7 ± 3.4
KAT120413-1	>80	**JWB111913-1**	>33
KAT101013-2	>80	**JWB111913-2**	33.14 ± 13.1
KAT101013-3	>100	**JWB111913-3**	>80
KAT100313-4	>80	**JWB111913-4**	27.7 ± 17.3
KAT101013-5	>100	**JWB111913-5**	26.7 ± 15.8

2-Hybrid transcription assay using a CMV-VDR plasmid and a luciferase reporter plasmid under control of a 24-hydroxylase promoter with GW0742-based oxazole analogs. The maximum concentration used was 150μM.

The two most promising compounds from each oxazole series were chosen for further investigation towards other nuclear receptors. These included PPARs α, γ, and δ, the RXRα, TRα and β, and the estrogen receptors α and β (ERα and β). The results are summarized in Table 17.

Table 17. Inhibition of transcription with an array of nuclear receptors in the presence of KAT092413-3, KAT092513-4, JWB091313-3, and JWB091313-4 to determine selectivity.

Compound	PPARα IC_{50} (μM)[a]	PPARγ IC_{50} (μM)[b]	PPARδ IC_{50} (μM)[c]	RXRα IC_{50} (μM)[d]	TRα IC_{50} (μM)[e]	TRβ IC_{50} (μM)[e]	ERα IC_{50} (μM)[f]	Erβ IC_{50} (μM)[f]
KAT092413-3	6.6 ± 2.9	7.6 ± 3.4	10.9 ± 3.9	11.1 ± 4.6	10.1 ± 3.3	9.8 ± 2.9	5.2 ± 1.5	23.6 ± 17.2
KAT092513-4	8.0 ± 6.6	6.3 ± 3.1	6.6 ± 2.9	4.4 ± 3.1	8.4 ± 2.7	7.6 ± 4.4	4.1 ± 1.7	10.0 ± 6.4
JWB091313-3	3.5 ± 2.1	7.6 ± 3.4	10.9 ± 4.1	4.6 ± 2.6	5.4 ± 2.5	8.8 ± 3.0	4.7 ± 1.1	5.9 ± 2.8
JWB091313-4	1.9 ± 1.3	6.7 ± 3.0	11.3 ± 6.8	2.0 ± 1.7	4.2 ± 2.2	0.97 ± 0.82	1.7 ± 0.96	7.4 ± 6.3

[a]GW7647 (30nM), [b]Rosiglitazone (300nM), [c]GW0742 (50nM), [d]Bexarotene (200nM), [e]T3 (10nM) and [f]Estradiol (10nM). The maximum concentration used was 100μM.

Interestingly, all four compounds inhibited the transcription mediated by all nuclear receptors investigated. Minor selectivity was observed for each compound. For instance KAT092413-3 were more effective towards ERα than ERβ, however selectivity between TR and PPAR isoforms was marginal. Still, VDR-mediated transcription was inhibited at low concentration with an IC_{50} of 2.5 μM. In addition, JWB091313-4 exhibited not only selectivity between ER isoforms but also was very selective towards PPARα in respect to PPARγ and PPARδ. Nevertheless the IC_{50} for VDR (0.6 μM) was still lower than that of PPARs with 1.9 μM. Triggered by the PAN activity by the four compounds chosen, possible inhibition of the luciferase enzyme was investigated by adding ATP and compounds to the Cell Titer Glo™ assay from Promega. None of the four compounds inhibited the formation of light as illustrated for JWB091313-3 and JWB091313-4 in Figure 47.

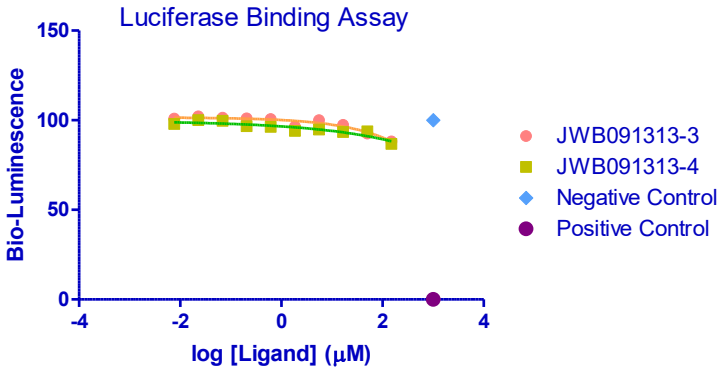

Figure 47. Dose response curve showing no inhibition of the luciferase enzyme by GW0742 oxazole derivatives

3.5 Determining Physiochemical Properties of Oxazole-based GW0742 Analogs

3.5.1 Solubility Assay

Drug solubility is defined as the amount of substance that dissolves in a given volume of solvent at a specific temperature.[161] In drug discovery, it is a physiochemical characteristic of a molecule that influences its success as a lead compound. For instance, the bioavailability of poorly soluble drugs is highly susceptible to food intake, active transport, and efflux.[162] In addition, compounds with poor solubility carry a higher risk of failure during discovery and development since it may compromise the success of biochemical and cell-based assays, induce aggregation, and complicate formulation for in vivo studies.[148] Experimentally, solubility can be measured either thermodynamically or kinetically. Thermodynamic solubility is defined by the addition of excess solid drug directly to an aqueous solution under constant agitation until equilibrium is established. This assay can take several days for completion due to and slow equilibration. Crystallinity plays an important factor for this assay thus variability in production of solids will change its solubility. As parallel synthesis and combinatorial chemistry have

increasingly become the most dominant methods of compound synthesis in the discovery stage of pharmaceuticals, there is an increasing probability that the physical form of the compounds is amorphous due to impurities and solvent residues. The non-crystalline materials will always be more soluble than their pure counterpart.[163] Therefore, early discovery stages adopted kinetic solubility as an alternative. For this process, compounds diluted in an organic solvent (i.e. DMSO) are added to an aqueous solution until precipitation is observed or the concentration of the dissolved compounds becomes constant.[164] The benefits of this method are that it is rapid and requires only a small amounts of test compounds thus making it suitable for high throughput. In general, there are two main approaches to determine kinetic solubility. The first one is done by removing the precipitate by filtration or centrifugation followed by the determination of compound concentrations by UV absorption or mass spectrometry. The second approach detects the formation of precipitate by monitoring the scattering of light by particles using UV absorbance or directly by detecting the light scattering by nephelometric turbidity detection.[165]

Within this section, we report the use of a miniaturized kinetic-based HTS assay for the determination of solubility of GW0742 oxazole derivatives developed by Dr. Megan Pawlak in our lab. Compounds tested included the ester and acid forms of the ortho and meta-methoxy GW0742 oxazoles.

Experimental Procedure

Reagents and Instrumentation: All materials were used as they were received, with no further purification. Five bioactive small molecules: 4,5-diphenylimidazole (Alfa Aesar), β-estradiol (Alfa Aesar), diethylstilbestrol (Spectrum Chemicals), 3-phenylazo-2,6-diaminopyridine (Alfa Aesar)

were used as standards. Each of the standards were made into a 10 mM solution in DMSO (Acros, Spectroscopic Grade 99.9+%). The buffer was prepared in 18 MΩ water with 90 mM ethanolamine (Alfa Aesar, ACS grade 99+%), 90 mM KH_2PO_4 (J.T. Baker), 90 mM potassium acetate (Fisher Biotech), and 30 mM NaCl (Fisher) and adjusted to pH 7.4 with HCl (Mallinckrodt).

HPLC grade acetonitrile (Columbus Chemical Industries) was used to make a 20% by volume solution in buffer for the preparation of the calibration plate. The calibration solutions (0-300 µM, 50µL each) were read in a 384-well UV plate (Greiner Bio-One, #781801), which was also used for the solubility assay absorbance readings. The incubation and filtration were performed in a 384-well filter plate (Pall, #5071), which was sealed with an aluminum cover (Corning, #6570) during incubation and mixing. The filtration of the plates was performed using a Millipore MultiScreen$_{HTS}$ Vacuum Manifold (MSVMHTS00). All of the absorbance readings were performed on an Infinite M1000 plate reader (Tecan).

Solubility Assay Protocol: Calibration plots were generated to obtain the relationship between solute concentration and absorbance. Molecules were serially diluted in 96-well plates (Table 18) and then 50 µL was transferred to 384-well UV plate so that one compound was in each row. Each concentration was plated in duplicate. The top of the plate was then covered with an aluminum plate cover. The UV plate was then carefully placed in the bench-top sonicator so that it floated on top of the water. It was sonicated for 1 minute and centrifuged at 1000 rpm for 3 minutes to ensure that all of the solution remained in the wells. The plate was then scanned for absorbance with the Tecan plate reader from 230-800 nm at 5 nm increments with 10 flashes per well.

Once the calibration plates were read, a calibration plot for each compound of adjusted absorbance vs. solute concentration at the maximum wavelength (λ_{max}) was generated. This was done by subtracting the average absorbance of the 0 µM (background) wells from the absorbance of each of the other wells. Each of the calibration plots was labeled with the compound name

Table 18. Preparation of 96 well calibration plate for solubility assay.

Well Number	**1**	**2**	**3**	**4**	**5**	**6**
Volume Buffer	291 µL	83.3 µL	125 µL	125 µL	125 µL	95 µL
Volume 10 mM DMSO Stock	9 µL					
Volume DMSO						5 µL
Volumes transferred from wells 1 to 2, 2 to 3, 3 to 4, 4 to 5	166.7 µL	125 µL	125 µL	125 µL		
Final Concentration	**300 µM**	**200 µM**	**100 µM**	**50 µM**	**25 µM**	**0 µM (blank)**

and maximum wavelength. Finally, a best fit linear trend line through the origin of the plot with the equation and r^2 value to 4 decimal places was added to the plot.

After the calibration plots were generated at the wavelength of maximum absorbance for each molecule, the solubility assay was performed. The wells in the 384-well filter plate were pre-wetted with 20-40 µL of buffer. The buffer was left to sit in the wells for about 5 minutes and subsequently removed by vacuum. An aluminum film cover was then adhered underneath

Table 19. Preparation of solution for solubility assay.

500 µM	**Blank**
47.5 µL buffer	47.5 µL buffer
2.5 µL of 10 mM stock DMSO solution	2.5 µL DMSO

the filter plate to prevent wicking out or evaporation of the solvents during the incubation period. The solubility assay was then mixed in the filter plate according to Table 19 with four wells per molecule. With an adhesive plate cover on top and underneath the filter plate, it was sonicated for 1 minute, and shaken on a reciprocating plate shaker overnight.

The next morning, the solution was filtered into a collection plate (384-well polystyrene plate). From the filtrate, 30 µL from each well from the collection plate was transferred into a 384-well UV plate using a multichannel pipette. Next, 20 µL of acetonitrile was added to each well by pipette and shaken for 5 minutes on the plate shaker followed by centrifugation at 1000 rpm for 3 minutes. The absorbance was scanned from 230-800 nm at 5 nm increments with 10 flashes per well.

Equation 3) $$Solubility = \frac{Adjusted\ Absorbance\ at\ \lambda_{max}}{Slope}\left(\frac{3}{5}\right)$$

Finally, the solubility was determined using Equation 3 with the slope from the calibration plot for the molecule. At the maximum wavelength for each compound, the average absorbance from the blank wells (no small molecule) was subtracted from the absorbance of the solution after filtration (adjusted absorbance at λ_{max}). The average of the solubility values were calculated and the standard deviations were determined. Five small molecules (4,5-diphenylimidazole, β-estradiol, diethylstilbestrol, 3-phenylazo-2,6-diaminopyridine) with known solubility values were analyzed as standards on each solubility assay plate.

3.5.2 Parallel Artificial Membrane Permeability Assay (PAMPA)

In addition to solubility, permeability is an important property of drug-like molecules and is necessary to determine the extent of oral absorption, bio-distribution and consequently the target tissue uptake.[166] Unlike solubility, permeability cannot be manipulated by formulations but rather is an inherent property of the molecule itself that can only be changed by adjustments to its structure.

The absorption of orally administered substances is widely determined by their ability to cross the gastrointestinal tract (GI-tract), its penetration of the blood brain barrier, and its transport across cell membranes.[167] This is governed by several different mechanisms of permeation including passive diffusion, active uptake, paracellular transport, and efflux. It is generally assumed that sufficiently lipophilic compounds are transported via passive diffusion, while small hydrophilic compounds (<200 Da) are transported through the paracellular route if not by active transport.[168] However, active transport of small molecules is difficult to replicate with *in vitro* assays. For this reason, the assessment of passive cellular absorption is the preferred method.

Passive diffusion is a physiochemical process that is governed by physiochemical properties like lipophilicity, molecular weight, pK_a, polar surface area, ionization state and hydrogen bond capacity.[169] Drug lipophilicity is commonly used as a predictor for membrane permeability because membranes are primarily lipophilic in nature.[170] Molecular size can also play a distinct role in the permeation process because larger molecules diffuse more slowly than smaller molecules. Lipids within a membrane that contain hydrogen-bonding acceptor groups

can associate with the hydrogen-bonding solutes. This hydrogen-bonding prevents the solutes from penetrating the membrane and slows down the diffusion process. Directly related to the hydrogen-bonding capacity is the polar surface area.[170] Polar surface area is the molecular surface area associated with hydrogen bonding acceptor atoms (i.e., oxygen and nitrogen) plus the area of the hydrogen atoms. Finally, membranes are more permeable to non-ionized forms of drug than the ionized species because of their greater lipid solubility and the charged nature of the membranes.[170]

The Caco-2 cells monolayer permeation has long been widely and successfully used to screen drug candidates. However, the Caco-2 method possessed many limitations including expensive cell culture that could take weeks to obtain confluency with full cell differentiation, low throughput, variable expression of transport and metabolizing proteins, and the complication of multiple permeation mechanisms.[167] Because of this, the Caco-2 method in many cases has been replaced by a parallel artificial membrane permeability assay (PAMPA). PAMPA is a high-throughput, inexpensive method that produces reproducible results without requiring cell culture.[170] Although, PAMPA methods are not completely predictive of *in vivo* permeability, they can identify definitive trends in the ability of a molecule to permeate membranes by passive diffusion.[163]

PAMPA is typically performed in a 96-well plate with two parts, the donor plate and the acceptor plate (Figure 48). The donor plate has a permeable membrane or filter along the bottom which aligns with the wells in the acceptor plate. The artificial membrane, which is either composed of lecithin, phosphatidylcholine, hexadecane, or porcine brain lipid extract, etc. in organic solvents, is impregnated into the filter of the donor plate. Buffer and compound are added to the donor wells while buffer is added to the acceptor wells. With the impregnated filter in contact with both solutions, the assay plates are incubated for a set amount of time, and the

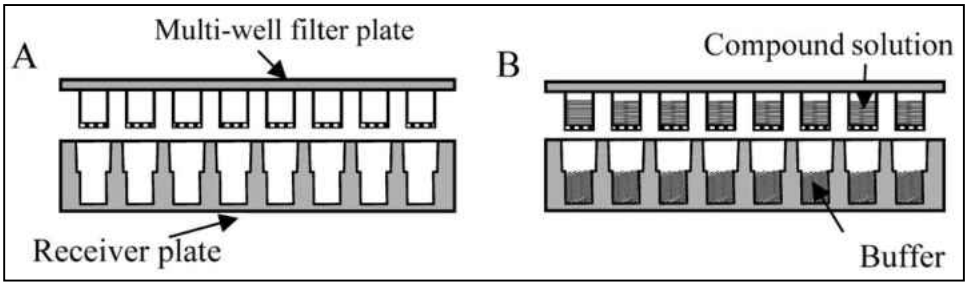

Figure 48. Illustration of PAMPA plates. A) 96-well filter plate pre-coated with an artificial membrane with a matched 96-well receiver plate. B) Solutions of the compounds in buffer are added to the filter plate on top of the artificial membrane (donor plate), while buffer is added to the receiver plate (acceptor plate).[11]

concentration of compound that has passed through the membrane is determined usually by absorbance spectroscopy, HPLC, or LC-MS. An illustration of the PAMPA method is shown in Figure 49.

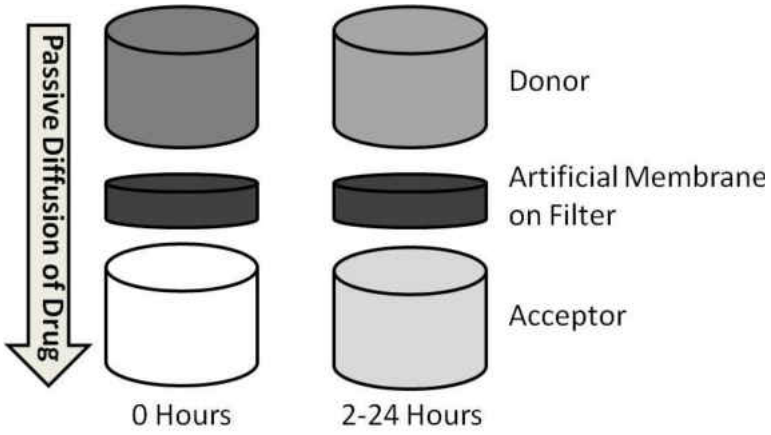

Figure 49. Example of a PAMPA assay performed in a multi-well plate.

The effective permeability determined by cell-based or PAMPA method is calculated using Equation 4. Here, dC_A/dt (mg/s·mL) is the increase of drug concentration in the acceptor well over the incubation period. The term A (cm^2) is the surface area of the membrane that is exposed to the compound. V_A (mL) is the volume of the solvent in the acceptor well. Finally, C_A and C_D (mg/mL) are the initial drug concentration in the acceptor and donor wells, respectively.[170]

Equation 4) $$P_{eff} = \frac{V_a}{A(C_D - C_A)}\left(\frac{dC_A}{dt}\right)$$

The PAMPA assay was used to evaluate oxazole-based GW0742 analogs for their ability to cross a hydrophobic membrane at biological pH. By doing so, a correlation could be made between their cellular bio-activity and their ability to cross the cell membrane. High, medium and low permeable standards were chosen based on their *in vivo* permeability values found in

the Biopharmaceutics Classification System (BCS) database. The logP values calculated for each molecule was compared to the standard molecules to provide the degree of *in vitro* permeability.

Experimental Procedure

Reagents and Instrumentation: All materials were used as received with no further purification. The following small molecules were used as standards: verapamil hydrochloride (Tocris Bioscience), 10,11-dihydrocarbamazepine (Alfa Aesar), and ranitidine hydrochloride (Alfa Aesar). Each of the small molecules were dissolved in DMSO to make 10 mM solutions (Acros, Spectroscopic Grade 99.9+%).

The PAMPA assay was performed with the Millipore MultiScreen filter plates (MAIPNTR10) and Millipore transport receiver plates (MATRNPS50) using a 5% by volume n-hexadecane (Acros) in n-hexane (Fisher) solution to create the artificial layer. The absorbance readings were completed with a Corning Costar 96 well UV plate (3635). 1x Phosphate buffered saline (PBS) was prepared in 1L batches using 18 MΩ water with 3.23 mM $K_2HPO_4 \cdot 7H_2O$ (J.T. Baker), 7.84 mM KH_2PO_4 (J.T. Baker), 5 mM KCl (Fisher), 150 mM NaCl (Fisher), and adjusted to pH 7.2 with HCl (Mallinckrodt) and NaOH (Fisher). All of the absorbance readings were performed on an Infinite M1000 plate reader (Tecan).

PAMPA Assay Protocol:

The artificial membrane was prepared by carefully pipetting 15 µL of the 5% (v/v) hexadecane in hexane solution to each of the wells of the donor plate (assay plates as shown in Figure 49). The plate was placed into a fume hood for 1 hour to ensure complete evaporation of the hexane. After the hexane had evaporated, 300 µL of PBS with 5% (v/v) DMSO was added to

each of the wells of the acceptor plate. The hexadecane treated donor plate was then placed on top of the acceptor plate taking care that the underside of the membrane is completely in contact with the solution in each of the acceptor wells. Each of the compounds solutions were prepared in triplicate in a separate 96-well plate to 300 µM (4.5 µL of 10 mM compound solution in DMSO, 3 µL DMSO, and 95 µL buffer). Then, 150 µL of the compound solution was added to the donor wells. For each plate, 10, 11-dihydrocarbamazepine (medium-high permeability), verapamil (high permeability), and ranitidine (low permeability) were used as standard molecules for reference.

The lid was placed on the plates and the entire plate sandwich was placed into a closed container with a wet paper towel along the bottom to circumvent evaporation during the incubation process. The container was then placed on a reciprocal shaker for agitation at about 100 rpm. The time at the beginning of the incubation was recorded, as this is a thermodynamic-based assay. The incubation was then allowed to continue for approximately eighteen hours.

The next day, the plates were removed from the incubation container and the incubation end time was noted. The donor plate was removed and 50 µL of the acceptor solution was transferred to the UV plate. Drug solutions at the theoretical equilibrium concentration (300 µM) was also prepared and transferred to the UV plate. The absorbance of the solutions in the UV plate was then scanned from 250-600 nm with 1 nm steps and a 5 nm bandwidth.

Equation 5) $$logP = log\left\{C \times -\ln\left(1 - \frac{[Drug]_A}{[Drug]_E}\right)\right\} ; Where\ C = \left(\frac{V_A \times V_D}{(V_D + V_A)A \times T}\right)$$

The relative permeability (cm/s) of the small molecules was calculated with Equation 5, where V_D is the volume of the donor well in cm^3 (150 µL), V_A is the volume in the acceptor well in cm^3 (300 µL), A is the active surface area of the membrane in cm^2 (0.283 cm^2), T is the incubation time of the assay in seconds, $[Drug]_A$ is the absorbance of the compound in the acceptor well after the incubation period, and $[Drug]_E$ is the absorbance of the compound at the concentration of the theoretical equilibrium (as if the donor and acceptor solutions were simply combined).[171] The equation is derived from Equation 4, described previously, in which the change in concentration of the solute is time dependent.

3.5.3 Results and Discussion

The ester and acid forms of the GW0742 oxazole analogs developed in our lab were evaluated for two physiochemical characteristics: aqueous solubility and permeability. The solubility results as well as the measured maximum wavelength obtained for these compounds are summarized in Table 20. Overall, the ester oxazole derivatives were less soluble than their

acid counterparts. When compared to the standards, the esters possessed low solubility while the acids had medium solubility in water.

Table 20. Solubility assay results. Table includes solubilites (μM) and maximum wavelengths (nm) measured for each standard and compound.

Compound	Aqueous Solubility (μM)	Maximum Wavelength (nm)
4,5-diphenylimidazole	18.71 ± 0.028	286
β-estradiol	47.61 ± 0.014	290
Diethylstilbestrol	60.6 ± 0.003	290
3-phenylazo-2,6-diaminopyridine	221.28 ± 0.012	425
KAT092013-1	67.71 ± 0.011	274
KAT092313-2	22.52 ± 0.0068	262
KAT092413-3	15.87 ± 0.0122	274
KAT092513-4	22.18 ± 0.0006	274
KAT092513-5	22.54 ± 0.0045	274
KAT120413-1	146.46 ± 0.0289	272
KAT101013-2	170.99 ± 0.0578	304
KAT101013-3	152.30 ± 0.0164	272
KAT100313-4	161.72 ± 0.058	272
KAT101013-5	144.18 ± 0.0264	272
JWB091313-1	20.1 ± 0.011	282
JWB091313-2	8.67 ± 0.004	282
JWB091313-3	6.19 ± 0.006	266
JWB091313-4	16.31 ± 0.0018	280
JWB091313-5	15.58 ± 0.0203	282
JWB111913-1	97.88 ± 0.0264	284
JWB111913-2	186.06 ± 0.0356	280
JWB111913-3	166.58 ± 0.0293	274
JWB111913-4	150.30 ± 0.0350	276
JWB111913-5	84.40 ± 0.0043	274

Maximum compound concentration was 500 μM.

The relative permeability for GW0742 oxazole analogs are summarized in Table 21. When compared to the standards, the ester form had medium permeability while the acids were more comparable to Ranitidine with low permeability across a hydrophobic barrier. Overall, the esters would be more drug-like.

Table 21. PAMPA assay results

Compound	LogP (cm/s)
Verapamil (high)	-2.81 ± 0.003
10, 11-Dihydrocarbamazepine (medium- high)	-3.22 ± 0.002
Ranitidine (low)	-3.92 ± 0.009
KAT092013-1	-3.33 ± 0.001
KAT092313-2	-3.35 ± 0.013
KAT092413-3	-3.42 ± 0.002
KAT092513-4	-3.56 ± 0.002
KAT092513-5	-3.34 ± 0.001
KAT120413-1	-3.63 ± 0.003
KAT101013-2	-3.67 ± 0.001
KAT101013-3	-3.58 ± 0.0001
KAT100313-4	-3.72 ± 0.001
KAT101013-5	-3.59 ± 0.0005
JWB091313-1	-3.29 ± 0.002
JWB091313-2	-3.37 ± 0.002
JWB091313-3	-3.43 ± 0.0005
JWB091313-4	3.32 ± 0.001
JWB091313-5	-3.34 ± 0.002
JWB111913-1	-3.63 ± 0.001
JWB111913-2	-3.88 ± 0.0003
JWB111913-3	-3.77 ± 0.003
JWB111913-4	-3.88 ± 0.012
JWB111913-5	-3.92 ± 0.005

Permeabilities were measured using the parallel artificial membrane permeation assay (PAMPA) at neutral pH (pH 7.4).

3.6 Conclusion

A good SAR could be established with the ortho- and meta-oxazole containing GW0742 analogs with an ester or acid moiety. Overall in the cell-based transcription assay, the *o*-OCH_3 and *m*-OCH_3 esters were more potent VDR inhibitors with reduced activation of PPARδ-mediated transcription. *m*-OCH_3 acids able to inhibit VDR transcription possessed partial PPARδ agonism making them not selective, while *o*-OCH_3 acids only showed partial agonism for PPARδ and no inhibition of VDR. Although none of these analogs demonstrated VDR inhibition in the FP binding

assay, we know that solubility did not play a role and that the VDR inhibitory effect seen in cells was not due the molecules binding to the luciferase enzyme. A coumarin-derived probe is being developed in our lab and will give insight into if these molecules bind in the LBP of VDR. Therefore this project is ongoing and just like the thiazole analogs, subject to further rational design. This project would also enormously benefit from a GW0742 analog VDR or PPARδ crystal structure, which is currently underway in Prof. Silvaggi's lab.

CHAPTER 4: SYNTHESIS OF NATURAL VDR LIGAND METABOLITES AND THEIR INTERACTION WITH THE VITAMIN D RECEPTOR

4.1 Introduction

4.1.1 Metabolism of $1,25(OH)_2D_3$

The major enzyme responsible for the catabolic breakdown of $1,25(OH)_2D_3$ is the mitochondrial inner-membrane cytochrome p450 enzyme, CYP24A1.[172, 173] As previously mentioned, $25(OH)D_3$ is formed in the liver and then shuttled to the kidney where the final hormonal form of vitamin D_3, $1,25(OH)_2D_3$, is made through the actions of CYP27B1. Once formed, $1,25(OH)_2D_3$ targets VDR in many different tissues. Interestingly, expression of CYP24A1 in target tissues is regulated by $1,25(OH)_2D_3$ through a classic endocrine negative feedback loop. Major catabolism of $1,25(OH)_2D_3$ occurs on the secosteroid's aliphatic chain either forming C24-oxidation pathway products or C23-hydroxylation path products (Figure 50).[174] The C24 pathway is comprised of five enzymatic steps beginning with the 24-hydroxylation of $1,25(OH)_2D_3$ to yield $1,24,25(OH)_3D_3$. This metabolite is oxidized to the ketone, 24-oxo-$1,25(OH)_2D_3$, and then hydroxylation at C-23 to generate 24-oxo-$1,23,25(OH)_3D_3$.[175, 176] This compound is metabolized by oxidative cleavage of the carbon-carbon bond between C-23 and C-24 to produce 24,25,26,27-tetranor-$1,23(OH)_2D_3$.[177] The C23 alcohol is converted to calcitroic acid, a main excretory product of $1,25(OH)_2D_3$ in bile.[178, 179] The $1,25(OH)_2D_3$-induced C24 pathway has been observed in many different cell lines including kidney, bone, intestine, skin and breast thus demonstrating this

pathway can occur in many different tissues.[180-182] The main role of C24 oxidation pathway is

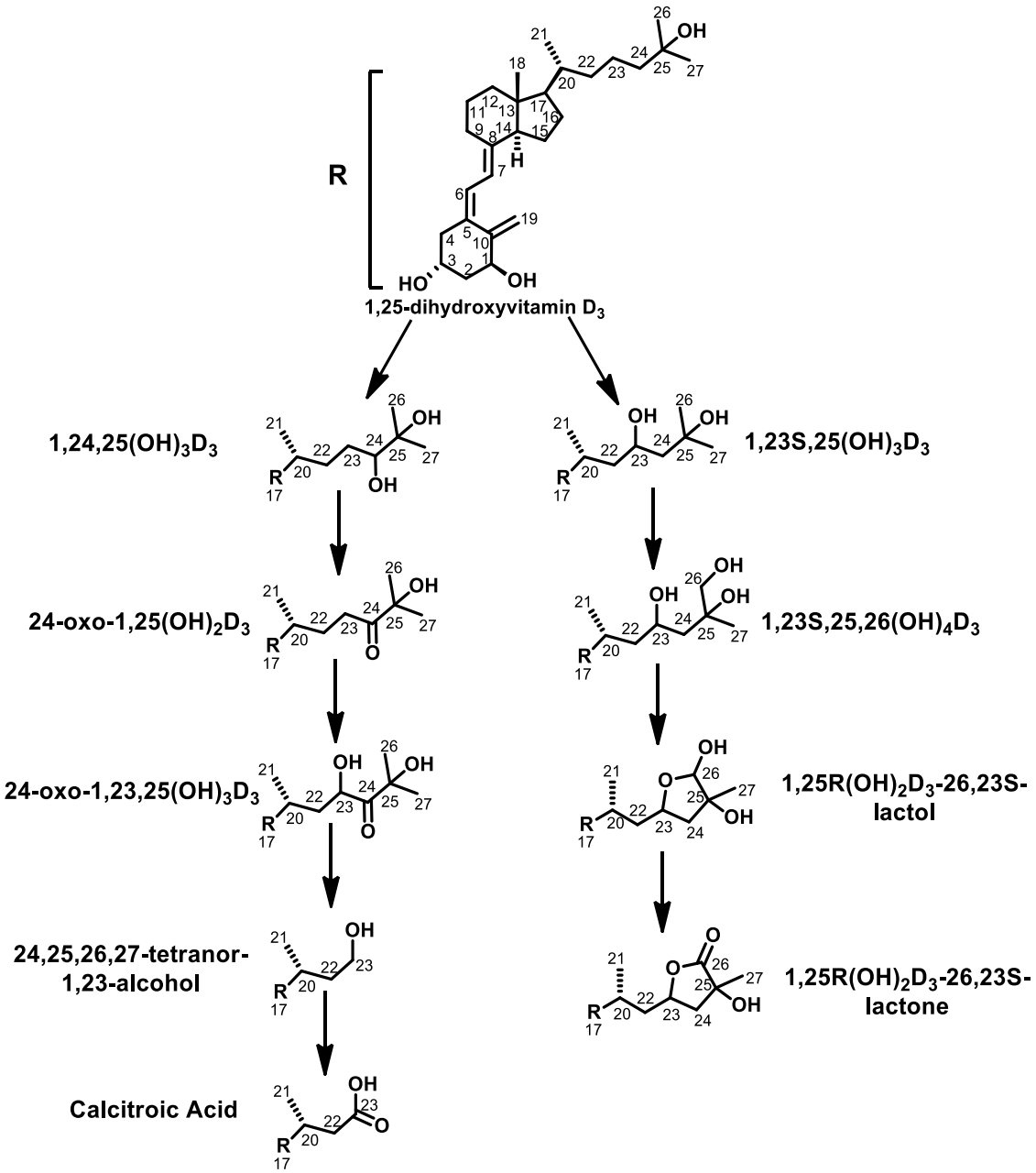

Figure 50. Enzymatic pathways catalyzed by CYP24A1 with $1,25(OH)_2D_3$ as a substrate. The C24-oxidation pathway products are on the left and the C23-hydroyxlation products are on the right.

most likely to regulate the $1,25(OH)_2D_3$ biological signal inside target cells. This is supported by cell-based experiments where CYP24A1 activity was blocked by ketoconazole, an antifungal

derivative known to inhibit P450 activity. The result is a build-up of 1,25$(OH)_2D_3$ and extended hormone action.[183] In CYP24A1 deficient mice, hypercalcemia and hypervitaminosis D_3 was observed due to high serum levels of 1,25$(OH)_2D_3$ and their inability of clearance.[184] Furthermore, when VDR-knockout mice were administered 1,25$(OH)_2D_3$, it was observed that the induction of CYP24A1 expression is dependent on VDR and is required for the production of calcitroic acid and 1,25R$(OH)_2D_3$-26,23S-lactone (final product of C23 hydroxylation pathway).[185, 186]

The C23 hydroxylation pathway consists of four enzymatic steps starting with the formation of 1,23S,25$(OH)_3D_3$ from 1,25$(OH)_2D_3$.[187] This is further converted to 1,23S,25,26$(OH)_4D_3$, then to 1,25R$(OH)_2D_3$-26,23S-lactol and finally 1,25R$(OH)_2D_3$-26,23S-lactone.[174] The biological activity of the C23 hydroxylation metabolites is unclear but it has been speculated that 1,25R$(OH)_2D_3$-26,23S-lactone could act as a VDR antagonist thus suggesting the lactone pathway proves a fail-safe mechanism to efficiently and rapidly diminish the vitamin D signal.[188, 189]

The binding and transcriptional activity of calcitroic acid with VDR was investigated in our lab. It was hypothesized that the final metabolite of the C24 pathway, a molecule that cannot be further oxidized by CYP24A1 enzymes, would be more metabolically stable and may bind and inhibit VDR-mediated transcription.

4.1.2 Lithocholic Acid Metabolism

Bile acids are the end products of hepatic cholesterol catabolism and acts as an emulsifier for ingestion and intestinal absorption of hydrophobic nutrients like cholesterol, fatty acids and

lipid-soluble vitamins like vitamin D. Primary bile acids are synthesized from cholesterol in the liver through a series of enzymatic reactions catalyzed by cytochrome p450 enzymes such as CYP7A1, CYP7B1 and/or CYP27A1 where CYP7A1 accounts for 50% or more of bile production in humans.[190] They are then secreted in bile as glycine or taurine conjugates where they assist in lipid digestion and absorption. Most bile acids are reabsorbed in the intestine and recirculate to the liver. Others are converted to secondary bile acids in the intestinal microflora, such as deoxycholic acid (DCA) and lithocholic acid (LCA).[191]

Secondary bile acids, like LCA, are toxic in higher concentrations when absorbed and can promote the development of liver disease and colorectal cancer. VDR has be found to act as a bile acid sensor and is involved with bile acid metabolism by inducing a LCA detoxification mechanism in the liver and intestine. The activation of VDR by either LCA or $1,25(OH)_2D_3$ induces expression of CYP3A4, the cytochrome p450 enzyme responsible for the removal of harmful secondary bile acids. The conversion of cholesterol to bile acids is tightly regulated to maintain homeostasis. Two receptors in particular, VDR and farnesoid X receptor (FXR), are part of this feedback regulation (Figure 51).[190] High concentrations of bile acids activate FXR resulting in suppressed bile acid biosynthesis. Activated FXR also stimulates fibroblast growth factor (FGF) 19 (in humans) and 15 (in mice) transcription which signals through hepatocytes to suppress CYP7A1 expression[192]. Interestingly, it has been observed that VDR-null mice have increased bile acid levels and decreased expression of FGF15. This phenotype has also been observed in FXR-null mice. Furthermore, $1,25(OH)_2D_3$ suppressed bile acid synthesis through a mechanism that involved regulation of FGF15 by VDR.[193, 194] This evidence shows that both FXR and VDR are

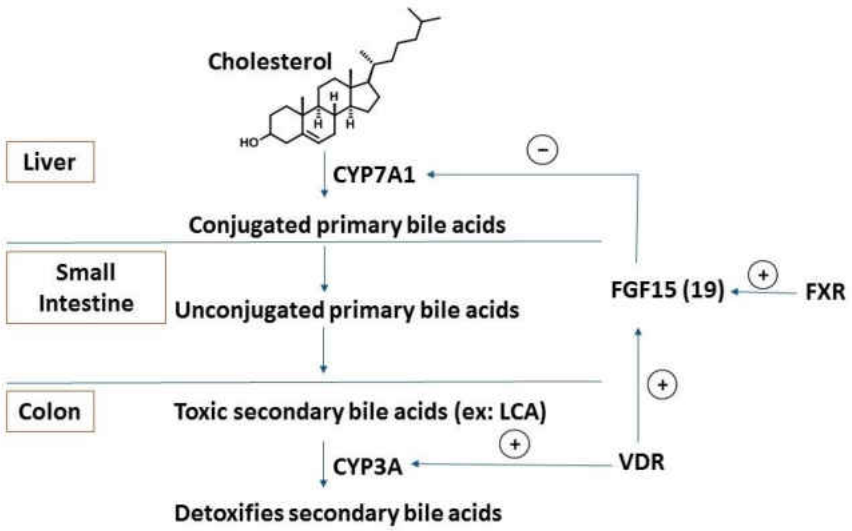

Figure 51. Summary of the role VDR and FXR in bile acid metabolism.

required for FGF15 (19) expression and that VDR plays an important role in the regulation of bile acids which may contribute to further protection against colorectal cancer.

4.1.3 VDR Ligand Metabolite Binding

In vivo studies conducted by DeLuca *et al* demonstrated that vitamin D deficient rats administered high concentrations of LCA showed induction of the vitamin D dependent calcium binding protein, calbindin-D_{9k}. However this link between LCA and calcium homeostasis was quickly dismissed when rats with normal vitamin D levels showed no effect from LCA. This could be explained by the lower binding affinity LCA has compared to $1,25(OH)_2D_3$.[195] In 2014, Rochel *et al* crystallographic studies revealed that two molecules of LCA bind to two distinct sites on the VDR LBD of zebra fish (Figure 52).[196] The first LCA molecule binds to the VDR ligand binding pocket (LBP) with a reversed orientation compared to $1,25(OH)_2D_3$. The binding requires VDR to rearrange near helix 6 (H6) where LCA interacts mainly through hydrophobic interactions and weaker H-bonds with residues through water molecules with zSer265, zArg302, zHis333, and

zHis423 and direct contacts with zTyr175 and zSer306. These weaker interactions explain the lower affinity of LCA for VDR and its ability to activate VDR-mediated transcription only at high micromolar concentrations. The second LCA molecules is slightly exposed to water and is anchored to VDR through its C3 hydroxyl group forming direct H-bonds with zSer263 (H3) and zGln267 (H3). This site is of considerably lower affinity compared to the first site but importantly

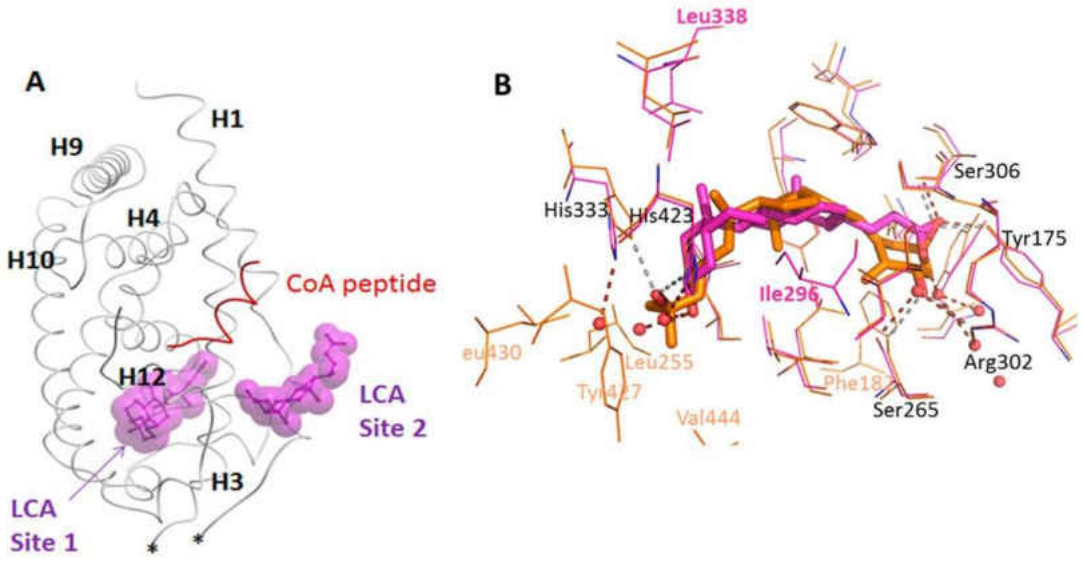

Figure 52. zVDR LBD crystal structure bound to two LCA molecules. A) The overall structure of VDR LBD receptor with two ligand binding sites. B) Comparison of the interactions between VDR and LCA (pink) and VDR and 1,25$(OH)_2D_3$ (orange) in the first binding site. The hydroxyl groups of LCA forming H-bonds are labeled in black. Specific interactions between VDR and 1,25$(OH)_2D_3$ that are absent in LCA are labeled in orange. Specific interactions between VDR and LCA that are absent for 1,25$(OH)_2D_3$ are labeled pink. Red spheres represent water molecules.

stabilizes the active protein conformation.

In recent years, LCA has been investigated as an important biological VDR ligand because of 1) its selectivity for VDR among other NRs and 2) its inability to induce hypercalcemia. Table 22 shows a list of compounds that have been investigated.[197, 198] The results show that esterification of the LCA side chain carboxyl group with methyl, ethyl, and benzyl moieties

drastically decreases transactivation. However, esterification of the C3 hydroxyl group increases VDR activity. LCA formate and LCA acetate activate VDR three times and thirty times the potency of LCA, respectively. Structure-function analysis and docking models have even shown that LCA acetate interacts with H3 and H4/5 residues in VDR LBP differently than $1,25(OH)_2D_3$ suggesting

Table 22. Derivatives based on LCA structure

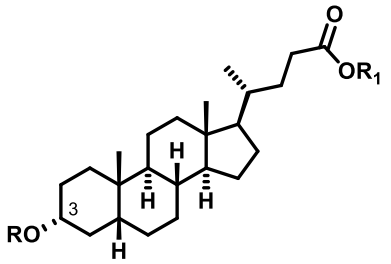

LCA Derivatives

R	R_1	Compound
OH	**H**	LCA
OH	**CH_3**	LCA methyl ester
OH	**C_2H_5**	LCA ethyl ester
OH	**$CH_2C_6H_5$**	LCA benzyl ester
HCOO	**H**	LCA formate
CH_3COO	**H**	LCA acetate
C_3H_7COO	**H**	LCA isobutyrate
$COOHC_2H_4COO$	**H**	LCA hemisuccinate
CH_3COO	**CH_3**	LCA acetate methyl ester
CH_3CH_2COO	**H**	LCA propionate

differential cofactor recruitment and selective physiological function. Furthermore, LCA propionate is as potent a VDR agonist as LCA acetate, while LCA isobutyrate and LCA hemisuccinate showed a decrease in VDR activation compared to LCA.

4.1.4 Proposed VDR Ligand Metabolites

Although many LCA derivatives have been investigated as VDR agonists, none have been studied as VDR-coactivator inhibitors. Herein we report the first look at LCA phase 1 and phase 2 metabolites evaluated as VDR-coactivator inhibitors. Phase 1 metabolic reactions include oxidation, hydrolysis and reduction reactions, while phase 2 are produced through conjugation

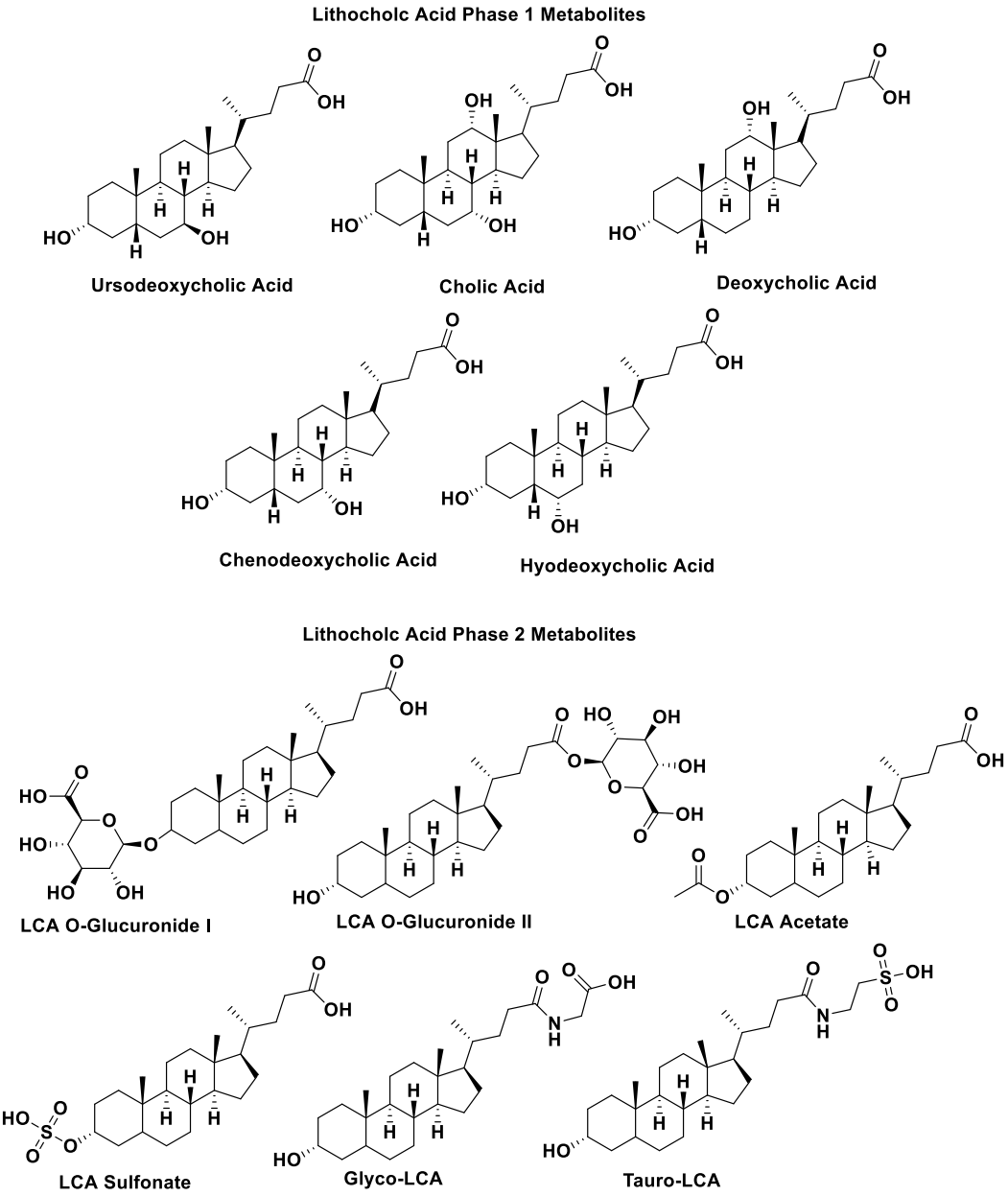

Figure 53. The phase 1 and phase 2 metabolites evaluated as VDR inhibitors.

reaction with glucuronic acid, sulfate and glycine. Our goal was to identify new natural VDR ligands. Figure 53 shows the phase 1 and phase 2 metabolites evaluated in our lab and their biological activity.

4.2 Chemistry

4.2.1 Synthetic Strategy

LCA was the starting material used to synthesize LCA acetate and LCA sulfonate (Scheme 7). A base catalyzed esterification reaction using 4-dimethylaminopyridine and acetyl chloride

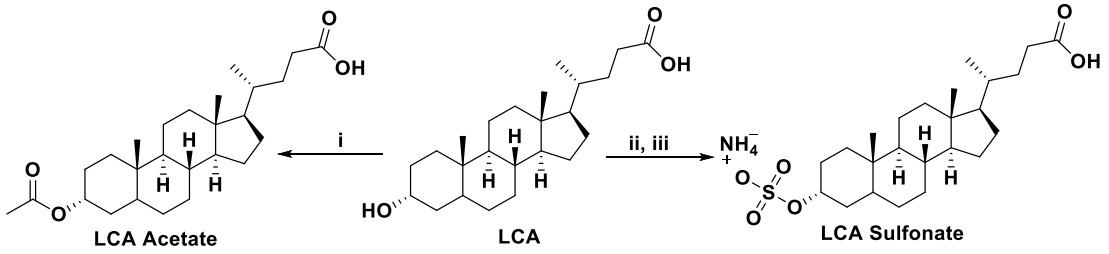

Scheme 7. Synthetic scheme for converting LCA to LCA acetate and LCA sulfonate. i) pyridine, acetyl chloride and 4-DMAP at room temperature, 1 hour. ii) sulfuric acid, acetic anhydride, and pyridine, 50-55°C, 30 minutes. iii) 25% ammonia water, 0°C, 15 minutes.

produced LCA acetate at a 95% yield.[199] To obtain LCA sulfonate, sulfuric acid and acetic anhydride in pyridine were used as oppose to the more "classical" method using pyridine sulfur trioxide to make sulfonate steroids.[200, 201] According to the literature, the "classical" method had low conversion of the starting alcohol (in this case LCA), produced polymeric byproducts resulting in difficulties during purification and low yields. The final product was converted into an ammonium salt using 25% ammonia acetate at 0°C to receive a final yield of 97%. For the synthesis of *O*-glucuronide I and II (Scheme 8), LCA methyl ester (LCME) was used as starting material. A Koenigs-Knorr condensation reaction of LCME with acetobromo-α-D-glucuronic acid methyl ester catalyzed by $CdCO_3$ in dry benzene at reflux was performed to make LCME *O*-

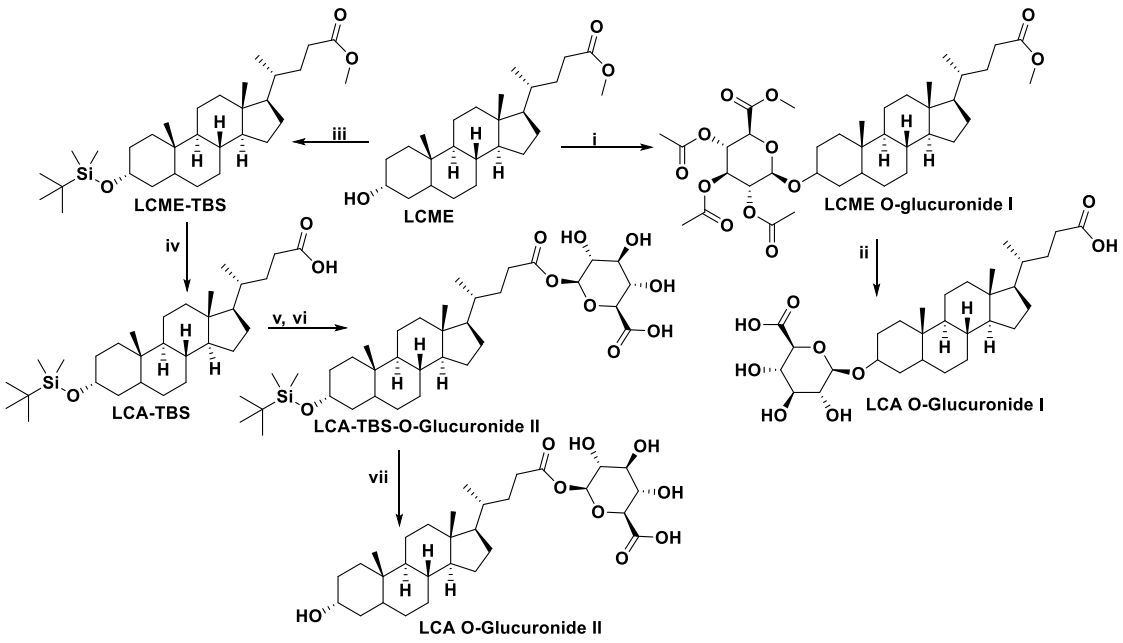

Scheme 8. Synthetic scheme for converting LCME to LCA *O*-glucuronide I and II. i) Dry benzene, $CdCO_3$, acetobromo-α-D-glucuronic acid methyl ester, reflux, 5 hours, ii) MeOH, 1M NaOH, room temperature, 4 hours followed by 5% HCl. iii) TBDMSCl, DMF, imidazole, room temperature, iv) THF, 2M NaOH, 75°C, 24 hours followed by 2M HCl, v) pyridine, CDI, reflux, 3 hours, vi) a) NaH, tetrabutylammonium glucuronate, 50°C, 4-5 hours, b) acetic acid, vii) THF,

glucuronide I.[202] The β-glycosidic linkage with LCA methyl ester at the C-3 position was confirmed by ^{1}HNMR with the appearance of a doublet at 4.69 ppm and the disappearance of the brominated anomeric proton doublet 6.67ppm. Hydrolysis with sodium hydroxide afforded the final product, LCA *O*-glucuronide I, at an overall yield of 61%. Figure 54 shows the proposed mechanism for the Koenigs-Knorr glycosylation reaction. The acyl protected sugar molecule is first activated through an S_N1 removal of the bromine. The reaction then proceeds through a process called neighboring group participation with the acetoxy substituent to form an acyloxonium cation intermediate that is stabilized by both acetoxy oxygen atoms. The sugar is now a good acceptor/electrophile for the donor/nucleophile, LCA, to attack at the anomeric carbon and form the final LCA O-glucuronide I product.[203-205]

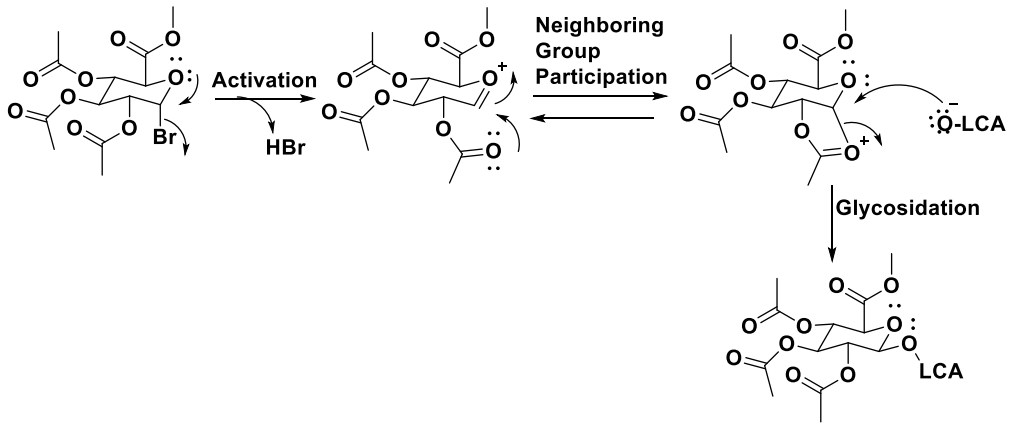

Figure 54. Mechanism of the Koenigs-Knorr glycosylation reaction to produce LCA *O*-glucuronide I.

LCA *O*-glucuronide II was synthesized in four steps starting with the protection as *t*-butyldimethylsilylether (TBS). TBS was chosen as a protecting group because it is 10^4 more stable to basic hydrolysis than trimethylsilyl (TMS).[206] However, a *t*-butyldiphenylsilylether would have allowed TLC monitoring omitting the use of a stain. Hydrolysis of LCME-TBS afforded the corresponding carboxylic acid, LCA-TBS. Next, glucuronic acid was converted into a tetrabutylammonium salt (Scheme 9), which not only protected the free carboxyl group but also rendered it soluble in organic solvents.[207] In a one pot reaction, LCA-TBS was activated with 1,1'-

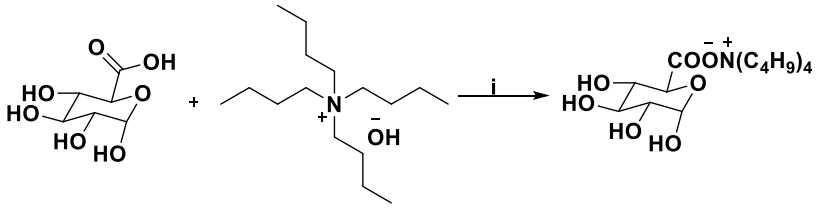

Scheme 9. Tetrabutylammonium salt formation of glucuronic acid.
i) MeOH, 40°C, 1 hour.

carbonyldi-imidazole followed by the addition of tetrabutylammonium glucoronate. The reaction was quenched with acetic acid to produce LCA-TBS *O*-glucuronide II. To avoid accidental cleavage of the coupled sugar ring, deprotection of the TBS group was accomplished under

neutral conditions with tetrabutylammonium fluoride as oppose to acidic conditions.[206] The fluoride-based deprotection is driven by the formation of a Si-F bond which is about 30kcal/mol stronger than a Si-O bond. This reaction was quenched with water to yield the final product, LCA *O*-glucuronide II. The final product was purified by silica gel column to remove any unreacted LCA and then recrystallized with EtOH to yield about 40 mg of product with an overall yield of 10%. Although this multistep synthesis produced little product, it was beneficial to have the sugar as the donor and LCA as the acceptor molecule because it omitted unnecessary protection and deprotection of the sugar hydroxyl groups.

4.2.2 Characterization

All phase 1 metabolites, lithocholic acid, lithocholic methyl ester and taurolithocholic acid were purchase from Sigma-Aldrich and glycolithocholic acid was purchased from Santa Cruz Biotechnology. Calcitroic acid was purchased from Toronto Research Chemicals. Synthesized compounds were either purified via recrystallization or normal phase flash chromatography (SPI Biotage, silica gel 230-400 mesh). Compound characterization was performed using a Shimadzu 2020 LC-MS (single quadrupole) instrument with compounds directly injected. NMR spectra were recorded on a Bruker 300MHz instrument with samples diluted in either $CDCl_3$ or DMSO-D_6.

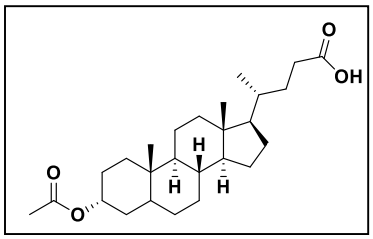

LCA Acetate: 95% yield; Lithocholic acid (0.5 g, 1.3 mmol), was dissolved in dry pyridine (10mL) under N_2 gas and cooled to 0^{o}C. 4-dimethylaminopyridine (0.02 g, 0.13 mmol) and acetyl chloride (1.1 mL, 16 mmol) were added to the solution. The reaction was

stirred at room temperature and monitored by TLC using EtOAc-Hexanes-MeOH (4:1:1, v/v/v) and cerium molybdate as a developing stain. After 1 hour, water (3 mL) was added and the solution was evaporated under reduced pressure. DCM (15 mL) was used to dissolve the residue, which was subsequently washed with saturated aqueous NaCl (20 mL) and water (15 mL). The organic phase was dried over Na_2SO_4, then filtered and evaporated to dryness. The crude product was co-evaporated with toluene (10 mL x2), ethanol (10 mL x2), acetonitrile (10 mL x 2) and DCM (10 mL x 2) in order to remove traces of pyridine and purified by silica gel chromatography with CH_3OH-CH_2Cl_2 (0%-5% strong). ^{1}H-NMR (300 MHz) ($CDCl_3$) δ 4.75 (m, 1H, H-3), 2.05 (s, 3H, -CH_3, Ac), 0.95 (m, 6H, H-18/19, 21), 0.67 (s, 3H, H-18/19); ^{13}C NMR δ 178.57, 170.72, 74.43, 56.51, 55.99, 42.75, 41.89, 40.42, 40.16, 35.79, 35.35, 35.03, 34.58, 32.25, 31.06, 29.69, 28.18, 26.32, 23.33, 20.83, 18.55, 18.28, 12.05; MS DUIS ($^-$ve) calcd. *m/z* for $C_{26}H_{42}O_4$ [(M)] 418.3, found [$(M-1)^-$] 417.4.

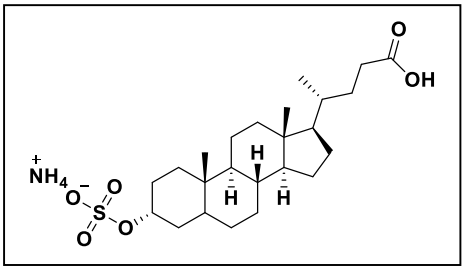

LCA Sulfonate: 97% yield; Sulfuric acid (0.16 mL, 3 mmol) and acetic anhydride (0.28 mL, 3 mmol) were mixed with dry pyridine (5 mL) and after 5 minutes of stirring at 50-55^{o}C a solution of lithocholic acid in 2 mL of pyridine was added. The mixture was stirred for 30minutes at the same conditions, cooled to 0^{o}C, and 25% ammonia water (0.74 mL) was added. After 15 minutes of stirring, the precipitate was filtered and the filtrate was placed on a rotary evaporator for concentrating. The product isolated was not purified further. ^{1}H-NMR (300 MHz) (DMSO-D_6) δ 3.96 (m, 1H, H-3), 0.88 (m, 6H, H-18/19, 21), 0.61 (s, 3H, H-18/19); ^{13}C NMR δ 175.18, 75.98, 56.41, 55.93, 42.66, 35.77, 35.47, 35.24, 24.53,

33.77, 31.21, 31.08, 28.16, 27.27, 26.52, 24.31, 23.65, 20.85, 18.59, 12.34; ^{13}CDEPT-135 δ Negative (-) CH_2: 76.05, 56.42, 55.94, 42.06, 40.33, 35.82, 35.51, 24.31, 18.59, 12.34 Positive (+) CH and CH_3: 40.09, 35.29, 33.80, 31.21, 31.13, 28.16, 27.27, 26.53, 23.64, 20.85; MS DUIS ($^-$ve) calcd. *m/z* for $C_{24}H_{40}O_6S$ [(M)] 456.3, found [$(M-1)^-$] 455.4.

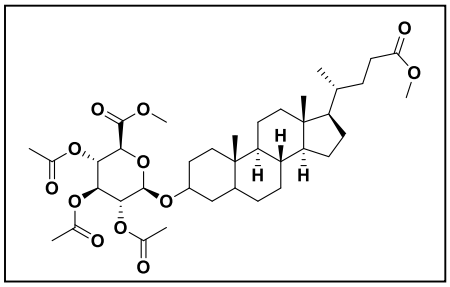

LCME *O*-glucuronide I: 43% yield; To a solution of lithocholic methyl ester (400 mg) in anhydrous benzene (16 mL) was added cadmium carbonate (400 mg), acetobromo-α-D-glucuronic acid methyl ester (400 mg) and a quantity of molecular sieves (400 mg). The mixture was stirred at reflux. After 1 hour and 3 hours, additional quantities of acetobromo-α-D-glucuronic acid methyl ester (200 mg) and cadmium carbonate (200 mg) were added and the mixture stirred for 7 hours and was monitored by TLC using hexane-EtOAc-AcOH (50:50:1, v/v/v) and cerium molybdate as the developing stain. The precipitate was removed by filtration and washed with EtOAc. The filtrate and washings were combine and evaporated to dryness under reduced pressure and the oily residue was recrystallized in MeOH (5mL) to make white crystals. ^{1}H-NMR (300 MHz) ($CDCl_3$) δ 5.28-5.24 (m,2H), 5.01-4.95 (t, 1H, J= 9Hz), 4.69-4.66 (d, 1H, J= 9Hz, anomeric), 4.06-4.03 (d, 1H, J= 9Hz), 3.78 (s, 3H, Ac), 3.69 (s, 3H, Ac), 3.62 (m, 1H, H-3), 2.07, 2.04 (s, 9H, $COCH_3$), 0.92 (m, 6H, H-18/19, 21), 0.65 (s, 3H, H-18/19); ^{13}C NMR δ 174.76, 170.21, 169.35, 169.28, 167.32, 99.57, 80.56, 72.61, 72.20, 71.57, 69.50, 56.28, 55.89, 52.82, 51.46, 42.70, 42.17, 40.30, 40.09, 35.81, 35.35, 35.09, 34.63, 33.99, 31.05, 30.99, 28.16, 27.09, 27.01, 26.23, 24.16, 23.35, 20.83, 20.71, 20.63, 20.51, 18.25, 12.01; MS DUIS ($^+$ve) calcd. *m/z* for $C_{38}H_{58}O_{12}$ [(M)] 706.4, found [$(M+ 18 (NH_4))^+$] 724.8.

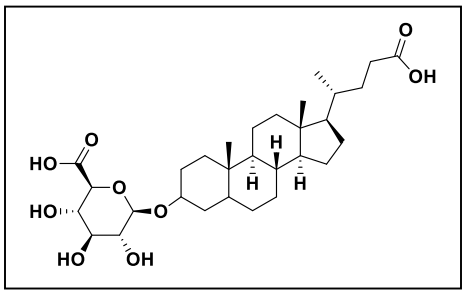

LCA *O*-glucuronide I: 100% yield; To a solution of LCME *O*-glucuronide I (70 mg) in MeOH (8 mL) an aqueous solution of 2M NaOH was added dropwise until the mixture was basic. The reaction was stirred at room temperature overnight and monitored by TLC using hexanes-EtOAc-AcOH (50:50:1, v/v/v) and cerium molybdate as the developing stain. After most of the solvent was removed by rotary evaporation, the reaction product was diluted with water, neutralized with 3M HCl and then evaporated to dryness. The residue was re-suspended in anhydrous EtOH (10 mL) and the insoluble material was filtered off and washed with EtOH. The combined filtrate was evaporated and the residue was recrystallized from MeOH resulting in white, flakey solid. ^{1}H-NMR (300 MHz) (DMSO-D_6) δ 4.34-4.31 (d, 1H, J= 9Hz, anomeric), 3.61-3.58 (d, 1H, J= 9Hz), 3.33-3.27 (2H, t, J= 9Hz), 3.20-3.14 (1H, t, J= 9Hz), 2.93 (m, 1H, H-3), 0.88 (m, 6H, H-18/19, 21), 0.61 (s, 3H, H-18/19); ^{13}C NMR δ 175.30, 170.86, 101.33, 77.75, 76.55, 76.00, 73.65, 72.01, 56.45, 55.97, 51.65, 42.72, 41.86, 35.80, 35.29, 34.26, 31.13, 30.83, 28.17, 27.20, 26.85, 26.55, 24.31, 26.55, 24.31, 23.49, 20.86, 18.59, 12.32 ; MS DUIS ($^{-}$ve) calcd. *m/z* for $C_{30}H_{48}O_9$ [(M)] 552, found [$(M-1)^{-}$] 551.

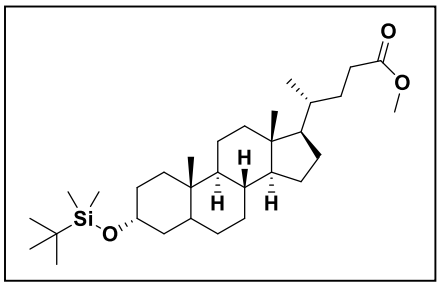

LCME-TBS: 84% yield; To a solution of LCME (3 g, 0.0077 mols) and imidazole (3.74 g, 0.0231 mol, 3 equiv.) in dry DMF (28 mL) tert-butyldimethylsilyl chloride (3.48 g, 0.0231 mols, 3 equiv.) was added dropwise. The mixture was stirred overnight at room temperature and monitored by TLC using EtOAc-DCM- AcOH (5:95:1, v/v/v) and cerium molybdate as the developing stain. Upon completion, the reaction was diluted with water and extracted with DCM (25 mL x 3) and then dried using rotary evaporation. The resulting

crude product was purified using silica gel chromatography using EtOAc-Hexanes with 1% AcOH (1% -20% strong). A white solid was isolated. ^{1}H-NMR (300 MHz) ($CDCl_3$) δ 3.67 (s, 3H, Ac) 3.59 (m, 1H, H-3), 0.92 (m, 6H, H-18/19, 21), 0.90 (s, 9H, t-butyl-Si), 0.63 (s, 3H, H-18/19), 0.06 (s, 6H, $2CH_3$-Si); ^{13}C NMR δ 174.90, 135.15, 121.89, 72.85, 56.39, 55.93, 51.49, 42.70, 42.27, 40.20, 40.12, 36.90, 36.49, 35.84, 35.56, 35.36, 34.57, 31.57, 31.06, 31.00, 28.18, 27.28, 26.39, 25.97, 25.74, 24.20, 23.38, 20.79, 18.33, 18.24, 12.00; MS DUIS ($^{+}$ve) calcd. *m/z* for $C_{31}H_{56}O_3Si$ [(M)] 504, found $[(M\text{-}TBDMS)]^{+}$ 373 and $[(M+1+imidazole)^{+}]$ 574.

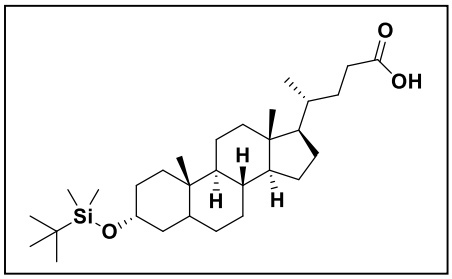

LCA-TBS: 64% yield; LCME-TBS (3.25 g, 6.45 mmol) was dissolved in THF (20 mL) and to it 2M NaOH was added until it reached pH=10. The reaction was stirred at 75^{o}C for 24 hours and monitored by TLC using EtOAc-Hexanes-AcOH (3:2:1, v/v/v) and cerium molybdate as the developing stain. Once complete, most of the solvent was removed by rotary evaporation. The reaction product was diluted with water and acidified with 3M HCl to pH=3. The solid formed was collected and purified by silica gel chromatography using EtOAc-Hexanes with 1% AcOH (1-20% strong). A white solid with low solubility in MeOH, EtOH and $CHCl_3$ was obtained. ^{1}H-NMR (500 MHz) (DMSO-D_6) δ 8.45 (s, 1H, COOH), 3.58 (m, 1H, H-3), 0.88 (m, 6H, H-18/19, 21), 0.85 (s, 9H, t-butyl-Si), 0.61 (s, 3H, H-18/19), 0.02 (s, 6H, $2CH_3$-Si); ^{13}C NMR δ 175.14, 72.56, 56.45, 56.09, 42.80, 42.05, 37.11, 35.90, 35.49, 35.24, 34.62, 31.34, 31.24, 28.11, 27.26, 26.53, 26.28, 24.28, 23.62, 20.92, 18.65, 18.23, 12.36; MS DUIS ($^{-}$ve) calcd. *m/z* for $C_{31}H_{54}O_3Si$ [(M)] 490.3, found $[(M\text{-}1)^{-}]$ 489.4.

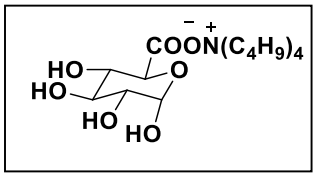

Tetrabutylammonium Glucuronate: ~100% yield; Glucuronic acid (2.9 g) was suspended in methanol (25 mL) to which tetrabutylammonium hydroxide 30-hydrate (12 g) was added. The mixture was stirred at room temperature for 1 hour until a clear solution resulted. The solvent was removed in a rotary evaporator at 40°C, thereby yielding a syrup. Addition of acetone (100 mL) resulted in precipitation of the tetrabutylammonium glucoronate. That salt was separated by filtration and washed with acetone. The filtrate and washings, on further concentration in a rotary evaporator, resulted in precipitation of more salt. A flakey, white solid was obtained. ^{1}H-NMR (500 MHz) (DMSO-D_6) δ 5.75- 5.72 (d, 1H, J= 9Hz), 4.50-4.58 (d, 1H, J= 6Hz), 3.86-3.58 (m, 4H,OHs), 3.19-3.14 (m, 8H), 1.57 (m, 8H), 1.37-1.25 (m, 8H), 0.96-0.91 (t, 12H, J= 7.5Hz); MS DUIS ($^{-}$ve) calcd. *m/z* for $C_{22}H_{45}NO_7$ [(M)] 435.2, found [(M-tetrabutylammonium)$^{-}$] 193.

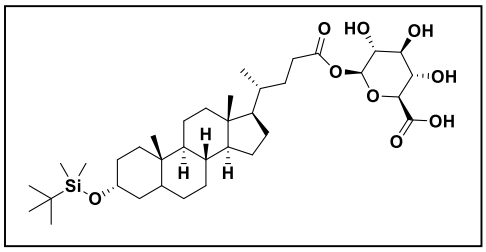

LCA-TBS-*O*-glucuronide II: >100% yield (crude); LCA-TBS (1.0 g, 2.04 mmol) and 1,1'-carbonyliimidazole (0.66 g, 4.08 mmol, 2 equiv.) were dissolved in dry pyridine (40 mL). The mixture was stirred at reflux overnight and was monitored by both TLC using EtOAc-Hexanes-AcOH (4:1:1, v/v/v) and cerium molybdate as a developing stain and mass spectrometry. The development of a peak at 542 *m/z* in the positive mode indicated the formation of LCA-TBS-imidazole coupled product. To the same reaction pot, tetrabutylammonium glucuronate (2.22 g, 5.1 mmol, 2.5 equiv.), dry pyridine (10 mL), and sodium hydride (15 mg, 0.04 mmol, 0.02 equiv.) were added and the reaction was stirred at 50°C for 5 hours. The reaction was monitored by TLC (same conditions as above) and mass spectrometry. The development of a peak at 666 *m/z* in the negative mode indicated the

formation of LCA-TBS-*O*-glucuronide II product. The reaction was stopped by careful addition of water. After the solution was made just acidic with acetic acid, the product was extracted with EtOAc (25mL x 3). The EtOAc layer was dried over Na_2SO_4 and then evaporated to dryness with a rotary evaporator. The final yellow oil was not purified and was directly used for the next reaction. Crude sample: ^{1}H-NMR (300 MHz) (DMSO-D_6) δ 4.69-4.67 (d, 2H, J= 6Hz anomeric), 3.47 (m, 1H, H-3), 0.89 (m, 6H, H-18/19, 21), 0.83 (s, 9H, t-butyl-Si), 0.63 (s, 3H, H-18/19), 0.07 (s, 6H, 2CH_3-Si); ^{13}C NMR δ 178.36 (glucuronic acid COOH) and 175.73 (LCA COOR) MS DUIS ($^-$ve) calcd. *m/z* for $C_{36}H_{62}O_9Si$ [(M)] 667, found [$(M-1)^-$] 666.

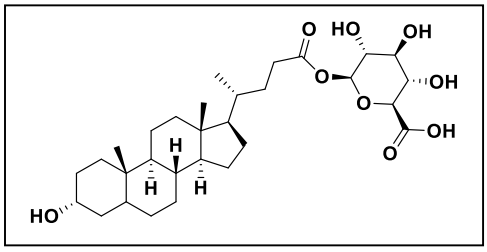

LCA *O*-glucuronide II: 10% yield; LCA-TBS-O-glucuronide II (1.3 g, 2.0 mmol) was dissolved in a 1.0M THF solution of tetrabutylammonium fluoride (1.66 mL, 3 equiv.). The reaction was stirred at 40^{o}C for 2 days and was monitored by mass spectrometry with the disappearance of the startming material peak at 666 *m/z* in the negative mode. When complete, the reaction was quenched with addition of water and washed with EtOAc (3x). The EtOAc layer was dried over $MgSO_4$ and dried by rotary evaporation. The crude yellow oil re-suspended in EtOH and the insoluble solid was filtered and washed with EtOH. The filtrate was collected and dried. The residue was then purified using silica gel chromatography with MeOH-EtOAc with 1%AcOH (0-60% strong) to remove the LCA impurity. Fractions containing the product were dried and then recrystallized with EtOH to produce a cream colored solid. ^{1}H-NMR (300 MHz) (DMSO-D_6) δ 5.23-3.77 (m, 5H, sugar-ring protons), 3.46 (m, 1H, H-3), 2.28-2.22 (m, 0.88 (m, 6H, H-18/19, 21), 0.62 (s, 3H, H-18/19); ^{13}DEPT-135 δ Negative (-) CH_2: 56.48, 40.25, 36.78, 35.64, 31.11, 30.86, 28.14, 27.38, 26.64, 20.89, Positive (+)

CH and CH_3: 93.07, 89.76, 70.77, 70.34, 56.52, 42.01, 40.81, 40.53, 40.43, 40.25, 39.98, 39.70, 35.86, 35.21, 23.74, 19.02, 18.62, 12.34. MS DUIS ($^-$ve) calcd. *m/z* for $C_{30}H_{48}O_9$ [(M)] 552, found [$(M-1)^-$] 551.

4.3 Modulation of VDR-Coactivator Binding by VDR Ligand Metabolites

Table 23 summarizes the binding results for phase 1 metabolites of VDR ligands. All compounds but LCA showed no induction of the VDR-SRC2-3 interaction. Surprisingly, LCA had low agonistic binding at an estimated value greater than 150 µM although activity of LCA has been reported in the range of 4-6 µM.[208] Interestingly, the VDR-SRC2-3 binding was inhibited with an IC_{50}= 13.6 ± 4.6 µM. Ursodeoxycholic acid, cholic acid, and deoxycholic acid were inactive as antagonist, while chenodeoxycholic acid and hyodeoxycholic acid exhibited low inhibition affinities at values greater than 150 µM. The poor inhibition by these compounds could be

Table 23. Modulation of VDR-Coactivator binding in the presence of phase 1 VDR ligand metabolites

Compound	Recruitment of SRC-2-3 to VDR EC_{50} (µM)	Inhibition of SRC2-3 VDR Interaction IC_{50} (µM)
Ursodeoxycholic Acid	Inactive	Inactive
Lithocholic Acid	>150	13.6 ± 4.6
Cholic Acid	Inactive	Inactive
Deoxycholic Acid	Inactive	Inactive
Chenodeoxycholic Acid	Inactive	>150
Hyodeoxycholic Acid	Inactive	>150
Calcitroic Acid	Inactive	6.12 ± 2.1

The maximum concentration used for this assay was 450 µM of each compound.

contributed to the additional hydroxyl groups. VDR-LBD has a very hydrophobic pocket with hydrogen bonding occurring at the outer ends of the pocket. Hydroxyl groups in this region might promote unfavorable binding. Interestingly, calcitroic acid was the most potent inhibitory metabolite with an IC_{50} value two times as potent as LCA. The comparable potency of these two

compounds could be contributed to the absence of any hydroxyl groups on the B and C rings and their ability to make favorable hydrogen bonds at each end of the molecules (C3 –OH and C25 –COOH). As expected, LCA showed agonistic behavior in the same experiments at higher concentrations, as seen in Figure 55, A. It can be speculated that the availability of two VDR binding sites for LCA might be responsible for this behavior. However, we also observed a large

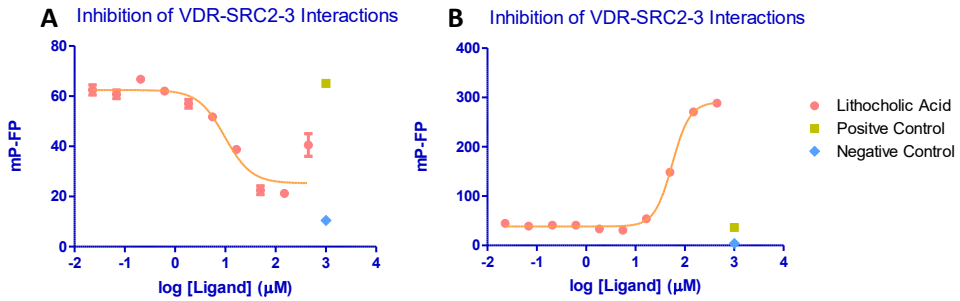

Figure 55. A) LCA effect on the interactions between VDR and Alexa Fluor 647-labeled SRC2-3 coactivator. B) LCA effect on VDR and Texas Red-labeled SRC2-3

increase in fluorescence polarization and fluorescence intensity using a Texas Red labeled SRC2-3 (Figure 55, B), which is an indication of aggregation between LCA and the fluorescent probe. This affect has been observed with other compounds for example GW0742, where aggregates between compound and probe and increases the fluorescence intensity and polarization in the absence of VDR.[150] LCA phase 2 metabolites were also investigated using the fluorescence polarization-based binding assay (Table 24). None of the compounds were able to induce VDR-coactivator binding. However, changes to the C3 hydroxyl group versus modification to the C25 position still allowed for inhibition of VDR-coactivator interactions. As previously discussed, LCA acetate is a known VDR agonist with potency 30 times greater than LCA but has never been evaluated as a VDR antagonist. Although agonistic binding of LCA acetate was not observed in

Table 24. Modulation of VDR-Coactivator binding in the presence of phase 2 VDR ligand metabolites this

Compound	Recruitment SRC2-3 VDR Interaction EC_{50} (μM)	Inhibition of SRC2-3 VDR Interaction IC_{50} (μM)
Glyco-LCA	Inactive	40.1 ± 8.0
Tauro-LCA	Inactive	14.5 ± 4.3
LCA Acetate	Inactive	11.02 ± 3.2
LCA *O*-Glucuronide I	Inactive	28.7 ± 8.8
LCA *O*-Glucuronide II	Inactive	2.90 ± 0.6
LCA Sulfonate	Inactive	23.3 ± 4.3

The maximum concentration used for this assay was 450 μM of each compound

assay, LCA and LCA acetate have comparable inhibitory effects on the interactions between VDR and coactivator. Tauro-LCA was about three times more potent than glycol-LCA and the sulfonate was less inhibitory than acetate. When comparing the positioning of glucuronic acid on LCA, LCA *O*-glucuronide II was 10 times more potent than LCA *O*-glucuronide I.

4.4 Modulation of VDR-Mediated Transcription by VDR Ligand Metabolites

Table 25 summarizes the VDR transcription data obtained for LCA, its phase 1 metabolites and calcitroic acid. Surprisingly, LCA was unable to activate VDR-mediated transcription in cells although the reported activation was observed in the presence of overexpressed RXR. Thus, the RXR dimer is essential to mediate the agonistic activity of LCA. As expected from the FP-binding data, all the other LCA phase 1 metabolites did not activate transcription. Calcitroic acid showed exciting transcription data. As previously thought, metabolites derived from CYP24A1-mediated catabolism like calcitroic acid would be inactive intermediates of vitamin D degradation and thus serve no physiological function. However, our data demonstrates that calcitroic acid possesses partial agonistic activity at 16.2%, although at higher concentration and to a lower degree than $1,25(OH)_2D_3$. In addition, calcitroic acid was the only compound in this series to inhibit VDR-mediated transcription at a low micromolar level with little toxic effects, which is consistent with the FP-binding data from above. Most interestingly, as calcitrioic acid inhibits the binding of

Table 25. Modulation of VDR transcription in the presence of phase 1 VDR ligand metabolites

Compound	VDR Transcription EC_{50} (μM)[a]	VDR Transcription IC_{50} (μM)[a]	Cytotoxicity LD_{50} (μM)[b]
Ursodeoxycholic Acid	Inactive	66.3 ± 39.5	Non-toxic
Lithocholic Acid	Inactive	35.9 ± 4.4	>50
Cholic Acid	Inactive	>100	Non-toxic
Deoxycholic Acid	Inactive	40.0 ± 2.24	>150
Chenodeoxycholic Acid	Inactive	61.3 ± 11.0	>150
Hyodeoxycholic Acid	Inactive	62.7 ± 26.9	Non-toxic
Calcitroic Acid	2.56 ± 1.04 (16.2%)	3.20 ± 2.4	>100

[a]Transcription assay using a CMV-VDR plasmid and a luciferase reporter plasmid under control of a 24-hydroxylase promoter with LCA and its phase 1 metabolites as well as $1,25(OH)_2D_3$ metabolite, calcitroic acid. Efficacy, shown in parenthesis, is in respect to full activation with $1,25(OH)_2D_3$. [b]Cell- TiterGlo (Promega). Maximum concentration used was 150 μM.

$1,25(OH)_2D_3$ it also acts a partial agonist at nearly the same concentration (Figure 56). Further studies will be conducted to determine the physiological role of calcitroic acid especially in

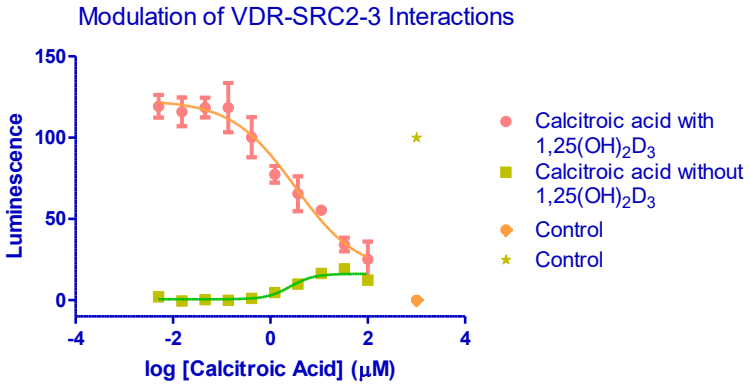

Figure 56. Combined dose response curves showing partial agonistic activity (pink) and competitive inhibition (in the presence of $1,25(OH)_2D_3$) (green) of calcitroic acid with VDR.

respect to calcium homeostasis. Only LCA had a moderately toxic effect on the cells.

In the 2-hybrid assay (Table 26), LCA showed agonistic results that coincides with the

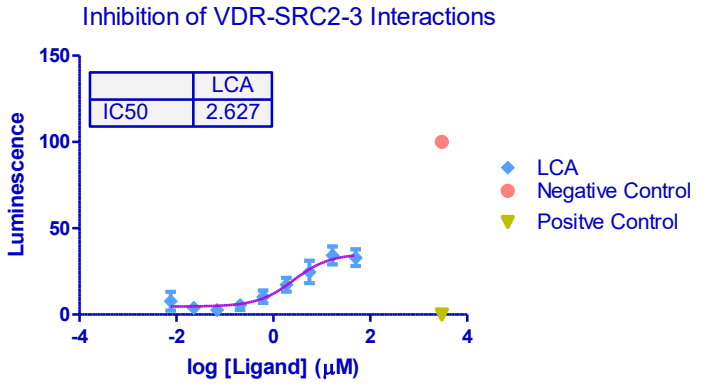

Figure 57. Dose-response curve showing the partial agonistic activity of LCA compared to $1,25(OH)_2D_3$.

Table 26. Mod ase 1 VDR ligand metaboli

Compc		
Ursodeoxyc		
Lithocho		
Cholic		
Deoxycholic acid	Inactive	57.36 ± 11.1
Chenodeoxycholic acid	Inactive	>60
Hyodeoxycholic acid	Inactive	66.6 ± 32.1
Calcitroic Acid	0.85 ± 0.33 (47.6%)	Inactive

Two-hydrid assay: HEK293T cells were transfected with a VP16-VDR-LBD, SRC1-GAL4, and luciferase reporter plasmid vector with or without $1,25(OH)_2D_3$ and LCA phase 1 metabolites or calcitroic acid. Efficacy, shown in parenthesis, is in respect to full activation with $1,25(OH)_2D_3$. Maximum concentration used was 150 µM.

literature.[198] It was able to recruit SRC1 coactivator and activate transcription with an IC_{50}= 2.63 ± 1.75 µM, however the effects was only 35.2% of that of $1,25(OH)_2D_3$ (Figure 57).

LCA inhibited transcription at a moderate level that was comparable to the results found in the transcription assay (Table 25). Again, calcitroic acid was a partial agonist but did not have any inhibitory effect on the recruitment of SRC1. All other LCA phase 1 metabolites did not activate transcription thus suggesting unfavorable interactions with VDR due to extra hydrogen bond donor/acceptors in the ring system. Deoxycholic acid, chenodeoxycholic acid, and hyodeoxycholic acid again showed moderate antagonistic effects on transcription.

Table 27 summarizes the transcription data obtained for LCA phase II metabolites. All compounds were non-toxic at a maximum concentration of 150 μM. Glyco-LCA, tauro-LCA, and

Table 27. Modulation of VDR transcription in the presence of phase 2 VDR ligand metabolites

Compound	VDR Transcription EC_{50} (μM)[a]	VDR Transcription IC_{50} (μM)	Cytotoxicity LD_{50} (μM)
Glyco-LCA	Inactive	>50	Non-toxic
Tauro-LCA	Inactive	Inactive	Non-toxic
LCA Acetate	17.6 ± 7.60	44.3 ± 16.4	Non-toxic
LCA *O*-Glucuronide I	3.73 ± 2.1 (22.1%)	>150	Non-toxic
LCA *O*-Glucuronide II	6.92 ± 3.9 (21.7%)	>150	Non-toxic
LCA Sulfonate	Inactive	Inactive	Non-toxic

[a]Transcription assay using a CMV-VDR plasmid and a luciferase reporter plasmid under control of a 24-hydroxylase promoter with LCA phase 2 metabolites. Percent partial agonistic activity is shown in parenthesis. Efficacy, shown in parenthesis, is in respect to full activation with $1,25(OH)_2D_3$. [b]Cell-TiterGlo (Promega). Maximum concentration used was 150 μM.

LCA sulfonate were unable to activate or inhibit transcription with glyco-LCA possessing very moderate inhibitory effects. LCA acetate agonist activity was confirmed but also inhibited VDR-mediated transcription at an IC_{50}= 44.3 ± 16.4 μM. In addition, LCA *O*-glucuronide I and II exhibited a potent partial agonist activity as seen in the dose-response curve in Figure 58.

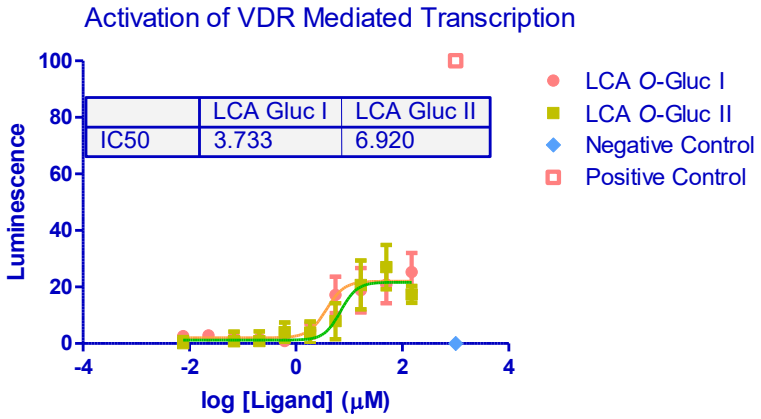

Figure 58. Dose-response curve showing the partial agonistic effect LCA *O*-glucuronide I and LCA *O*-glucuronide II have on VDR-mediated transcription.

In the 2-hydrid assay (Table 28), LCA acetate was able to recruit SRC1 and activate VDR-mediated transcription reported. LCA *O*-glucuronide II but not LCA *O*-glucuronide I was also a potent agonist with a partial agonistic effect of 30.7% compared to $1,25(OH)_2D_3$. Other phase 2 metabolites exhibited no activity.

Table 28. Modulation of VDR-SRC1 interaction in cells in the presence of phase 2 VDR ligand metabolites.

COMPOUND	2-Hybrid: VDR Transcription EC_{50} (μM)	2-Hybrid: VDR Transcription IC_{50} (μM)
Glyco-LCA	Inactive	>50
Tauro-LCA	Inactive	Inactive
LCA Acetate	1.79 ± 1.16	>150
LCA *O*-Glucuronide I	>150	>150
LCA *O*-Glucuronide II	8.39 ± 4.60 (30.7%)	>150
LCA Sulfonate	Inactive	Inactive

Two-hydrid assay: HEK293T cells were transfected with a VP16-VDR-LBD, SRC1-GAL4, and luciferase reporter plasmid vector with or without $1,25(OH)_2D_3$ and LCA phase 2 metabolites. Percent partial agonistic activity is shown in parenthesis. Efficacy, shown in parenthesis, is in respect to full activation with $1,25(OH)_2D_3$. Maximum concentration used was 150 μM.

4.5 Semi-Quantitative Real Time PCR

Polymerase chain reaction (PCR) is an important tool in molecular biology, medicine and forensics sciences because it can amplify DNA from a selected region of a genome by a billion-fold thus effectively purifying the DNA from the remainder of the genome.[209] The process relies on thermal cycling which consists of repeated cycles of heating and cooling of the DNA in the presence of reverse and forward primers, deoxynucleoside triphosphates (dNTPs) and polymerase enzyme. The DNA is first heated to about 90°C to denature it into single stranded DNA. After strand separation, cooling of the DNA allows for the hybridization of the primers to the strand. This occurs usually between 50-60°C for a few seconds, where it is typically 3-5°C below the melting temperature (T_m) of the primers being used. The single stranded DNA is then ready for extension. Starting at the primers, the dNTPs are added to the single strand with the help of DNA polymerase. The number of double stranded (dsDNA) produced is exponential and dependent on the number of cycles. Once the desired amount of dsDNA is produce, it can be quantified and identified using gel electrophoresis. In addition to DNA, trace amounts of RNA can be analyzed in the same way by first transcribing them into DNA with reverse transcriptase. The procedure for semi-quantitative real time polymerase chain reaction (qRT-PCR) is very similar to classic PCR except for the ability to obtain real time analysis through the incorporation of a fluorescent marker into the PCR product with every cycle. In our

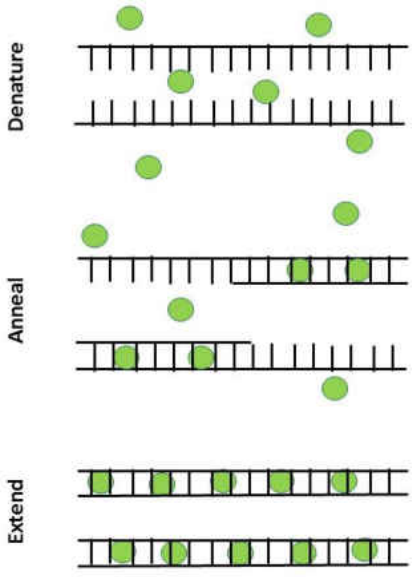

Figure 59. SYBR green binding to dsDNA to produce a fluorescent signal.

case, fluorescence was detected using a SYBR™ Green probe. It is a DNA binding dye that binds to the minor groove of dsDNA and emits light (Figure 59). When only single stranded DNA is present, the dye weakly binds and low fluorescence is observed therefore making the dye a selective tool for detecting the PCR product being produced.

As previously mentioned, $1,25(OH)_2D_3$ upregulates its own catabolic degradation through the C24-oxidation and C23-hydroxylation pathways of CYP24A1 rendering it biologically unstable. Because many VDR agonist contain the secosteroidal scaffold, they too experience metabolic instability requiring them to be given in combined therapies with CYP inhibitors. Herein we report the use of a qRT-PCR to investigate the effect VDR ligands, LCA *O*-Glucuronide I, LCA *O*-Glucuronide II, LCA or calcitroic acid, would have on CYP24A1 gene regulation.

4.5.1 Experimental Procedure

Reagents and Instrumentation: The prostate cancer cell line, DU 145, was purchased (ATCC) and in cultured in 75 cm^2 flasks (CellStar). Cells were grown in DMEM/High Glucose (Hyclone, #SH3024301) media to which non-essential amino acids (Hyclone, #SH30238.01), 10 mM HEPES (Hyclone, #SH302237.01), 5 x 10^6 units of penicillin and streptomycin (Hyclone, #SV30010), and 10% of heat inactivated fetal bovine serum (Gibco, #10082147) were added. Cells were harvested using 0.05% Trypsin (Hyclone, #SH3023601), which disrupts the cell monolayer and proteolytically cleaves the bonds between the cells and flask. Cells were re-plated into 6 well plates (coated in matrigel (BD Bioscience, #354234) using DMEM/High Modified buffer without phenol red (Hyclone, #SH30284.01) that contained all the above mentioned additives plus 10mM sodium pyruvate and 2% percent charcoal treated FBS (Invitrogen, #12676-011) instead of HI FBS

prior to dosing. Compounds were diluted to either 10 mM or 30 mM solutions with DMSO. The cells were lysed using a QIAshredder (Qiagen) and total RNA was isolated using RNAeasy kit (Qiagen). RNA concentration was determine by UV at 260nm using the Tecan Infinite M1000 plate reader. A QuantiFast SYBR Green RT-PCR Kit (Qiagen) was used for the real time PCR following manufacturer's recommendations. Primers used in these studies are as follows: GAPDH FP 5'-ACCACAGTCCATGCCATCAC-3', GAPDH RP 5'-TCCACCACCCTGTTGCTGTA-3'; CYP24A1 FP 5'-CTTTGCTTCCTTTTCCCAGAAT-3'; CYP24A1 RP 5'- CGCCGTAGATGTCACCAGTC-3'; Real-time rt-PCR was carried out on a Mastercycler (Eppendorf).

Semi-Quantitative RT-PCR Protocol: 80-90% confluent DU145 cells were harvested using 0.05% Trypsin and transferred to 6 well plates coated in matrigel. Cells were cultured in DMEM media without phenol red and incubated at 37°C overnight to allow the cells to settle and adhere to the plate. The next day, either DMSO (0.03%), test compound (7.5 µM, LCA *O*-glucuronide I, LCA *O*-glucuronide II, Calcitroic acid, LCA) or 1,25(OH)2D3 (20 nM) were added to the 6-well plate and incubated at 37 °C for 18 hours. Cells were harvested following the RNAeasy Mini Handbook "Protocol for the Purification of Total RNA from Animal Cells using Spin Technology".[210] After 18 hours, cells were first harvested with 0.05% Trypsin and added to media to be counted using a hemocytometer. The cell suspension was then spun down for 2 minutes at 1000 rpm to form a pellet. Media was removed and the cell pellet was resuspended in RTL buffer and vortexed for 5 seconds each. RTL buffer and cell mixture was added to a QIAshredder spin column and spun for 2 minutes at 10,000 rpm. One volume of 70% ethanol was added to the homogenized lysate and mixed well by pipetting. Afterwards, the solution transferred to an RNAeasy spin column and spun for 15s at 10,000 rpm. At this point, all RNA is attached to the spin column and washed

several times with different buffers provided by the RNAeasy Qaigen kit. All flow throughs were discarded. Once thoroughly washed and dried, the RNA is collected by adding 30-50 µL RNase-free water to the spin column and collecting it in a 1.5 mL tube by spinning for 1 minute at 10,000 rpm. Total RNA concentration was determined by UV at 260nm. Once isolated, RNA was diluted accordingly and a QuantiFast SYBR Green RT-PCR Kit (Qiagen) was used for the real time PCR following the "Quantifast^{TM} SYBR^{TM} Green RT-PCR Handbook". The cycling conditions used for Quantifast SYBR Green was 10 minutes at 50^{o}C (reverse transcriptase), 5 minutes at 95^{o}C (PCR initial activation step), 10s at 95 ^{o}C (denaturation), and 30s at 60 ^{o}C (combined annealing/extension) for 50 cycles. The forward and reverse primers used were the house keeping gene, GAPDH and the gene of interest, CYP24A1. We used the ΔΔCt method to measure the fold change in gene expression of target genes. Standard errors of mean were calculated from two biological independent experiments performed in triplicates.

4.5.2 Results and Discussion

The expression levels of VDR target gene, CYP24A1, was determined in DU145 cells treated with 7.5µM of LCA *O*-glucuronide I and II, LCA and calcitroic acid as seen in Figure 60. As expected, a strong induction of CYP24A1 by $1,25(OH)_2D_3$ (20nM) was observed. Cells treated with

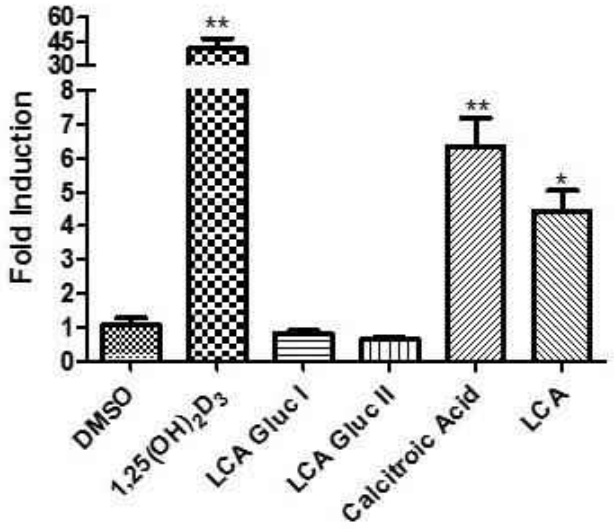

Figure 60. CYP24A1 regulation by LCA phase 2 metabolites, LCA, and calcitroic acid (7.5µM) in DU145 compared to $1,25(OH)_2D_3$ and DMSO after 18hrs. Standard errors of mean were calculated from two biological independent experiments performed in triplicate.

the two synthetically made LCA phase 2 metabolites, LCA *O*-Glucuronide I and II did not induce the expression of CYP24A1 gene. However, LCA and the $1,25(OH)_2D_3$ catabolic metabolite, calcitroic acid, induced the induction of transcription but not to the extent of $1,25(OH)_2D_3$, supporting the agonistic effect seen for both of these compounds in the transcription assay.

4.6 Conclusion

Overall, LCA-based phase 2 metabolites and LCA itself but not phase 1 metabolites were able to competitively inhibit the recruitment of Alexa Fluor 647-labeled SRC2-3 to VDR-LBD. Importantly, calcitroic acid was identified as partial VDR agonist. Unfortunately, aggregation between LCA analogs and Texas Red omitted the application of different coregulator peptides, which were only available as Texas-Red conjugates. All but LCA showed minor activation of binding in the absence of LG190187 and LCA *O*-glucuronide II was the most potent molecule among LCA phase 1 and phase 2 metabolites with an IC_{50} five time more potent than LCA.

Judging from the results of the 2-hybrid assay, none of the metabolites were novel VDR inhibitors. However, the lower efficacy compared to $1,25(OH)_2D_3$ was observed for LCA *O*-glucuronide I and II and calcitroic acid in the transcription assay means that it could be used to restrict full activation of VDR-mediated transcription. Further studies are necessary to evaluate these partial agonist in respect to calcium homeostasis and metabolic stability.

The qRT-PCR study revealed that LCA and calcitroic acid but not LCA *O*-Glucuronide I and II up-regulate CYP24A1 and produce 24-hydroxylase. Interestingly, because expression was conducted in DU145 cells, a prostate cancer cell line, it can be postulated that these molecules may promote anti-proliferation and differentiation of cancer cells. This is evidenced in the literature by other analogs, such as P450 enzyme inhibitors that deactivate 24-hydroxylase thus increasing the concentration of $1,25(OH)_2D_3$ induced anti-proliferation.[211, 212]

CHAPTER 5: IDENTIFICATION OF VDR ANTAGONISTS AMONG NUCLEAR RECEPTOR LIGANDS USING VIRTUAL SCREENING

5.1 Introduction

NRs are one of the most important drug targets today.[213] Over the last decades thousands of small molecules have been synthesized to improve the activity of NR ligands identified by HTS or rational drug design. Although the activity of NR ligands is very important in terms of dosage and suppression of side effects, the selectivity of ligands towards a particular NR is crucial for specific pharmacological effects. Usually NR ligands are investigated in respect to their NR isoform-selectivity. For instance, ER ligands are evaluated for their selectivity towards ERα and ERβ, which are distributed tissue-selectively in the human body.[214] Once a promising ligand has been identified, further analysis in respect to other closely related NRs is conducted based on phylogenetic distance or NR sequence similarity.[215, 216] Schapira et al. introduced an alternative concept of NR similarity based on the likelihood that two NRs share a common ligand.[217] Therefore, sixteen NR crystal structures and 78 NR ligands were used in a computational approach to determine the cross-reactivity of NR ligands. Herein, we present an alternative approach by using a large library of NR ligands and only one receptor, VDR. Among 14330 compounds, we identified four new VDR antagonists that were originally developed as ligands for other nuclear receptor. Thus, virtual screening represents a useful tool to identify those NRs that are likely to interact with a new NR ligand.

5.2 Experimental Procedure

5.2.1 Virtual Screens

A library of nuclear receptor ligands were assembled using “the Binding Database”. The database included 14330 compound structures and their nuclear receptor binding data (EC_{50}, IC_{50}, or K_D). Weakly active ligands that had estimated binding data (e.g. >5000 μM) or inactive compounds (e.g. no binding observed) were assigned a zero activity. Compounds that were not tested were assigned an empty field. The database only included compounds that were at least tested with one nuclear receptor. For racemic compounds only one stereoisomer was used for the screen. All compounds were minimized and the ionization state of functional groups was adjusted to pH 7. Molecule conformations were generated from a single 3D conformer by applying a collection of preferred torsion angles to the rotatable bond during the virtual screen. The crystal structure of VDR bound to $1,25(OH)_2D_3$ (PDB ID 1DB1)[218] was prepare for docking using the MOE structure preparation function to repair any structural defects in the pdb file. In addition, a protonation 3D function was used to optimize the hydrogen bond network and hydrogen positions. Finally unbound water molecules were removed. The virtual screen was carried out by selecting VDR-bound $1,25(OH)_2D_3$ as binding site and a triangle matcher for the placement of compounds. The triangle matcher function generated poses by superposition of ligand atom triplets and triplets of receptor site points. The receptor site points are alpha sphere centers which represent locations of tight packing. At each iteration, a random triplet of ligand atoms and a random triplet of alpha sphere centers were used to determine the pose. The poses were scored using affinity London dG scoring that estimated the free energy of binding (ΔG) from each given pose given in kJ/mol. Compound conformations that do not satisfy the pharmacophore model 1 or 2 depicted in Figure 4 were eliminated.

5.2.2 Fluorescence Polarization Assay with VDR-SRC2-3

Reagents and Instrumentation: LG190178 was synthesized using a published procedure.[153] The peptide SRC2-3 (CLQEKHRILHKLLQNGNSPA),[219] was purchased and labeled with the cysteine-reactive fluorophore (Alexa Fluor 647 maleimide) in a 50:50 DMF/PBS mixture. After purification by high performance liquid chromatography, the corresponding labeled peptide was dissolved in DMSO and stored at -20ºC. The VDR-LBDmt DNA was kindly provided by D. Moras[218] and cloned into the pMAL-c2X vector (New England Biolabs). A detailed expression and purification protocol for VDR was reported previously.[219]

Fluorescence Polarization Assay Protocol: Agonistic and antagonistic activity was studied using a FP assay. This assay was conducted in 384-well black polystyrene plates (Corning) using a buffer (25 mM PIPES (pH 6.75) 50 mM NaCl, 0.01% NP-40, 2% DMSO), VDR-LBD protein (0.1 µM), LG190178 (3 µM), and Alexa Fluor 647-labeled SRC2-3. Small molecule transfer into a 20 µL assay solution was accomplished using a stainless steel pin tool (V&P Scientific), delivering 100 nL of the serially diluted compound solution. Fluorescence polarization was detected after 1 hour at excitation and emission wavelengths of 650 nm and 665 nm, respectively. Three independent experiments were conducted in quadruplicate. The data were analyzed using nonlinear regression with a variable slope (GraphPadPrism).

5.3 Results

A library of 14330 NR ligands were compiled using "The Binding Database.org".[220] The sets of NR ligands were downloaded individually and merged as a virtual small molecule library using MOE (molecular operating environment). The number of ligands downloaded per NR is given in Figure 61. The NRs with the largest ligand databases are the peroxisome proliferator-

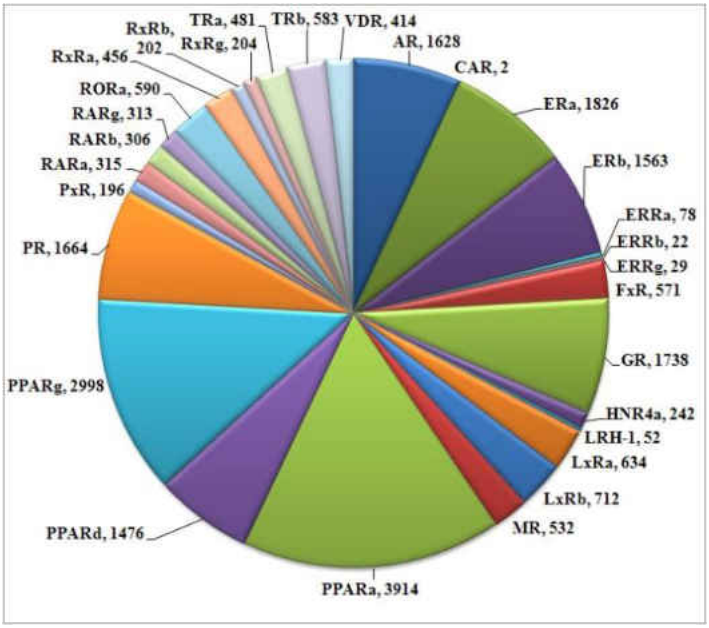

Figure 61. Number of NR ligands deposited with "The Binding Database".

activated receptor (PPAR)γ, PPARδ, PPARα, the progesterone receptor (PR), the androgen receptor (AR), the ERα, the ERβ, and the glucocorticoid receptor (GR) with more than a thousand ligands each. Overall, 30 NRs are represented by their ligands in "The Binding Database" with a total of 14330 unique NR ligands. Many of these ligands were investigated in regards to multiple NR binding and some of them exhibited a significant potency to more than one NR.

The analysis to determine global selectivity of ligand among nuclear receptors is restricted by the fact that limited data are available. We were surprised that for the majority of ligands only one NR was evaluated. 4006 ligands out of 14330, thus a quarter of the ligands, were investigated with only two different NRs as illustrate in Figure 62. Most of NR ligands tested with two NRs

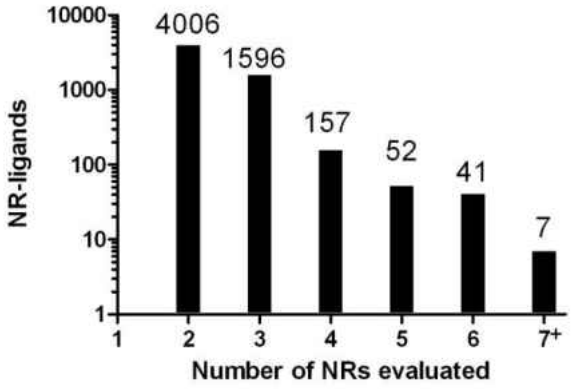

Figure 62. Number of NR ligands that bind to multiple NRs.

were able to bind two NR isoforms with different affinity, such as α and β, which applies to the liver X receptor (LXR), ER, and TR. Ligands that were developed for NRs having three isoforms such as PPAR, estrogen related receptor (ERR), RXR, and retinoic acid receptor (RAR) represent almost half of the NR library members (Figure 61). However, only a fraction of these ligands (1853) were evaluated with more than two NRs (Figure 62). Some examples of ligands that bind multiple NRs, although with different affinity, are depicted in Figure 63. Compound 1 (Figure 63, A) was developed by Ligand Pharmaceuticals as RXRα antagonist.[221] Although the selectivity in respect to RARs is very high, there is a moderate selectivity toward other RXR subtypes. In addition, a synergistic activation of transcription was observed when cotransfected with PPARγ in the presence of selective PPARγ ligand. Guggulsterone (Figure 63, B) was predominately

evaluated with steroid hormone receptors.[222] The compound has a strong affinity for the

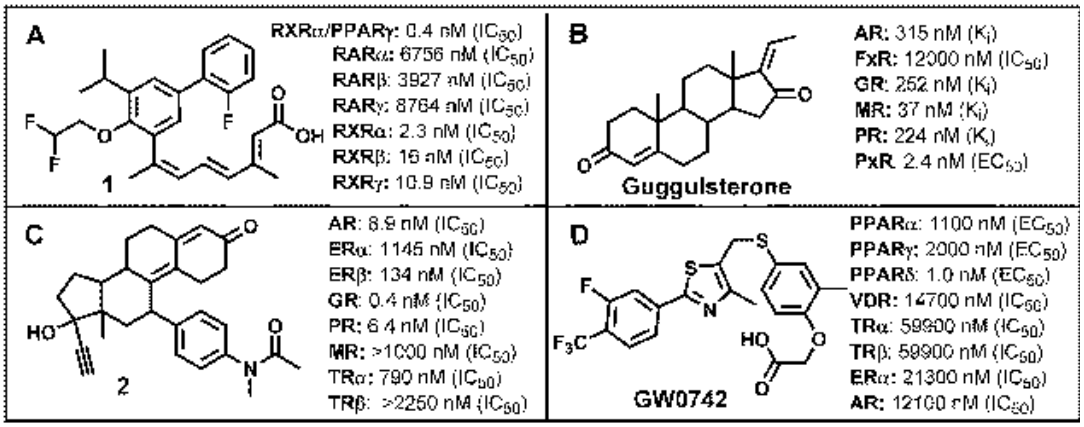

Figure 63. NR ligands that were evaluated towards multiple nuclear receptors.

mineralocorticoid receptor (MR) and the pregnane X receptor (PXR).[223] Compound 2 (Figure 63, C) is a very potent GR antagonist, which still has a significant activity towards PR and AR.[224] Finally, GW0742 (Figure 63, D) was developed by GlaxoSmithKline as highly a selective agonist for the PPARδ.[225] The evaluation of GW0742, in respect to NR-mediated inhibition of transcription, identified this compound as antagonist for AR and VDR.[152]

Nevertheless, the exhaustive characterization of NR ligands is limited by the sheer number of different NRs resulting in a cost and time-intensive analysis for research labs and the pharmaceutical industry. Therefore, a prediction of NR-selectivity of new ligands using computational approaches might enable a selection of a smaller pool of NRs to be considered for evaluation. In addition, this approach might also identify groups of NRs that bind similar ligands, thus introducing a new relationship between NRs that is different from phylogenetic distance or NR sequence similarity. In order to test this hypothesis, we used the library of NR ligands and carried out two virtual screens applying the first crystal structure of liganded VDR.[218] For each

screen, we applied a different pharmacophore model to filter all molecule conformations. The two different pharmacophore models are depicted in Figure 65.

The virtual screen 1 was carried out with a pharmacophore model that specifies three electron donor/acceptor elements depicted as purple spheres (Figure 64, A). These three elements represent the spatial configuration of three hydroxyl groups of the most active endogenous VDR ligand 1,25-dihydroxy vitamin D_3 ($1,25(OH)_2D_3$).[226] $1,25(OH)_2D_3$ is a metabolic product of vitamin D_3 formed from $25(OH)D_3$ by 1α-hydroxylase.[227] The binding affinity of $1,25(OH)_2D_3$ is 0.1-1 nM, whereas $25(OH)D_3$ binds with a moderate affinity of 1420 nM towards VDR.[228] The virtual screen

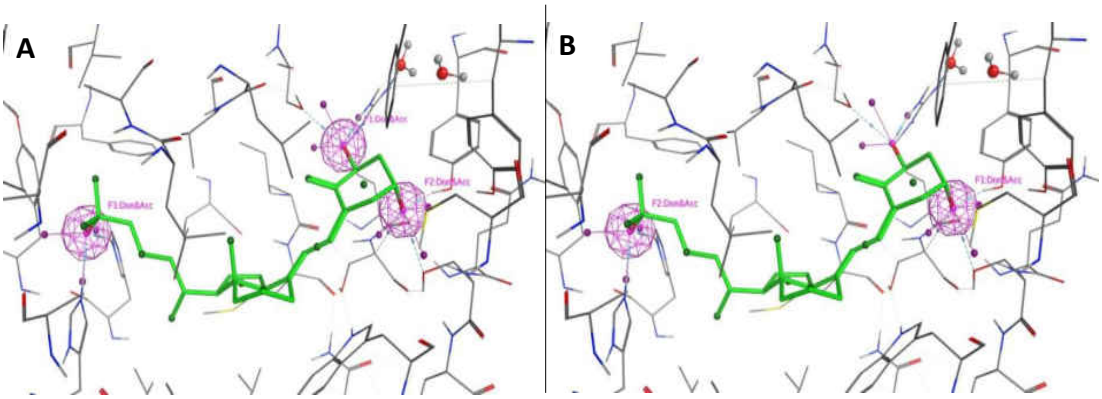

Figure 64. Two different pharmacophore models for VDR ligands. Pharmacophore models were established using MOE.

of 14330 compounds using model A (Figure 64) identified 64 compounds. 32 of the 64 compounds had a significant calculate free energy of VDR binding of more than -6.0 kJ/mol. Nordihydroguaiaretic acid (NDGA) was the only non-VDR ligand identified with a calculate ΔG of -11.1 kJ/mol (Figure 65, B). NDGA is a bioactive compound that inhibits lipoxygenases, functions as an antioxidant, and has shown promising anti-cancer activities.[229] The compound has also been reported to weakly interact with the androgen receptor by binding to a new BF3 binding site.[230]

Herein, we confirmed the activity NDGA towards VDR using a fluorescence polarization assay. In the presence of $1,25(OH)_2D_3$, NDGA was able to inhibit the interaction between VDR and coactivator peptide SRC2-3 with an IC_{50} values of 15.8 ± 2.1 µM. In the absence of

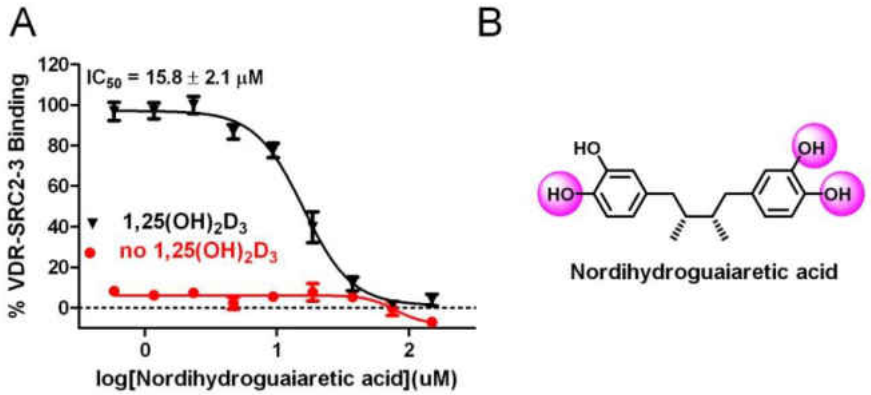

Figure 65. Nordihydroguaiaretic acid is inhibiting the interaction between VDR and coactivator peptide SRC2-3.

$1,25(OH)_2D_3$, NDGA was not able to promote the recruitment of coactivator towards VDR (Figure 65, A). Because of the fact that the interactions between VDR and coactivators are essential for VDR-mediated transcription we identified NDGA as novel VDR antagonist.

Virtual screen 2 was carried out using a less stringent pharmacophore model depicted in Figure 64, B bearing two acceptor/donor groups representative of VDR ligand $25(OH)D_3$. Among the

14330 molecules, 397 compounds were identified and 162 compounds exhibited a free energy of binding of more than -6.0 kJ/mol (Figure 66). Among the hit compounds of virtual screen 2,

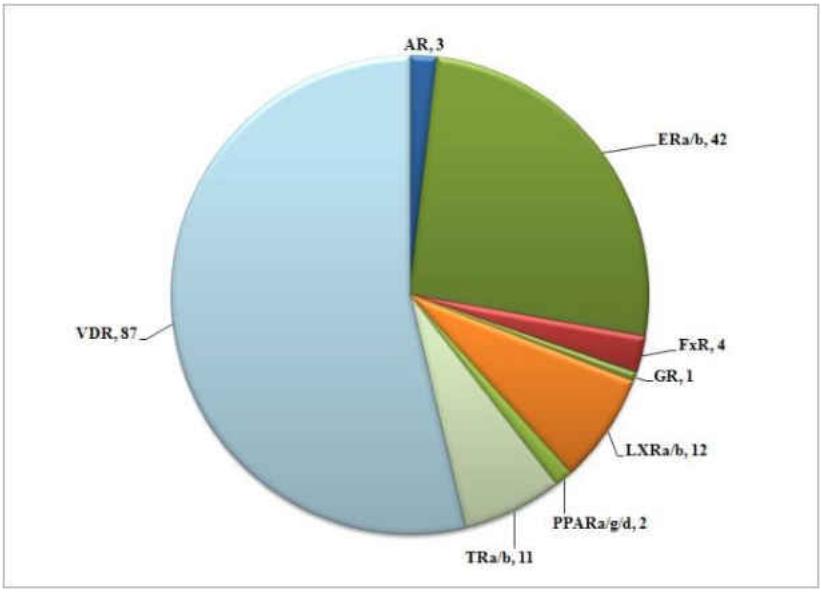

Figure 66. Number and affiliation of NR ligands identified by virtual screen 2 using the pharmacophore model depicted in Figure 4, B.

the majority of molecules were developed as ligands for VDR. Ligands developed for LxRα/β, TRα/β, and ERα/β ligands were among the most frequent ligands that potentially interact with VDR. We picked one TRα ligand (3) and one ERα ligand (H6036) in order to confirm the activity in

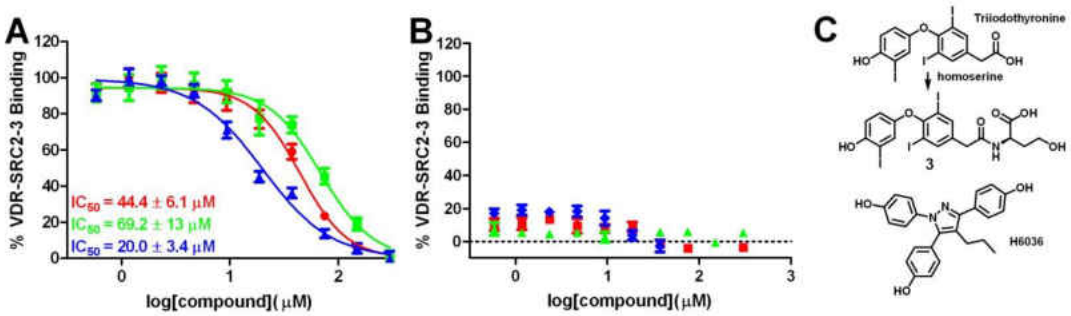

Figure 67. Interaction between virtual screen hit compounds (♦H6036, ■ compound 3, ▲triiodothyronine) and VDR. A) Hit compound inhibition of the interaction between SRC2-3 and VDR in the presence of VDR agonist LG190178; B) Association of VDR-LBD and SRC2-3 in the presence of hit compounds; C) Structure and generation of NR ligands.

regard to VDR (Figure 67). Fortunately, both compounds (1 and H6036), identified by virtual

screen 2, were able to inhibit the interaction between VDR and SRC2-3 with IC_{50} values of 44.5 ± 6.1 µM and 20.0 ± 3.4 µM, respectively (Figure 67, A). The original docking score for these compounds was -7.9 kJ/mol (3) and -9.1 kJ/mol (H6036). The thyroid receptor ligand triiodothyronine did not score during the virtual screen 2 because it did not satisfy the pharmacophore model. However, we observed that triiodothyronine did inhibit the interaction between VDR–SRC2-3, although at higher concentrations. In the absence of VDR ligand LG190178 no recruitment of SRC2-3 to VDR was observed in the presence of any of these ligands (Figure 67, B).

5.4 Discussion

We showed that databases such as the "Binding database" can function as starting point for virtual screening. During the compilation of this focused library we were surprised by the small number of developed NR ligands that have been evaluated with other NRs. The main reason for this lack of investigation is the size of the NR superfamily in addition to the existing agonism and antagonism that would make an exhaustive evaluation with a panel of NRs very time intensive and costly. An alternative approach to predict NR selectivity might be realized by virtual screening. Using the first published VDR crystal structure and pharmacophore models representing the essential features of VDR ligands, we showed that among NR ligands those with higher affinities for VDR can be identified by virtual screening. The essential features of VDR ligand $1,25(OH)_2D_3$ are three hydroxyl functions that interact with VDR via hydrogen bonding. In addition, this ligand induces a large hydrophobic effect due to the non-polar vitamin D_3 scaffold. Using a pharmacophore model based on $1,25(OH)_2D_3$ that defines the spatial orientation of three

OH groups as filter, we were able to identify compounds that interact with VDR with 100% accuracy during the first virtual screen using a cutoff of -6 kJ/mol for the calculated free energy of binding. 31 out of the 32 hit compounds were VDR ligands such as agonists 2MD[231] or antagonist 4[232]. Both compounds have been shown to bind VDR, however 2MD promoted the recruitment of coactivators, whereas antagonist 4 inhibited the interaction between VDR and coactivator. Thus, our virtual screen 1 was very efficient to identify VDR ligands but did not differentiate between VDR agonists and antagonists.

Our virtual screen 2 applied a less stringent pharmacophore model based on VDR ligand 25(OH)D_3, which is at least 1000-fold less potent than 1,25(OH)D_3. As expected, we identified more and different NR ligands that are likely to interact with VDR. In total we found 162 compounds with a calculated free energy of VDR binding of more than -6.0 kJ/mol. 54% of these ligand were developed for VDR. The next biggest group included ER ligands (26%) with different affinities for the ERα and ERβ, followed by TR ligands (7%) and LxR ligands (7%). Thus, there is a relationship between VDR, TR and ER that is beyond the phylogenetic distance or NR sequence similarity. We picked two compounds that were commercially available or in case of 3 easy to synthesize. Fortunately, both compounds inhibited the interaction between VDR and coactivator peptide SRC2-3 although at different concentrations. We were very pleased that the calculated free energy of binding correlated with the IC_{50} values observed for the new VDR antagonists. NDGA exhibited the highest VDR affinity and largest free energy of VDR binding followed by H6036 and 3, respectively. Interestingly, triiodothyronine was not among the hit compounds because it failed to satisfy the pharmacophore used for virtual screen 2. Nevertheless, we confirmed triiodothyronine as a weak VDR antagonist highlighting the fact that other

pharmacophore models exist to identify VDR ligands. One approach to develop a new pharmacophore for this kind of virtual screening could include the application of a VDR crystal structure bound to a VDR ligand with a low calculated free energy of VDR binding for the virtual screen 1 but a relative high reported affinity for VDR. Another approach could include the optimization of our current pharmacophore model by changing the volume of the donor/acceptor elements or by adding additional pharmacophore elements.

Overall, the development of NR-specific pharmacophore models is important because it can assist in the choice of NRs that should be evaluated in order to determine NR-selectivity of novel NR ligands. Although this approach can drastically decrease the cost and time to determine NR-selectivity of new ligands it is not a full substitute for an exhaustive investigation of a comprehensive panel of NRs in respect to agonism and antagonism. In addition, NR-specific pharmacophore models can be used to identify new NR ligands. We demonstrate the utility of this approach using a library of NR ligands to identify new VDR antagonists. The application of larger virtual compound libraries such as the “Zinc Library” might result in the identification of even more compounds that interact with VDR. Overall it can be concluded that virtual screening can support both the identification of new NR ligands as well as the identification of NRs that are likely to interact with new NR ligands in order to accelerate the determination of NR selectivity.

PART II. THE DEVELOPMENT OF A UNIVERSAL GTPase ASSAY

CHAPTER 1: INTRODUCTION

GTPases act as molecular switches in which their "on" and "off" functions are triggered by the binding and hydrolysis of GTP.[233, 234] Their highly conserved function allows GTPases to play an important role in regulation of cellular processes ranging from cell growth and differentiation to vesicular and nuclear transport. As depicted in Figure 68, activation of GTPases requires the dissociation of protein bound guanosine diphosphate (GDP) an intrinsically slow process that is accelerated with the help of guanine nucleotide-exchange factors (GEFs). The switch-ON process involves the exchange of GDP for guanosine triphosphate (GTP), which in theory is a reversible reaction. The switch-off process involves hydrolysis of GTP to GDP, which is an irreversible reaction. This additional slow process is accelerated by GTPase-activating proteins (GAPs).

Several proteins belong to the GTPase superfamily including small Ras-related proteins

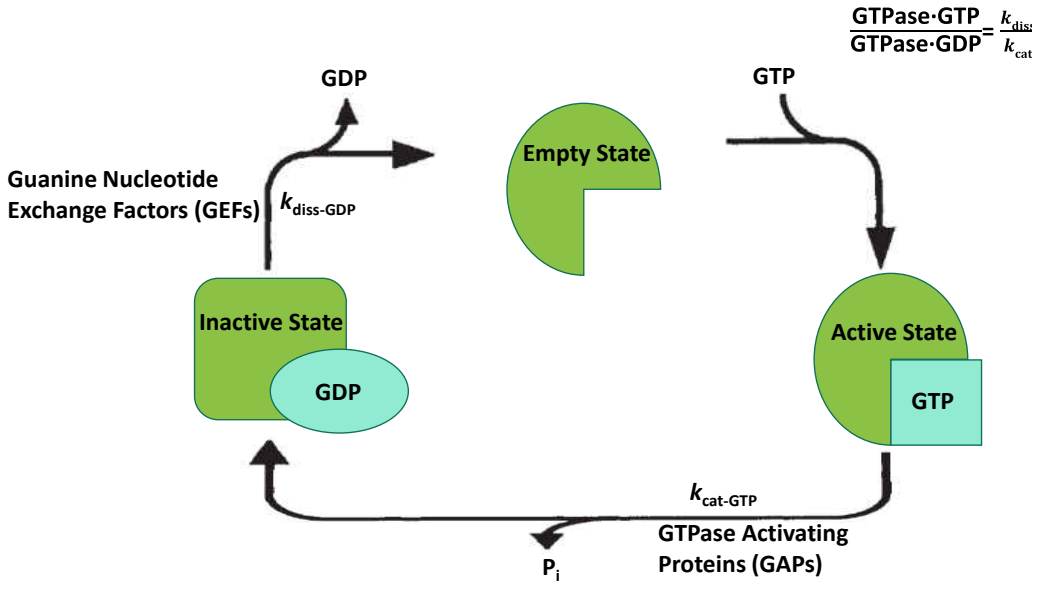

Figure 68. The basic "on" and "off" switch cycle of GTPases.

with many subfamilies (Rho, Rab, Arf and Ran), heterotrimeric G proteins with α, β and γ subunits,

and large proteins such as dynamin, which is responsible for endocytosis in eukaryotic cells.[234] With growing research in this area, many members of the GTPase family have been linked to diseases like cancer, diabetic renal disease, and neurological diseases such as Parkinson's disease.[235, 236] Especially Ras GTPases (HRas, KRas, and NRas), which control cell proliferation, differentiation, cellular growth and apoptosis, have been implicated in a large number of cancers and hyperproliferative diseases.[237, 238] Ras GTPase-mediated regulation is disrupted by specific gene mutations coding these proteins, specifically at codon 12, 13, and 61. The single point mutation promotes oncogenesis and promotes GTP binding and activation of Ras. The presence of mutations in cancer does vary between different types of tumors with predominate isoforms in particular cancers. For instance, K-Ras has been shown to be the most frequently mutated GTPase in cancers with 90% of pancreatic tumors harboring this mutation.[237]

Due to their relationship to many diseases, numerous GTPase targeting drugs have been developed. One third of all drugs targeting proteins are either interacting with kinases (22% of drugs) or GTPases (15% of drugs). The growing interest in GTPase targeting drugs has promoted the development of assays that can efficiently test these compounds in a high throughput and inexpensive way. Although many commercially available kinase/GTPase assays are on the market, they do not necessarily directly monitor the conversion of NTP to NDP. Activity-based assays are advantageous because of their sensitivity and ability to directly detect changes in the biochemical activity of the enzyme. However, many of these activity-based assays utilize antibodies to detect the phosphorylated peptide produced. This makes them specific but not universal. Monitoring the formation of GDP is universal because it is the most basic function of GTPases irrespectively which substrate is phosphorylated. The available assays a variety of

detections including proximity-based scintillation, fluorescence polarization, UV, and fluorescence resonance energy transfer (FRET).

AviMed Pharmaceuticals, LLC, is a local company founded by Dr. Daniel Sem with interest in developing a universal kinase/GTPase assay kit that is affordable and commercially available

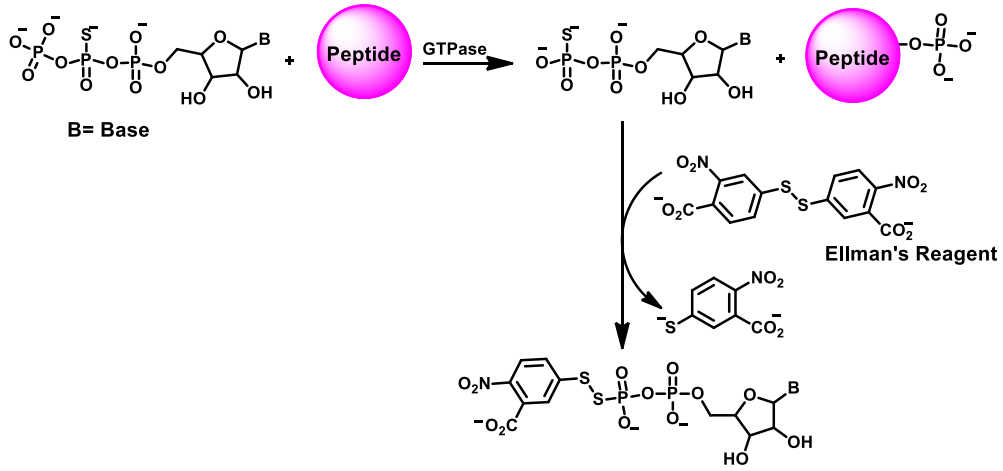

Figure 69. The dithio-coupled reaction using Ellman's reagent to detect the enzymatic activity of kinases or GTPases.

for industry and research labs to test potential drug candidates. Dr. Sem is the inventor of two kinase/GTPase assay patents describing the assay to be used in for these kits.[239, 240] The assay designed relies on the fact that a beta thiol substituted ATP (GTP for GTPases) can be enzymatically hydrolyzed and produce ADP (GDP). The exposure of the thiol makes it nucleophilic and reactive towards thiol-sensitive fluorescent or calorimetric reagents such as Ellman's reagent.[241] The assay is illustrated in the Figure 69. Enzymatic reaction rates can be measured in the presence or absence of inhibitors as a way to identify and screen potential kinase (GTPase) targeting drug candidates. Herein, we report the synthesis of assay reagents and the preliminary development of a universal, inexpensive, sensitive GTPase assay kit that directly detects the GTPβ-S hydrolysis product, GDPβ-Se.

CHAPTER 2: THE SYNTHESIS OF GTPase ASSAY REAGENTS: GTPβ-S AND GTPβ-Se

2.1 Chemistry

2.1.1 Synthetic Strategy

The overall synthetic scheme used in our lab to make GTPβ-S and GTPβ-Se was adopted from the literature and is shown in Scheme 10.[242] Essentially, it's a two-step one pot reaction to convert GDP to GTP without the use of enzymes. First, (2-cyanoethyl) phosphate barium salt (2.1) was converted into its triethylammonium salt (2.2) using the ion-change resin Dowex and triethylamine (TEA). The reaction with imidazole in the presence of 2,2'-dithiopyridine,

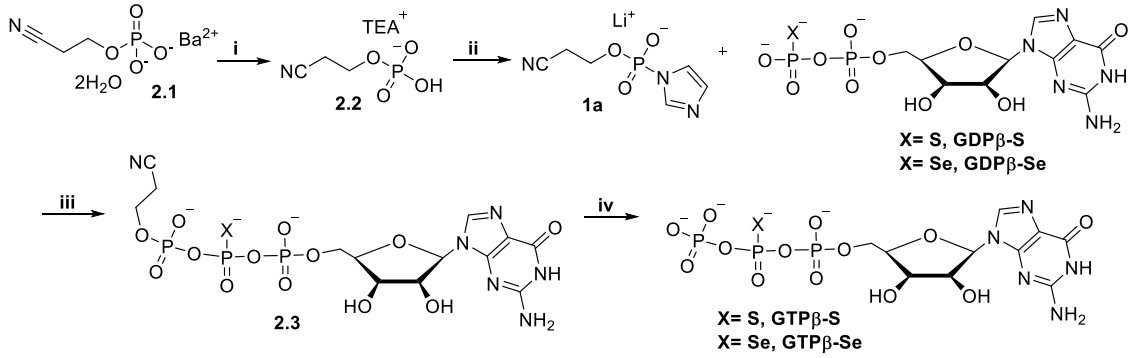

Scheme 10. General synthetic scheme for GTPβ-X analogs. i) a) H_2O, Dowex (50Wx8, 200-400mesh), rt, 1 hour b) TEA, EtOH; ii) a) imidazole, 2,2'-DTDP, Ph_3P, TEA, DMF, rt, 6-8 hours, b)

triphenylphosphine and TEA in DMF generated the phosphorylating agent, 1a. GTPβ-S or GTPβ-Se were synthesized by coupling of 1a with GDPβ-S or GDPβ-Se in the presence of $MgCl_2$ followed by β-elimination of the cyanoethyl (CE) group using 1,8-diazabicycloundec-7-ene (DBU). Due to a possible conjugate addition of acrylonitrile with the nucleotide, dithiothreitol (DTT) was added to scavenge formed acrylonitrile during the reaction. In addition, either an open flask capped

with anhydrous calcium chloride to protect the reaction from moisture, or a weak vacuum applied to the sealed reaction can aided in the removal of acrylonitrile.

The syntheses of GDPβ-S and GDPβ-Se are summarized in Scheme 11 and 12, respectively. First, guanosine 5'-monophosphate disodium salt (2.4) was transformed to the TEA salt (GMP-

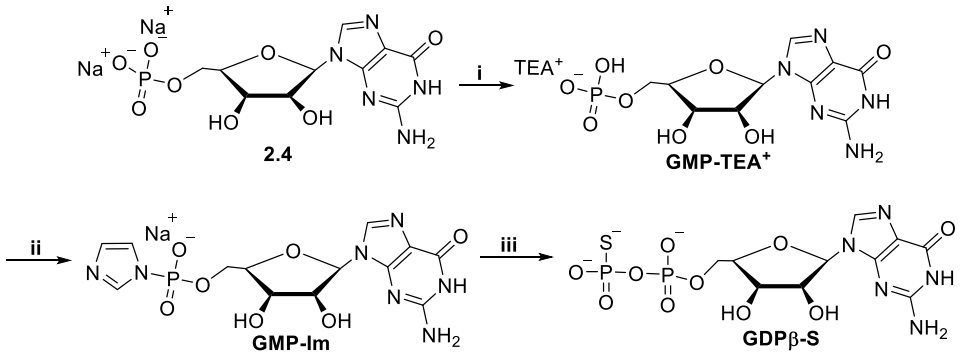

Scheme 11. Synthesis for GDPβ-S. i) a) H_2O, Dowex (50Wx8, 200-400mesh), rt, 1 hour, b) TEA, EtOH; ii) a) imidazole, 2,2'-DTDP, Ph_3P, TEA, DMF, rt, 6-8 hours, b) $NaClO_4$, dry acetone; iii) a) DMF, ZnCl2, thiosphophate TEA^+ salt, rt, 30 minutes, b) EDTA, $NaHCO_3$, H_2O.

TEA^+) following the same ion-exchange procedure reported previously. Activation yielded guanosine monophosphate phosphorimidazolide (GMP-Im), which was coupled with thiophosphate to yield guanosine 5'-*O*-(2-thiodiphosphate) (GDPβ-S).

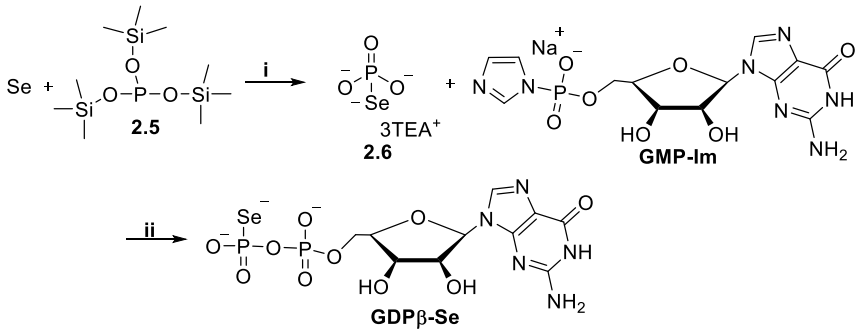

Scheme 12. Synthesis of GDPβ-Se. i) a) dry pyridine, CH_3CN, rt, 30 minutes, b) TEA, MeOH, rt, 3 hours; ii) DMF, $ZnCl_2$, rt, 20 minutes b) EDTA, $NaHCO_3$, H_2O, pH= 7.5, room temperature, 3 hours.

Elemental selenium and tris(trimethylsilyl)phosphite (2.5) were mixed and transformed with TEA to synthesize triethylammonium selenophosphate (2.6).[243] Inert and dry conditions were essential to suppress the formation of Se-Se bonds. ^{31}P-NMR confirmed the formation of triethylammonium selenophosphate, which due to its instability, was immediately coupled with GMP-Im in the presence of $ZnCl_2$ to yield the final product, guanosine 5'-*O*-(2-selenodiphosphate) (GDPβ-Se). All diphosphate and triphosphate nucleotides were purified by ion-exchange chromatography on DEAE-Sephadex A-25 (HCO_3^-) column. Briefly, the crude product was loaded on the column and washed with excess water to remove metal salt/EDTA complexes. Subsequently, the nucleotide was eluted using a linear gradient of triethylammonium bicarbonate (TEAB, pH= 8.0).

2.1.2 Characterization

All starting reagents were purchased from either Sigma-Aldrich or Fisher Scientific. Synthesized nucleotides were purified using a fast protein liquid chromatography system (FPLC, GE Healthcare AktaPurifier UPC 10, #28406268). 5 mL proteus FPLC columns were purchased from NuSep (#Nu-FliQ1-25) and loaded manually. GTPβ-Se reaction was monitored by HPLC using a Agilent Tech. Series 1220 Infinity LC with a Supelcosil LC-18-T HPLC column (Sigma, #58971, 4.6 x 250mm, flow rate 1mL/min) with a linear gradient 1-25% of methanol in 0.05M ammonium acetate buffer (pH=5.9) in 15 minutes, UV-detection at 260 nm. Compound characterization was performed using a Shimadzu 2020 LC-MS (single quadrupole) instrument with compounds directly injected. NMR spectra were recorded on a Bruker 300MHz instrument with samples diluted in D_2O.

General Procedure for Converting to TEA Salt using Dowex: 5 g of starting salt (i.e. Ba^{2+}, Na^{+}) was suspended in water (100mL) and mixed with a calculated amount of Dowex 50W x 8 (200-400mesh) resin in H^{+} form (see calculation below) in a beaker covered with parafilm. The mixture was agitated on a reciprocal shaker for 1 hour. The suspension was then filtered and the eluate was collected in a round bottom flask containing a solution of trimethylamine (3.2mL) in absolute ethanol (100mL). The solvents were mostly evaporated by rotary evaporation and then further dried in vacuum over P_4O_{10} to obtain the final TEA salt.

Ion Exchange Capacity Calculation with Dowex 50Wx8 200-400 mesh H^{+} form:

In general, the capacity of an ion exchange resin can be expressed as the quantity of ions that can be taken up by a specific volume of resin. This can be expressed in quantity/unit volume such as milli-equivalents/milliliter (meq/mL). Equivalents refers to the equivalent weight (EW) of the substance expressed in grams (or meq in milligrams), which is the molecular weight (MW) divided by valence.[244] For example: (2-cyanoethyl) phosphate barium salt dihydrate

Ba^{2+} MW= 137.3 g/mol and is divalent

Dowex 50Wx8 200-400 mesh H^{+} form total exchange capacity= 1.7 meq/mL[245]

$$\frac{137.3g}{mol} \div 2 = 68.65\ EW$$

$$1.7\ \times 68.65\ EW = \frac{116.7\ g\ Ba^{2+}\ salt}{L\ of\ resin}$$

Grams of Ba^{2+} in 5g of (2-cyanoethyl) phosphate barium salt dehydrate:

$$15.5mmol \times \frac{137.3g}{mol} = 2.1g$$

$$\frac{2.1g}{XL} = \frac{116.7gBa^{2+}}{1L\ resin}$$

X= 17mL of resin needed to exchange ions with TEA^+

General Purification Procedure with FPLC: Synthesized nucleotides were purified by ion exchange chromatography on DEAE-sephadex A-25 (HCO_3^- form) column. Resin was soaked in water for 1 day at room temperature before being loaded to a 5 mL proteus FPLC column. The reaction mixture was loaded to the column and washed through with excess water to remove metal (II) salt/EDTA complex. Nucleotides were eluted slowly over 7 hours (flow rate of 2.5 mL/min) using a linear gradient (0-100%) of triethylammonium bicarbonate (TEAB) buffer in 18 MΩ water (0.7M, pH=8.5). Afterwards, fractions were collected and buffer was evaporated under reduced pressure. Several 15 mL portions of absolute ethanol were added to decompose the TEAB and produce the TEA salts.

Triethylammonium Bicarbonate Buffer Recipe: To make TEAB at 1M, 120 mL of HPLC grade triethylamine was diluted in 740 mL of 18 MΩ water. Dry ice was placed into a separate vessel with a nozzle connected to a hose. The CO_2 from the dry ice was bubbled into the triethylamine solution for 2-3 hours and stopped once the solution reached a pH=8.5. The buffer was filtered using HVLP 0.45µM filter paper.

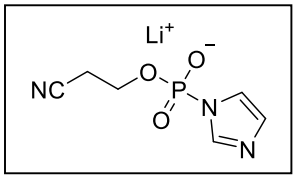

1a: 82% yield; (2-cyanoethyl) phosphate barium salt dihydrate (5g, 15.5mmol) converted to the TEA salt using 20 mL of Dowex 50W x 8 (200-400mesh) resin in H^+ form (see general procedure above). About 3.91 g (92% yield) of (2-cyanoethyl) phosphate TEA salt was obtained. Thereafter, (2-cyanoethyl) phosphate TEA salt (2.9 g, 11.9 mmols) was mixed with imidazole (10 equiv., 8.07

g, 0.119 mols), 2,2'dithiodipyridine (3 equiv., 7.85 g, 35.6 mmol), DMF (25 mL), trimethylamine (3 equiv., 3.6 mL, 35.6 mmol), and triphenylphosphine (3 equiv., 9.34 g, 35.6 mmol) and the mixture was stirred for 6-8 hours. The product was precipitated from the reaction mixture with a solution of anhydrous $LiClO_4$ (4 equiv., 5.05 g, 47.5 mmol) in dry acetonitrile (187.5 mL). After cooling to 4°C, the precipitate was filtered off, washed repeatedly with cold, dry acetonitrile, and dried in vacuum over P_4O_{10}. The resulting product, 1a, was stored at 4°C in a closed vessel for several months. ^{1}H-NMR (300 MHz) (D_2O) δ 7.84 (s, 1H), 7.22 (s, 1H), 7.03 (s, 1H), 3.95-3.88 (q, 2H, J= 7Hz), 2.68-2.65 (t, 2H, J= 6Hz), 1.96 (s, 1H); ^{31}P NMR (121 MHz) δ -8.56 (s, 1P); MS DUIS ($^-$ ve) calcd. *m/z* for $C_6H_7N_3O_2P^-$ [$(M-H^+)^-$] 200.2, found [$(M-H^+)^-$] 200.2.

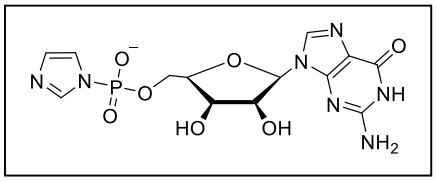

Guanosine monophosphate phosphorimidazolides (GMP-Im): 75% yield; Guanosine 5'monophosphate (GMP) disodium salt (5 g, 12.3 mmol) was converted to the TEA salt using 14.4mL of Dowex 50W x 8 (200-400 mesh) resin in H^+ form (see general procedure above). About 4.78 g (84% yield) of GMP TEA salt was obtained. Thereafter, GMP TEA salt (1 equiv., 4.78 g, 10 mmol), imidazole (10 equiv. 7.0 g, 0.103 mols), and 2,2'dithiodipyridine (3 equiv., 6.82 g, 31 mmol), were mixed in 30mL of DMF. Trimethylamine (3 equiv., 4.33 mL, 31.0 mmol) and triphenylphosphine (3 equiv., 8.13 g, 31.0 mmol) were added and the mixture was stirred for 6-8 hours. The reaction was monitored by ^{31}P-NMR to confirm the disappearance of GMP at 3.76 ppm. The product was precipitated from the reaction mixture with anhydrous $NaClO_4$ (4 equiv., 4.9 g, 40.0 mmol) solution in dry acetone. To ensure the acetone was completely dry, it was distilled over $MgSO_4$ and stored with 4Å molecular sieves at 4°C. After cooling the mixture to 4°C, the precipitate was filtered, washed repeatedly with cold, dry acetone and the solvent was

removed under reduced pressure. ^{1}H-NMR (300 MHz) (D_2O) δ 7.79 (s, 1H), 7.71 (s, 1H) 7.02 (s, 1H), 6.82 (s, 1H), 5.74-5.72 (d, 1H, J= 6Hz), ~4.70-4.66 (overlapped with water, m, 1H), 4.32-4.29 (t, 1H, J= 3Hz), 4.14 (s, 1H), 4.00-3.98 (m, 2H), 2.91 (s, 1H); ^{31}P NMR (121 MHz) δ -7.96 (s, 1P); MS DUIS ($^{-}$ve) calcd. *m/z* for $C_{13}H_{15}N_7O_7P^-$ [$(M-H^+)^-$] 412.2, found [$(M-H^+)^-$] 412.2.

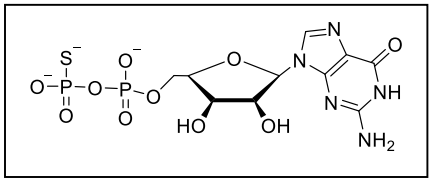

Guanosine 5'-*O*-(2-thiodiphosphate) (GDPβ-S): 99% yield; GMP-Im (1 equiv., 0.435 g, 1.0 mmol), thiophosphate TEA salt (converted sodium thiophosphate tribasic hydrate to TEA salt using general procedure, 2 equiv., 0.431 g, 2.0 mmol), and anhydrous $ZnCl_2$ (8 equiv., 1.09 g, 8.0 mmol) were dissolved in DMF (10 mL) and stirred at room temperature. After 30 minutes, the reaction was quenched by the addition of a solution of EDTA (8 equiv., 2.34 g, 8.0 mmol) and $NaHCO_3$ (18 equiv., 1.51 g, 18 mmol) in water. The resulting product was purified on DEAE-sephadex and isolated as a TEA salt according to the general procedure. ^{1}H-NMR (300 MHz) (D_2O) δ 8.03 (s, 1H), 5.83-5.81 (d, 1H, J= 6Hz), 3.25-1.13 (TEA residues); ^{31}P NMR (121 MHz) δ 31.1 (broad s, 1P), -11.7 (d, 1P, J= 31.5Hz) (; MS DUIS ($^{-}$ve) calcd. *m/z* for $C_{10}H_{14}N_5O_{10}P_2S^-$ [$(M-H^+)^-$] 458.0, found [$(M-H^+)^-$] 458.2.

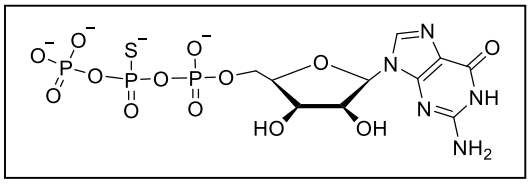

Guanosine 5'-*O*-(2-thiotriphosphate) (GTPβ-S): 10% yield; GDPβ-S TEA salt (1 equiv., 167 mg, 0.30 mmol) was suspended in 3 mL of DMF. Then, 1a (3 equiv., 186 mg, 0.90 mmol) and anhydrous $MgCl_2$ (8 equiv., 228 mg, 2.4 mmol) were added to the suspension. The mixture was stirred at room temperature for 24 hours. Next, the product was subjected to cyanoethyl group removal (one-pot reaction) with the addition of more DMF (3 mL), 1.1 mL of DBU and DTT (3 equiv., 138 mg 0.9 mmol). The reaction was carried out at 50°C in

either an open flask protected from moisture (capped with drying tube packed with anhydrous calcium chloride) or a sealed flask with a rubber septum pierced with a needle attached to a weak pressure vacuum. The deprotection reaction went for 5 hours and was stopped by the addition of 1% acetic acid to pH=7, diluted with water and washed 3 times with ethyl acetate. Finally, the product was purified on DEAE-Sephadex and isolated as a TEA salt. ^{31}P NMR (121 MHz) δ 28.1 (broad s, 1P), -6.70 (dd, 1P, J= 6Hz, J= 28Hz), -12.1 (d, 1P, J= 28Hz); MS DUIS ($^{-}$ve) calcd. *m/z* for $C_{10}H_{15}N_5O_{13}P_3S^-$ [(M-H$^+$)$^-$] 537.9, found [(M-H$^+$)$^-$] 538.0.

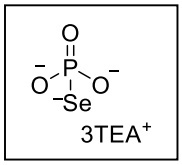

Triethylammonium Selenophosphate: 98% yield; **Note: This procedure should be performed under a fume hood, including all evaporations of solvents.* Prior to the reaction, pyridine was distilled over CaH_2 to ensure complete removal of water. A suspension of selenium (160 mg, 2 mmol) in dry pyridine (1 mL) was added dropwise through a syringe into a septum-sealed and nitrogen-bubbled solution of tris(trimethylsilyl) phosphite (600 µL, 1.8 mmol) in dry CH_3CN (10 mL). The resulting solution was held at room temperature for 30 minutes, and then was evaporated to dryness. Next, a solution of trimethylamine (250 µL, 1.8 mmol) in dry MeOH (10 mL) was added and the mixture was stirred at room temperature for 3 hours. During this time, the initially colorless solution turned yellow with black particulates (elemental Se falling out of solution). The reaction was then filtered and the solvent removed under reduced pressure. The residue was re-dissolved in MeOH and dried under reduced pressure two times. The product isolated was a semi-solid yellow residue and confirmed by ^{31}P NMR. It was immediately used for the following coupling to make GDPβ-Se. ^{31}PNMR (121 MHz) δ 26.8 (s, 1P)

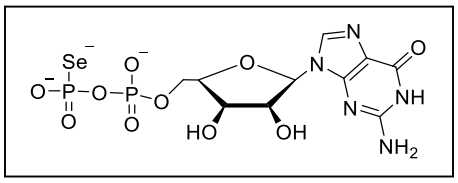

Guanosine 5'-*O*-(2-selenodiphosphate) (GDPβ-Se): 98% yield; To a suspension of GMP-Im (250 mg, 0.42 mmol) and selenophosphate TEA salt (prepared from 600 µL tris(triemthylsilyl)phosphite) in 5 mL of dry DMF, anhydrous $ZnCl_2$ (580 mg, 4.20 mmol) was added and the mixture was vigorously shaken until all reagents dissolved (2-3 minutes). The resulting solution was stirred for 20 minutes at room temperature (during this time a precipitation of small red, slowly turning black, solid, presumably selenium, was observed). The reaction was quenched by diluting a solution of disodium EDTA (1.6 g, 4.20 mmol) and $NaHCO_3$ (800 mg) in 300 mL of water. The pH was checked and, if necessary, adjusted with a small portion of $NaHCO_3$ to pH=7.5. The mixture was stirred at room temperature for 1-2 hours and the precipitated selenium was filtered off using 0.45 µm PVDF syringe filters. The product was isolated on DEAE Sephadex according to the general procedure. **Note: Sephadex resin is irreversibly stained a bright red-orange but still remains useable for other purifications.* ^{31}P NMR (121 MHz) δ 15.53 (d, 1P, J= 37Hz), -12.37 (d, 1P, J= 37Hz); MS DUIS ($^{-}$ve) calcd. *m/z* for $C_{10}H_{15}N_5O_{13}P_2Se^-$ [$(M-H^+)^-$] 505.9, found [$(M-H^+)^-$] 506.0 in addition to selenium isotope peaks.

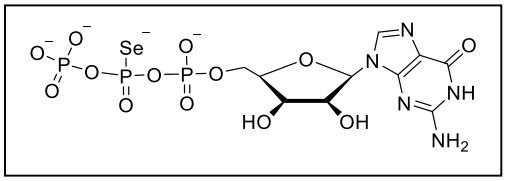

Guanosine 5'-*O*-(2-selenotriphosphate) (GTPβ-Se): 30% yield; GDPβ-Se TEA salt (1 equiv., 167 mg, 0.30 mmol) was suspended in 3 mL of DMF. Then, 1a (3 equiv., 186 mg, 0.90 mmol) and anhydrous $MgCl_2$ (8 equiv., 228 mg, 2.4 mmol) were added to the suspension. The mixture was stirred at room temperature for 24 hours. The coupling reaction was monitored by HPLC with a linear gradient 1-25% of methanol in 0.05M ammonium acetate buffer (pH=5.9) over 15minutes and UV-detection at 260 nm. Next, the product was subjected to

cyanoethyl group removal (one-pot reaction) with the addition of more DMF (3 mL), 1.1mL of DBU and DTT (3 equiv., 138 mg 0.9 mmol). The reaction was carried out at 50°C in either an open flask protected from moisture (capped with drying tube packed with anhydrous calcium chloride) or a sealed flask with a rubber septum pierced with a needle attached to a weak pressure vacuum. The deprotection reaction was monitored by HPLC with the same parameters as the coupling reaction. After 2 hours, the reaction was stopped by the addition of 1% acetic acid to pH=7, diluted with water and washed 3 times with ethyl acetate. Finally, the product was purified on DEAE-Sephadex and isolated as a TEA salt. ^{31}PNMR (121 MHz) δ 16.7 (broad s, 1P), -8.54 (d, 1P, J= 31.5Hz), -12.68 (d, 1P, J= 31.5Hz); MS DUIS ($^{-}$ve) calcd. *m/z* for $C_{10}H_{15}N_5O_{13}P_3Se^-$ [$(M-H^+)^-$] 585.9, found [$(M-H^+)^-$] 586.0.

2.2 Preliminary GTPase Assay Development

For this assay, we wanted a rapid, sensitive and selective fluorescent probe to detect the hydrolysis of GTPβ-S or Se independent of the GTPases. A panel of sulfur-sensitive fluorophores were tested but the most promising probe was Thiofluor 623 (Figure 70). In 2008, Bouffard *et al* at

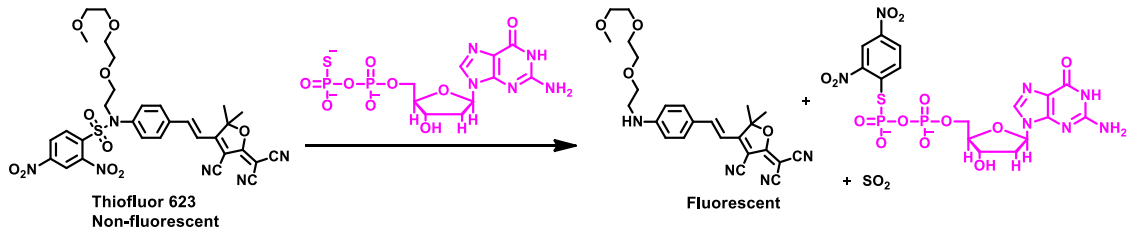

Figure 70. The "turn-on" reaction that occurs when Thiorfluor 623 is cleaved with a thiol like GDPβ-S.

Harvard University developed this Thiofluor probe to address the many drawbacks associated with already commercially available thiol-detecting chromophores and fluorophores.[246] Thiofluor 623 is a "turn-on" probe whose structure is based on a classical donor-π-acceptor

design. The probe will undergo a nucleophilic substitution with nucleophilic compounds liberating the aniline based fluorescence compound (Figure 71). This increases the push-pull character of the dye and results in a higher quantum yield and large bathochromic shifts in the absorption and emission spectra. Arenesulfonamides are stable towards oxygen and nitrogen nucleophiles but react with thiols in contrary to arene-sulfonate-based probes.[247] Furthermore, the long triethyleneglycol methyl ether chain substituted on the nitrogen allows for a wide pH range in which this probe can be used and increases its water solubility. Figure 71 shows that

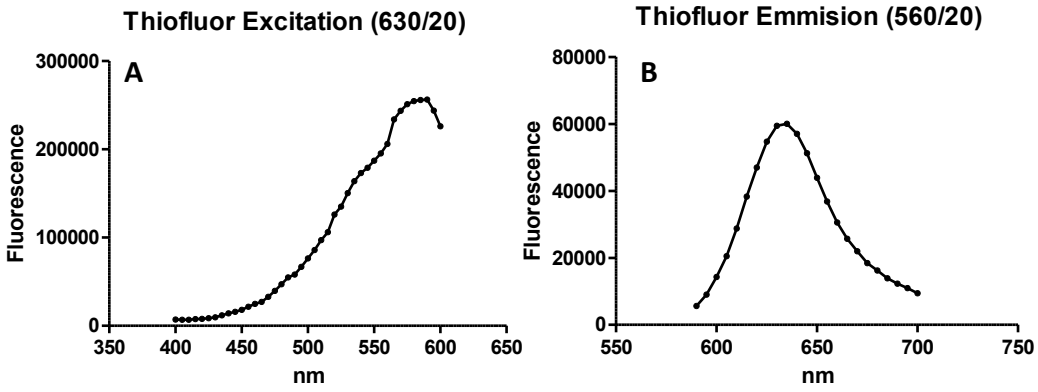

Figure 71. Thiofluor 623 excitation and emission spectra; A) Excitation spectra at 630 nm emission B) Emission spectra at 560 nm excitation.

Thiofluor 623 has an Ex_{max} of 560 nm and Em_{max} at 630 nm.

Within this section, we report the use of Thiofluor 623 to determine the limit of detection with Glutathione (GSH), GDPβ-S and GDPβ-Se over a range of different concentrations and time. The optimizations resulted in the detection of GTPβ-Se in the presence of H-Ras. The activity of H-Ras was determined using a calorimetric assay that detects inorganic phosphate liberated when H-Ras hydrolyzes GTP to GDP.

2.2.1 Experimental Methods

Optimization of Assay Conditions:

Reagents and Instrumentation: The buffer was prepared from phosphate buffered saline, pH 7.4 (Hyclone, #SH30256.01) and 0.001% Tween. Thiofluor 623 was purchased from Cayman Chemical Company (#13083). The reagents tested were L-Glutathione reduced (GSH) (Sigma-Aldrich #G4251), GDPβ-S and GDPβ-Se (both synthesized in our lab). All fluorescence readings were performed with Tecan Infinite M1000 plate reader. Small volume transfers were performed on the Tecan Freedom EVO liquid handling system with a 100 nL pin tool transfer (V&P Scientific). Serial dilutions were done in 96-well polypropylene plates (Corning, #3365) and assays were conducted in 384-well black polystyrene microplates (Nunc, #262260).

Probe Determination Assay Protocol: Solid Thiofluor 623 was diluted in DMF at 10 mM. 10 mM stock solutions of GSH, GDPβ-S and GDPβ-Se in water were serially diluted in the prepared PBS buffer (2.5 μM-0.00488 μM).

Determining H-Ras Functionality using a GTPase Calorimetric Assay[248]:

Reagents and Instrumentation: The assay buffer was prepared by adding 50 mM Tris (Acros Organics, #201-064-4) , 5 μg/mL BSA (Thermo Scientific, #23209), 0.01% (v/v) Tween 20 (Fisher Scientific, #BP337), 5 mM DTT (Gold Biotechnology, #DTT100) to 18 MΩ water. The final buffer was pH to 7.5 and filtered to remove any particulates. A 12.5 mM $MgCl_2$ (Fisher Scientific, #AB-0359) solution was prepared in 18MΩ water. A 30 mM stock solution of guanosine 5'-triphosphate sodium salt hydrate (Sigma, #G8877) was prepared in 18MΩ water. The 25 μM stock GTPase protein, H-Ras, was a gift from Prof. Evgueni Kovriguine (Marquette University). The calorimetric dye, Biomol Green™ (Enzo Life Sciences, #BML-AK111), reacts with inorganic

phosphate to produce a product that absorbs light at 620 nm. Controls used were buffer (negative control) and KH_2PO_4 (J. T. Baker Chemical Company, #3246, positive control) Serial dilutions were done in 96-well polypropylene plates (Corning, #3365) while reactions were performed in clear, 384-well UV plates (Greiner Bio-One, #781801). Each concentration was done in triplicate. All UV readings were performed with a Tecan Infinite M1000 plate reader.

GTP Hydrolysis Assay Protocol: GTP was serially diluted (1:2) to produce concentrations ranging from 30 mM to 0.001524 mM. H-Ras was diluted to 80 nM in buffer. In a clear, 384 well UV plate each well contained 6.75 µL H-Ras (final concentration 40 nM), 6.75µL of GTP (final concentrations ranging from 15 mM-0.000762 mM) and 1.5 µL of $MgCl_2$ to equal a total volume of 15 µL. The plate was incubated for 1 hour at 37°C. After 1 hour, 25 µL of Biomol Green™ was added to each well and the plate was incubated for an additional 30 minutes at 37°C. Absorbance was read at 620 nm to determine if phosphate was in fact hydrolyzed from GTP by the GTPase actions of H-Ras.

H-Ras Hydrolysis of GTPβ-Se Monitored with Fluorescence:

Reagents and Instrumentation: Buffer was made by adding 50mM Tris (Acros Organics, #201-064-4), 0.03% (v/v) Tween 20 (Fisher Scientific, #BP337), 80 mM NaCl (Fisher Scientific, #S640), 8 mM $MgCl_2$ (Fisher Scientific, #AB-0359), 1 mM EDTA (Fisher Scientific, #S80007) to 18MΩ water. The buffer was pH to 7.4 with HCl and filtered to remove any particulates. 10 mM stock solutions of GDPβ-Se, GTPβ-Se and GSH (Sigma-Aldrich #G4251) were diluted in 18MΩ water. The probe, Thiofluor 623, was diluted in the buffer to 1 µM and GTPase protein, H-Ras, at 40 nM concentration. All fluorescence readings were performed on a Tecan Infinite M1000 plate reader with excitation read at 570 nm and emission at 630 nm. The gain was set manually at 100 and

10 nm bandwidth was used. Serial dilutions were done in 96-well polypropylene plates (Corning, #3365) and assays were conducted in 384- well black polystyrene microplates (Nunc, #262260).

H-Ras Activation using Thiofluor 623 Assay Protocol: First, to check if GDPβ-Se and GTPβ-Se had different fluorescence intensities without the presence of H-Ras they were serially diluted (1:2) in 96 well plates to obtain concentrations ranging from 10 mM-0.000508 mM. 10 µL of each concentration of compound was transferred to a 384 well black plate. To each well 10 µL of a 20 µM Thiofluor 623 solution (diluted in buffer) was added. Therefore, the resulting plate had the final concentrations of compound ranging from 5 mM- 0.000254 mM and 10 µM Thiofluor 623. To determine if H-Ras hydrolyzes GTPβ-Se to GDPβ-Se, another experiment was set up where GTPβ-Se was serially diluted (1:2) to in 96 well plates and 10 µL was transferred to 384 well black plates just like before. To the 20 µM Thiofluor 623 solution, H-Ras protein was added to yield a final concentration of 80 nM. To each well, 10 µL of the probe/protein solution was added. Therefore, the final concentrations in each well were: 5 mM- 0.000254 mM GTPβ-Se, 40nM H-Ras and 10 µM Thiofluor 623. For both experiments, the plate was incubated at room temperature and fluorescence was read at 10, 20, 30, 40, 50, 90 and 120 minutes.

2.2.2 Results and Discussion

Initial experiments were conducted to determine the best assay conditions to monitor the formation of GDPβ-S or GDPβ-Se by fluorescence. Thiofluor 623 was incubated with GSH over a range of concentrations over 60 minutes (Figure 72, A). After 40 minutes, it was evident that the fluorescence intensity reached its maximum before starting to decrease at 60 minutes. In addition, the fluorescence signal was high at about 25,000 units. When GDPβ-S was used, the fluorescence intensity was much lower even after 30 minutes (Figure 72, B). This indicated that a large amount of the GDPβ-S would be necessary to obtain a significant window of detection.

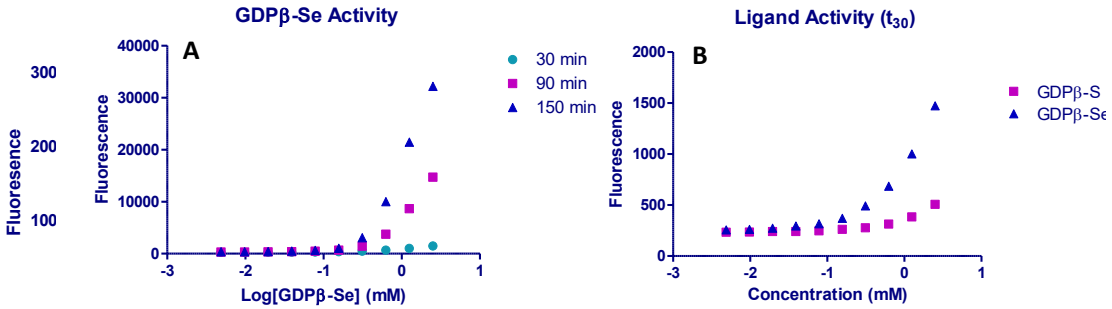

Figure the flu **Figure 73.** Determining if GDPβ-S or GDPβ-S would be more suitable for assay kit. A) A dose response curve with GDPβ-Se and probe, Thiofluor 623 react, over time. B) Comparison of fluorescence intensity between GDPβ-S and GDPβ-Se over a range of concentrations at 30 minutes.

With these results, it was concluded that GDPβ-S may not be a good substrate for the assay being developed. Therefore, GDPβ-Se was investigated as a possible GTPase substrate because of the higher nucleophilicity of the larger selenium atom. GDPβ-Se gave higher fluorescence when compared to GDPβ-S (Figure 73, A and B). A concentration of 1mM of GDPβ-Se appeared to be necessary to observe a significant window of detection. The initial assay development was conducted with the GTPase, H-Ras. Prior to its use, the functionality was evaluated using a calorimetric assay developed at UWM by Sweeney *et al*.[248] GTP was serially diluted and

incubated with H-Ras. The production of inorganic phosphate (P_i) was detected by its reaction with Biomol Green™, a dye that absorbs UV light at 620nm (Figure 74). The H-Ras protein was capable of hydrolyzing GTP to GDP with a concentration of less than 1.0 mM GTP was necessary to create a workable signal.

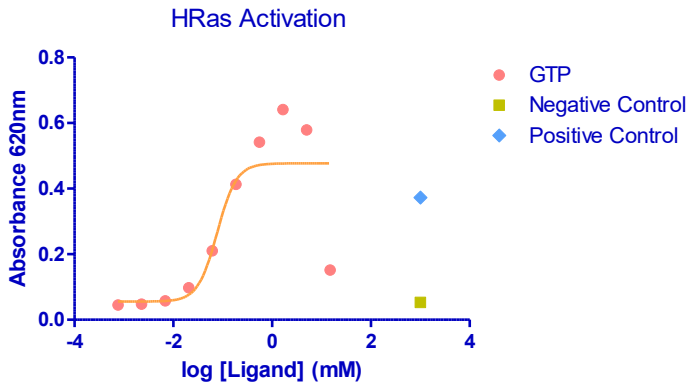

Figure 74. Dose response curve representing the hydrolysis of GTP to GDP with H-Ras using the calorimetric assay.

GDPβ-Se and GTPβ-Se were first compared without H-Ras present in Figure 76, A. As observed before, GDPβ-Se reacted with Thiofluor 623 showing an increased fluorescence with increasing concentration over 90 minutes (figure 75, A). However, GTPβ-Se with a "capped" selenium atom did not induce fluorescence (Figure 75, A). Thus, thiofluor 623 was capable of

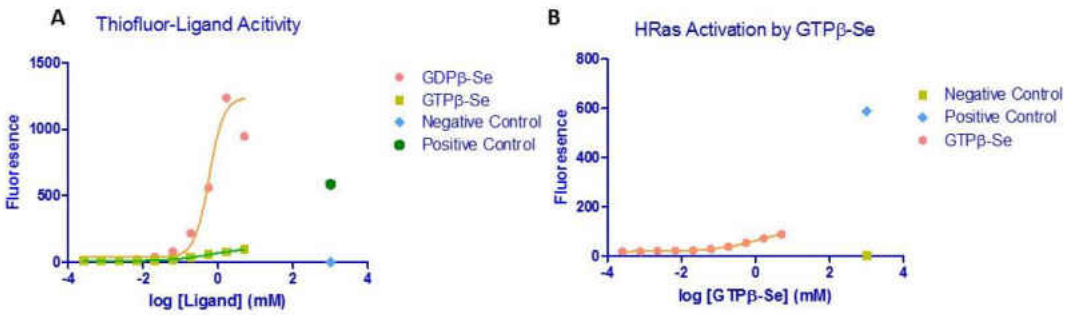

Figure 75. A) A comparison of GTPβ-Se and GDPβ-Se and their ability to turn "on" the probe, Thiofluor 623. B) The activation of H-Ras with the binding of GTPβ-Se using Thiofluor 623 to detect the production GDPβ-Se.

detecting GDPβ-Se in the presence of GTPβ-Se. With H-Ras present, GTPβ-Se was not

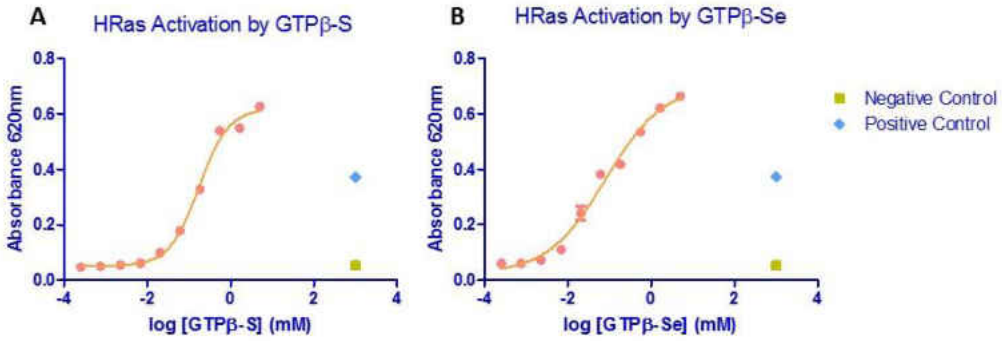

Figure 76. A comparison of GTPβ-S and GTPβ-Se in activating H-Ras using a calorimetric assay. A) GTPβ-S and B) GTPβ-Se.

enzymatically converted into GDPβ-Se and therefore no fluorescence was observed even in the presence of increasing amounts of GTPβ-Se substrate (Figure 75, B). One hypothesis is that H-Ras is not able to convert GTPβ-Se to GDPβ-Se. Therefore, the Biomol Green™ –based calorimetric assay was used in the presence of GTPβ-Se and GTPβ-S and H-Ras (Figure 76, A and B). Initially, H-Ras appeared to be capable of hydrolyzing both substrates, however the absorbance was higher than the control concentration of phosphate. When the reactions were carried out in the absence of H-Ras a similar curve was obtained, thus the substrates GTPβ-Se and GTPβ-S reacted with Biomol Green™ to increase the absorbance at 620 nm. Another possibility is that traces of seleno- and thio-phosphate or compound 1a might react with Biomol Green™. We are currently in the process to purify the final products with HLPC and scan the absorbance spectra from 250-800 nm to identify if the GTP analogs change the absorbance spectra of the molybdate-malachite green complex.

2.2.3 Conclusion

The synthesis of GDPβ-S/Se and GTPβ-S/Se was successfully executed. In addition, an appropriate probe, Thiofluor 623, was identified for the detection of GDPβ-S and GDPβ-Se.

Interestingly, H-Ras was not able to convert the heavy atom analogs of GTP, which prompted us to investigate other GTPases with our assay system. In addition, we will continue the search for a fluorescence probe that will work for the GDP/GTPβ-S system. The Biomol Green™ –based assay did identify phosphate species in the purified end products or reacted with the GTP analogs itself. . Overall, a significant progress has been made to develop a universal GTPase assay, which encourages us to continue this work in the future with AviMed Pharmaceuticals, LLC.

REFERENCES

1. Shaffer, P. L.; Gewirth, D. T., Structural Basis of VDR-DNA Interactions on Direct Repeat Response Elements *EMBO Journal* **2002,** *21*, 2242-2252.

2. Orlov, I.; Rochel, N.; Moras, D.; Klaholz, B. P., Structure of the full human RXR/VDR nuclear receptor heterodimer complex with its DR3 target DNA. *The EMBO Journal* **2012,** *31*, 291-300.

3. Whitfield, G. K.; Jurutka, P. W.; Haussler, C. A.; Hsieh, J.-C.; Barthel, T. K.; Jacobs, E. T.; Dominguez, C. E.; Thatcher, M. L.; Haussler, M. R., Nuclear Vitamin D Receptor: Stucture-Function, Molecular Control of Gene Transcription, and Novel Bioactions. In *Vitamin D Recptor, 2nd Edition*, Feldman, D.; Pike, J. W.; Glorieux, F. H., Eds. Elsevier Academic Press: Burlington, MA, 2005; Vol. 1, pp 219-261.

4. Jurutka, P. W.; Whitfield, G. K.; Hsieh, J.-C.; Thompson, P. D.; Haussler, C. A.; Haussler, M. R., Molecular Nature of the Vitamin D Receptor and its Role in Regulation of Gene Expression. *Reviews in Endocrine & Metabolic Disorders* **2001,** *2*, 203-216.

5. Dowd, D. R.; MacDonald, P. N., Coregulators of VDR-mediated Gene Expression. In *Vitamin D, 3rd edition*, Freedman, D.; Pike, J. W.; Adams, J. S., Eds. Elsevier: 2011; Vol. 1.

6. *Molecular Operating Environment (MOE)*, Chemical Computing Group, Inc.: Sherbook St. West, Suite #910, Montreal, QC, Canada, H3A, 2R7, 2015.

7. Parker, C.; Zhang, J.-H., High Throughput Screening for Small-Molecule Drug Discovery. In *Development of Therapeutic Agents Handbook, 1st Ed.*, Cox, S., Ed. John Wiley & Sons: 2012.

8. Rochel, N.; Wurtz, J. M.; Mitschler, A.; Klaholz, B.; Moras, D., The Crystal Structure of the Nuclear Receptor for Vitamin D Bound to Its Natural Ligand. *Molecular Cell* **2000,** *5*, 173-179.

9. Teichert, A.; Arnold, L. A.; Otieno, S.; Oda, Y.; Augustinaite, I.; Geistlinger, T. R.; Kriwacki, R. W.; Guy, R. K.; Bikle, D. D., Quantification of the Vitamin D Receptor- Coregulator Interaction. *Biochemistry* **2009,** *48*, 1454-1461.

10. Batista, F. A. H.; Trivella, D. B. B.; Bernardes, A.; Gratieri, J.; Oliveira, P. S. L.; Figueira, A. C. M.; Webb, P.; Polikarpov, I., Structural Insights into Human Peroxisome Proliferator Activated Receptor Delta (PPAR-Delta) Selective Ligand Binding. *PLoS ONE* **2012,** *7*, 1-7.

11. Chen, X.; Murawski, A.; Patel, K.; Crespi, C. L.; Balimane, P. V., A Novel Design of Artificial Membrane for Improving the PAMPA Model. *Pharmaceutical Research* **2008,** *25*, 1511-1520.

12. Rosenfeld, L., Vitamine-Vitamin. The Early Years of Discovery. *Clinical Chemistry* **1997,** *43*, 680-685.

13. Hopkins, F. G., Feeding Experiments Illustrating the Importance of Accessory Food Factors in Normal Dietaries. *J. Physiol* **1912,** *44*, 425-460.

14. Funk, C., On the Chemical Nature of the Substance Which Cures Polyneuritis in Birds Induced by a Diet of Polished Rice. *J. Physiol* **1911,** *43*, 395-402.

15. McCollum, E. V.; Davis, M., The Necessity of Certain Lipins int he Diet During Growth. *J. Biol. Chem* **1913,** *15*, 167-175.

16. McCollum, E. V.; Simmonds, N.; Pitz, W., The Relation of the Unidentified Dietary Factos, the Fat-Soluble A, and Water-Soluble B, of the Diet to the Growth-Promoting Properties of Milk. *J. Biol. Chem* **1916,** *27*, 33-38.

17. McCollum, E. V.; Simmonds, N.; Becker, J. E., An Experimental Demonstration of the Existence of a Vitamin Which Promotes Calcium Deposition. *J Biol. Chem* **1922,** *53*, 293-298.

18. Deluca, H. F., Historical Overview of Vitamin D. In *Vitamin D, 3rd Edition*, Feldman, D.; PIke, J. W.; Adams, J. S., Eds. 2011; Vol. 1.

19. Huldschinsky, K., Heilung con rachitis durch kunstalich hohen-sonne. *Deut. Med. Wochenschr* **1919,** *45*, 712-713.

20. Chick, D. H., Study of Rickets in Vienna 1919-1922. *Medical Research Council, Special Report* **1923**.

21. Wolf, G., The Discovery of Vitamin D: The Contribution of Adolf Windaus. *J. Nutr.* **2004,** *134*, 1299-1302.

22. Steenbock, H.; Black, A., Fat Soluble Vitamins: XVII. The Induction of Growth-Promoting and Calcifying Properties in a Ration by Exposure to Ultra-Violet Light. *J Biol. Chem* **1924,** *61*, 405-422.

23. Steenbock, H.; Black, A., XXIII. The Induction of Growth-Promoting and Calcifying Propterties in Fats and their Unsaponifiable Constituents by Exposure to Light. *J Biol. Chem* **1925,** *64*, 263-298.

24. Hess, A.; Weinstock, M.; Helman, F. D., The Antirachitic Value of Irradiated Phytosterol and Cholesterol. *J Biol. Chem* **1925,** *63*, 305-309.

25. Askew, F. A.; Bourdillon, R. B.; Bruce, H. M.; Jenkins, R. G. C.; Webster, T. A., The Distillation of Vitamin D. *Proc. R. Soc.* **1930,** *B107*, 76-90.

26. Rosenheim, O.; Webster, T. A., XCV. The Specificity of Ergosterol as Parent Substance of Vitamin D. *J Biol. Chem* **1928**, 762-766.

27. Rosenheim, O.; Webster, T. A., LVI. The Parent Substance of Vitamin D. *Biochem J.* **1927,** *21*, 389-397.

28. Windaus, A.; Schenck, F., Uber das antirachitsch wirksame bestrahlungs-produkt aus 7-dehydrocholesterin. *Hoppe.-Seylers. Z. Physiol. Chem* **1936,** *241*, 100-103.

29. Windaus, A.; Lettre, H.; Schenck, F., 7-Dehydrocholesterol. *Justus Liebigs Annalen der Chemie* **1935,** *520*, 98-106.

30. Kodicek, E., The Metabolism of Vitamin D. In Umbreit, W.; Molitor, H., Eds. 1960; pp 198-208.

31. Kodicek, E., Metabolic Studies on Vitamin D. In *Ciba Foundation Sypmosium on Bone Structure and Metabolism*, Wolstenholme, G. W. E.; O'Connor, C. M., Eds. Boston, Massachusetts, 1956; pp 161-174.

32. Blunt, J. W.; Deluca, H. F., The Synthesis of 25-hydroxycholecalciferol. A Biologically Active Metabolite of Vitamin D_3. *Biochemistry* **1969,** *8*, 671-675.

33. Blunt, J. W.; DeLuca, H. F.; Schnoes, H. K., 25-Hydroxycholecalciferol. A Biologically Active Metabolite of Vitamin D_3. *Biochemistry* **1968,** *7*, 3317-3322.

34. Deluca, H. F., History of the Discovery of Vitamin D and its Active Metabolites. *BoneKEy Reports* **2014,** *3*.

35. Holick, M. F.; Schnoes, H. K.; DeLuca, H. F.; Suda, T.; Cousins, R. J., Isolation and Identification of 1,25-Dihydroxycholecalciferol A Metabolite of Vitamin D Acite in Instestine. *Biochemistry* **1971,** *10*, 2799-2804.

36. Chalk, K. J. I.; Kodicek, E., The Association of ^{14}C-Labelled Vitamin D_2 with Rat Serum Protiens. *Biochem J.* **1961,** *79*.

37. Rikkers, H.; DeLuca, H. F., An in vivo study of the carrier proteins of ^{3}H-vitamins D_3 and D_4 in rat serum. *American Journal of Physiology* **1967,** *213*, 380-386.

38. Ponchon, G.; Kennan, A. L.; DeLuca, H. F., "Activation" of Vitamin D by the Liver. *The Journal of Clinical Investigations* **1969,** *48*.

39. Cheng, J. B.; Levine, M. A.; Bell, N. H.; Mangelsdorf, D. J.; Russel, D. W., Genetic Evidence that the Human CYP2R1 Enzyme is a Key Vitamin D 25-hydroxylase. *Proc Natl Acad Sci U S A* **2004,** *101*, 7711-7715.

40. Takeyama, K.-i.; Kitanaka, S.; Sato, T.; Kobori, M.; Yanagisawa, J.; Kato, S., 25-hydroxyvitamin D_3 1α-Hydroxylase and Vitamin D Synthesis. *Science* **1997,** *277*, 1827-1829.

41. Haussler, M. R.; Norman, A. W., Chromosomal Receptor for Vitamin D Metabolite. *Proc Natl Acad Sci* **1969,** *62*, 155-162.

42. Brumbaugh, P. F.; Haussler, M. R., Specific Binding of 1a-25-dihydroxycholecalciferol to Nuclear Components of Chick Intestine. *The Journal of Biological Chemistry* **1974,** *250*, 1588-1594.

43. Brumbaugh, P. F.; Hughes, M. R.; Haussler, M. R., Cytoplasmic and Nuclear Binding Components for 1a,25-dihydroxyvitamin D3 in Chick Parathyrid Glands. *Biochemistry* **1975,** *72*, 4871-4875.

44. Evans, R. M., The steroid and thyroid hormone receptor superfamily. *Science* **1988,** *240*, 889-895.

45. Robinson-Rechavi, M.; Carpentier, A.-S.; Duffraisse, M.; Laudet, V., How many nuclear hormone recewptor are there in the human genome. *Trends in Genetics* **2001,** *17*, 554-556.

46. Mangelsdorf, D. J.; Thummel, C.; Beato, M.; Herrlich, P.; Schutz, G.; Umesono, K.; Blumberg, B.; Kastner, P.; Mark, M.; Chambon, P.; Evans, R. M., The Nuclear Receptor Superfamily: The Second Decade. *Cell* **1995,** *83*, 835-839.

47. Pike, J. W.; Meyer, M. B.; Lee, S. M., The Vitamin D Receptor. In *The Vitamin D Receptor, 3rd Edition*, Feldman, D.; PIke, J. W.; Adams, J. S., Eds. Elsevier: 2011; Vol. 1.

48. Berg, J. M., DNA Binding Specificity of Steroid Receptors. *Cell* **1989,** *57*, 1065-1068.

49. Luisi, B. F.; Xu, W. X.; Otwinowski, Z.; Freedman, L. P.; Yamamoto, K. R.; Sigler, P. B., Crystallographic Analysis of the Interaction of the Glucocoricoid Receptor with DNA. *Nature* **1991,** *352*, 497-505.

50. Pike, W.; Shevde, N. K., The Vitamin D Receptor. In *Vitamin D, 2nd Edition*, Feldman, D.; Pike, J. W.; Glorieux, F. H., Eds. Elsevier Academic Press: 2005; Vol. 1, pp 167-191.

51. Carlberg, C.; Bendik, I.; Wyss, A.; Meier, E.; Sturzenbecker, L. J.; Grippo, J. F.; Hunziker, W., Two Nuclear Signaling Pathways for Vitamin D. *Nature* **1993,** *361*, 657-660.

52. Shaffer, P. L.; Gewirth, D. T., Structural basis of VDR-DNA interactions on direct repeat repsonse elements. *EMBO J.* **2002,** *21*, 2242-2252.

53. Kurokawa, R.; Yu, V. C.; Nααρ, A.; Kyakumoto, S.; Han, Z.; Silverman, S.; Rosenfeld, M. G.; Glass, C. K., Differential orientations of the DNA-binding domain and carboxy-terminal dimerization interface regulate binding site selection by nuclear receptor heterodimers. *Genes Dev.* **1993,** *7*, 1423-1435.

54. Moras, D.; Gronemeyer, H., The Nuclear Receptor Ligand-binding Domain: Structure and Function. *Current Opinion in Cell Biology* **1998,** *10*, 384-91.

55. Rochel, N.; Moras, D., Structural Basis for Ligand Activity in VDR. In *Vitamin D, 3rd Edition*, Feldman, D.; Pike, J. W.; Adams, J. S., Eds. Elsevier Inc: 2011; Vol. II, pp 171-191.

56. Makishima, M.; Yamada, S., Targeting the Vitamin D Receptor: Advances in Drug Discovery. *Expert Opinion* **2005**, 1133-1145.

57. Rachez, C.; Lemon, B. D.; Suldan, Z.; Bromleigh, V.; Gamble, M.; Naar, A. M.; Erdjument-Bromage, H.; Tempst, P.; Freedman, L. P., Ligand-independent transcription activation by nuclear receptors requires the DRIP complex. *Letters to Nature* **1999,** *298*, 824-828.

58. Perissi, V.; Jepsen, K.; Glass, C. K.; Rosenfeld, M. G., Deconstructing Repression: Evolving Models of Co-repressor Action. *Nature Reviews* **2010,** *11*, 109-123.

59. Horlein, A. J.; Naar, A. M.; Heinzel, T.; Tochia, J.; Gloss, B.; Kurokawa, R.; Ryan, A.; Kamei, Y.; Soderstrom, M.; Glass, C. K.; Rosenfeld, M. G., Ligand-idependent repression by the thyroid hormone receptor mediated by nuclear receptor co-repressor. *Nature* **1995,** *377*, 397-403.

60. Nagy, L.; Kao, H.-Y.; Chakravarti, D.; Lin, R. J.; Hassig, C. A.; Ayer, D. E.; Schreiber, S. L.; Evans, R. M., Nuclear Receptor Repression Mediated by a Complex Containing SMRT, mSin3A and Histone Deacetylase. *Cell* **1997,** *89*, 373-380.

61. Blanco, J. C. G.; Wang, I.-M.; Tsai, S. Y.; Tsai, M.-J.; O'Malley, B. W.; Jurutka, P. W.; Haussler, M. R.; Ozato, K., Transcription factor TFIIB and the vitamin D receptor cooperatively activate ligand-dependent transcription. *Biochemistry* **1995,** *92*, 1535-1539.

62. Masuyama, H.; Stephen C. Jefcoat, J.; MacDonald, S. N., The N-terminal domain of transcription factor IIB is require for direct interaction with the Vitamin D Receptor and participiates in Vitamin D-mediate transcription. *Molecular Endocrinology* **1997,** *11*, 218-228.

63. Xu, J.; Wu, R.-C.; O'Malley, B. W., Normal and Cancer-Related Functions of the p160 Steroid Receptor Coactivator (SRC) Family. *Nat Rev Cancer* **2009,** *9*, 615-630.

64. McInerney, E. M.; Rose, D. W.; Flynn, S. E.; Westin, S.; Mullen, T.-M.; Krones, A.; Inostroza, J.; Torchia, J.; Nolte, R. T.; Ass-Munt, N.; Milburn, M. V.; Glass, C. K.; Rosenfeld, M. G., Determinants of Coactivators LXXLL Motif Specificity in Nuclear Receptor Transcriptional Activation. *Genes Dev.* **1998,** *12*, 3357-3368.

65. Bikle, D. D.; Teichert, A.; Arnold, L. A.; Uchida, Y.; Elias, P. M.; Oda, Y., Differential Regulation of Epidermal Function by VDR Coactivators. *J. Steroid Biochem. Mol. Biol.* **2010,** *121*, 308-313.

66. Chen, H.; Lin, R. J.; Schiltz, R. L.; Chakravarti, D.; Nash, A.; Nagy, L.; Privalsky, M. L.; Nakatani, Y.; Evans, R. M., Nuclear Receptor Coactivator ACTR is a Novel Histone Acetyltransferase and Forms a Mutimeric Ativation Complex with P/CAF and CBP/p300. *Cell* **1997,** *90*, 569-580.

67. Mengus, G.; May, M.; Carre, L.; Chambon, P.; Davidson, I., Human $TAF_{II}135$ potentiates transcriptional activation by the AF-2s of the retinoic acid, vitamin D3, and thyroid hormone receptors in mammalian cells. *Genes Dev.* **1997,** *11*.

68. Rachez, C.; Gamble, M.; Chang, C.-P. B.; Atkins, G. B.; Lazar, M. A.; Freedman, L. P., The DRIP Complex and SRC-1/p160 Coactivators Share Similar Nuclear Receptor Binding Determinants but Constitute Functionally Distinct Complexes. *Molecular and Cellular Biology* **2000,** *20*, 2718-2726.

69. Cantin, G. T.; Stevens, J. L.; Berk, A. J., Activation domain-mediator interactions promote trancription preinitiation complex assembly on promoter DNA. *Proc Natl Acad Sci* **2003,** *100*, 12003-12008.

70. Feldman, D.; Pike, J. W.; Glorieux, F. H., *Vitamin D, 2nd Edition*. Elsevier Academic Press: 2005; Vol. 1-2.

71. Franceschi, R. T.; Li, Y., Vitamin D Regulation of Osteoblast Function. In *VItamin D, 3rd Edition*, Feldman, D.; Pike, J. W.; Glorieux, F. H., Eds. Elsvier Academic Press: 2011; Vol. 1, pp 321-333.

72. Rojas-Rivera, J.; Piedra, C. D. L.; Ramos, A.; Ortiz, A.; Egido, J., The expanding spectrum of biological actions of Vitamin D. *Nephrol Dial Transplant* **2010,** *25*, 2850-2865.

73. Hsu, H.; Lacey, D. L.; Dunstan, C. R.; Solovyev, I.; Colombero, A.; Timms, E.; Tan, H.-L.; Elliott, G.; Kelley, M. J.; Sarosi, I.; Wang, L.; Xia, X.-S.; Elliott, R.; Chui, L.; Black, T.; Scully, S.; Capparelli, C.; Morny, S.; Shimamoto, G.; Bass, M. B.; Boyle, W. J., Tumor necrosis factor receptor family member RANK mediates osteoclast differentiation and activation induced by osteoprotegerin ligand. *Proc. Natl. Acad. Sci* **1999,** *96*, 3540-3545.

74. Dusso, A. S.; Brown, A. J.; Slatopolsky, E., Vitamin D. *Am J Physiol Renal Physiol* **2005,** *289*, F8-F28.

75. Nishii, Y.; Okano, T., History of the development of new vitamin D analogs: studies on 22-oxacalcitriol (OCT) and 2B-(3-hydroxypropoxy)calcitriol (ED-71). *Steroids* **2001,** *66*, 137-146.

76. Matsumoto, T.; Kubodera, N., ED-71, a New Active Vitamin D3, Increases Bone Mineral Density Regardless of Serum 25(OH)D Levels in Osteoporotic Subjects. *Journal of Steroid Biochemistry & Molecular Biology* **2007,** *103*, 584-586.

77. Uchiyama, Y.; Higuchi, Y.; Takeda, T.; Masaki, T.; Shira-Ishi, A.; Sato, K.; Kubodera, N.; Ikeda, K.; Ogata, E., ED-71, a Vitamin D Analog, is a More Potent Inhibitor of Bone Resportion than Alfacalcidol in an Estrogen-Deficient Rat Model of Osteoporosis. *Bone* **2002,** *30*, 582-588.

78. Noguchi, Y.; Kawate, H.; Nomura, M.; Takayanagi, R., Eldecalcitol for the treatment of osteoporosis. *Clinical Interventions in Aging, Review* **2013,** *8*, 1313-1321.

79. Matsumoto, T.; Miki, T.; Hagino, H.; Sugimoto, T.; Okamoto, S.; Hirota, T.; Tanigawara, Y.; Hayashi, Y.; Fukunaga, M.; Shiraki, M.; Nakamura, T., A New Active Vitamin D, ED-71, Increases Bone Mass in Osteoporotic Patients under Vitamin D Supplementation: A Randomized, Double-Blind, Placebo Controlled Clincal Trial. *The Journal of Clinical Endocrinology & Metabolism* **2005,** *90*, 5031-5036.

80. Eisman, J. A.; Martin, T. J.; MacIntyre, I.; Moseley, J. M., 1,25-dihydroxyvitamin-D-receptor in breast cancer cells. *Lancet* **1979,** *2*, 1335-6.

81. Colston, K.; Colston, M. J.; Feldman, D., 1,25-dihydroxyvitamin D3 and malignant melanoma: the presence of receptors and inhibition of cell growth in culture. *Endocrinology* **1981,** *108*, 1083-6.

82. Gross, C.; Stamey, T.; Hancock, S.; Feldman, D., Treatment of early recurrent prostate cancer with 1,25-dihydroxyvitamin D3 (calcitriol). *J Urol* **1998,** *159*, 2035-9; discussion 2039-40.

83. Beer, T. M.; Myrthue, A., Calcitriol in cancer treatment: from the lab to the clinic. *Mol Cancer Ther* **2004,** *3*, 373-81.

84. Gulliford, T.; English, J.; Colston, K. W.; Menday, P.; Moller, S.; Coombes, R. C., A phase I study of the vitamin D analogue EB 1089 in patients with advanced breast and colorectal cancer. *Br J Cancer* **1998,** *78*, 6-13.

85. Jain, R. K.; Trump, D. L.; Egorin, M. J.; Fernandez, M.; Johnson, C. S.; Ramanathan, R. K., A phase I study of the vitamin D3 analogue ILX23-7553 administered orally to patients with advanced solid tumors. *Invest New Drugs* **2011,** *29*, 1420-5.

86. VanWeelden, K.; Flanagan, L.; Binderup, L.; Tenniswood, M.; Welsh, J., Apoptotic regression of MCF-7 xenografts in nude mice treated with the vitamin D_3 analog, EB1089. *Endocrinology* **1998,** *139*, 2102-2110.

87. Koshizuka, K.; Koike, M.; Asou, H.; Cho, S. K.; Stephen, T.; Rude, R. K.; al, e., Combined effect of vitamin D_3 analogs and paclitaxel on the growth of MCF-7 breast cancer cells in vivo. *Breast Cancer Res. Treat.* **1999,** *53*, 113-120.

88. Koshizuka, K.; Kubota, T.; Said, J.; Koike, M.; Binderup, L.; Uskokovic, M.; al, e., Combination therapy of a viatmin D_3 analog and all-trans-retinoic acid: effect on human breast cancer in nude mice. *Anticancer Res* **1999,** *19*, 519-524.

89. Sundaram, S.; Sea, A.; Feldman, S.; Strawbridge, R.; Hoopes, P. J.; Demidenko, E.; al, e., The combination of a potent vitamin D_3 analog, EB1089, with ionizing radiation reduces tumor growth and induces apoptosis of MCF-7 breast tumor xenografts in nude mice. *Clin. Cancer Res.* **2003,** *9*, 2350-2356.

90. Wu, G.; Fan, R. S.; Li, W.; Ko, T. C.; Brattain, M. G., Modulation of cell cycle control by vitamin D_3 and its analogue, EB1089, in human breast cancer cells. *Oncogene* **1997,** *15*, 1555-1563.

91. Verlinden, L.; Verstuyf, A.; Convents, R.; Marcelis, S.; Camp, M. V.; Bouillon, R., Action of 1,25(OH)2D3 on teh cell cycles genes, cyclin D1, p21, p27 in MCF-7 cells. *Mol Cell Endocrinol* **1998,** *142*.

92. James, S. Y.; Mackay, A. G.; Colston, K. W., Effects of 1,25 dihydroxyvitamin D_3 and its analogues on induction of apoptosis in breast cancer cells. *J. Steroid Biochem. Mol. Biol* **1996,** *58*, 395-401.

93. Bettoun, D. J.; Buck, D. W.; Lu, J.; Khalifa, B.; Chin, W. W.; Nagpal, S., A vitamin D receptor-Ser/Thre phosphatase-p70 S6 kinase complex and modulation of its enzymatic activities by the ligand. *J. Biol. Chem.* **2002,** *277*, 24847-24850.

94. Simboli-Campbel, M.; Narvaez, C. J.; vanWeelden, K.; Tenniswood, M.; Welsh, J., Comparative effects of 1,25(OH)2D3 and EB1089 on cell cycle kinestics apoptosis in MCF-7 breast cancer cells. *Breast Cancer Res. Treat.* **1997,** *42*, 31-41.

95. James, S. Y.; Mackay, A. G.; Colston, K. W., Vitamin D derivatives in combination with 9-cis retinoic aicd promote active cell death in breast cancer cells. *J Mol Endocrinol* **1995,** *14*, 391-394.

96. Narvaez, C. J.; Welsh, J., Role of mitochondria and caspases in vitamin D-mediated apoptosis of MCF-7 breast cancer cells. *J. Biol. Chem.* **2001,** *276*, 9101-9107.

97. Flanagan, L.; Packman, K.; Juba, B.; O'Neill, S.; Tenniswood, M.; Welsh, J., Efficacy of vitamin D compounds to modulate estrogen receptor negative breast cancer growth and invasion. *J. Steroid Biochem. Mol. Biol* **2003,** *84*, 181-192.

98. Koli, K.; Keski-Oja, J., 1alpha,25-dihydroxyvitamin D_3 and its analogues down-regulate cell invasion-associated proteases in cultured malignant cells. *Cell Growth Differ.* **Cell Growth Differ.,** *11*, 221-229.

99. Majewski, S.; Skopinska, M.; Marczak, M.; Szmurlo, A.; Bollag, W.; Jablonska, S., Vitamin D_3 is a potent inhibitor of tumor cell-induced angeiogenesis. *J. Investig. Dermatol. Symp. Proc.* **1996,** *1*, 97-101.

100. Kato, Y.; Nakano, Y.; Sano, H.; tanatani, A.; Kobayashi, H.; Shimazawa, R.; Koshino, H.; Hashimoto, Y.; Nagasawa, K., Synthesis of 1a-25-dihydroxyvitamin D3-26,23-lactams (DLAMs)- a novel series of 1a,25-dihydroxyvitamin D3 antagonist. *Bioorganic & Medicinal Chemistry Letters* **2004,** *14*, 2579-2583.

101. Lamblin, M.; Spingarn, R.; Wang, T.-T.; Burger, M. C.; Dabbas, B.; Moitessier, N.; White, J. H.; Gleason, J. L., An *o*-aminoanilide. *J. Med. Chem.* **2010,** *53*, 7461-7465.

102. Nandhikonda, P.; Lynt, W. Z.; McCallum, M. M.; Ara, T.; Baranowski, A. M.; Yuan, N. Y.; Pearson, D.; Bikle, D. D.; Guy, R. K.; Arnold, L. A., Discovery of the first irreversible small molecule inhibitors of the interaction between the vitamin D receptor and coactivators. *J. Med. Chem.* **2012,** *55*, 4640-4651.

103. Toell, A.; Gonzalez, M. M.; Ruf, D.; Steinmeyer, A.; Ishizuka, S.; Carlberg, C., Different molecular mechanisms of vitamin D(3) receptor antagonists. *Mol Pharmacol* **2001,** *59*, 1478-85.

104. Herdick, M.; Steinmeyer, A.; Carlberg, C., Antagonistic action of a 25-carboxylic ester analogue of 1alpha, 25-dihydroxyvitamin D3 is mediated by a lack of ligand-induced vitamin D receptor interaction with coactivators. *J Biol Chem* **2000,** *275*, 16506-12.

105. Perakyla, M.; Molnar, F.; Carlberg, C., A structural basis for the species-specific antagonism of 26,23-lactones on vitamin D signaling. *Chem Biol* **2004,** *11*, 1147-56.

106. Zella, L. A.; Chang, C. Y.; McDonnell, D. P.; Pike, J. W., The vitamin D receptor interacts preferentially with DRIP205-like LxxLL motifs. *Archives of biochemistry and biophysics* **2007,** *460*, 206-12.

107. Yamaoka, K.; Kim, M. S.; Takada, I.; Takeyama, K.; Kamimura, T.; Kato, S., Culture serum-induced conversion from agonist to antagonist of a Vitamin D analog, TEI-9647. *J Steroid Biochem Mol Biol* **2006,** *100*, 177-83.

108. Sanchez-Martinez, R.; Zambrano, A.; Castillo, A. I.; Aranda, A., Vitamin D-dependent recruitment of corepressors to vitamin D/retinoid X receptor heterodimers. *Mol Cell Biol* **2008,** *28*, 3817-29.

109. van Driel, M.; Koedam, M.; Buurman, C. J.; Roelse, M.; Weyts, F.; Chiba, H.; Uitterlinden, A. G.; Pols, H. A. P.; van Leeuwen, J. P. T. M., Evidence that both 1 alpha,25-dihydroxyvitamin D-3 and 24-hydroxylated D-3 enhance human osteoblast differentiation and mineralization. *Journal of Cellular Biochemistry* **2006,** *99*, 922-935.

110. Kim, S.; Yamazaki, M.; Zella, L. A.; Shevde, N. K.; Pike, J. W., Activation of receptor activator of NF-kappa B ligand gene expression by 1,25-dihydroxyvitamin D-3 is mediated through multiple long-range enhancers. *Molecular and Cellular Biology* **2006,** *26*, 6469-6486.

111. Castillo, A. I.; Sanchez-Martinez, R.; Jimenez-Lara, A. M.; Steinmeyer, A.; Zugel, U.; Aranda, A., Characterization of vitamin D receptor ligands with cell-specific and dissociated activity. *Mol Endocrinol* **2006,** *20*, 3093-104.

112. Fujishima, T.; Kojima, Y.; Azumaya, I.; Kittaka, A.; Takayama, H., Design and synthesis of potent vitamin D receptor antagonists with A-ring modifications: remarkable effects of 2alpha-methyl introduction on antagonistic activity. *Bioorg Med Chem* **2003,** *11*, 3621-31.

113. Wang, X.; Wang, T. T.; White, J. H.; Studzinski, G. P., Expression of human kinase suppressor of Ras 2 (hKSR-2) gene in HL60 leukemia cells is directly upregulated by 1,25-dihydroxyvitamin D(3) and is required for optimal cell differentiation. *Exp Cell Res* **2007,** *313*, 3034-45.

114. Studzinski, G. P.; Wang, X. N.; Ji, Y.; Wang, Q.; Zhang, Y. Y.; Kutner, A.; Harrison, J. S., The rationale for deltanoids in therapy for myeloid leukemia: Role of KSR-MAPK-C/EBP pathway. *J Steroid Biochem* **2005,** *97*, 47-55.

115. Wang, X.; Wang, T. T.; White, J. H.; Studzinski, G. P., Induction of kinase suppressor of RAS-1(KSR-1) gene by 1, alpha25-dihydroxyvitamin D3 in human leukemia HL60 cells through a vitamin D response element in the 5'-flanking region. *Oncogene* **2006,** *25*, 7078-85.

116. Ji, Y.; Studzinski, G. P., Retinoblastoma protein and CCAAT/enhancer-binding protein beta are required for 1,25-dihydroxyvitamin D3-induced monocytic differentiation of HL60 cells. *Cancer Res* **2004,** *64*, 370-7.

117. Hughes, P. J.; Lee, J. S.; Reiner, N. E.; Brown, G., The vitamin D receptor-mediated activation of phosphatidylinositol 3-kinase (PI3K alpha) plays a role in the 1 alpha,25-dihydroxyvitamin D3-stimulated increase in steroid sulphatase activity in myeloid leukaemic cell lines. *Journal of Cellular Biochemistry* **2008,** *103*, 1551-1572.

118. Belkacemi, L.; Zuegel, U.; Steinmeyer, A.; Dion, J. P.; Lafond, J., Calbindin-D28k (CaBP28k) identification and regulation by 1,25-dihydroxyvitamin D3 in human choriocarcinoma cell line JEG-3. *Mol Cell Endocrinol* **2005,** *236*, 31-41.

119. Chang, C.; Norris, J. D.; Gron, H.; Paige, L. A.; Hamilton, P. T.; Kenan, D. J.; Fowlkes, D.; McDonnell, D. P., Dissection of the LXXLL nuclear receptor-coactivator interaction motif using combinatorial peptide libraries: discovery of peptide antagonists of estrogen receptors alpha and beta. *Mol Cell Biol* **1999,** *19*, 8226-39.

120. McDonnell, D. P.; Chang, C. Y.; Norris, J. D., Development of peptide antagonists that target estrogen receptor-cofactor interactions. *The Journal of steroid biochemistry and molecular biology* **2000,** *74*, 327-35.

121. Hall, J. M.; Chang, C. Y.; McDonnell, D. P., Development of peptide antagonists that target estrogen receptor beta-coactivator interactions. *Mol Endocrinol* **2000,** *14*, 2010-23.

122. Pathrose, P.; Barmina, O.; Chang, C. Y.; McDonnell, D. P.; Shevde, N. K.; Pike, J. W., Inhibition of 1,25-dihydroxyvitamin D3-dependent transcription by synthetic LXXLL peptide antagonists that target the activation domains of the vitamin D and retinoid X receptors. *Journal of bone and mineral research : the official journal of the American Society for Bone and Mineral Research* **2002,** *17*, 2196-205.

123. Caboni, L.; Lloyd, D. G., Beyond the ligand-binding pocket: targeting alternate sites in nuclear receptors. *Medicinal research reviews* **2013,** *33*, 1081-118.

124. Misawa, T.; Demizu, Y.; Kawamura, M.; Yamagata, N.; Kurihara, M., Structural development of stapled short helical peptides as vitamin D receptor (VDR)-coactivator interaction inhibitors. *Bioorganic & medicinal chemistry* **2015,** *23*, 1055-61.

125. Demizu, Y.; Nagoya, S.; Shirakawa, M.; Kawamura, M.; Yamagata, N.; Sato, Y.; Doi, M.; Kurihara, M., Development of stapled short helical peptides capable of inhibiting vitamin D receptor (VDR)-coactivator interactions. *Bioorg Med Chem Lett* **2013,** *23*, 4292-6.

126. Mita, Y.; Dodo, K.; Noguchi-Yachide, T.; Miyachi, H.; Makishima, M.; Hashimoto, Y.; Ishikawa, M., LXXLL peptide mimetics as inhibitors of the interaction of vitamin D receptor with coactivators. *Bioorg Med Chem Lett* **2010,** *20*, 1712-7.

127. Vanhooke, J. L.; Benning, M. M.; Bauer, C. B.; Pike, J. W.; DeLuca, H. F., Molecular structure of the rat vitamin D receptor ligand binding domain complexed with 2-carbon-substituted vitamin D3 hormone analogues and a LXXLL-containing coactivator peptide. *Biochemistry-Us* **2004,** *43*, 4101-10.

128. Mita, Y.; Dodo, K.; Noguchi-Yachide, T.; Hashimoto, Y.; Ishikawa, M., Structure-activity relationship of benzodiazepine derivatives as LXXLL peptide mimetics that inhibit the interaction of vitamin D receptor with coactivators. *Bioorg Med Chem* **2013,** *21*, 993-1005.

129. Nandhikonda, P.; Lynt, W. Z.; McCallum, M. M.; Ara, T.; Baranowski, A. M.; Yuan, N. Y.; Pearson, D.; Bikle, D. D.; Guy, R. K.; Arnold, L. A., Discovery of the first irreversible small molecule inhibitors of the interaction between the vitamin D receptor and coactivators. *J Med Chem* **2012,** *55*, 4640-51.

130. Han, A.; Sidhu, P. S.; Chen, E.; Hill, E. K.; Horan, T. C.; Nandhikonda, P.; Teske, K.; Yuan, N. Y.; Guthrie, M. L.; Sidorko, M.; Kodali, R.; Cook, J. M.; Han, L.; Silvaggi, N. R.; Bikle, D. D.; Moore, R. G.; Singh, R. K.; Arnold, L. A., Anti-tumor activity of vitamin D receptor coregulator inhibitor 31B in ovarian cancer. *accepted* **2015**.

131. Sidhu, P. S.; Nassif, N.; McCallum, M. M.; Teske, K.; Feleke, B.; Yuan, N. Y.; Nandhikonda, P.; Cook, J. M.; Singh, R. K.; Bikle, D. D.; Arnold, L. A., Development of novel Vitamin D Receptor-Coactivator Inhibitors. *Acs Med Chem Lett* **2014,** *5*, 199-204.

132. Sidhu, P. S.; Teske, K.; Feleke, B.; Yuan, N. Y.; Guthrie, M. L.; Fernstrum, G. B.; Vyas, N. D.; Han, L.; Preston, J.; Bogart, J. W.; Silvaggi, N. R.; Cook, J. M.; Singh, R. K.; Bikle, D. D.; Arnold, L. A., Anticancer activity of VDR-coregulator inhibitor PS121912. *Cancer Chemother Pharmacol* **2014,** *74*, 787-98.

133. Dunn, I. S., Searching for Molecule Solutions: Empirical Discovery and Its Future. In *An Empirical-Rational Loop Forwards*, John Wiley & Sons, Inc.: 2009; pp 315-342.

134. Wang, W.; Joyner, S.; Khoury, K. A. S.; Domling, A., (-)-Bacillamide C: the convergent approach. *Organic & Biomolecular Chemistry* **2009,** *8*, 529-532.

135. Ganem, B., Strategies for Innovation in Multicomponent Reaction Design. *Accounts of Chemical Research* **2009,** *42*, 463-472.

136. Strecker, A., *Liebigs Ann. Chem.* **1850,** *75*, 27.

137. Ivachtchenko, A. V.; Ivanenkov, Y. A.; Kysil, V. M.; Krasavin, M. Y.; Ilyin, A. P., Multicomponent Reactions of Isocyanides in the Synthesis of Heterocycles. *Russian Chemical Reviews* **2010,** *79*, 787-817.

138. Ugi, I., Recent Progress in the Chemistry of Multicomponent Reactions. *Pure Appl. Chem.* **2001,** *73*, 187-191.

139. Ugi, I.; Werner, B.; Domling, A., The Chemistry of Isocyanides, their Multicomponent Reactions and their Library. *Molecules* **2003,** *8*, 53-66.

140. Katzung, B. G.; Masters, S. B.; Trevor, A. J., *Basic and Clinical Pharmacology*. The McGraw-Hill Companies, Inc: 2009.

141. Boehm, M. F.; Fitzgerald, P.; Zuo, A.; Elgort, M. G.; Bischoff, E. D.; Mere, L.; Mais, D. E.; Bissonnette, R. P.; Heyman, R. A.; Nadzan, A. M.; Reichman, M.; Allegretto, E. A., Novel non-secosteroidal vitamin D mimics exert VDR-modulating activities with less calcium moibilization than 1,25-dihydroxyvitamin D_3. *Chemistry & biology* **1999,** *6*, 265-275.

142. Hakamata, W.; Sato, Y.; Okuda, H.; Honzawa, S.; Saito, N.; Kishimoto, S.; Yamashita, A.; Sugiura, T.; Kittaska, A.; Kurihara, M., (2,S,1'R)-Analogue of LG190178 is a major active isomer. *Bioorg Med Chem Letters* **2008,** *18*, 120-123.

143. Arnold, L. A.; Kosinski, A.; Estebanez-Perpina, E.; Fletterick, R. J.; Guy, R. K., Inhibitors of the interaction of a thyroid hormone receptor and coactivators: preliminary structure-activity relationships. *J Med Chem* **2007,** *50*, 5269-80.

144. Noah, J. W., New Developments and Emerging Trends in High-Throughput Screening Methods for Lead Compound Identification. *Int. J. of HTS* **2010,** *1*, 141-149.

145. Macarron, R., Critical Review of the Role of HTS in Drug Discovery. *Drug Discovery Today* **2006,** *11*.

146. Fox, S.; Farr-Jones, S.; Sopchak, L.; Boggs, A.; Comley, J., High-Throughput Screening: Searching for High Productivity. *Journal of Biomolecular Screening* **2004,** *9*.

147. Valler, M. J.; Green, D., Diversity Screening Versus Focused Screening in Drug Discovery. *DDT* **2000,** *5*.

148. Lipinski, C. A.; Lombardo, F.; Dominy, B. W.; Feeney, P. J., Experimental and Computational Approaches to Estimate Solubility and Permeabillity in Drug Discovery and Development Settings. *Advanced Drug Delivery Reviews* **2001,** *46*, 3-26.

149. Hertzberg, R. P.; Pope, A. J., High-Throughput Screening: a New Technology of the 21st Century. *Current Opinion in Cell Biology* **2000,** *4*, 445-451.

150. Nandikonda, P.; Yasgar, A.; Barnowski, A. M.; Sidhu, P. S.; McCallum, M. M.; Pawlak, A. J.; Teske, K.; Feleke, B.; Yuan, N. Y.; Kevin, C.; Bikle, D. D.; Ayers, S. D.; Webb, P.; Rai, G.; Simeonov, A.; Jadhav, A.; Maloney, D.; Arnold, L. A., Peroxisome Proliferation-Activated Receptor δ Agonist GW0742 Interacts

Weakly with Multiple Nuclear Receptors, Including the Vitamin D Receptor. *Biochemistry* **2013,** *52*, 4193-4203.

151. Sznaidman, M. L.; Haffner, C. D.; Maloney, P.; Fivush, A.; Chao, E.; Goreham, D.; Sierra, M.; LeGrumellec, C.; Xu, H. E.; Montana, V. G.; Lambert, M. H.; Wilson, T. M.; William R. Oliver, J.; Sternbach, D. D., Novel Selective Small Molecule Agonists for Peroxisome Proliferator-Activated Receptor δ (PPARδ)-Synthesis and Biological Activity. *Bioorganic & Medicinal Chemistry Letters* **2003,** *13*, 1517-1521.

152. Nandhikonda, P.; Yasgar, A.; Baranowski, A. M.; Sidhu, P. S.; McCallum, M. M.; Pawlak, A. J.; Teske, K.; Feleke, B.; Yuan, N. Y.; Kevin, C.; Bikle, D. D.; Ayers, S. D.; Webb, P.; Rai, G.; Simeonov, A.; Jadhav, A.; Maloney, D.; Arnold, L. A., Peroxisome proliferation-activated receptor delta agonist GW0742 interacts weakly with multiple nuclear receptors, including the vitamin D receptor. *Biochemistry* **2013,** *52*, 4193-203.

153. Boehm, M. F.; Fitzgerald, P.; Zou, A.; Elgort, M. G.; Bischoff, E. D.; Mere, L.; Mais, D. E.; Bissonnette, R. P.; Heyman, R. A.; Nadzan, A. M.; Reichman, M.; Allegretto, E. A., Novel nonsecosteroidal vitamin D mimics exert VDR-modulating activities with less calcium mobilization than 1,25-dihydroxyvitamin D3. *Chem Biol* **1999,** *6*, 265-75.

154. Keil, S.; Urmann, M.; Bernardelli, P.; Glein, M.; Wendler, W.; Chandross, K. Phenyl-1,2,4-oxadiazolone derivatives, processes for their preparation and their use and pharmaceuticals. 2007.

155. Moon, H.-S.; Yoo, M.-H.; Kim, S.-H.; Lim, J.-I. Novel Phenylpropionic Acid Derivatives as Peroxisome Proliferator-Activated Gamma Receptor Modulators, Method of the Same, and Pharmaceutical Composition Comprising the Same. 2008.

156. *Microwave Assisted Organic Synthesis*. Blackwell Publishing: Oxford, 2005; p 280.

157. Nandhikonda, P.; Lynt, W. Z.; McCallum, M. M.; Ara, T.; Baranowski, A. M.; Yuan, N. Y.; Pearson, D.; Bikle, D. D.; Guy, R. K.; Arnold, L. A., Discovery of the First Irreversible Small Molecule Inhibitors of the Interaction between the Vitamin D Receptor and Coactivators. *J Med Chem* **2012,** *55*, 4640-4651.

158. Sznaidman, M. L.; Haffner, C. D.; Maloney, P. R.; Fivush, A.; Chao, E.; Goreham, D.; Sierra, M. L.; LeGrumelec, C.; Xu, H. E.; Montana, V. G.; Lambert, M. H.; Willson, T. M.; William R. Oliver, J.; Sternbach, D. D., Novel Selective Small Molecule Agonists for Peroxisome Proliferator-Activated Receptor δ (PPARδ)-Synthesis and Biological Activity. *Bioroganic & Medicinal Chemistry Letters* **2003,** *13*, 1517-1521.

159. Desroy, N.; Moreau, F.; Briet, S.; Fralliec, G. L.; Floquet, S.; Durant, L.; Vongsouthi, V.; Gerusz, V.; Denis, A.; Escaich, S., Towards Gram-negative Antivirulence Drugs: New Inhibitors of HldE Kinase. *Bioroganic & Medicinal Chemistry* **2008,** *17*, 1276-1289.

160. Nagaya, A.; Yamagishi, Y.; Yonezawa, Y.; Akai, S.; Shin, C.-g.; Sato, K.-i., Scope and Limitations of a Modified Hantzch Reaction for the Synthesis of Oxazole-Dehydroamino Acid Derivatives from Dehydroamino Acid Amides. *Heterocycles* **2012,** *85*, 313-331.

161. Alsenz, J.; Kansey, M., High Throughput Solubility Measurement in Drug Discovery and Development. *Advanced Drug Delivery Reviews* **2007,** *59*, 546-567.

162. Loftsson, T., Aqueous Solubility and True Solutions. *Pharmazie* **2010,** *65*.

163. Waterbeemd, H. v. d.; Lennernas, H.; Artursson, P., *Drug Bioavailability: Methods and Principles in Medicinal Chemistry*. Wiley - VCH: Germany, 2003; Vol. 18.

164. Kerns, E., *Drug-like Properties: Concepts, Structure Design and Methods, 1st Edition*. Academic Press, 2008.

165. Alsenz, J.; Kansy, M., High throughput solubility measurement in drug discovery and development. *Advanced Drug Delivery Reviews* **2007,** *59*, 546-567.

166. Fortuna, A.; Alves, G.; Soares-Da-Silva, P.; Falcao, A., Optimization of a parallel artificial membrane permeability assay for the fast and simulateous predication of human intestinal absorption and plasma protein binding of drug candidates: application to dibenz[b,f]azepine-5-carboxamide derivatives. *Journal of Pharmaceutical Sciences* **2011,** *101*.

167. Kerns, E. H.; Di, L.; Petusky, S.; Farris, M.; Ley, R.; Jupp, P., Combined Application of Parallel Artificial Membran Permeability Assay and Caco-2 Permeability Assays in Drug Discovery. *Journal of Pharmaceutical Sciences* **2004,** *93*.

168. Winiwarter, S.; Bonham, N. M.; Ax, F.; Hallberg, A.; Lennernas, H.; Karlen, A., Correlation of Human Jejunal Permeability (in Vivo) of Drugs with Experimentally and Theoretically Derived Parameters. A Multivariate Data Analysis Approach. *Journal of Medicinal Chemistry* **1998,** *41*, 4939-4949.

169. Wohnsland, F.; Faller, B., High Throughput Permeability pH Profile and High Throughput Alkane/water Log P with Artificial Membranes. *J. Med. Chem.* **2001,** *44*, 923-930.

170. Gad, S. C., *Preclinical Development Handbook: ADME and Biopharmaceutical Properties*. Wiley-Interscience: 2008.

171. Schmidt, D.; Lynch, J. *MultiScreen Filter Plates for PAMPA and Permeability Assays: Data review and optimization of PAMPA and permeability assays*; Millipore Corporation: Billerica, MA, 2003.

172. Omdahl, J. L.; Morris, H. A.; Morris, B. K., Hydroxylase enzymes of the vitamin D pathway: expression, function and regulation. *Annu. Rev. Nutr.* **2002,** *22*, 139-166.

173. Tanaka, Y.; Castillo, L.; Deluca, H. F., The 24-hydroxylation of 1,25-dihydroxyvitamin D_3. *J. Biol. Chem* **1977,** *252*, 1421-1424.

174. Sakaki, T.; Sawada, N.; Komai, K.; Shiozawa, S.; Yamada, S.; Yamamoto, K.; Ohyama, Y.; Inouye, K., Dual metabolic pathway of 25-hydroxyvitamin D_3 catalyzed by human CYP24. *Eur. J. Biochem.* **2000,** *267*, 6158-6165.

175. Napoli, J. L.; Horst, R. L., C(24) and C(23)-oxidation, converging pathways of intestinal 1,25-dihydroxyvitamin D3 metabolism: identifcation of 24-keto-1,23,25-trihydroxyvitamin D3. *Biochemistry* **1983,** *22*, 5848-5853.

176. Takasaki, Y.; Yamada, S.; Takayama, H.; Nishii, Y., Isolation, identification, and biological acitivity of 25-dihydroxy-24-oxovitamin D3: a new metabolite of vitamin D3 generated by in vitro incubations with kidney homogenates. *Biochemistry* **1981,** *20*.

177. Esvelt, R. P.; Schnoes, H. K.; DeLuca, H. F., Isolation and characterization of 1 alpha-hydroxy-23-carboxytetranorvitamin D: a major metabolite of 1,25-dihydroxyvitamin D3. *Biochemistry* **1979,** *18*, 3977-3983.

178. Makin, G.; Lohnes, D.; Byford, V.; Ray, R.; Jones, G., Target cell metabolism of 1,25-dihydroxyvitamin D3 to calcitroic acid. Evidence for a pathway in kidney bone involving 24-oxidation. *Biochem. J.* **1989,** *262*, 173-180.

179. Reddy, G. S.; Tserng, K. Y., Calcitroic acid, end product of renal metablism of 1,25-dihydroxyvitamin D3 through C-24 oxidation pathway. *Biochemistry* **1989,** *28*, 1763-1769.

180. Masuda, S.; Strugnell, S.; Calverley, M. J.; Makin, H. L.; Kremer, R.; Jones, G., In vitro metabolism of the anti-psoriatic vitamin D analog, calcipotriol, in two cultured human keratinocyte models. *J. Biol. Chem* **1994,** *269*, 4794-4803.

181. Tomon, M.; Tenenhouse, H. S.; Jones, G., Expression of 25-hydroxyvitamin D3-24-hydroxylase activity in Caco-2 cells. An in vitro model of intestinal vitamin D catabolism. *Endocrinology* **1990,** *126*, 2868-2875.

182. Reinhardt, T. A.; Horst, R. L., Self-induction of 1,25-dihydroxyvitamin D3 metabolism limits receptor occupancy and target tissue responsiveness. *J. Biol. Chem.* **1989,** *264*, 15917-15921.

183. Reinhardt, T. A.; Horst, R. L., Ketoconazole inhibits self-induced metabolism of 1,25-dihydroxyvitamin D3 and amplifies 1,25-dihydroxyvitamin D3 receptor up-regulation in rat osteosarcoma cells. *Arch. Biochem. Biophys.* **1989,** *272*, 459-465.

184. St-Arnaud, R.; Arabian, A.; Travers, R.; Barletta, F.; Raval-Pandya, M.; Chapin, K.; al., e., Deficient mineralization of intramembranous bone in vitamin D-24-hydroxylase-ablated mice is due to elevated 1,25-dihydroxyvitamin D and not to the absence of 24,25-dihydroxyvitamin D. *Endocrinology* **2000,** *141*, 2658-2666.

185. Endres, B.; Kato, S.; DeLuca, H. F., Metabolism of 1alpha,25-dihydroxyvitamin D3 in vitamin D receptor-ablated mice in vivo. *Biochemistry* **2000,** *39*, 2123-2129.

186. Masuda, S.; Byford, V.; Arabian, A.; Sakai, Y.; Demay, M. B.; St-Arnaud, R.; al, e., Altered pharacokinetics of 1alpha,25-dihydroxyvitamin D3 and 25-hydroxyvitamin D3 in the blood and tissues of the 25-hydroxyvitamin D-24-hydroxylase (CYP24A1) null mouse. *Endocrinology* **2005,** *146*, 825-834.

187. Ohnuma, N.; Norman, A. W., Identification of a new C-23 oxidation pathway of metabolism for 1,25-dihydroxyvitamin D3 present in intestine and kidney. *J. Biol. Chem* **1982,** *257*, 8261-8271.

188. Toell, A.; Gonzalez, M. M.; Ruf, D.; Steinmeyer, A.; Ishizuka, S.; Carlberg, C., Different molecular mechanisms of vitamin D3 receptor antagonists. *Mol. Pharmacol* **2001,** *59*, 1478-1485.

189. Miura, D.; Manabe, K.; Ozono, K.; Saito, M.; Gao, Q.; Norman, A. W.; Ishizuka, S., Antagonistic action of novel 1alpha,25-dihydroxyvitamin D3-26, 23-lactone analogs on differentiation of human leukemia cells (HL-60) induced by 1alpha,25-dihydroxyvitamin D3. *J Biol Chem* **1999,** *274*, 16392-9.

190. Russell, D. W., The enzymes, regulation and genetics of bile acid synthesis. *Annual Review of Biochemistry* **2003,** *72*, 137-174.

191. Ridlon, J. M.; Kang, D.-J.; Hylemon, P. B., Bile salt biotransformations by human intestinal bacteria. *J. Lipid Res.* **2006,** *47*, 241-259.

192. Chiang, J. Y., Bile Acids: regulation of synthesis. *J. Lipid Res.* **2009,** *undefined*.

193. Inagaki, T.; Choi, M.; Moschetta, A.; Peng, L.; Cummins, C. L.; McDonald, J. G.; al, e., Fibroblast growth factor 15 functions as an enterohepatic signal to regulate bile acid homeostasis. *Cell Metab* **2005,** *2*, 217-225.

194. Schmidt, D. R.; Holmstrom, S. R.; Fon, K. T.; Bookout, A. L.; Kliewer, S. A.; Mangelsdorf, D. J., Regulation of bile acid synthesis by fat-soluble vitamins A and D. *J. Biol. Chem* **2010,** *285*, 14486-14494.

195. Nehring, J. A.; Zierold, C.; Deluca, H. F., Lithocholic acid can carry out *in vivo* functions of vitamin D. *Proc Natl Acad Sci* **2007,** *104*, 10006-10009.

196. Belorusova, A. Y.; Eberhardt, J.; Potier, N.; Stote, R. H.; Dejaegere, A.; Rochel, N., Structural insights into the molecular mechanisms of vitamin D receptor activation by lithocholic acid involving a new mode of ligand recognition. *J. Med. Chem.* **2014,** *57*, 4710-4719.

197. Ishizawa, M.; Matsunawa, M.; Adachi, R.; Uno, S.; Makishima, M.; al, e., Lithocholic acid derivatives act as selective vitamin D receptor modulators without inducing hypercalcemia. *J. Lipid Res.* **2008,** *49*, 763-772.

198. Adachi, R.; Homna, Y.; Masuno, H.; Kawana, K.; Shimomura, I.; Yamada, S.; Makishima, M., Selective activation of vitamin D receptor by lithocholic acid acetate, a bile acid derivative. *J. Lipid Res.* **2005,** *46*, 46-57.

199. Petrova, N. S.; Chernikov, I. V.; Meschaninova, M. I.; Dovydenko, I. S.; Aliya G, V.; Zenkova, M. A.; Vlassov, V. V.; Chernolovskaya, E. L., Carrier-free cellular uptake and the gene-silending activity of the lipophilic siRNAs is strongly affected by the length of the linker between siRNA and lippphilic group. *Nucleic Acids Research* **2012,** *40*, 2330-2344.

200. Bureeva, S.; Andia-Pravdivy, J.; Symon, A.; Bichucher, A.; Moskaleva, V.; Popenko, V.; Shpak, A.; Shvets, V.; Kozlov, L.; Kaplun, A., Selective inhibition of the interaction of C1q with immunoglobulins and the classical pathway of complement activation by steroid and triterpenoids sulfates. *Bioorganic & medicinal chemistry* **2007,** *15*, 2489-2498.

201. Sobel, A. E.; Spoerri, P. E., Steryl Sulfates. I. Preparation and Properties. *J. Am. Chem. Soc.* **1941,** *63*, 1259-1261.

202. Iida, T.; Tazawa, S.; Ohshima, Y.; Niwa, T.; Goto, J.; Nambara, T., Analysis of conjugated bile acids in human biological fluids. Synthesis of hyodeoxycholic acid 3- and 6-glycosides and related compounds. *Chem. Pharm. Bull* **1994,** *42*, 1479-1484.

203. Ranade, S. C.; Demchenko, A. V., Mechanism of chemical glycosylation: focus on the mode of activation and departure of anomeric leaving groups. *Journal of Carbohydrate Chemistry* **2013,** *32*, 1-43.

204. Isbell, H. S.; Frush, H. L., Mechanisms for the formation of acetylglycosides and othoestes from acetylglycosyl halides. *Journal of Research of the National Bureau of Standards* **1949,** *43*, 161-171.

205. Carey, F. A.; Sundberg, R. J., *Advanced Organic Chemistry Part A: Structure and Mechanisms, 5th Edition*. Springer: New York City, 2007.

206. Wuts, P. G. M.; Greene, T. W., *Greene's Protective Groups in Organic Synthesis*. John Wiley & Sons, Inc.: Hoboken, New Jersey, 2007.

207. Becker, B.; Barua, A. B.; Olsen, J. A., All-trans-retinoyl B-glucuronide: new procedure for chemical synthesis and its metabolism in vitamin A-deficient rats. *Biochem J.* **1996,** *314*, 249-252.

208. Adachi, R.; Shulman, A. I.; Yamamoto, K.; Shimomura, I.; Yamada, S.; Mangelsdorf, D. J.; Makishima, M., Structural determinants for vitamin D receptor response to endocrine and xenobiotic signals. *Mol Endocrinol* **2004,** *18*, 43-52.

209. Alberts, B.; Johnson, A.; Lewis, J.; Raff, M.; Roberts, K.; Walter, P., *Molecular Biology of The Cell, 4th Ed.* 2002.

210. http://www.genome.duke.edu/cores/microarray/services/rna-qc/documents/RNeasy_Mini_Handbook.pdf

211. Posner, G. H.; Crawford, K. R.; Yang, H. K.; al., e., Potent, low calcemin, selective inhibitors of CYP24 hydroxylase: 24-sulfone analogs of the hormone 1alpha,25-dihydroxyvitamin D3. *J. Steroid Biochem. Mol. Biol* **2004,** *89*, 5-12.

212. Schuster, I.; Egger, H.; Astecker, N.; Herzig, G.; Schussler, M.; Vorisek, G., Selective inhibitors of CYP24: mechanistic tools to explore vitamin D metabolism in human keratinocytes. *Steroids* **2001,** *66*, 451-462.

213. Overington, J. P.; Al-Lazikani, B.; Hopkins, A. L., How many drug targets are there? *Nat Rev Drug Discov* **2006,** *5*, 993-6.

214. Kuiper, G. G.; Carlsson, B.; Grandien, K.; Enmark, E.; Haggblad, J.; Nilsson, S.; Gustafsson, J. A., Comparison of the ligand binding specificity and transcript tissue distribution of estrogen receptors alpha and beta. *Endocrinology* **1997,** *138*, 863-70.

215. Escriva, H.; Safi, R.; Hanni, C.; Langlois, M. C.; Saumitou-Laprade, P.; Stehelin, D.; Capron, A.; Pierce, R.; Laudet, V., Ligand binding was acquired during evolution of nuclear receptors. *Proc Natl Acad Sci U S A* **1997,** *94*, 6803-8.

216. Garcia-Vallve, S.; Palau, J., Nuclear receptors, nuclear-receptor factors, and nuclear-receptor-like orphans form a large paralog cluster in Homo sapiens. *Mol Biol Evol* **1998,** *15*, 665-82.

217. Schapira, M.; Abagyan, R.; Totrov, M., Nuclear hormone receptor targeted virtual screening. *J Med Chem* **2003,** *46*, 3045-59.

218. Rochel, N.; Wurtz, J. M.; Mitschler, A.; Klaholz, B.; Moras, D., The crystal structure of the nuclear receptor for vitamin D bound to its natural ligand. *Mol Cell* **2000,** *5*, 173-9.

219. Teichert, A.; Arnold, L. A.; Otieno, S.; Oda, Y.; Augustinaite, I.; Geistlinger, T. R.; Kriwacki, R. W.; Guy, R. K.; Bikle, D. D., Quantification of the vitamin D receptor-coregulator interaction. *Biochemistry* **2009,** *48*, 1454-61.

220. http://www.bindingdb.org/bind/index.jsp.

221. Michellys, P. Y.; Boehm, M. F.; Chen, J. H.; Grese, T. A.; Karanewsky, D. S.; Leibowitz, M. D.; Liu, S.; Mais, D. A.; Mapes, C. M.; Reifel-Miller, A.; Ogilvie, K. M.; Rungta, D.; Thompson, A. W.; Tyhonas, J. S.; Yumibe, N.; Ardecky, R. J., Design and synthesis of novel RXR-selective modulators with improved pharmacological profile. *Bioorg Med Chem Lett* **2003,** *13*, 4071-5.

222. Burris, T. P.; Montrose, C.; Houck, K. A.; Osborne, H. E.; Bocchinfuso, W. P.; Yaden, B. C.; Cheng, C. C.; Zink, R. W.; Barr, R. J.; Hepler, C. D.; Krishnan, V.; Bullock, H. A.; Burris, L. L.; Galvin, R. J.; Bramlett, K.; Stayrook, K. R., The hypolipidemic natural product guggulsterone is a promiscuous steroid receptor ligand. *Mol Pharmacol* **2005,** *67*, 948-54.

223. Owsley, E.; Chiang, J. Y., Guggulsterone antagonizes farnesoid X receptor induction of bile salt export pump but activates pregnane X receptor to inhibit cholesterol 7alpha-hydroxylase gene. *Biochem Biophys Res Commun* **2003,** *304*, 191-5.

224. von Geldern, T. W.; Tu, N.; Kym, P. R.; Link, J. T.; Jae, H. S.; Lai, C.; Apelqvist, T.; Rhonnstad, P.; Hagberg, L.; Koehler, K.; Grynfarb, M.; Goos-Nilsson, A.; Sandberg, J.; Osterlund, M.; Barkhem, T.; Hoglund, M.; Wang, J.; Fung, S.; Wilcox, D.; Nguyen, P.; Jakob, C.; Hutchins, C.; Farnegardh, M.; Kauppi, B.; Ohman, L.; Jacobson, P. B., Liver-selective glucocorticoid antagonists: a novel treatment for type 2 diabetes. *J Med Chem* **2004,** *47*, 4213-30.

225. Sznaidman, M. L.; Haffner, C. D.; Maloney, P. R.; Fivush, A.; Chao, E.; Goreham, D.; Sierra, M. L.; LeGrumelec, C.; Xu, H. E.; Montana, V. G.; Lambert, M. H.; Willson, T. M.; Oliver, W. R., Jr.; Sternbach, D. D., Novel selective small molecule agonists for peroxisome proliferator-activated receptor delta (PPARdelta)--synthesis and biological activity. *Bioorg Med Chem Lett* **2003,** *13*, 1517-21.

226. Holick, M. F.; Schnoes, H. K.; DeLuca, H. F.; Suda, T.; Cousins, R. J., Isolation and identification of 1,25-dihydroxycholecalciferol. A metabolite of vitamin D active in intestine. *Biochemistry* **1971,** *10*, 2799-804.

227. Norman, A. W., Evidence for a new kidney-produced hormone, 1,25-dihydroxycholecalciferol, the proposed biologically active form of vitamin D. *Am J Clin Nutr* **1971,** *24*, 1346-51.

228. Barycki, R.; Sicinski, R. R.; Plum, L. A.; Grzywacz, P.; Clagett-Dame, M.; Deluca, H. F., Removal of the 20-methyl group from 2-methylene-19-nor-(20S)-1alpha,25-dihydroxyvitamin D(3) (2MD) selectively eliminates bone calcium mobilization activity. *Bioorg Med Chem* **2009,** *17*, 7658-69.

229. Lu, J. M.; Nurko, J.; Weakley, S. M.; Jiang, J.; Kougias, P.; Lin, P. H.; Yao, Q.; Chen, C., Molecular mechanisms and clinical applications of nordihydroguaiaretic acid (NDGA) and its derivatives: an update. *Med Sci Monit* **2010,** *16*, RA93-100.

230. Lack, N. A.; Axerio-Cilies, P.; Tavassoli, P.; Han, F. Q.; Chan, K. H.; Feau, C.; LeBlanc, E.; Guns, E. T.; Guy, R. K.; Rennie, P. S.; Cherkasov, A., Targeting the binding function 3 (BF3) site of the human androgen receptor through virtual screening. *J Med Chem* **2011,** *54*, 8563-73.

231. Sicinski, R. R.; Prahl, J. M.; Smith, C. M.; DeLuca, H. F., New 1alpha,25-dihydroxy-19-norvitamin D3 compounds of high biological activity: synthesis and biological evaluation of 2-hydroxymethyl, 2-methyl, and 2-methylene analogues. *J Med Chem* **1998,** *41*, 4662-74.

232. Inaba, Y.; Yoshimoto, N.; Sakamaki, Y.; Nakabayashi, M.; Ikura, T.; Tamamura, H.; Ito, N.; Shimizu, M.; Yamamoto, K., A new class of vitamin D analogues that induce structural rearrangement of the ligand-binding pocket of the receptor. *J Med Chem* **2009,** *52*, 1438-49.

233. Bourne, H. R.; Sanders, D. A.; McCormick, F., The GTPase superfamily: a conserved switchfor the diverse cell functions. *Nature* **1990,** *348*.

234. Cherfils, J.; Zeghouf, M., Regulation of Small GTPases by GEFs, GAPs and GDIs. *Physiol Rev* **2012,** *93*, 269-309.

235. Hong, L.; Sklar, L. A., Targeting GTPases in Parkinson's Disease: Comparison to the historic path of kinase drug discovery and perspectives. *Molecular Neuroscience* **2014,** *7*.

236. Peng, F.; Wu, D.; Gao, B.; Ingram, A. J.; Zhang, B.; Chorneyko, K.; McKenzie, R.; Krepinsky, J. C., RhoA/Rho-Kinase Contribute to the Pathogenesis of Diabetic Renal Disease. *Diabetes* **2008,** *57*.

237. Prior, I. A.; Lewis, P. D.; Mattos, C., A Comprehensive Survey of Ras Mutations in Cancer. *Cancer Research* **2012,** *72*, 2457-67.

238. Cox, A. D.; Der, C. J., Ras History: The Saga Continues. *J. Der.* **2010,** *1*, 2-27.

239. Sem, D. S. Methods for detecting ditho-containing proteins using quenched fluorphores conjugated to peptides via linker containing dithio groups. 2015.

240. Sem, D. S.; Pullela, P. K. Dithio Compounds. 2010.

241. Chiku, T.; Pullela, P. K.; Sem, D. S., A Dithio-Couled Kiase and ATPase Assay. *Journal of Biomolecular Screening* **2006,** *11*, 844.

242. Strenkowska, M.; Wanat, P.; Ziemniak, M.; Jemielity, J.; Kowlask, J., Preparation of Synthetically Challenging Nucleotides Using Cyanoethyl P-Imidazolides and Microwaves. *Organic Letters* **2012,** *14*, 4782-4785.

243. Kowalska, J.; Lukaszewicz, M.; Zuberek, J.; Darzynkiewicz, E.; Jemielity, J., Phosphoroselenoate Dinucleotides for Modification of mRNA 5' End. *ChemBioChem* **2009,** *10*.

244. Michaud, C. F. C., Defining Ion Exchange Capacity. *Water Conditioning & Purification* **2011**.

245. Dechow, F. J., Separation and Purification Techniques in Biotechnology. In Noyes Publications: 1989.

246. Bouffard, J.; Kim, Y.; Swager, T. M.; Weissleder, R.; Hilderbrand, S. A., A Highly Selective Fluorescent Probe for Thiol Bioimaging. *Organic Letters* **2008,** *10*, 37-40.

247. Maeda, H.; Matsuno, H.; Ushida, M.; Katayama, K.; Saeki, K.; Itoh, N., 2,4-Dinitrobenzenesulfonyl Fluoresceins as Fluorescent Alternatives to Ellman's Reagent in Thiol-Quantification Enzyme Assays. *Angew. Chem., Int. Ed.* **2005,** *44*, 2922-2925.

248. Sweeney, N. L.; Hanson, A. M.; Mukherjee, S.; Ndjomou, J.; Geiss, B. J.; Steel, J. J.; Frankowski, K. J.; Li, K.; Schoenen, F. J.; Frick, D. N., Benzothiazole and Pyrrolone Flavivirus Inhibitors Targeting the Viral Helicase. *ACS Infect. Dis* **2015**, 140-148.

APPENDIX A: VDR BINDING AND TRANSCRIPTION DATA FOR GW0742 ANALOGS

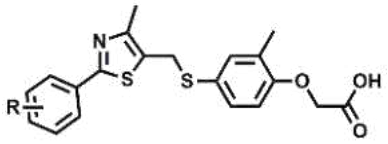

Table 29. Evaluation of mono-substituted GW0742 analogs

Entry	R	VDR-SRC2-3 interaction IC_{50} (μM)[a]	VDR transcription IC_{50} (μM)[b]
NCGC00319174-01	H	16.95± 1.64	41.5± 11.9
NCGC00319046-01	*o*-CH_3	43.88± 8.54	19.2 ± 5.6
NCGC00319053-01	*m*-CH_3	47.45± 6.61	38.2± 8.6
NCGC00319065-01	*p*-CH_3	37.52± 6.12	42.0± 11.1
NCGC00319061-01	*o*-Cl	32.27± 3.19	28.9± 5.0
NCGC00319050-01	*m*-Cl	24.10± 3.39	19.4 ± 8.5
NCGC00319056-01	*p*-Cl	29.72± 2.28	17.5± 5.7
NCGC00319063-01	*o*-F	35.53± 4.46	40.0± 8.5
NCGC00319048-01	*m*-F	42.68± 5.14	28.3± 7.1
NCGC00319055-01	*p*- F	45.61± 3.87	16.8± 4.64
NCGC00319064-01	*o*-CF_3	32.27± 5.28	31.5± 9.1
NCGC00319049-01	*m*-CF_3	24.5± 2.27	19.0± 6.01
NCGC00241455-04 (GW501516)	*p*-CF_3	22.92± 2.08	16.0 ± 3.6
NCGC00319047-01	*o*-OCH_3	45.18± 5.65	31.4± 8.1
NCGC00319052-01	*m*-OCH_3	48.82± 6.56	26.3± 6.9
NCGC00319051-01	*m*-OCF_3	13.86± 1.0	24.5± 8.6
NCGC00319058-01	*p*-OCF_3	15.63± 0.94	27.9± 7.4
NCGC00319036-01	*m*- CN	>100	25.1± 10.0
NCGC00319057-01	*p*-CN	>100	>50
NCGC00319069-01	*p*- $N(CH_3)_2$	>100	24.5 ± 6.1
NCGC00319067-01	*p*-$NHCH_3$	12.22± 1.93	16.0 ± 7.1
NCGC00319066-01	*p*- $COOCH_2CH_3$	19.52± 1.20	17.6± 10.9
NCGC00319054-01	*m*-methylsulfinyl	>100	>100
NCGC00319070-01	*p*-methanesulfonamide	>100	Inactive
NCGC00319071-01	*p*-$NHCOCH_3$	40.11± 9.26	inactive
NCGC00319151-01	*m*-$CONH(CH_2)_3N(CH_3)_2$	30.28± 4.5	inactive
NCGC00319150-01	*p*-$CONH(CH_2)_2N(CH_3)_2$	52.03± 12.79	>100
NCGC00319169-01	*p*-(4-methylpiperazinyl) methanone	>100	inactive
NCGC00319072-01	*p*-piperazinyl	>100	inactive
NCGC00319068-01	Morpholino-methanone	>100	>100

[a]VDR-LBD concentration used was 0.1μM. Inhibition of VDR-SRC2-3 interaction in the presence of LG190178 (0.75 μM). The maximum concentration used for this assay was 300 μM of each compound; [b]Transcription assay using a CMV-VDR plasmid and a luciferase reporter plasmid under control of a 24-hydroxylase promoter with GW0742 analogs. [c]Cell-TiterGlo (Promega) The maximum concentration used for transcription and toxcitiy assay was 100 μM of each compound. Data were analyzed using a nonlinear regression with a variable slope (GraphPad Prism).

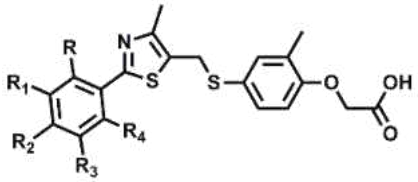

Table 30. Evaluation of poly-substituted GW0742 analogs

Entry	R	R_1	R_2	R_3	R_4	VDR-SRC2-3 interaction IC_{50} μM[a]	VDR transcription IC_{50} (μM)[b]
NCGC00092344-05 (GW0742)	H	F	CF_3	H	H	9.32 ± 1.14	20.7 ± 4.5
NCGC00319082-01	H	CF_3	CF_3	H	H	9.02 ± 0.982	15.0± 4.7
NCGC00319145-01	CF_3	H	CF_3	H	H	16.4 ± 2.78	28.5± 5.2
NCGC00319172-01	Cl	H	CF_3	H	H	9.71 ± 2.24	9.9± 3.2
NCGC00344925-01	H	Cl	CF_3	H	H	15.6 ±2 9.1	22.6 ± 7.1
NCGC00344922-01	H	Cl	OCF_3	H	H	10.3 ± 1.07	22.1 ± 4.3
NCGC00344921-01	H	F	OCF_3	H	H	17.2 ± 3.7	27.3 ± 5.1
NCGC00319077-01	H	OCH_3	OCH_3	H	H	>100	>50
NCGC00319159-01	H	F	OCH_3	H	H	68.6 ± 12.24	>50
NCGC00319154-01	H	CH_3	OCH_2CF_3	H	H	39.42 ± 4.45	22.3± 6.1
NCGC00319171-01	H	CF_3	F	H	H	17.0 ± 1.64	14.8± 6.3
NCGC00319147-01	F	F	F	H	H	51.55 ± 9.74	36.9± 13.0
NCGC00319168-01	H	F	F	F	H	19.57 ± 3.06	8.7 ± 4.4
NCGC00344924-01	H	Cl	F	H	H	10.2 ± 2.11	>50
NCGC00319153-01	H	CN	F	H	H	53.5 ± 16.0	23.7± 4.7
NCGC00319148-01	CF_3	H	Cl	H	H	34.02± 6.59	35.4± 12.2
NCGC00319143-01	H	CF_3	Cl	H	H	6.9 ± 0.99	21.4± 4.2
NCGC00344923-01	H	F	Cl	H	H	22.90 ± 4.2	>50
NCGC00319075-01	H	Cl	Cl	H	H	5.55 ± 1.17	6.5± 3.1
NCGC00319142-01	Cl	H	CN	H	H	17.4 ± 2.06	39.4± 11.0
NCGC00344926-01	H	Cl	H	F	H	15.6 ± 2.01	28.7 ± 8.2
NCGC00344927-01	H	CF_3	H	Cl	H	11.2 ± 3.24	32.6 ± 16.4
NCGC00319146-01	H	Cl	H	Cl	H	6.29 ± 0.79	22.2± 9.6
NCGC00344928-01	Cl	H	H	H	Cl	40.3 ± 8.07	33.0 ± 7.2
NCGC00344929-01	Cl	Cl	H	H	H	15.6 ± 2.01	14.3 ± 5.7
NCGC00344930-01	Cl	H	H	Cl	H	14.5 ±2.21	>50
NCGC00319170-01	H	F	Benzyl-morpholine	H	H	68.8 ± 13.0	>50

[a]VDR-LBD concentration used was 0.1μM. Inhibition of VDR-SRC2-3 interaction in the presence of LG190178 (0.75 μM). The maximum concentration used for this assay was 300 μM of each compound; [b]Transcription assay using a CMV-VDR plasmid and a luciferase reporter plasmid under control of a 24-hydroxylase promoter with GW0742 analogs. [c]Cell-TiterGlo (Promega) The maximum concentration used for transcription and toxcitiy assay was 100 μM of each compound. Data were analyzed using a nonlinear regression with a variable slope (GraphPad Prism).

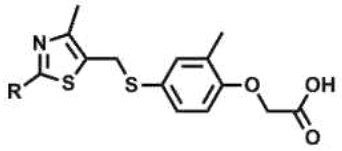

Table 31. Evaluation of heteroaromatic-substituted GW0742 analogs

entry	R	VDR-SRC2-3 interaction IC_{50} μM	VDR transcription IC_{50} (μM)
NCGC00319037-01	3,5-dimethylisoxazol-4-yl	>100	>60
NCGC00319078-01	1*H*-indazol-4-yl	50.2 ± 7.49	>20
NCGC00319073-01	4-pyridine	43.9 ± 8.54	inactive
NCGC00319074-01	2-(benzofuran-2-yl)	52.8 ± 8.65	>50
NCGC00319040-01	2,3-dihydrobenz[1,4]dioxin-6-yl	40.9 ± 5.67	>50
NCGC00319076-01	Naphthalene-1-yl	20.2 ± 1.89	26.3±0 8.3
NCGC00319038-01	Benzo[1,3]dioxol-5-yl	65.8 ± 15.54	42.5± 19.4
NCGC00319039-01	Benzo[1,2,5]oxadiazol-5-yl	20.7 ± 1.18	>50
NCGC00319155-01	Furan-2-yl	>100	>50
NCGC00319173-01	Pyridin-3-yl	>100	>100
NCGC00319059-01	Benzothiophen-2-yl	47.7 ± 8.29	>100
NCGC00319162-01	Piperazin-1-yl	>100	>50
NCGC00319164-01	Pyrimidin-yl	>100	inactive
NCGC00319149-01	1*H*-indazol-6-yl	57.9 ± 8.69	inactive
NCGC00319160-01	Benzothiazol-6-yl	53.0 ± 7.35	32.0± 14.5
NCGC00319166-01	Isoquinolin-4-yl	53.5 ± 7.45	21.6± 6.05
NCGC00319163-01	6-fluoropyridin-3-yl	>100	>50
NCGC00319167-01	1-methyl-1*H*-indazol-6-yl	57.1 ± 11.04	>50
NCGC00319165-01	6-(trifluoromethyl)pyridin-3-yl	>100	>80
NCGC00319144-01	1-methyl-1*H*-indol-6-yl	20.9 ± 3.58	>50
NCGC00319157-01	1*H*-indol-5-yl	15.1 ± 11.8	>50
NCGC00319156-01	1*H*-pyrazol-4-yl	>100	inactive
NCGC00319152-01	2-fluoropyridin-4-yl	>100	>100
NCGC00319158-01	1*H*-indazol-5-yl	51.1 ± 5.55	inactive
NCGC00344920-01	Benzothiophen-5-yl	20.4 ± 1.96	>50
NCGC00344919-01	1*H*-indol-4-yl	28.9 ± 4.69	Inactive
NCGC00344918-01	1*H*-indol-2-yl	22.6 ± 3.83	30.1 ± 10.2

[a]VDR-LBD concentration used was 0.1μM. Inhibition of VDR-SRC2-3 interaction in the presence of LG190178 (0.75 μM). The maximum concentration used for this assay was 300 μM of each compound; [b]Transcription assay using a CMV-VDR plasmid and a luciferase reporter plasmid under control of a 24-hydroxylase promoter with GW0742 analogs. [c]Cell-TiterGlo (Promega) The maximum concentration used for transcription and toxcitiy assay was 100 μM of each compound. Data were analyzed using a nonlinear regression with a variable slope (GraphPad Prism).

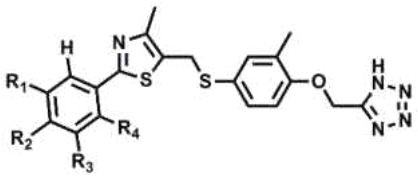

Table 32. Evaluation of tetrazole-substituted GW0742 analogs

Compound ID	R_1	R_2	R_3	R_4	VDR-SRC2-3 Interaction IC_{50} μM[a]	VDR Transcription IC_{50} (μM)[b]
NCGC00264097-01	H	CF_3	F	H	4.25 ± 0.692	7.11± 1.74
NCGC00344870-01	Cl	H	Cl	H	4.55 ± 0.738	11.8 ± 6.5
NCGC00344869-01	H	Cl	H	CF_3	11.85± 4.54	19.9 ± 1.06
NCGC00344871-01	H	Cl	Cl	H	2.66± 0.487	9.03 ± 2.3

[a]VDR-LBD concentration used was 0.1μM. Inhibition of VDR-SRC2-3 interaction in the presence of LG190178 (0.75 μM). The maximum concentration used for this assay was 300 μM of each compound; [b]Transcription assay using a CMV-VDR plasmid and a luciferase reporter plasmid under control of a 24-hydroxylase promoter with GW0742 analogs. [c]Cell-TiterGlo (Promega) The maximum concentration used for transcription and toxcitiy assay was 100 μM of each compound. Data were analyzed using a nonlinear regression with a variable slope (GraphPad Prism).

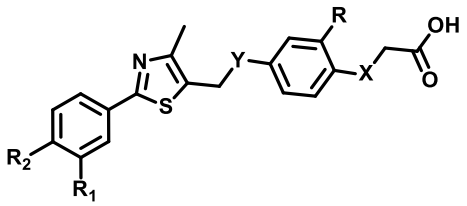

Table 33. Evaluation of linker-substituted GW0742 analogs.

entry	R_1	R_2	Y	R	X	VDR-SRC2-3 interaction (IC50) μM	VDR transcription IC_{50} (μM)
NCGC00264098-01	H	CF_3	S	CH_3	CH_2	16.0 ± 1.22	3.62 ± 0.99
NCGC00264099-01	F	CF_3	S	H	--	34.9 ± 3.75	15.9 ± 6.46
NCGC00263796-01	F	CF_3	S	H	O	17.2 ± 1.52	13.33 ± 4.7
NCGC00264094-01	F	CF_3	O	CH_3	O	19.8 ± 1.66	6.33 ± 3.18
NCGC00264104-01	F	CF_3	O	H	CH_2	33.3 ± 3.71	6.40 ± 4.91
NCGC00264093-01	F	CF_3	O	H	S	15.0 ± 1.18	5.5 ± 2.0
KAT-031513	H	CF_3	O	H	CH_2	>100	>33
NCGC00264101-01	F	CF_3	N	CH_3	O	62.4±8.52	11.78± 6.32
NCGC00264103-01	F	CF_3	N	H	O	>100	21.0 ± 7.5
NCGC00264102-01	F	CF_3	N	H	CH_2	>100	22.3± 7.1
KAT-050713	CH_2OH	H	O	H	CH_2	>100	Inactive

[a]VDR-LBD concentration used was 0.1μM. Inhibition of VDR-SRC2-3 interaction in the presence of LG190178 (0.75 μM). The maximum concentration used for this assay was 300 μM of each compound; [b]Transcription assay using a CMV-VDR plasmid and a luciferase reporter plasmid under control of a 24-hydroxylase promoter with GW0742 analogs. [c]Cell-TiterGlo (Promega) The maximum concentration used for transcription and toxcitiy assay was 100 μM of each compound. Data were analyzed using a nonlinear regression with a variable slope (GraphPad Prism).

APPENDIX B: SOLUBILITY ASSAY WITH GW0742 OXAZOLE ANALOGS: CALIBRATION CURVES

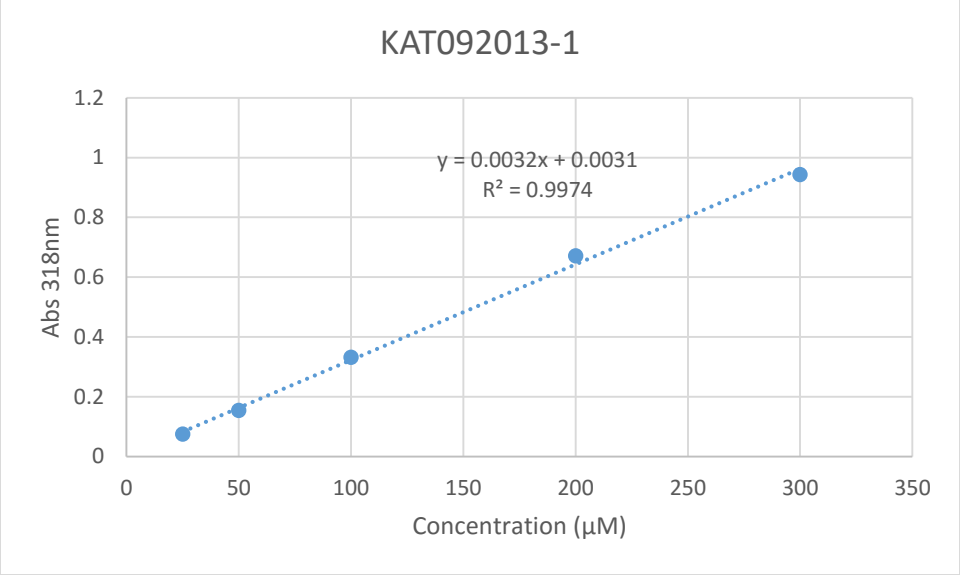

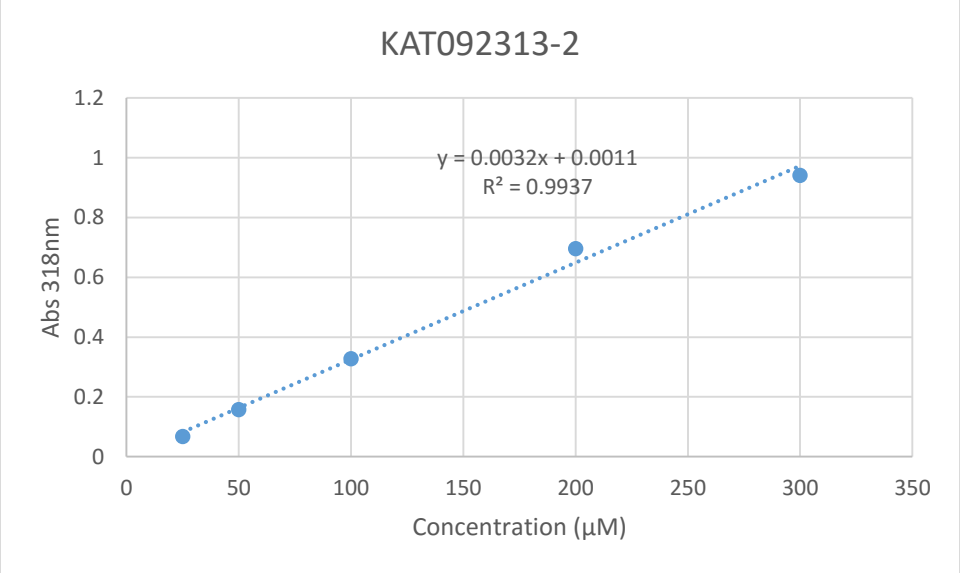

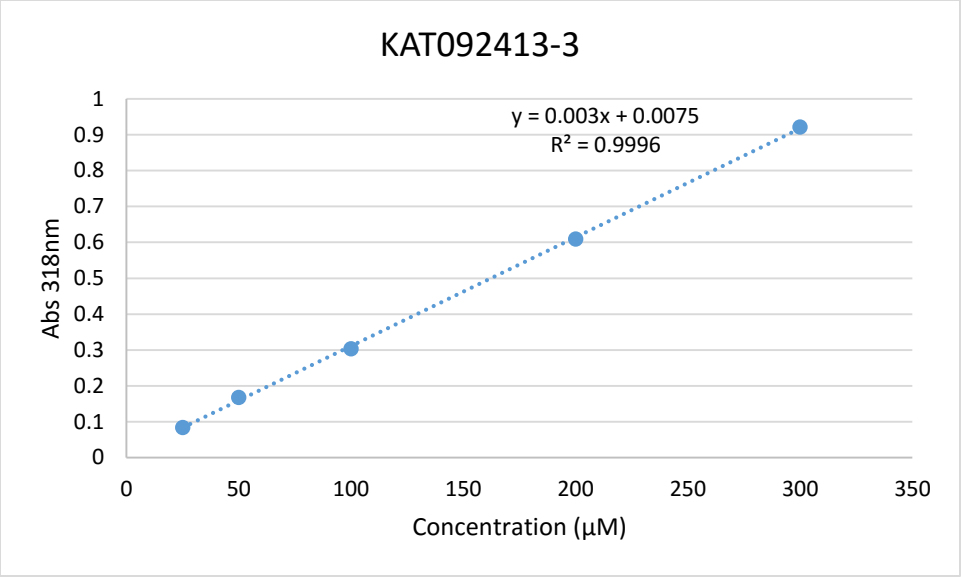
KAT092413-3
y = 0.003x + 0.0075
R² = 0.9996
Abs 318nm
Concentration (µM)
0
0.1
0.2
0.3
0.4
0.5
0.6
0.7
0.8
0.9
1
0
50
100
150
200
250
300
350

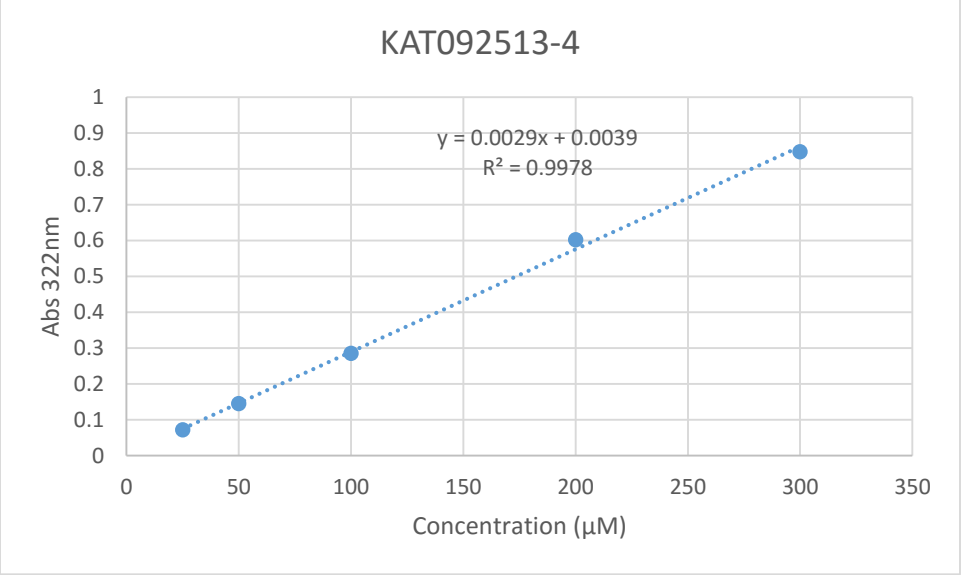
KAT092513-4
y = 0.0029x + 0.0039
R² = 0.9978
Abs 322nm
Concentration (µM)
0
0.1
0.2
0.3
0.4
0.5
0.6
0.7
0.8
0.9
1
0
50
100
150
200
250
300
350

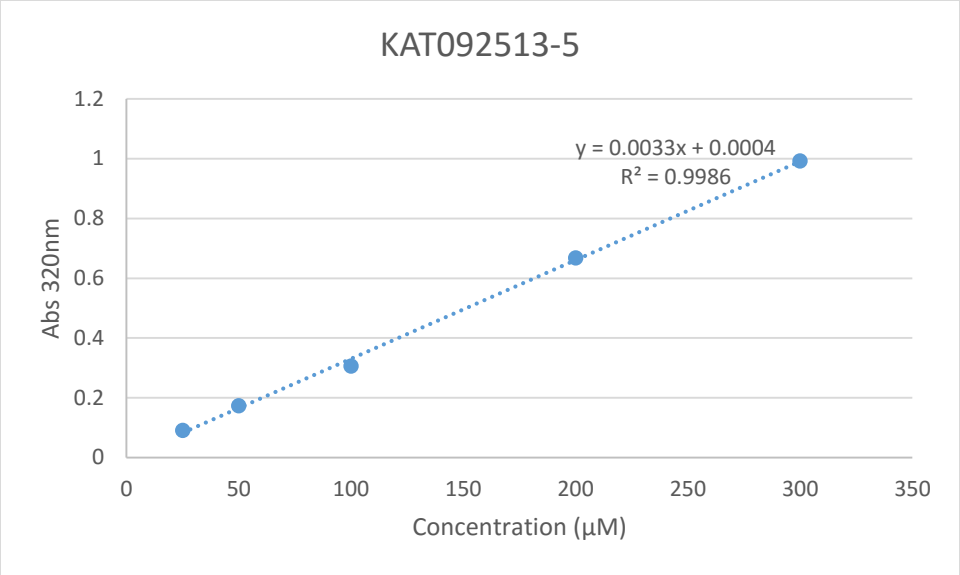
KAT092513-5
y = 0.0033x + 0.0004
R² = 0.9986
Abs 320nm
Concentration (µM)
0
0.2
0.4
0.6
0.8
1
1.2
0
50
100
150
200
250
300
350

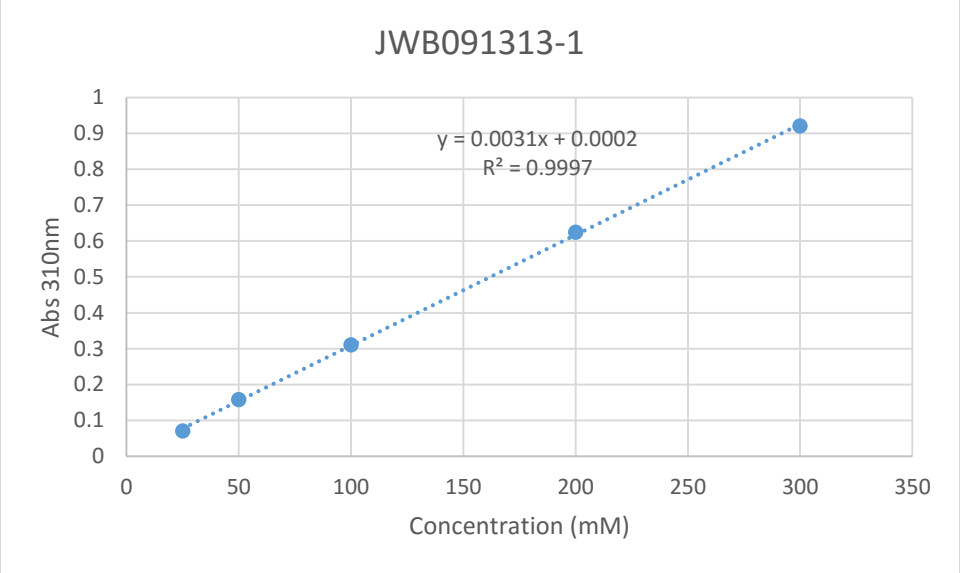
JWB091313-1
y = 0.0031x + 0.0002
R² = 0.9997
Abs 310nm
Concentration (mM)
0
0.1
0.2
0.3
0.4
0.5
0.6
0.7
0.8
0.9
1
0
50
100
150
200
250
300
350

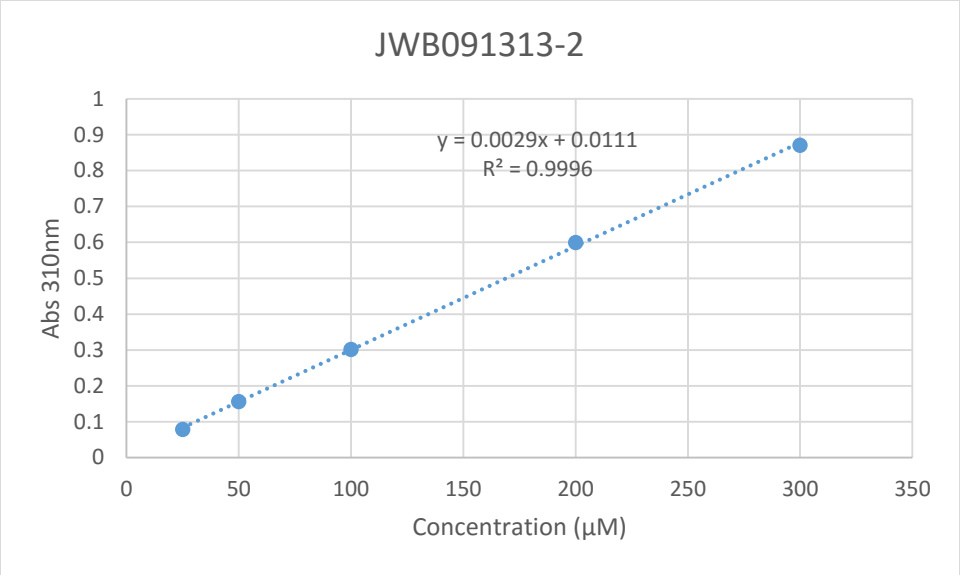
JWB091313-2
y = 0.0029x + 0.0111
R² = 0.9996
Abs 310nm
Concentration (µM)
0
0.1
0.2
0.3
0.4
0.5
0.6
0.7
0.8
0.9
1
0
50
100
150
200
250
300
350

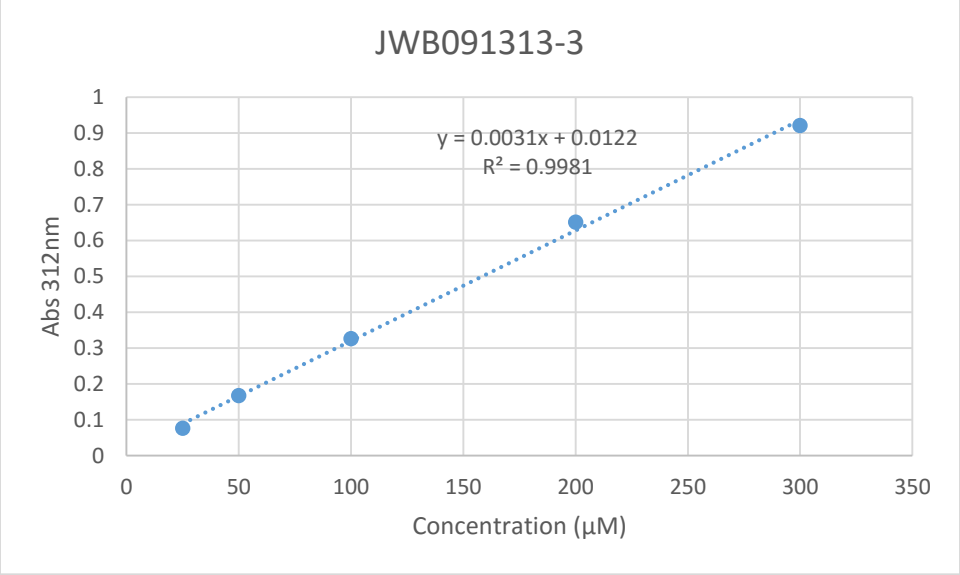
JWB091313-3
y = 0.0031x + 0.0122
R² = 0.9981
Abs 312nm
Concentration (µM)
0
0.1
0.2
0.3
0.4
0.5
0.6
0.7
0.8
0.9
1
0
50
100
150
200
250
300
350

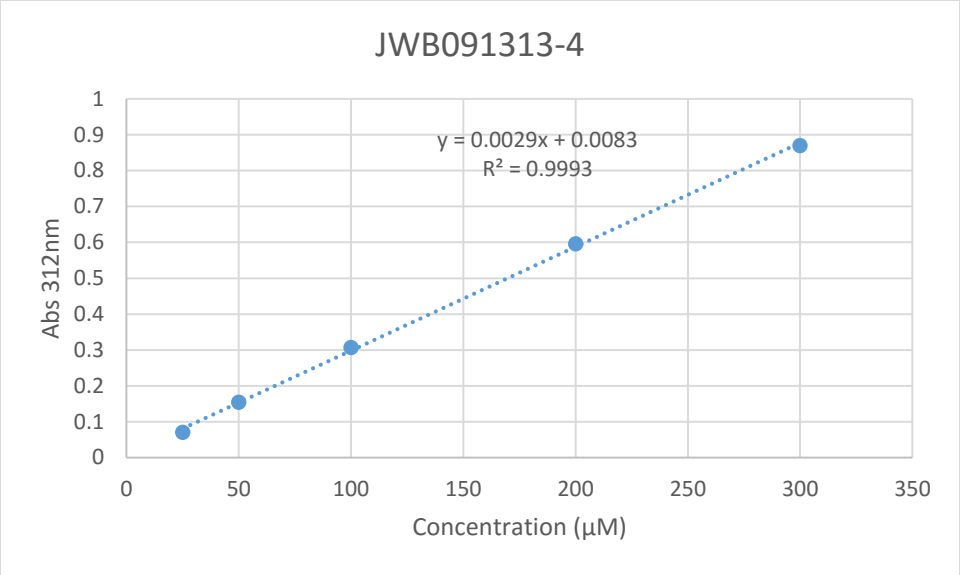
JWB091313-4
y = 0.0029x + 0.0083
R² = 0.9993
Abs 312nm
Concentration (µM)
0
0.1
0.2
0.3
0.4
0.5
0.6
0.7
0.8
0.9
1
0
50
100
150
200
250
300
350

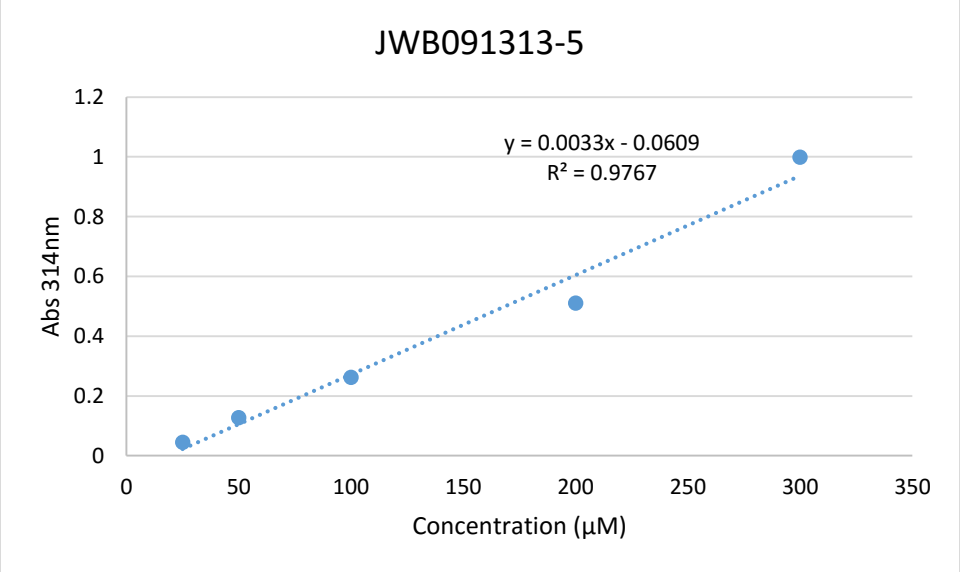
JWB091313-5
y = 0.0033x - 0.0609
R² = 0.9767
Abs 314nm
Concentration (µM)
0
0.2
0.4
0.6
0.8
1
1.2
0
50
100
150
200
250
300
350

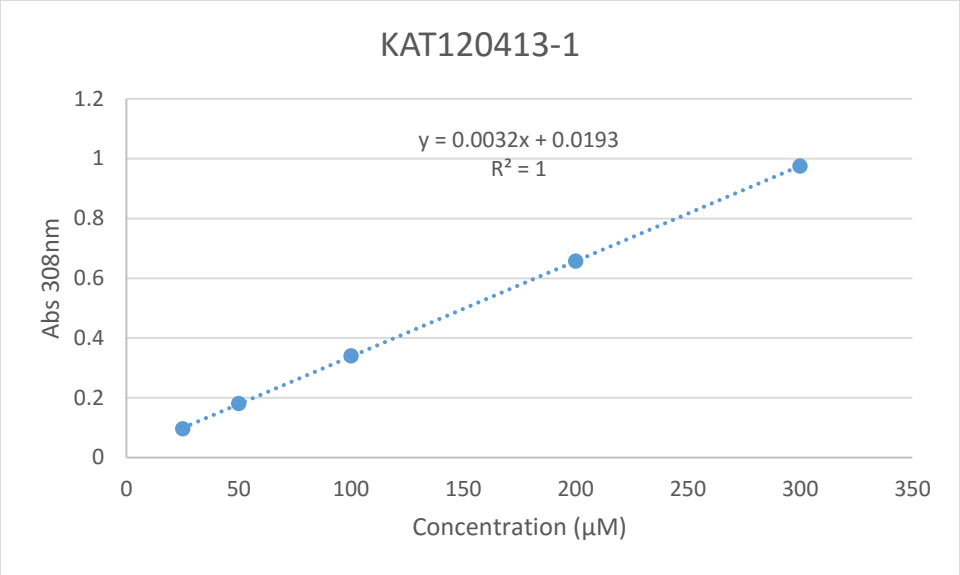
KAT120413-1
y = 0.0032x + 0.0193
R² = 1
Abs 308nm
Concentration (µM)
0
0.2
0.4
0.6
0.8
1
1.2
0
50
100
150
200
250
300
350

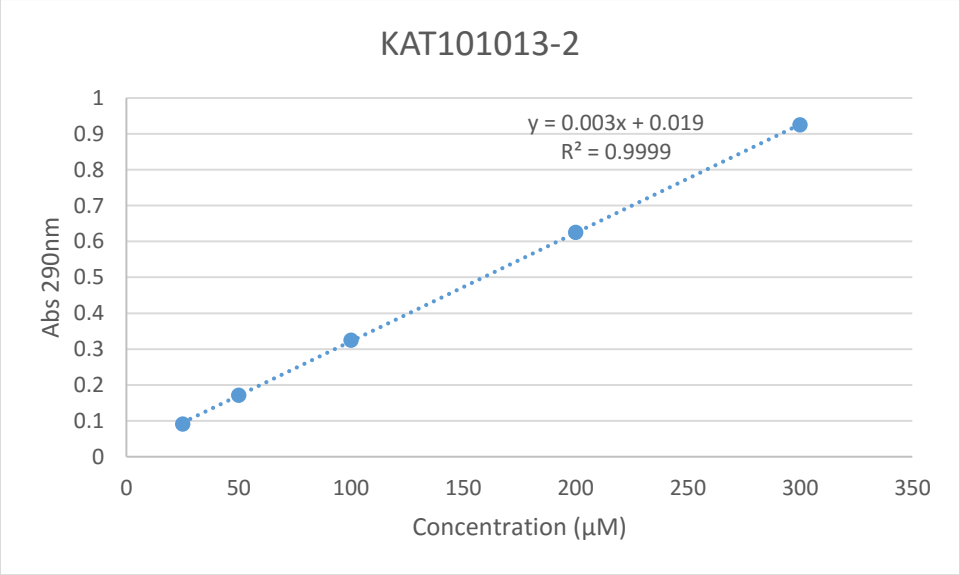
KAT101013-2
y = 0.003x + 0.019
R² = 0.9999
Abs 290nm
Concentration (µM)
0
0.1
0.2
0.3
0.4
0.5
0.6
0.7
0.8
0.9
1
0
50
100
150
200
250
300
350

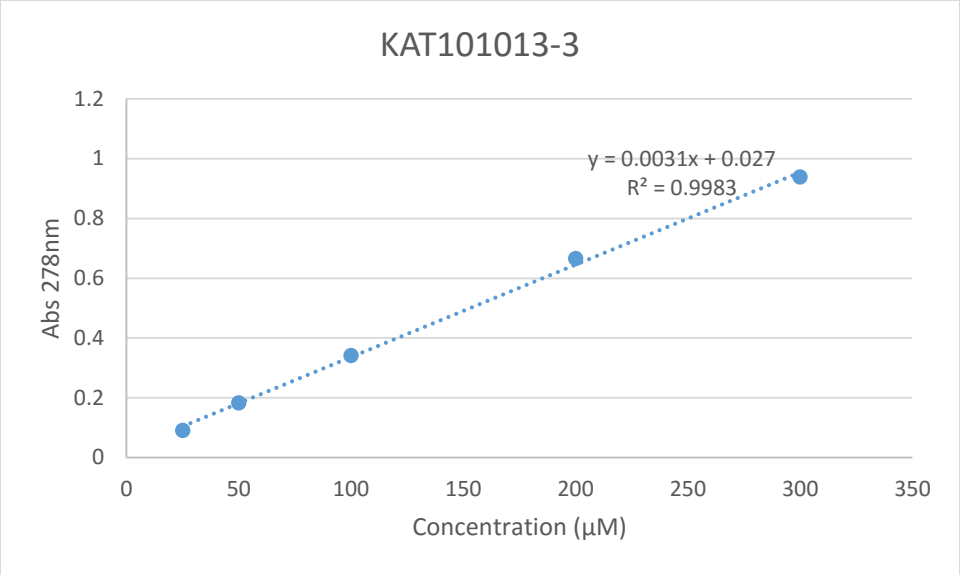
KAT101013-3
y = 0.0031x + 0.027
R² = 0.9983
Abs 278nm
Concentration (µM)
0
0.2
0.4
0.6
0.8
1
1.2
0
50
100
150
200
250
300
350

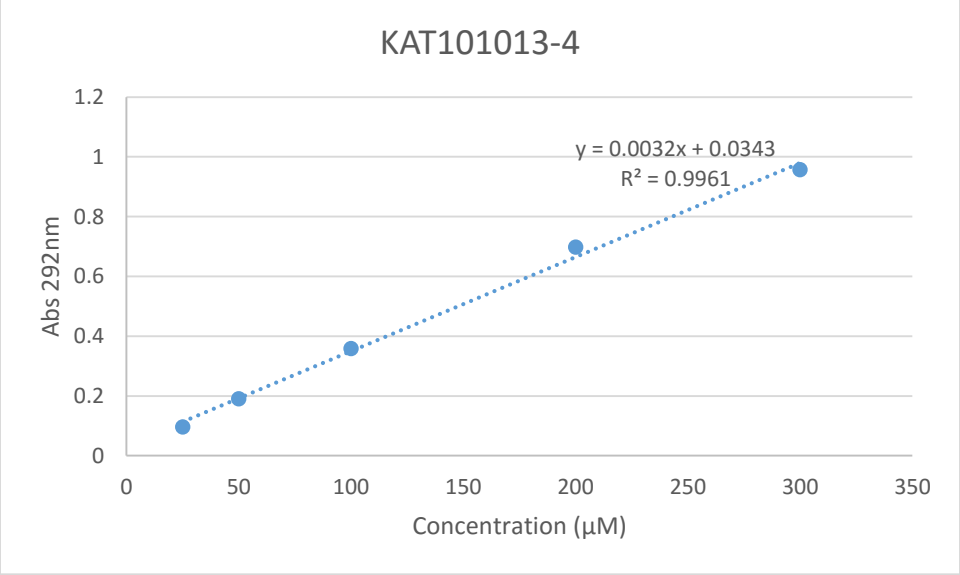
KAT101013-4
y = 0.0032x + 0.0343
R² = 0.9961
Abs 292nm
Concentration (µM)
0
0.2
0.4
0.6
0.8
1
1.2
0
50
100
150
200
250
300
350

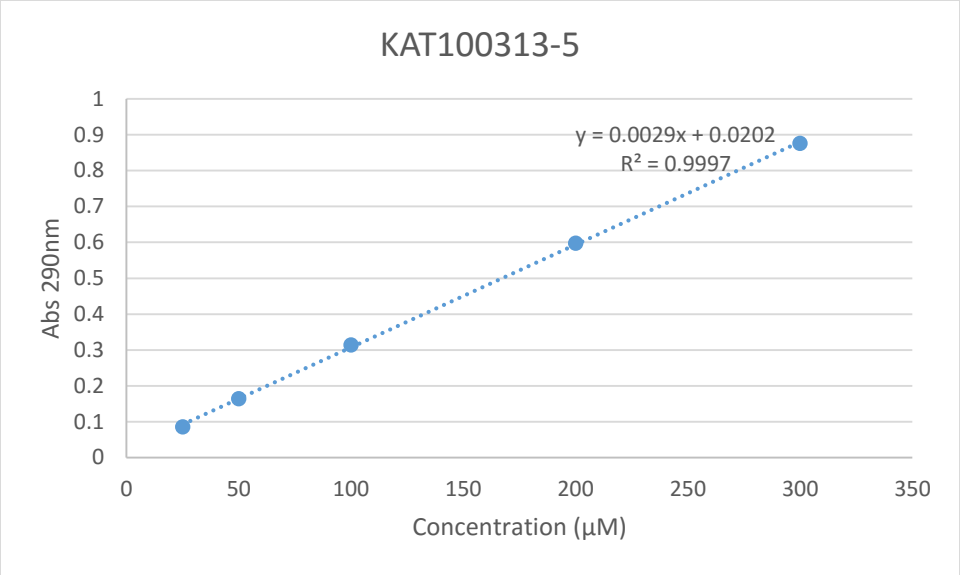
KAT100313-5
y = 0.0029x + 0.0202
R² = 0.9997
Abs 290nm
Concentration (µM)
0
0.1
0.2
0.3
0.4
0.5
0.6
0.7
0.8
0.9
1
0
50
100
150
200
250
300
350

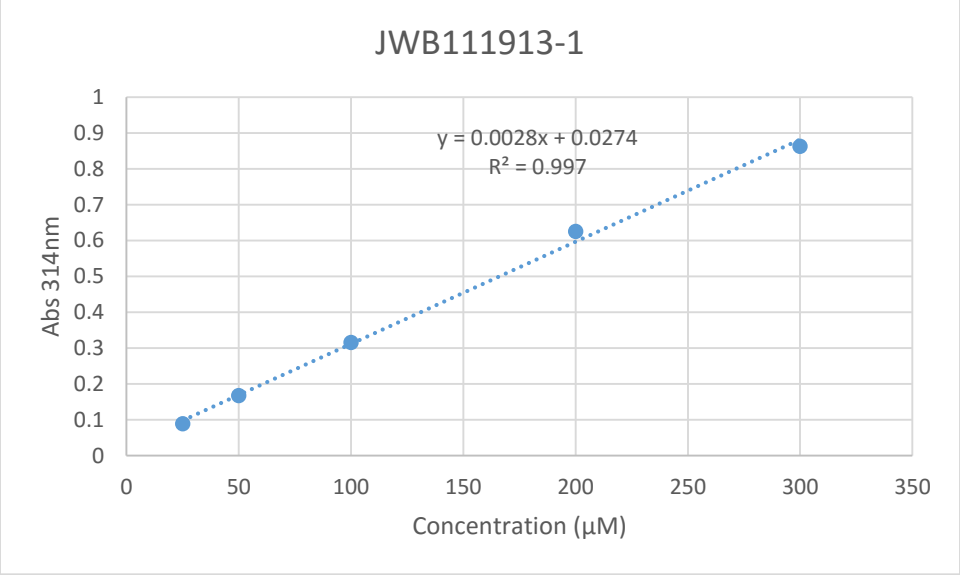
JWB111913-1
y = 0.0028x + 0.0274
R² = 0.997
Abs 314nm
Concentration (µM)
0
0.1
0.2
0.3
0.4
0.5
0.6
0.7
0.8
0.9
1
0
50
100
150
200
250
300
350

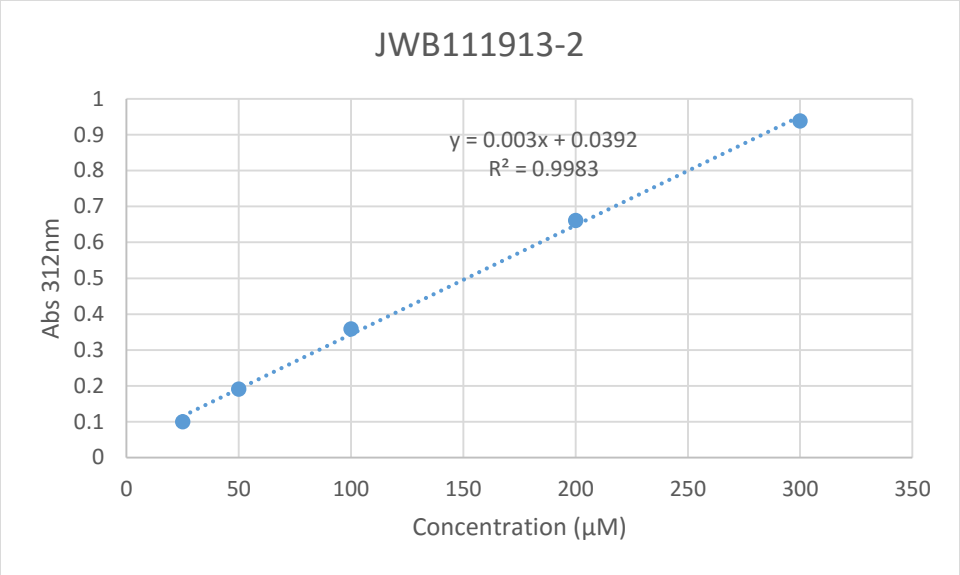
JWB111913-2
y = 0.003x + 0.0392
R² = 0.9983
Abs 312nm
Concentration (µM)
0
0.1
0.2
0.3
0.4
0.5
0.6
0.7
0.8
0.9
1
0
50
100
150
200
250
300
350

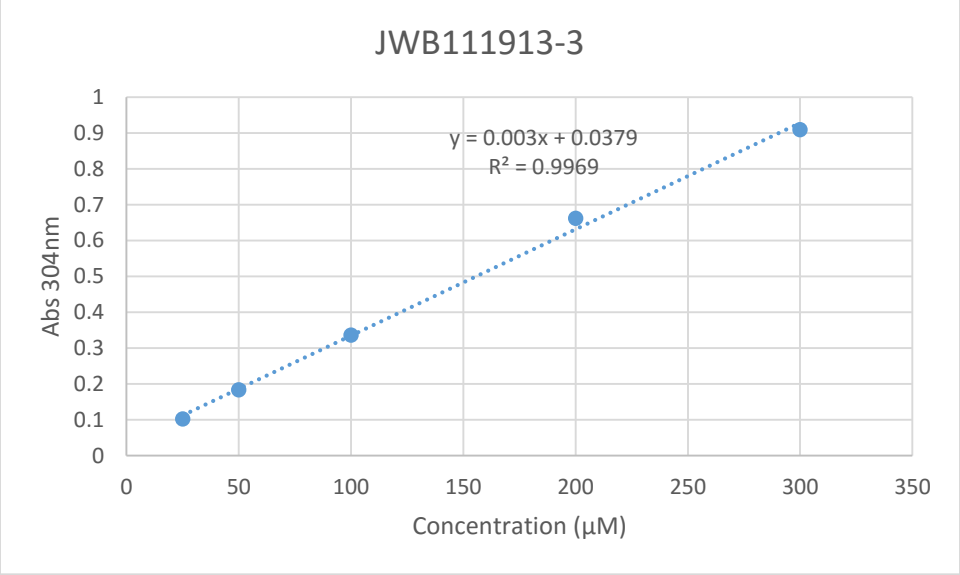
JWB111913-3
y = 0.003x + 0.0379
R² = 0.9969
Abs 304nm
Concentration (µM)
0
0.1
0.2
0.3
0.4
0.5
0.6
0.7
0.8
0.9
1
0
50
100
150
200
250
300
350

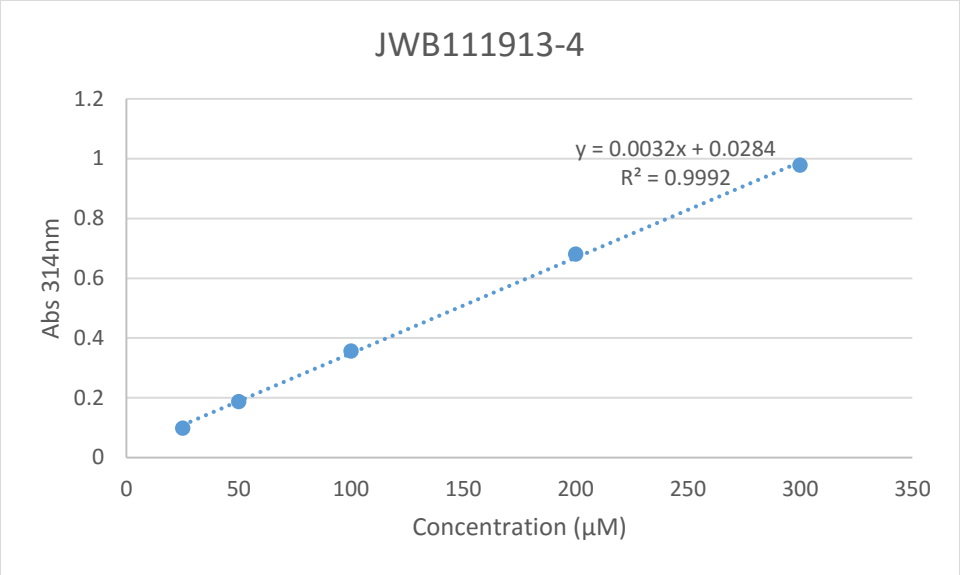
JWB111913-4
y = 0.0032x + 0.0284
R² = 0.9992
Abs 314nm
Concentration (µM)
0
0.2
0.4
0.6
0.8
1
1.2
0
50
100
150
200
250
300
350

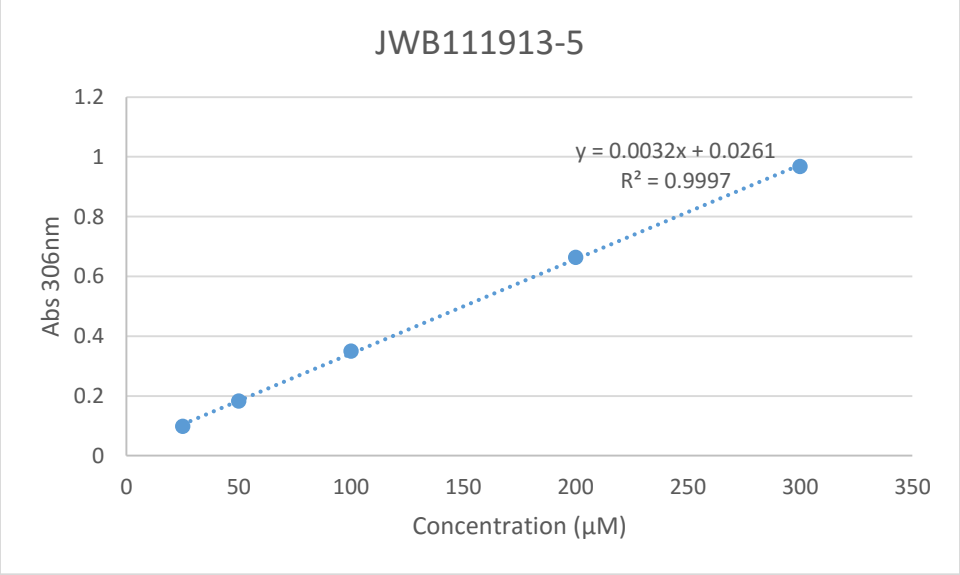
JWB111913-5
y = 0.0032x + 0.0261
R² = 0.9997
Abs 306nm
Concentration (µM)
0
0.2
0.4
0.6
0.8
1
1.2
0
50
100
150
200
250
300
350

CURRICULUM VITAE

Kelly A. Teske

EDUCATION

Ph.D., Organic (Medicinal) Chemistry, August 2010- August 2015
University of Wisconsin- Milwaukee, WI
Dissertation: "Part 1. The Development of Non-Secosteroidal Vitamin D Receptor Modulators and Part 2. The Development of a Universal GTPase Assay"
Advisor: Prof. Alexander (Leggy) Arnold

B.S., Chemistry and Biochemistry & Molecular Biology, August 2006-May 2010
Illinois State University, Normal, Il
Research: "The Reaction of Gold (I) and Gold (III) Cyanide with Cysteine Hydrochloride"
Advisor: Prof. Frank C. Shaw, III

RESEARCH EXPERIENCE

GTPase and Kinase Assay: Developed a universal kinase and GTPase Assay kit in collaboration with AviMed Pharmaceuticals LLC. This included the synthesis of assay components, development, miniaturization, and quality control.

Designing and Evaluating Vitamin D Receptor (VDR) Modulators: VDR is a therapeutically relevant drug target for the treatments of osteoporosis, psoriasis, cancer, and autoimmune diseases such as Crohn's disease and sarcoidosis. Applied rational design and high throughput screening hit compounds to develop novel inhibitors for VDR-coregulator interactions. The techniques used included different biochemical and cell-based assays for nuclear receptors, multi-step and parallel synthesis, and analysis such as NMR and LCMS. Molecular modeling was used to identify new analogs based on docking as well as calculations of preclinical properties.

Interaction of Gold with Sulfur-based Compounds: The reactions of $[Au(CN)_2]^-$ and $[Au(CN)_4]^-$ were studied separately with cysteine hydrochloride in order to understand the underlying pharmacology of gold based drugs (i.e. auranofin) as treatment for rheumatoid arthritis. The reactions were analyzed using LC-MS, NMR, and UV-Spectrometry.

LABORATORY TECHNIQUES

- 1D, 2D NMR (^{13}C, ^{31}P, ^{1}H and ^{77}Se)
- Chromatography:
    - HPLC (reverse phase)
    - Automated Flash Chromatography
    - Fast Protein Liquid Chromatography (Ion-exchange and size exclusion columns)

- Mass Spectrometry (Single Quadrupole)
- Fluorescence-based assays (F, FP, and FRET), 384-well format
- Luminescence-based assays (luciferase reporter and toxicity assay), 384-well format
- Mammalian cell culture (HEK293, DU145, HL-60, and LNCaP)
- Solubility and permeability assay, 384-well format
- qRT-PCR
- Multi-step organic synthesis (drug-like compounds and nucleoside synthesis)
- Molecular Modeling using Molecular Operating Environment (MOE)
    - Ligand: Receptor docking of small molecules
    - Contact statistics, electrostatic and interaction maps
    - Pharmacophore modeling
    - Production of ligand databases
- Animal Studies
    - Handling, drug administration, and euthanasia
    - Mouse xenograft studies
    - Dissection and organ harvesting

TEACHING EXPERIENCE

Graduate Chemistry Teaching Assistant August 2010- May 2014

University of Wisconsin-Milwaukee

General Chemistry for Non-majors (100), engineering (105) and nursing (101), Introductory Biochemistry for nursing (103), Organic Chemistry for Majors and Pre-professional (344)

Undergraduate Chemistry Teaching Assistant January 2009- May 2010

Illinois State University

General Chemistry (Majors and non-majors), Organic Chemistry, and Analytical Chemistry

MENTORSHIP

- Angela Zivkovic, Undergraduate research student 2011-2012
  Research: "Synthesis of Novel Non-secosteroidal Vitamin D Receptor Agonist"
- Rajwana Jahan, Graduate student teaching assistant Fall 2012
- Nicholas Nassif, Undergraduate research student 2012-2013
  Research: "Expression and Purification of the Vitamin D Receptor Ligand Binding Domain for the Identification of Vitamin D Receptor-Coactivator Inhibitors"
- Praveen Ghosh, Undergraduate student teaching assistant Spring 2013
- Quint Owen, Graduate student teaching assistant Fall 2013
- Jon Bogart, Undergraduate research student 2013-2014
  Research: "The Synthesis and Evaluation of Potential Non-secosteroidal VDR-Coactivator Inhibitors"

- Surajadeen Omolabake, Graduate student teaching assistant Spring 2014
- Luis Sanchez, Undergraduate research student 2014-2015
  Research: "Development and Synthesis of Potential Non-secosteroidal VDR-Coactivator Inhibitors"
- Charlie Stangl, Undergraduate research student Spring 2015-Current
  Research: "Synthesis of Hydrazine Derivatives as Potential Vitamin D Receptor Modulators"

PUBLICATIONS

PUBLISHED

1. Guthrie, M. L.; Sidhu, P. S.; Hill, E. K.; Horan, T. C.; Nandhikonda, P.; Teske, K. A.; Yuan, N. Y.; Sidorko, M.; Kodali, R.; Cook, J. M.; Han, L.; Silvaggi, N. R.; Bikle, D. D.; Moore, R. G.; Singh, R. S.; Arnold, L. A., Anti-tumor Activity of 3-Indoylmethanamines 31B and PS121912. *Anticancer Research* **2105**, 35.
2. Sidhu, P. S.; Teske, K.; Feleke, B.; Yuan, N. Y.; Guthrie, M. L.; Fernstrum, G. B.; Vyas, N. D.; Han, L.; Preston, J.; Bogart, J. W.; Silvaggi, N. R.; Cook, J. M.; Singh, R. K.; Bikle, D. D.; Arnold, L. A., Anticancer Activity of VDR-coregulator inhibitor PS121912. *Cancer Chemother Pharmacol* **2014**.
3. Teske, K.; Nanhikonda, P.; Bogart, J. W.; Feleke, B.; Sidhu, P.; Yuan, N. Y.; Preston, J.; Goy, R.; Han, L.; Silvaggi, N. R.; Singh, R. K.; Bikle, D. D.; Cook, J. M.; Arnold, L. A., Identification of VDR Antagonists Among Nuclear Receptor Ligands Using Virtual Screening. *Nuclear Receptor Research* **2014,** *1*, 1-8.
4. Teske, K.; Nandhikonda, P.; Bogart, J. W.; Feleke, B.; Sidhu, P.; Yuan, N.; Preston, J.; Goy, R.; Arnold, L. A., Modulation of Transcription Mediated by the Vitamin D Receptor and the Peroxisome Proliferator-Activated Receptor δ. *Biomolecular Research & Therapeutics* **2014,** *3* (1).
5. Sidhu, P. S.; Nassif, N.; McCallum, M. M.; Teske, K.; Feleke, B. D.; Yuan, N. Y.; Nandhikonda, P.; Cook, J. M.; Singh, R. K.; Bikle, D. D.; Arnold, L. A., Development of Novel Vitamin D Receptor-Coactivator Inhibitors. *ACS Medicinal Chemistry Letters* **2014,** *5* (2), 199-204.
6. Nandhikonda, P.; Yasgar, A.; Baranowski, A.; Sidhu, P. S.; McCallum, M. M.; Pawlak, A. J.; Teske, K.; Feleke, B.; Yuan, N. Y.; Kevin, C.; Bikle, D. D.; Ayers, S. D.; Webb, P.; Rai, G.; Simeonov, A.; Jadhav, A.; Maloney, D.; Arnold, L. A., Peroxisome Proliferation- Activated Receptor δ Agonist GW0742 Interacts Weakly with Multiple Nuclear Receptors, Including the Vitamin D Receptor. *Biochemistry* **2013,** *52*, 4193-4203.

SUBMITTED

7. Teske, K. A.; Yu, O.; Arnold, L. A., Arnold "Vitamin and Hormones: Chapter 7. Inhibitors for the Vitamin D Receptor–Coregulator Interaction **(published by the end of the year)**.
8. Min, J.; Arnold, L. A.; Attia, R. R.; Connelly, M.; Teske, K.; Shelat, A.; Guy, R. K. Inhibitors of the Interaction of PPARγ and SMRT. Submitted to J*BC.*

PRESENTATIONS

1. Teske, K. A.; Bogart, J. W.; Sanchez, L.; Arnold, L. A. Synthesis of Natural VDR Ligand Metabolites and Their Interaction with the Vitamin D Receptor. *250th American Chemical Society National Conference,* Boston, MA, **2015**
2. Teske, K. A.; Bogart, J. W.; Sanchez, L.; Bantukallu, G.; Simeonov, A.; Jadhav, A.; Yasgar, A.; Maloney, D.; Arnold, L. A., Development of Selective Non-Secosteroid Vitamin D Receptor Inhibitors, *248th American Chemical Society National Conference*, San Francisco, CA, **2014**
3. Teske, K. A.; Bogart, J. W.; Sanchez, L.; Arnold, L. A., Identification of New Vitamin D Receptor-Coregulator Inhibitors Among Nuclear Receptor Ligands, *248th American Chemical Society National Conference*, San Francisco, **2014**
4. Teske, K. A.; Yasgar, A; Bantukallu, G.; Bogart, J.; Simeonov, A.; Jadhav, A.; Maloney, D.; Arnold, L. A., Further Investigation of the First Non-Secosteroid Antagonist for the Vitamin D Receptor, *Awards Day*, University of Wisconsin- Milwaukee, **2014**
5. Teske, K. A.; Yasgar, A; Bantukallu, G.; Bogart, J.; Simeonov, A.; Jadhav, A.; Maloney, D.; Arnold, L. A., Further Investigation of the First Non-Secosteroid Antagonist for the Vitamin D Receptor, *The 4th Yao Yuan Biotech/Pharma International Symposium*, University of Illinois-Chicago, **2014**
6. Min, J.; Attia, R. N.; Arnold, L. A.; Teske, K.; Connelly, M.; Lemieux, G.; Ashrafi, K.; Shelat, A.; Guy, R. K., Discovery of Small Molecule Inhibitors of the Interaction between PPARγ and SMRT, *105th Annual Meeting of the American Association for Cancer Research,* San Diego, CA, **2014**.
7. Teske, K. A.; Yasgar, A; Bantukallu, G.; Bogart, J.; Simeonov, A.; Jadhav, A.; Maloney, D.; Nassif, N. D.; Arnold, L. A., Identification of the First Non-Secosteroid Antagonist for the Vitamin D Receptor, *Awards Day*, University of Wisconsin- Milwaukee, **2013**
8. Teske, K. A.; Yasgar, A; Bantukallu, G.; Bogart, J.; Simeonov, A.; Jadhav, A.; Maloney, D.; Nassif, N. D.; Arnold, L. A., Identification of the First Non-Secosteroid Antagonist for the Vitamin D Receptor, *245th American Chemical Society National Conference*, New Orleans, **2013**
9. Teske. K. A.; Zivkovic, A.; Arnold, L.A., Rational Development of Reversible Inhibitors of the Vitamin D Receptor-Coregulator Interactions, *Awards Day*, University of Wisconsin-Milwaukee, **2012**
10. Teske. K. A.; Zivkovic, A.; Arnold, L.A., Rational Development of Reversible Inhibitors of the Vitamin D Receptor-Coregulator Interactions, *243rd American Chemical Society National Conference*, San Diego, **2012**
11. Teske, K.; Webb, J. W.; and Shaw, III, C. F., Studies of Ligand Exchange and Oxidation-Reduction Reactions of Gold(I) and Gold(III) Cyanides with Cysteine, *Undergraduate Students Awards Day*, Illinois State University, **2010**
12. Teske, K.; Webb, J. W.; and Shaw, III, C. F., Studies of Ligand Exchange and Oxidation-Reduction Reactions of Gold(I) and Gold(III) Cyanides with Cysteine, *2nd Annual Georgian Bay International Conference on Bioinorganic Chemistry (CanBic)*, **2009**

13. Teske, K.; Webb, J. W.; and Shaw, III, C. F., Studies of Ligand Exchange and Oxidation-Reduction Reactions of Gold(I) and Gold(III) Cyanides with Cysteine, *Undergraduate Students Awards Day,* Illinois State University, **2009**
14. Shaw, III, C. F.; Yangyuoru, P. M.; Manthey, A.; O'Neill, J.; Teske, K. A.; Minser, J., Mixed Cyano-Thilato-Complexes of Gold (III) and Gold (I): Relevance to Chrysotherapy Metabolites, *40th Central Regional Meeting of the American Chemical Society,* Columbus, Ohio, **2008**
15. Teske, K.; Webb, J. W.; and Shaw, III, C. F., Studies of Ligand Exchange and Oxidation-Reduction Reactions of Gold(I) and Gold(III) Cyanides with Cysteine, *Undergraduate Students Awards Day*, Illinois State University, **2008**

AFFILIATIONS

American Chemical Society Member 2010- Present

Graduate Student Council June 2014-May 2015
Department of Chemistry and Biochemistry, University of Wisconsin-Milwaukee

New Graduate Student Mentor December 2012-May 2014
Department of Chemistry and Biochemistry, University of Wisconsin- Milwaukee

Society for Applied Spectroscopy August 2012-May 2013
University of Wisconsin-Milwaukee Student Chapter

AWARDS

Student Travel Award; Awarded by the Chemistry and Biochemistry Graduate Student Council at the University of Wisconsin- Milwaukee *(May 2015)*

Dr. and Mrs. George Sosnovsky Award for Excellence in Graduate Research; University of Wisconsin-Milwaukee *(April 2015)*

Chancellor's Graduate Fellowship; University of Wisconsin- Milwaukee *(2010-2014)*

MEDI-Chem Travel Award; Awarded by the National American Chemical Society MEDI- Chem Division *(August 2014)*

Mentoring Travel Award; Awarded by University of Wisconsin- Milwaukee New Graduate Student Mentor Program *(August 2014)*

Graduate School Research Poster Award; University of Wisconsin- Milwaukee *(April 2014)*

Graduate Student Travel Award; Awarded by the Graduate School at the University of Wisconsin – Milwaukee *(April 2014)*

Student Travel Award; Awarded by the Milwaukee, WI section of the American Chemical Society *(April 2013)*

Graduate Student Travel Award*;* Awarded by the Graduate School at the University of Wisconsin – Milwaukee *(April 2013)*

Mentoring Travel Award; Awarded by University of Wisconsin- Milwaukee New Graduate Student Mentor Program *(April 2013)*

The Gloria Moczynski Student Teacher Award; Awarded by the University of Wisconsin Milwaukee Department of Chemistry and Biochemistry *(April 2013)*

Student Travel Award*;* Awarded by the Graduate School at the University of Wisconsin – Milwaukee *(April 2012)*

The American Chemical Society Undergraduate Award in Inorganic Chemistry*;* Awarded by The American Chemical Society nominated by Illinois State University Department of Chemistry and Biochemistry *(May 2010)*

The Shulman Scholarship for Outstanding Achievements in Chemistry; Awarded by Illinois State University Department of Chemistry and Biochemistry *(August 2009)*